

REPORT

Christian  
Michelsen  
Research

*Research for  
Industrial Development*

**CFD GAS EXPLOSION SIMULATIONS  
TO SUPPORT THE INVESTIGATION  
INTO THE CAUSE OF THE  
EXPLOSION IN THE CENTER WING  
TANK OF TWA-800**

**Client:**  
**National Transportation Safety Board**

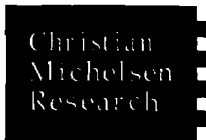
**Authors:**  
Kees van Wingerden  
Jerome Renoult  
Simen Armond

Bergen, April 2000  
**Ref. No.: CMR-00-F30026**

CONFIDENTIAL  
Copy No.: 1/14

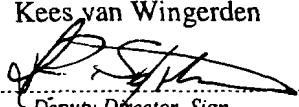
**Christian Michelsen Research AS**  
P.O.Box 6031 Postterminalen  
N-5892 Bergen, NORWAY  
Telephone +47 55 57 40 40  
Telefax +47 55 57 40 41  
Internet <http://www.cmr.no>

Christian Michelsen Research AS  
 Fantoftvegen 38, P.O.Box 6031  
 N-5020 Bergen, Norway  
 Telephone +47 55 57 40 40  
 Telefax +47 55 57 40 41  
 Bank 5201 05 11755



Research for  
 Industrial Development

**REFERENCE PAGE**

<b>REPORT</b>		<i>Ref. No.:</i> <b>CMR-00-F30026</b>	
<i>Author(s)</i> Kees van Wingerden Jerome Renoult Simen Armond		<i>Security Classification</i>  Report Confidential, (F) This ref.page open	
<i>Title</i> CFD Gas Explosion Simulations to Support the Investigation into the Cause of the Explosion in the Center wing Tank of TWA-800			
<i>Extract</i>  The report describes CMR's contribution to find the cause of the explosion in the Center Wing Tank of a Boeing 747-131 used for flight TWA-800. This accident occurred on 17 July 1996 shortly after take-off from New York.			
<i>Client</i>	National Transportation Safety Board	<i>Client's Ref.</i>	Joseph Kolly
<i>Project</i>	TWA-800 Accident Investigation		
<i>CMR-Project No.</i>	38011		
<i>CMR Department</i>	Process and Safety		
<i>Manager</i>	Kees van Wingerden		
<i>Program Manager</i>	Olav Roald Hansen		
<i>Project Manager</i>	Kees van Wingerden		
<i>Approved</i>	 <i>Deputy Director, Sign.</i>		
<i>Indexing Terms</i>			
<i>Norwegian</i> Ulykkesgransking Gasseksplosjon CFD-simuleringer Validering		<i>English</i> Accident investigation Gas explosion CFD simulations Validation	
<i>Number of pages</i>	167	<i>Price Group</i>	
		<i>Date:</i>	April 2000

## TABLE OF CONTENTS

DISCLAIMER	2
1. INTRODUCTION	3
2. DESCRIPTION OF CENTER WING TANK AND CONDITIONS PREVAILING IN THE TANK	5
2.1 Center Wing Tank	5
2.2 Conditions prevailing in Tank	9
3. SHORT OVERVIEW OF 1/4-SCALE EXPERIMENTS	10
3.1 Description of the test facility	10
3.2 Fuel	11
3.3 Experimental programme	13
4. DESCRIPTION OF THE FLACS CODE	16
4.1 Governing equations	18
4.2 Equilibrium chemistry thermodynamics	19
4.3 Turbulence modelling	19
4.4 Combustion modelling	20
4.5 Other models in FLACS	24
4.6 Validation	25
5. MODEL IMPROVEMENTS	27
5.1 Representation of flammable mixtures used in 1/4-scale experiments	27
5.1.1 Hydrogen-propane mixture	27
5.1.2 Jet-A mixtures	30
5.2 Flame propagation through holes	32
5.3 Heat transfer	34
5.4 Quenching	35
6. SIMULATIONS PERFORMED	45
6.1 Model validation: comparison to 1/4-scale experiments	45
6.2 Predictions: effect of ignition position: 1/4 scale	63
6.3 Predictions: effect of ignition source position: full-scale	66
7. DISCUSSION	90
8. CONCLUSIONS	94
9. REFERENCES	96

## **DISCLAIMER**

Christian Michelsen Research does not accept any legal liability or responsibility whatsoever for the consequences of use or misuse of results from this work by anyone.

## 1. INTRODUCTION

The investigation of the accident with flight TWA-800 on July 17, 1996, has been concentrating on the possibility of a gas explosion in one of the fuel tanks of the aeroplane, viz. the so-called Center Wing Tank. As part of this investigation Christian Michelsen Research has been performing gas explosion simulations.

The main aim of the contribution of Christian Michelsen Research has been to help finding the most likely scenario of the fuel-air explosion, which led to failure of parts of the Center Wing Tank escalating into the loss of the aeroplane.

Important parts of the investigation were the following:

- Laboratory experiments to determine physical, chemical and flammability properties of the fuel (Jet A).
- Field experiments in a ¼-scale model of the Center Wing Tank.
- Gas explosion simulations to support the performance of the ¼-scale experiment and to extrapolate therefrom (in scale and explosion scenario).

The laboratory experiments were performed at the California Institute of Technology. The California Institute of Technology also performed the field experiments in a ¼-scale model of the Center Wing Tank in co-operation with Applied Research Associates. Sandia National Laboratories and Christian Michelsen Research performed gas explosion simulation work. An important role is played by Combustion Dynamics considering structural response and the development of a rule based scenario analysis. The latter would potentially lead to indicating the most likely explosion scenario leading to the observed damage based on explosion loading characteristics and structural response of the various parts of the Center Wing Tank.

At Christian Michelsen Research a 3D-Computational Fluid Dynamics (CFD) model is used. This model, known as FLACS, has been developed for describing gas explosion propagation in complex geometries, such as offshore modules.

The reconstruction of the Center Wing Tank revealed a certain failure pattern of the tank.

The investigation is aiming at establishing a single explosion scenario event explaining the observed damage.

Christian Michelsen Research was involved in:

- Supporting the 1/4-scale field experiments,
- Simulating the outcome of a part of the field experiments performed,
- Validation of the FLACS code against the results of the field experiments,
- Inclusion of some improvements in the code
- Simulating the course of full-scale fuel tank explosions.

## 2. DESCRIPTION OF CENTER WING TANK AND CONDITIONS PREVAILING IN THE TANK

### 2.1 Center Wing Tank

Flight TWA-800 was performed with a Boeing 747-131. The Center Wing Tank is located in between the wings of this type of aeroplane.

The tank consists of four main compartments and an additional compartment in which no fuel is present. The compartments, in this report referred to as bays, are subdivided by partitions. Figure 1 shows the Center Wing Tank and the nomenclature of the partitions and bays as used during the investigation by all partners.

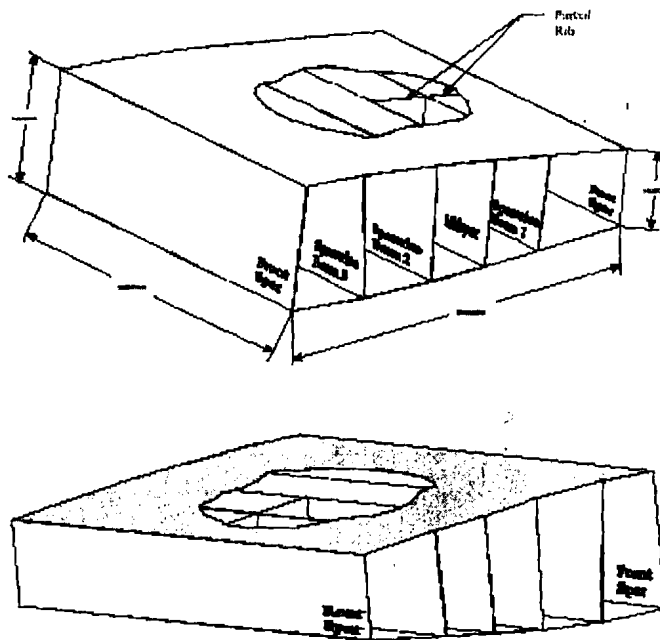


Figure 1a View of the Center Wing Tank as in reality.

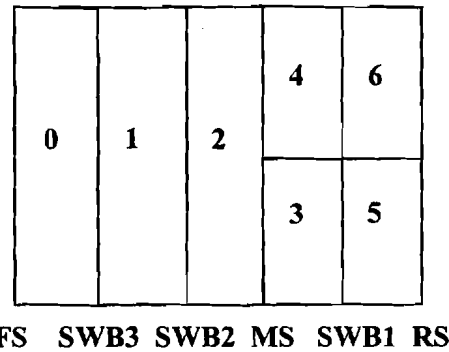


Figure 1b Schematic view of the Center Wing Tank showing nomenclature of bays and partitions.

The partition separating bay 0 (which is a dry bay, i.e. no fuel) from the cargo bay of the aeroplane is known as the Front Spar (FS). Bay 0 is separated from Bay 1 by Spanwise Beam 3 (SWB3). The partition between Bay 1 and Bay 2 is known as Spanwise Beam 2 (SWB2). The Midspar (MS) separates Bay 2 from the next compartment, which is subdivided in two, (Bay 3 and 4) by a partial rib. Similarly, a partial rib subdivides the rear compartment into two bays (Bay 5 and 6). Spanwise Beam 1 (SWB1) and the Rear Spar (RS) represent the boundary walls of these bays.

The bays can communicate via a number of openings in the partitions. There are two main types of openings: passageways, which are open, and access doors, which are closed off by doors. There are passageways in all partitions but the Front Spar and Spanwise Beam 3. Access doors are present in Spanwise Beam 1, Midspar and Spanwise Beam 2.

The reconstruction of the Center Wing Tank revealed that the Front Spar, Spanwise Beam 3 and a manufacturing door in the Midspar had failed early during the total event. The access doors in Spanwise Beam 1 were deformed but had not failed. The main aim of the investigation is to find scenarios explaining this damage.

The tank is connected to the outside atmosphere by two vent stringers. These stringers are approximately 30 m long and also connect Bays 3 and 1 and Bays 6 and 1.



The Center Wing Tank has a wetted volume of 50 m<sup>3</sup> excluding the dry bay. The volumes of the various bays are as follows: Bays 5 and 6: 6.25m<sup>3</sup>, Bays 3 and 4: 5.55 m<sup>3</sup>, Bay 2: 11.1m<sup>3</sup> and Bay 1: 15.4m<sup>3</sup>. The dry bay (Bay 0) has a volume of 15.2m<sup>3</sup>. The dimensions of the tank are:

At front spar:	6.48m wide	At rear spar:	6.48m wide
	1.98m high		1.22m high
Length:	6.15m		

The failure of the various partitions and access doors will depend on the structural details. Thibault (1999) presented pressure differences across each of the partitions needed for failure. These are presented in Table 1 as a range.

**Table 1: Failure pressure of partitions of the Center Wing Tank**

Structural element	Minimum failure pressure (bar)	Maximum failure pressure (bar)
Front Spar	1.4	1.7 - 2.1
SWB3	1.4	1.7
SWB2	1.4	2.1 - 2.4
MS	1.4	2.4 - 2.8
SWB1	1.7	3.1 - 3.5
RS	2.1	3.1 - 3.5

Based upon the observed deformation of the recovered pieces of wreckage, the pressure that the doors in Spanwise Beam 1 experienced are estimated as 3.1 - 3.8 bar and 1.4 - 1.7 bar for the left door and right door respectively. There is no mention of any difference in failure pressure with regard to from which direction these pressure differences are acting on the door.

In order to start an explosion event one needs an ignition source with sufficient energy. The only ignition sources in the tank that have been considered in this study is the Fuel Quantity Indication System consisting of 7 fuel indicator probes and a compensator.

The location of the Fuel Quantity Indication System is shown in Figure 2. Three fuel probes are located in bay 1, the compensator and one fuel probe are located in bay 2, one fuel probe is located in bay 5 and one in bay 6.

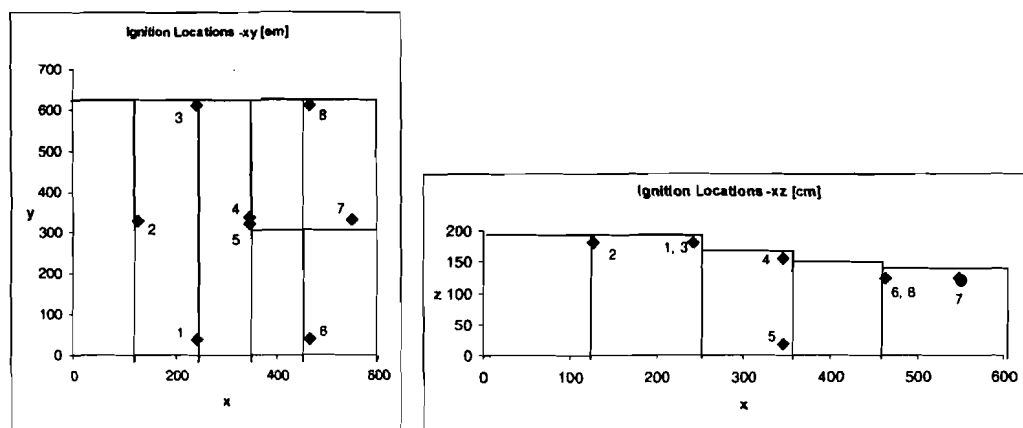


Figure 2 Location of the eight ignition source locations in the Center Wing Tank that were considered in this study. Please note that the shape of the tank has been idealised in this Figure. In the actual tank the upper and lower surfaces are continuous and curved.

## 2.2 Conditions prevailing in Tank

Based on simulation flights it is assumed that the temperature prevailing in the tank at the moment of the explosion was 40 °C to 50 °C. The atmospheric pressure at the height at which the aeroplane exploded (about 4206 m) is 0.585 bar. The Center Wing Tank was almost empty, i.e. there had been no refill of the tank. The amount of liquid fuel present in the tank at the moment of the explosion has been estimated to between 0.2 and 0.4 m<sup>3</sup>. This occupies a small fraction of the tanks' volume so that almost the entire 50 m<sup>3</sup> of the tank can be filled with a fuel vapour-air mixture.

At the time of the accident, relatively little was known about the combustion products of Jet A. An extensive research program was carried out in order to determine properties such as fuel vapour pressure, explosion pressures, and flame speeds. The pressure, temperature, and previous handling of the fuel are all significant factors. The results of this research are given in Shepherd et al., 1997b, and 1999, Lee and Shepherd, 1999 and Nuyt et al., 2000.

### 3. SHORT OVERVIEW OF 1/4-SCALE EXPERIMENTS

An important part of the investigation concerns tests carried out in a 1/4-scale representation of the Center Wing Tank. These tests were used to develop both an understanding of the course of explosions in the fuel tank and a database for validation of the two computer codes involved in the investigation.

#### 3.1 Description of the test facility

A detailed description of the 1/4-scale facility is given by Shepherd et al., 1997a and Shepherd et al., 1998. Hence, only a brief description is given here.

The 1/4-scale facility was chosen to be a rectangular box neglecting the height variation of the real Tank. The dimensions of the 1/4-scale facility are:

Width:	1.5 m
Length:	1.5 m
Height:	0.46 m

The locations of the various partitions were chosen such that the volume of each bay was an exact downscaled volume. The passageways were scaled by area, but their shape was not maintained. Their locations were scaled. The vent stringers were represented as 2.54 cm diameter tubing, connected to the atmosphere through a restricting orifice to simulate the 30 m length of the vent stringer. In some tests also the failure of the partitions was simulated. The mass of the partitions was properly scaled to assure a similar course of failure on 1/4-scale as on full scale. The failure pressures were chosen to be 1.4 bar for Spanwise Beams 2 and 3. The Front Spar was given a failure pressure of 0.48 bar.

Figure 3 shows a drawing of the 1/4-scale test facility with its dimensions and the ignition points used.

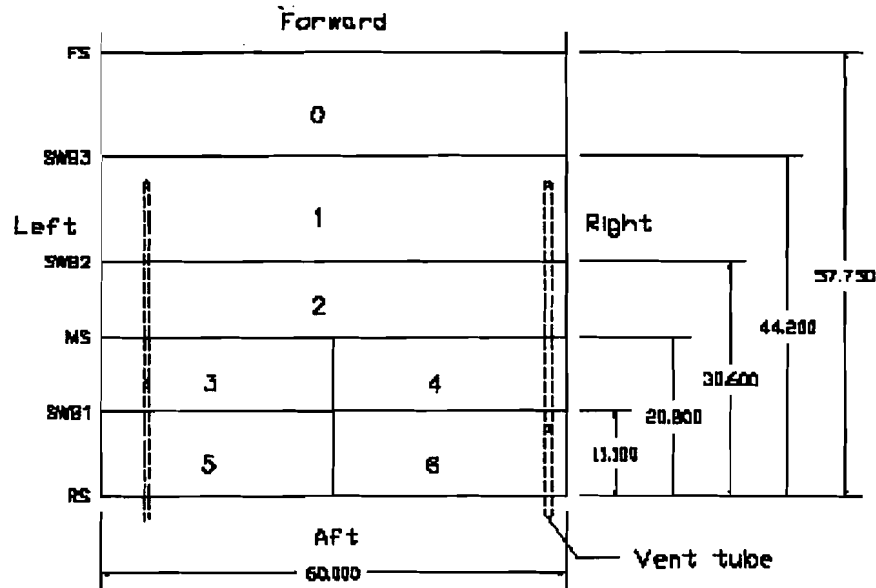


Figure 3 Drawing of the 1/4-scale test facility (Shepherd et al., 1997a)

During the tests several diagnostics were used. These diagnostics have been described in detail in Shepherd et al., 1998.

At a number of positions in the various bays, pressure measurements were carried out. For some of the experiments where failure of the Front Spar occurs, blast wave strengths were measured as well. Thermocouples were used to measure the flame time of arrival at two locations in each bay. Flame propagation was also recorded using high-speed and video cameras. Motion of the partitions in case of failure was monitored using the high-speed and video cameras and switches detecting loss of electrical contact in case of failure.

### 3.2 Fuel

In the first 30 tests in the 1/4-scale facility, the test fixture temperature was not controlled. For this reason, Jet A could not be used as the fuel and a mixture of gases was developed at the California Institute of Technology to simulate combustion speed and pressure rise of Jet A vapour. The simulant fuel was adjusted so that the maximum overpressure obtained with a starting pressure appropriate to

the Denver (location of test site) ambient pressure (0.83 bar) was the same as the Jet A vapour maximum overpressure starting from the explosion altitude pressure of 0.585 bar.

Closed vessel explosions (carried out in the so-called Hyjet facility (Shepherd et al., 1997a and Shepherd et al., 1998) were used to find a mixture that could have both properties. In this way one arrived at a mixture consisting of 7% v/v hydrogen and 1.4% v/v propane.

As also pointed out by Shepherd et al. (1997a) the mixture choice does not account for flame quenching phenomena which could occur at the passageways. A reduction of scale would possibly enhance the possibility of quenching. The turbulence generated at the edges of the passageways during an explosion event may be so strong that a flame entering such a highly turbulent region is quenched. This may have effects on the entire explosion event.

Another problem that has to be considered when choosing an alternative fuel for practical reasons is flame instabilities. Hydrodynamic flame instabilities can arise on the flame surface area when the flame has propagated over a certain distance after ignition. The hydrodynamic flame instabilities appear as a cellular structure on the flame surface (often referred to as a cauliflower structure). The cellular structure could be enhanced or counteracted if chemical diffusive processes start playing a role. The latter depends on the fuel concentration and appears when there is a difference between diffusion rates of reactants involved (e.g. oxygen and propane). The cellular structure causes an increase of the combustion rate depending on the distance from the point of ignition. The choice of a fuel-air mixture representing this effect correctly as well will complicate the choice of the fuel even more. The choice of the above mentioned hydrogen-propane mixture does not take the effect of flame instabilities into account either.

During the later phases of the investigation (Brown et al., 1999, Shepherd et al., 2000) tests were performed with Jet A liquid and vapour. To avoid the aforementioned problems with condensation, non-homogeneity and possibly poor repeatability the rig was heated and put into an insulated building which could be heated up to 60 °C. Temperature control of the building would assure an even temperature distribution in the 1/4-scale rig.

### **3.3 Experimental programme**

A summary of the tests that were performed is shown below. In most of these tests the afore-mentioned hydrogen-propane mixture was used but in some tests a leaner mixture was used. Moreover several tests were performed where apart from the aforementioned mixture also a layer of liquid Jet-A was present.

#### **Alpha-tests (test nos. 1-3, 9-12)**

Few or no partitions, partitions are not allowed to fail, no ignition point variation (ignition point 5 is used, see Figure 3), no venting through stringers to outside.

#### **Beta-tests (test nos. 4-8, 15-16)**

All partitions are present, no failing of partitions, ignition point variation, venting through stringers to the outside, in 1 test liquid fuel was present (test 8).

#### **Gamma-tests (test nos. 13-14, 17-29)**

In most tests all partitions are present and can fail or a part of them can fail (in most of these latter cases only SWB3, FS and the manufacturing door in SWB2 can fail), ignition point variation, venting through stringers to the outside (with exception of test 25), in many tests liquid fuel was present.

#### **Delta-test (test no. 30)**

In this single test the test facility was coupled to a structure simulating the cargo bay next to bay 0. The SWB3, FS and the manufacturing door in SWB2 were allowed to fail, a layer of liquid was present in the facility, venting through the stringers was possible, ignition was effected in bay 5.

#### **Replica-tests (test nos. 31, 31a, 31b, 32-34, 34a, 35, 35a, 35b, 36, 39)**

The tests were performed to investigate the repeatability of the tests. All partitions were present and were not allowed to fail, ignition source position was varied, no liquid, venting through stringers.

All other tests were performed with Jet A (supplied by Arco<sup>1</sup> unless otherwise stated). The initial pressure during these tests was always 0.585 bar.

---

<sup>1</sup> The flash point of the Arco fuel is 46 °C.

**Jet A-Demo tests (test nos. 40 and 42)**

Two tests were performed with Jet A ignited at position 2L, all partitions were present and not allowed to fail, vent through stringers. One test was performed at an initial temperature of 40 °C and one at 50 °C.

**Jet A-40 tests (test nos. 44, 46 and 48)**

Three tests were performed at an initial temperature of 40 °C varying the point of ignition. All partitions are present and strong, venting through stringer.

**Jet A-50 tests (test nos. 51, 53 and 55)**

Three tests were performed at an initial temperature of 50 °C varying the point of ignition. All partitions are present and strong, venting through stringer.

**Jet A-45 test (test no. 58)**

One test was performed at an initial temperature of 45 °C. Ignition was effected at 2L. All partitions are present and strong, venting through stringer.

**Quenching tests (test nos. 61-66)**

In some of the Jet-A tests mentioned above flame quenching occurred, i.e. the flame did not propagate through the openings present in the partitions. This feature was investigated in two-bay tests, i.e. tests where the flame was allowed to propagate from 1 bay into another through a partition containing only 1 hole. The hole size was varied (holes of 5.08 cm diameter and slit of 0.635 cm x 2.54 cm). All tests were performed at 50 °C and repeated once. In addition to the quenching tests, 2 tests were performed in a single bay to determine the reactivity of the flammable mixture and to study heat transfer to the walls of the facility for Jet A at 50 °C.

**Alternate fuel tests (test nos. 67 and 68)**

Two tests were performed with another Jet-A type. All partitions present and strong, ignition at 2L, initial temperature 50 °C, venting through stringers.

**Part strong tests (test nos. 69 and 70)**

Two tests were performed at 40 °C with all partitions present and SWB3, FS and manufacturing door in SWB2 allowed to fail. Ignition was effected at 2L, vent stringers are open.

**Jet A flame speed tests (test nos. 71-73)**



Tests were performed in a single bay to determine the reactivity of two types of Jet A fuel (ref. Arco and Denver<sup>2</sup>) at 40 °C initial temperature.

**Jet A Quenching tests (test nos. 74-79)**

Two-bay tests were performed to determine when quenching occurs in case of flame propagation through a single hole. Variations involve initial temperature (40 °C and 50 °C) and hole size and shape. All tests were performed with Jet A supplied by Arco.

The test programme and results are described in Shepherd et al., 1998, Brown et al., 1999 and Shepherd et al., 2000. Some results are presented in the present report when comparing to results of simulations performed with the FLACS code.

---

<sup>2</sup> The flashpoint of the Denver fuel is 54 °C.

#### 4. DESCRIPTION OF THE FLACS CODE

The production and processing of high-pressure natural gas on offshore platforms implies an inherent explosion hazard on these facilities. The acknowledgement of this hazard kicked-off a twenty-year and still continuing research programme at Christian Michelsen Research in Norway. The most important outcome of this research has been a 3-D CFD prediction tool named FLACS (FLame ACceleration Simulator) (Hjertager, 1982, Van Wingerden et al., 1993). The first version of this tool was released in 1986. Since then versions were released in 1989, 1993, 1994, 1995, 1996, 1997 and 1998. The code allows for describing release and dispersion processes involving gaseous substances and in case of successful ignition the subsequent explosion. The code has especially been developed to describe the flame propagation processes in congested environments that can be found on chemical plants and petro-chemical installations including offshore facilities. The development of the code including experimental work supporting the development and used for validation of the tool has cost approximately 27 million US\$ up till now.

FLACS is a CFD-code (CFD = Computational Fluid Dynamics) solving a set of mathematical equations describing compressible fluid flow, turbulence and combustion processes. The equations are based on conservation principles and involve the following quantities:

- Mass
- Momentum
- Enthalpy
- Mass fraction of fuel
- Mixture fraction
- Turbulent kinetic energy
- Dissipation rate of turbulent kinetic energy

Before performing calculations the calculation domain is subdivided in many grid cells. The equations are solved in each cell. As both release, dispersion and explosion events are transient phenomena the equations also have to be solved in time, i.e. the total event is subdivided in small time steps where the equations are solved in each grid cell for each time step. For large calculation domains computational resources still put restrictions on the spatial and temporal resolution used during calculations. This, especially for applications where FLACS is used,

often implies that certain details cannot be resolved on the grid. In order to account for these details FLACS has in-built subgrid models.

One example of subgrid models is the geometry representation. The influence of equipment present in a petro-chemical installation (see Figure 4) is very strong and a good representation of this equipment is of paramount importance to be able to predict accurately what the outcome of an explosion will be. In most situations it will not be possible to represent the smaller obstacles on the grid and these have to be treated by proper subgrid models.

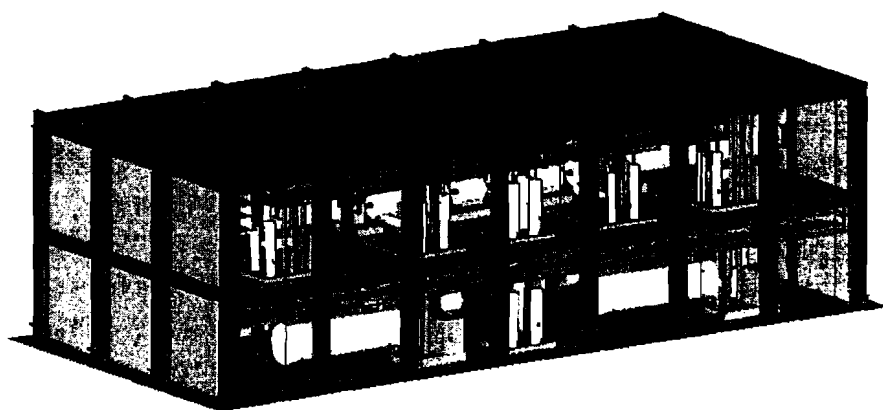


Figure 4 Example of offshore geometry as represented in FLACS.

To build geometries (as the one in Figure 4) every element inside the geometry is represented by two types of objects, viz. boxes and cylinders. Boxes have a location, dimensions ( $L_x$ ,  $L_y$ ,  $L_z$ ) and area porosities. Cylinders have a location, a diameter, a length, a direction and porosities. If all specified sizes are bigger than zero a volume porosity has to be specified in addition. The characteristic length of the object is used for specification of the length scale of the turbulence in the wake of the object. Thus, the geometry is represented on the numerical grid, with area porosities on the grid cell faces and volume porosity in the grid cells. Representation of subgrid geometry (objects which are smaller than the grid in at least one direction inside a grid cell) is done by subgrid turbulence generation factors, a typical diameter, flame folding factors and drag factors.

## 4.1 Governing equations

The governing equations used in FLACS are presented below.

**The equation of state is that of an ideal gas:**

$$PW = \rho RT$$

**Conservation of mass:**

$$\partial/\partial t(\beta_v \rho) + \partial/\partial x_j(\beta_j \rho u_j) = \dot{m}/V$$

**Conservation of momentum:**

$$\partial/\partial t(\beta_v \rho u_i) + \partial/\partial x_j(\beta_j \rho u_j u_i) = -\beta_v \partial p / \partial x_i + \partial/\partial x_j(\beta_j \sigma_{ij}) + R_i + R_W + (\rho - \rho_0)g_i$$

where  $R_i$  represents distributed resistance in  $i$ -direction due to subgrid obstruction:

$$R_i = -f_i A_i \rho |u_i| u_i$$

$$A_i = (1 - \beta_i) / \Delta x_i$$

$f_i$  = non-dimensional constant depending on type and orientation of obstruction

**Conservation of enthalpy  $h$ :**

$$\partial/\partial t(\beta_v \rho h) + \partial/\partial x_j(\beta_j \rho u_j h) = \partial/\partial x_j(\beta_j \mu_{eff} / \sigma_h \cdot \partial h / \partial x_j) + \beta_v Dp/Dt + Q$$

**Conservation of mass fraction of a chemical specie  $Y$ :**

$$\partial/\partial t(\beta_v \rho Y) + \partial/\partial x_j(\beta_j \rho u_j Y) = \partial/\partial x_j(\beta_j \mu_{eff} / \sigma_m \cdot \partial Y / \partial x_j) + R_m$$

**Conservation of mixture fraction  $f$ :**

$$\partial/\partial t(\beta_v \rho f) + \partial/\partial x_j(\beta_j \rho u_j f) = \partial/\partial x_j(\beta_j \mu_{eff} / \sigma_f \cdot \partial f / \partial x_j)$$

**Conservation of turbulent kinetic energy  $k$ :**

$$\partial/\partial t(\beta_v \rho k) + \partial/\partial x_j(\beta_j \rho u_j k) = \partial/\partial x_j(\beta_j \mu_{eff} / \sigma_k \cdot \partial k / \partial x_j) + P_k - \beta_v \rho \epsilon$$

**Conservation of dissipation rate of turbulent kinetic energy  $\epsilon$ :**

$$\partial/\partial t(\beta_v \rho \epsilon) + \partial/\partial x_j(\beta_j \rho u_j \epsilon) = \partial/\partial x_j(\beta_j \mu_{eff}/\sigma_\epsilon \partial \epsilon/\partial x_j) + P_\epsilon - C_2 \beta_v \rho \epsilon^2/\kappa$$

**4.2 Equilibrium chemistry thermodynamics**

In order to predict explosion overpressures correctly accurate thermodynamic data have to be used. In FLACS the thermodynamic data assume formation of H<sub>2</sub>O, CO, H<sub>2</sub>, O<sub>2</sub>, OH and CO<sub>2</sub> as products for burning of hydrocarbon fuels. The mass fraction in the products of each of these compounds is calculated from equilibrium constants, which are depending on and calculated from the equivalence ratio of the reactants.

The specific heat and enthalpy of formation as a function of temperature have been curve fitted with a second order polynomial for several reactants and products using data from the Chemkin data base (Kee et al., 1987). The temperature of the mixture can then be calculated from the mass fraction of each component in the mixture.

A comparison of temperature of combustion products and maximum explosion pressure in closed vessels calculated by FLACS and the so-called ThermoChemical Calculator (Goodwin) from Sandia gives for pure hydrocarbon fuels an agreement within 1 %, which is acceptable (Renoult, 1999).

**4.3 Turbulence modelling**

FLACS uses a so-called *k-ε* model to describe convection, diffusion, production and dissipation of turbulence during a release, dispersion and explosion. The model includes the two aforementioned conservation equations for generation and dissipation of turbulent kinetic energy. The Boussinesq eddy viscosity model models the turbulent viscosity:

$$\mu_t = c_\mu \rho (k^2/\epsilon)$$

The effective viscosity is set equal to the sum of the laminar and turbulent viscosity:

$$\mu_{\text{eff}} = \mu + \mu_t$$

The compressible Reynolds stresses in the  $k$ - $\epsilon$  model used in FLACS are modelled as the rate of strain through the eddy-viscosity concept.

Constants in the  $k$ - $\epsilon$  model have been chosen fixed although they vary for wake flow, recirculating flow and jets.

The application of the  $k$ - $\epsilon$  model for explosion problems is not straightforward. The model was developed for steady flow in pipes and not for transient reactive flow. As an example it can be mentioned that an analysis of transient flow fields with the  $k$ - $\epsilon$  model gave turbulence build-up times, which strongly depended on the initial conditions chosen and the grid resolution. In FLACS this was solved by introducing a large enough minimum value of turbulence production.

A subgrid model in FLACS represents flow at a wall (boundary layers). The model assures an increase in both turbulent energy and length scale proportional to flow distance (boundary layer thickness) as seen in experiments.

Turbulence generated at obstructions that are resolved by the grid is calculated directly by the  $k$ - $\epsilon$  model. Turbulence generated at obstructions not resolved by the grid is treated as follows. The turbulent kinetic energy is expressed as a function (fraction) of the shape of the obstruction (drag coefficient), the area they block of a grid cell and the flow speed (squared). The turbulence dissipation can be calculated from the turbulence length scale (a fraction of the obstacle dimension) and the turbulent kinetic energy. The models, for representation of both ongrid and subgrid obstructions have been validated extensively against results of experiments performed with obstructions in both steady and transient flows (Arntzen, 1998).

#### 4.4 Combustion modelling

The purpose of a combustion model for premixed combustion is to localise the reaction zone and convert reactants to products at a rate similar to that a real flame would do in an explosion. To model turbulent combustion processes mixing controlled type of combustion models of the eddy break-up type are often used. In FLACS a different approach is chosen. The mixing control implies a flame thickness

at a maximum equal to the integral turbulence length scale. To resolve the flame the size of the grid that is used should be smaller than the integral length scale (which for the usual applications for FLACS implies a flame thickness of the order of 10 % of the obstruction dimensions (i.e. typically 10 % of 5-50 cm)). This puts a strong restriction to the application of this type of models. Another restriction is that the model only can be used for turbulent flames and not for laminar flames, where turbulent mixing does not play a role. In FLACS the combustion model is divided in a separate flame model and a burning velocity model. The flame model allows for implementing a specified burning velocity into the CFD-code (laminar flame and turbulent flame). FLACS can use two flame models: the  $\beta$ -flame model and the so-called SIF-model.

The  $\beta$ -model introduces a new co-ordinate system for the flame through a so-called  $\beta$ -transformation allowing for using more than one grid cell (three grid cells) for representing the flame. This flame model uses correction functions concerning flame thickness due to numerical diffusion, flame curvature and burning towards walls.

The obvious disadvantage of the  $\beta$ -flame model is the flame thickness. Therefore an alternative flame model was developed: the SIF model (Simple Interface Flame model). Here the flame is represented as an interface between products and reactants (Arntzen, 1998). As for the  $\beta$ -flame model a separate burning velocity model determines the propagation speed of the flame.

The burning velocity model consists of several parts:

- Laminar burning velocity model
- Quasi-laminar burning velocity model
- Turbulent burning velocity model

During the initial stages of flame propagation the flame will propagate with a velocity known as laminar burning velocity  $S_L$ . In FLACS normally experimentally determined values are used (e.g. from Gibbs and Calcote, 1959), also as a function of equivalence ratio.

A mixing rule has been developed for estimation of the burning velocity of mixtures of fuels. This rule is based on the energy released for each of the fuel components.

Little is known on the effect of temperature and pressure on laminar burning velocities. In FLACS a relationship is used which is also often used in literature:

$$S_L = S_{L0}(T/T_0)^\alpha(P/P_0)^\beta$$

The coefficients  $\alpha$  and  $\beta$  are fuel dependent. In FLACS data from Metghalchi and Keck (1980) is used: for methane  $\alpha=2.0$  and  $\beta=-0.5$ ; for ethylene and propane  $\alpha=2.13$  and  $\beta=-0.17$ . Due to lack of data the latter values are used for all other fuels over the entire range of concentrations. This is obvious a huge simplification but proves to be acceptable as a first estimate. The above reported values have not been corrected for effect of flame stretch during especially the early stages of flame propagation neither for cellular flame instabilities, which are pressure dependent, during later stages of flame propagation.

Chemical kinetic, diffusive-thermal and hydrodynamic flame instabilities cause an increase of the flame surface area and as such an increase of the laminar burning velocity. The instabilities appear very early during flame propagation and start affecting the flame speed almost immediately after ignition. Due to the coarse grid that is used in FLACS simulations and because of the representation of the flame (too thick, at least when using the  $\beta$ -flame model) an enhancement factor has been introduced to describe the effect of flame instabilities on laminar flame speeds. Based on experiments performed at Christian Michelsen Research in a large tent (for various fuels and fuel mixtures) and by others (such as by Lind and Whitson (1977) in hemispherical balloons) the following model has been introduced:

$$S_{QL} = S_L(1 + aR)^{1/2}$$

where  $R$  is the distance the flame travelled after ignition and  $a$  is a constant depending on the fuel.

Flame instabilities occurring inside chambers such as acoustically driven flame instabilities (Markstein, 1964) are not taken into account.

Turbulence in the reactants may increase the combustion rate considerably. This may be due to distortion of the flame surface increasing its area, due to increase of the rate of transport of heat and active species and by mixing of reactants and products. For very high turbulent strain rate the combustion rate may decrease and even cause quenching of the flame.



Many investigators have measured turbulent burning velocities over a wide range of turbulence intensities and integral length scales. Bradley and collaborators have been collecting and evaluating such data. Figure 5 shows a representation of the data. The turbulent burning velocity has been plotted as a function of the turbulence intensity, and made non-dimensional using the laminar burning velocity.

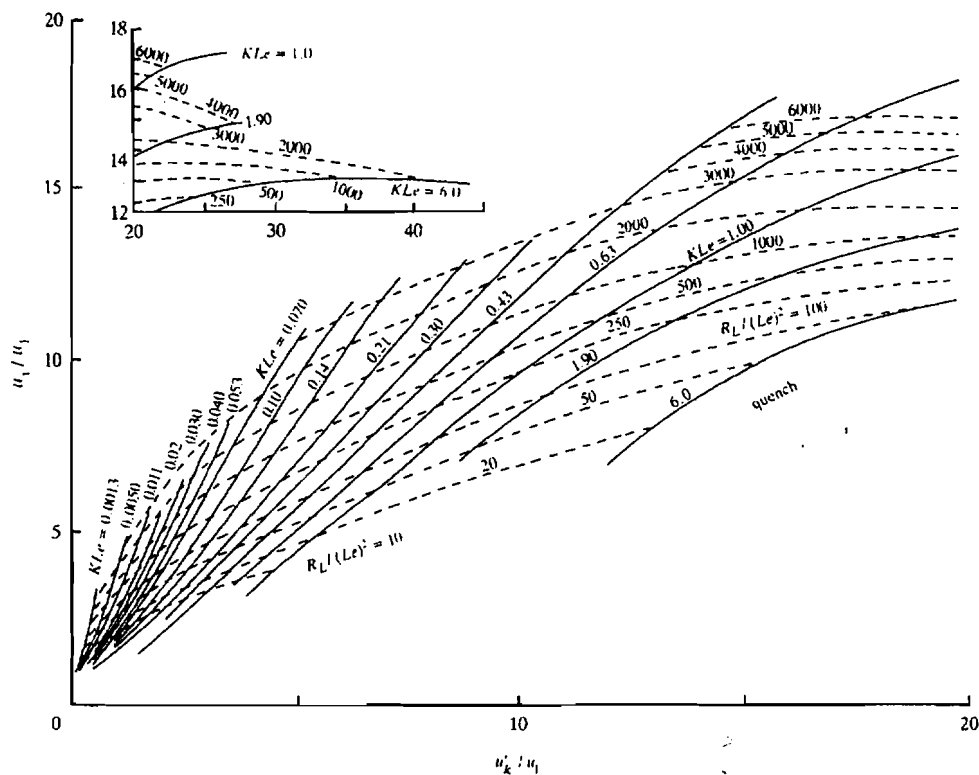


Figure 5 Correlation of turbulent burning velocities as presented by Bradley et al. (1992)

From the correlation developed by Bradley and collaborators relationships have been developed allowing for using the data in a model such as FLACS. In FLACS the following relationships are used:

$$S_{T1} = 1.8 S_L^{0.784} u'^{0.412} I_L^{0.196} v^{-0.196}$$

$$S_{T2} = 0.96 S_L^{0.284} u'^{0.912} I_L^{0.196} v^{-0.196} + S_L$$

$$S_T = \min(S_{T1}, S_{T2})$$

Quenching is not modelled in FLACS. Beyond a certain strain rate (expressed by the Karlovitz number  $K$  (ratio of flow strain rate and flame gradient, which can be expressed by ratio of reaction time scale ( $\delta/S_L$ ) and turbulence time scale (Taylor time scale:  $u'/\lambda$ )) the turbulent burning velocity is assumed to remain constant for increasing turbulence intensity  $u'$ . In reality the turbulent burning velocity would decrease beyond the aforementioned strain rate and turbulence time scale and eventually the flame would quench.

The effect of pressure on turbulent burning velocities (which can be as high as a 30 % increase when increasing from 1 to 5 bar absolute pressure, Kobayashi et al., 1996) has not been taken into account in the combustion model but is probably compensated for by the absence of quenching for very turbulent flames in FLACS.

Presence of obstructions will in addition to turbulence cause flow gradients and as a result of that folding of the flame around these obstructions. The flow gradients and therefore flame folding around obstructions resolved by the computational grid will be described by FLACS but flame folding around subgrid obstructions will not be described. Therefore an additional subgrid model has been included to take this feature into account.

#### 4.5 Other models in FLACS

FLACS contains several other models including a model describing blast waves propagating away from the explosion and a model describing the effect of water spray on gas explosions.

A feature that is used in the present investigation is the possibility of describing failing walls. The failure can be described as a "pop-out panel" or alternatively as a hinged panel. In the first alternative the wall moves away from its original position with its face parallel to the way it was mounted. In the second alternative the wall stays fixed at one of its sides and rotates around this side. The wall is defined with a failure pressure, a weight and dimensions. The movement of the wall is described analytically based on the weight of the panel and the local static and dynamic pressure. In FLACS the movement is translated into an increasing porosity of the relevant wall.

## 4.6 Validation

Each version of FLACS that is issued is validated thoroughly (see e.g. Van Wingerden et al., 1995). This involves both the sub-models of FLACS as well as the model as a whole. The full model is tested against both lab scale, medium scale and full scale experiments. For explosions data is available from experiments performed in experimental set-ups ranging from 0.170 m<sup>3</sup> to 2688 m<sup>3</sup>. These set-ups were generally speaking all vented enclosures with varying levels of congestion inside.

A general description of the way FLACS is validated is presented below:

1. Testing of submodels: turbulence models, flame models, burning velocity models and flame folding models. An example is the testing of the ability of the flame to propagate according to the specified burning velocity in 1D, 2D and 3D.
2. Study of the effect of grid resolution for subgrid models to assure a code with limited grid dependency.
3. Validation of explosion models for free flames propagating from a point: testing of ignition and quasi-laminar burning velocity models. Comparison with experiments.
4. Validation against experiments performed in empty vented enclosures.
5. Validation against experiments where obstructions can be resolved ongrid.
6. Validation against experiments where obstructions have to be represented subgrid.
7. Validation against experiments in medium-scale realistic geometries (50-550 m<sup>3</sup>).
8. Validation against experiments in full-scale realistic geometries (1638-2688 m<sup>3</sup>).

Examples of how FLACS predicted the maximum local pressures found during tests performed in various medium-scale and full-scale tests is shown in Figures 6 and 7.

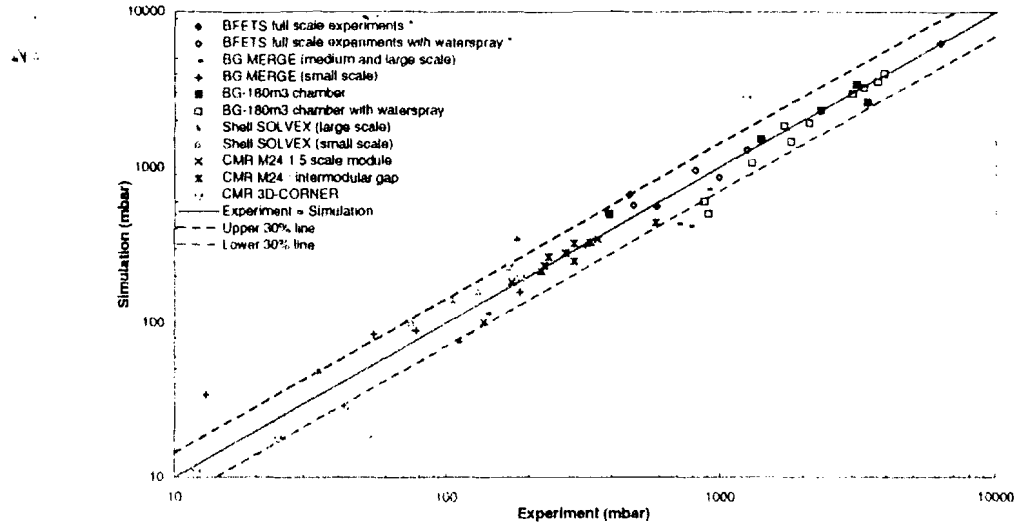


Figure 6 Prediction of peak pressures compared to those observed in medium-scale explosion experiments.

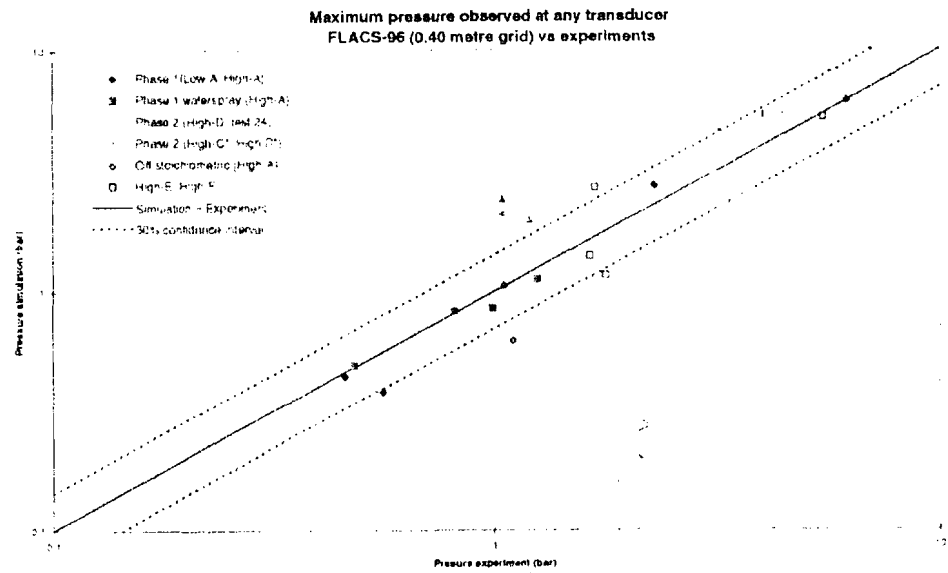


Figure 7 Prediction of peak pressures compared to those observed in full-scale explosion experiments.

## 5. MODEL IMPROVEMENTS

As FLACS was developed for slightly different applications than predicting the course of multi-compartment explosions such as for the present investigation the code needed a few improvements. These improvements involved the inclusion of a description of flame propagation through holes, inclusion of a model for radiative heat transfer and a model predicting quenching conditions during flame propagation through holes. In addition to that the code needed to be validated for the propane-hydrogen mixture that was used in the initial 1/4-scale experiments and an appropriate stand-in fuel-air mixture had to be found for the Jet-A mixtures at 40 °C and 50 °C.

### 5.1 Representation of flammable mixtures used in 1/4-scale experiments

#### 5.1.1 Hydrogen-propane mixture

The 1/4-scale experiments were initially performed with a mixture of 1.4 % v/v propane, 7 % v/v hydrogen and 91.6 % v/v air. The mixture was chosen on the basis of the fact that this mixture would result in maximum explosion overpressures in a closed vessel typical for Jet A at an initial temperature of 50 °C and an initial pressure of 0.585 bar but for an initial pressure as prevailing at the Denver test site, i.e. 0.83 bar. Moreover the rate of pressure rise was more or less similar (Shepherd et al., 1997a).

Comparative simulations were performed to see whether the models in FLACS reproduced the properties of this mixture satisfactory or that upgrades were necessary.

Tests performed by Shepherd et al. (1997a) in their Hyjet facility were simulated. Figure 8 shows a sketch of the Hyjet facility. The facility as used in the relevant investigations consists of a 0.86-m internal diameter cylinder closed by semi-elliptical heads, with a length of approximately 1.6 m (64 in) between head seams and a volume of 1.18 m<sup>3</sup>. The vessel is of heavy construction, rated to withstand internal pressures of up to 70 bar. The vessel is equipped with electrical heaters and digital controllers that enable the temperature of the receiver to be adjusted between

room temperature and about 100 °C. The vessel is also equipped with a driver which was closed during these very experiments.

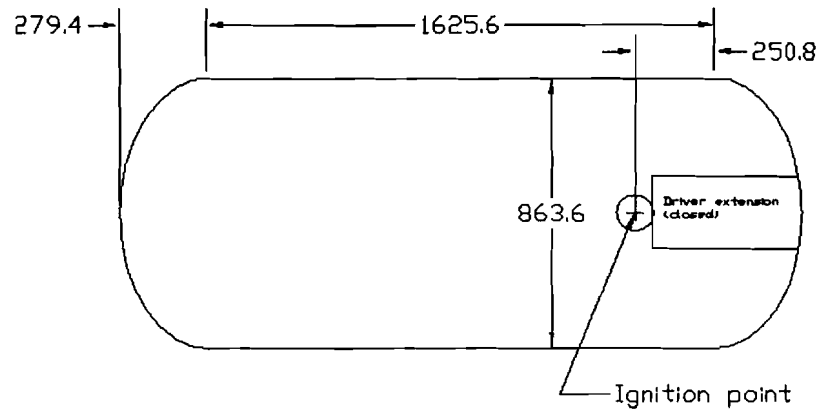


Figure 8 Hyjet facility of California Institute of Technology used by Shepherd et al. (1997 a and b).

The results of the simulation are compared to the results of an experiment in Figure 9 as two pressure-time histories. The Figure shows that the agreement is reasonable. The pressure in the experiments starts rising earlier than in the simulation but the subsequent rate of pressure rise is slightly lower. The flames seem to reach the wall more or less simultaneously as can be seen from the moment a drop in the rate of pressure rise occurs. The pressure in the experiment then increases considerably faster than in the experiment potentially caused by an acoustically driven flame instability witnessed by the oscillations superposed on the pressure-time history. The effect of such an instability cannot be modelled in the FLACS code. The maximum overpressure is overpredicted by 0.3 bar.

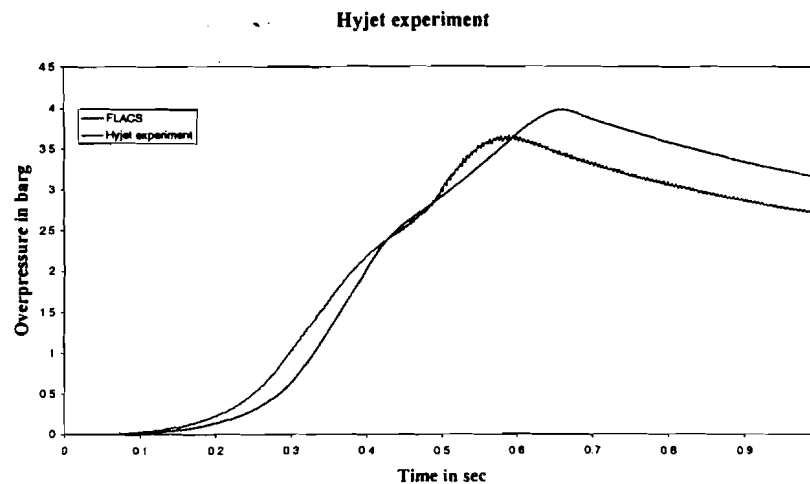


Figure 9 Comparison of FLACS simulation and experiment for a 1.4 % v/v propane, 7 % v/v hydrogen, 91.6 % v/v air mixture in the California Institute of Technology Hyjet test facility (test 484; initial pressure 0.83 bar).

A single bay experiment carried out in the 1/4-scale facility was also simulated. The results are shown in Figure 10. In Figure 10a the results of a direct simulation are shown whereas in Figure 10b the mixture used in the experiment was represented by a slightly richer mixture (ER=0.56 instead of ER=0.55). These two simulations show that representing the results with a slightly richer mixture gives a better agreement. The simulation highlights that small deviations in the mixture composition used during the experiments can give rise to quite some variation of the mixture reactivity. Note that also in the single bay 1/4-scale experiment an acoustically driven flame instability appears affecting the pressure-time history during the final phases of the event.

On the basis of these results it was decided to continue with the representation of the 1.4 % v/v propane, 7 % v/v hydrogen mixture in air as represented by FLACS. No changes were made to the code in spite of the small deviations seen between the simulations and experiments.

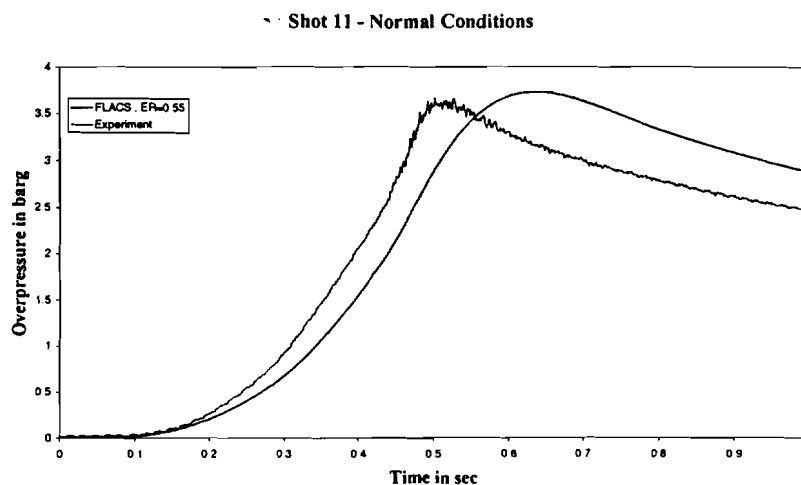


Figure 10a Comparison of FLACS simulation and experiment for a 1.4 % v/v propane, 7 % v/v hydrogen, 91.6 % v/v air mixture (ER=0.55) in a single bay 1/4-scale experimental set-up (Test no. 11, initial pressure 0.83 bar).

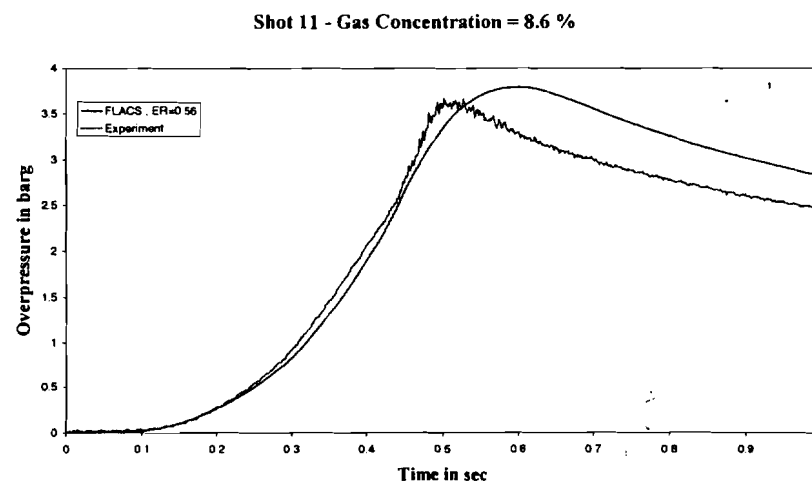


Figure 10b Comparison of FLACS simulation and experiment for a 1.4 % v/v propane, 7 % v/v hydrogen, 91.6 % v/v air mixture in a single bay 1/4-scale experimental set-up.. In the simulation a mixture of 1.43 % v/v propane, 7.17 % v/v hydrogen, 91.4 % v/v air mixture (ER=0.56) was used instead (Test no. 11, initial pressure 0.83 bar).

### 5.1.2 Jet-A mixtures

Jet A consists of over one hundred distinct hydrocarbon molecules and there are no reliable models available for predicting the burning speed or such a complex mixture. As an alternative, a single hydrocarbon fuel was chosen that had burning speeds and expansion ratios similar to those measured in laboratory tests with Jet A. Hence, Jet-A was represented with the heaviest standard alkane in FLACS, viz. n-



butane. Bearing in mind the initial pressure of 0.585 bar it was found that the 50 °C Jet-A mixture (Arco-type) could be represented relatively well with a ER=0.79 butane-air mixture (2.49 % v/v butane in butane-air mixture) at an initial temperature of 50 °C. The burning velocity of this mixture is 43 cm/s. Figure 11 shows the results of a test performed in a ¼-scale single bay geometry (test 61) compared to simulations for two different butane-air mixtures (ER=0.79 and ER=0.75). The Figure shows that the reactivity of an ER=0.79 mixture agrees very well with that of the Jet-A mixture but the maximum overpressure is slightly underestimated (by 0.26 bar).

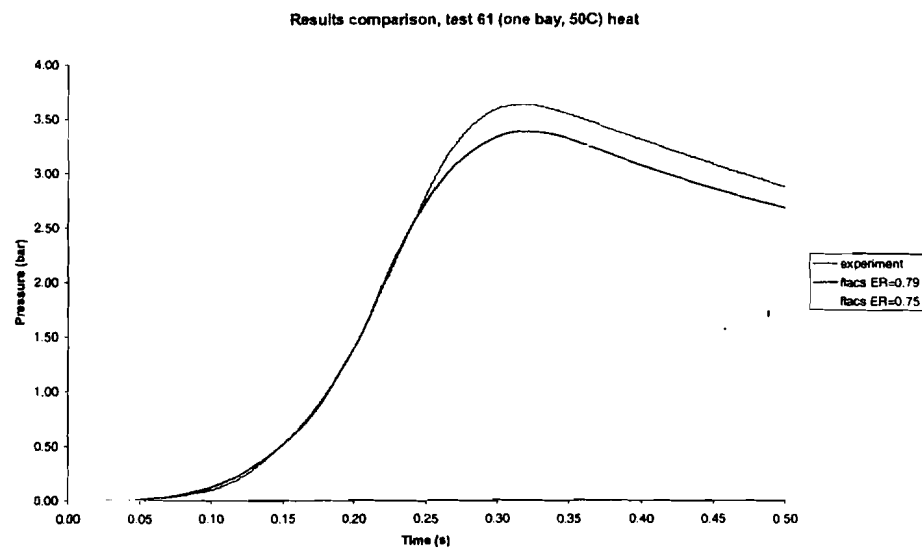


Figure 11 Comparison of measured (test 61) and simulated pressure time histories of an explosion of Jet-A, initial temperature 50 °C in a ¼-scale single bay geometry. The simulations concern butane-air mixtures, initial temperature 50 °C, ER=0.79 and ER=0.75.

Similarly it was found that a 40 °C mixture could be represented using a mixture of butane-air ER=0.62 (1.96 % v/v butane in butane-air mixture) at 40 °C. This mixture has a laminar burning velocity of 21.6 cm/s. A comparison of the simulation results for this mixture with the 40 °C Jet-A mixture in a ¼-scale single bay geometry is shown in Figure 12. A mixture slightly more reactive than seen in the experiments was chosen for the simulations (Shepherd et al., 2000). The graph also contains a simulation with a mixture of butane-air ER=0.55 which is clearly less reactive than seen in the experiments.

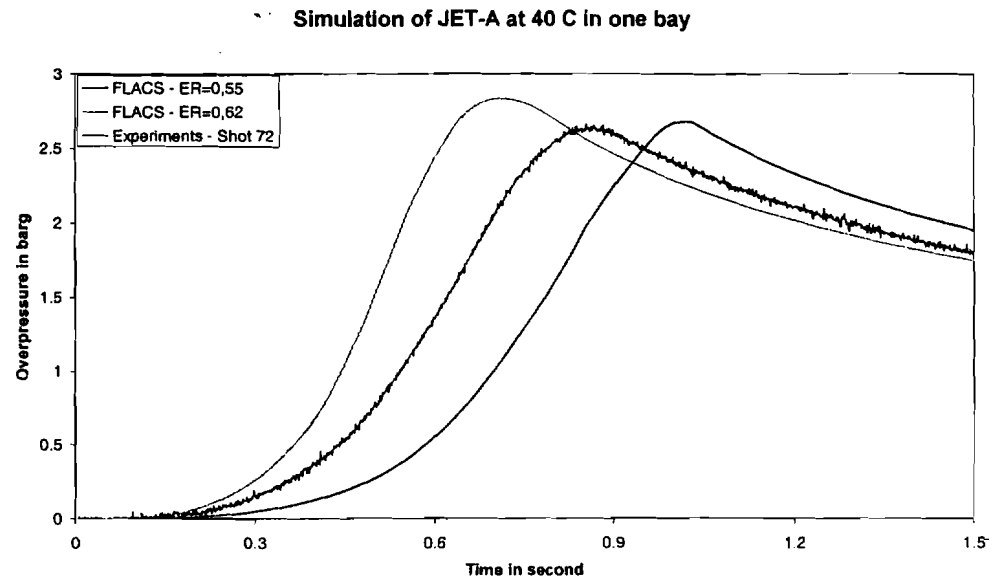


Figure 12 Comparison of measured (test 72) and simulated pressure time histories of an explosion of Jet-A, initial temperature 40 °C in a ¼-scale single bay geometry. The simulations concern butane-air mixtures, initial temperature 40 °C, ER=0.62 and ER=0.55.

## 5.2 Flame propagation through holes

As mentioned above FLACS has been developed for description of dispersion and explosion in congested petrochemical installations. As such FLACS has been designed to describe the turbulence generated by the shear layers in the wake of a cylinder but not for predicting shear layers in a jet, as relevant for the present study. Nevertheless the original version of FLACS has been used as a first alternative for representing holes. In this way holes smaller than a grid cell will be represented as porosity. The shear layer will be developed at the edges of the holes or at the edges of the porous area.

The second alternative that was considered was the inclusion of a special jet model. A jet is positioned at the location of the opening. The jet velocity is driven by the pressure difference across the opening. The relative turbulence intensity was set to 20 % of the main jet velocity and the length scale of the turbulence was chosen to be to 10% of the opening diameter.

Both representations do not allow for supersonic flow. FLACS has an inbuilt restriction of flow through holes allowing for a maximum flow velocity equal to the local speed of sound.

To investigate which of these two representations should be chosen for the full investigation comparisons were made to special experiments performed in the 1/4-scale rig. The experiments involve a two-bay 1/4-scale facility with the Midspar as only partition. Ignition was effected in the centre of one of the two remaining bays. In test 12 a single hole was introduced into the Midspar. Figure 12 shows a plot of the measured pressure difference across the Midspar compared to the pressure difference simulated using the two aforementioned ways of opening representation. "Geometrical" hole refers to the use of the original FLACS-code, whereas "Jet" hole refers to the new subgrid model. The two type of simulations give more or less the same result but the agreement between experiment and simulations is not very good especially regarding the timing. The maximum pressure difference across the Midspar was overpredicted by 0.2 to 0.25 bar respectively for the two alternative ways of opening representation.

Shot12 - Differential Pressure - Comparison "Geometrical" & "Jet" Hole

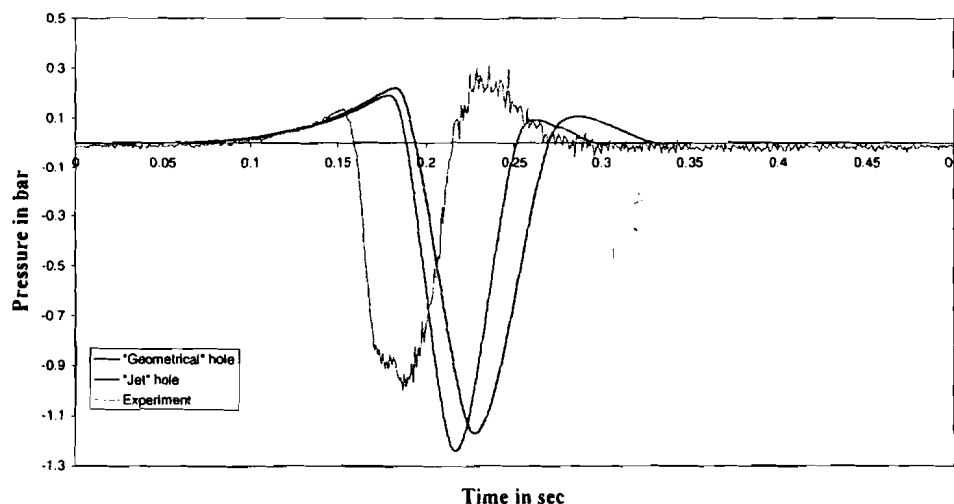


Figure 12 Comparison of pressure difference across single partition with single hole developed during a two-bay 1/4-scale experiment with those of FLACS simulations performed for two ways of representing the single hole (test 12, initial pressure 0.83 bar, flammable mixture: 1.4 % v/v propane, 7 % v/v hydrogen).

Based on these results and on results of other similar simulations (two-bay, four-bay and six-bay 1/4-scale experiments, variation of discharge coefficient) it was decided

to use the representation of holes as in the original FLACS code, i.e. no changes were made to the FLACS-code.

### 5.3 Heat transfer

FLACS normally assumes adiabatic conditions, i.e. no heat losses to the environment. For the present application, however, one can expect heat losses that can be considerable and may have an impact on the pressure differences across partitions depending on the course of the explosion. The heat losses can be recognised from the pressure decay after the explosion event in each bay for "all strong" tests, i.e. tests where none of the partitions including the front spar were made weak. In fact the heat transfer to the environment causes the pressure-time history to have a decrease of the rate of pressure rise towards the final stages of combustion.

The heat transfer to the environment can be twofold: radiative and convective.

FLACS already has a built-in model for convective heat transfer to walls which, however, has been used very little. This model is based on the assumption that the heat losses to the wall (heat flux  $Q_{\text{conv}}$ ) are directly related to the temperature difference between the hot combustion products ( $T_{\text{com}}$ ) close to the wall and the wall temperature ( $T_{\text{wall}}$ ):

$$Q_{\text{conv}} = h (T_{\text{com}} - T_{\text{wall}})$$

For the present application this model was applied.

A second and more important source of heat losses to the environment is radiation (Baer and Gross, 1998). This heat loss is volumetric and effective immediately after ignition. A model had to be included to describe this type of heat loss.

The model that was included was based on the assumptions that the combustion product temperature ( $T_g$ ) was uniform, that the tank walls could be considered as black and cold and that the degree of re-radiation was negligible.

In the model it assumed that the heat flux to the environment due to radiation can be expressed as:

$$Q_{\text{rad}} = \epsilon_g(L_e, p, T_g, X, Y)\sigma T_g^4$$

The gas emittance  $\epsilon_g$  is dependent on many factors including the characteristic radiation length  $L_e = 3.5.V/A$  (Ratzel and Shepherd, 1985), the prevailing pressure in the various bays, the gas temperature and the composition of the combustion products (X, Y). In the model it is assumed that the combustion products consist of water vapour and CO<sub>2</sub> only. The effect of pressure and temperature on the emission coefficients of water vapour and CO<sub>2</sub> are taken into account.

The model has been compared to tests in the Hyjet facility and the 1/4-scale single bay test set-up such as those shown in Figures 9-12 clearly showing that the heat losses are described satisfactory.

## 5.4 Quenching

Tests 40, 51, 53, 55 and 58 carried out in the 1/4 scale CWT facility using Jet-A as a fuel showed that flames passing through the small openings in the partitioning walls were sometimes quenched. This quenching is likely to be caused by flame stretch due to large velocity gradients existing at the interface of the turbulent jet emerging from the opening. Quenching in openings may have a strong influence on the course of the explosion (the mixture is not ignited in some bays as seen in the aforementioned experiments) and may lead to bigger pressure differences across partitions than one would get without flame quenching.

Hence it was decided to develop a criterion which indicated when one could expect flames to be quenched in openings.

The quenching criterion was developed on the basis of small-scale experiments carried out at the University of Bergen to find critical dimensions of holes for transmission of gas explosions (Larsen, 1998). On the basis of these experiments a criterion was developed independent from the Jet-A experiments performed in the 1/4 scale CWT facility. Thus it was possible to obtain a more independent basis for a criterion allowing for extrapolation to larger scales and other fuels.

The criterion that was developed is based on the so-called Karlovitz number  $K$ . The Karlovitz number describes flame stretch due to flow strain as the ratio of flow strain and flame gradient. Abdel-Gayed et al. (1987) expressed the Karlovitz number as the ratio of a combustion time scale ( $\delta/S_L$ ) and a turbulence time scale ( $u'/\lambda$ ) and used this to express conditions at which quenching due to flame stretch would occur.

Using the aforementioned expression as a starting point one can derive the following relationship for  $K$  where the strain rate has been expressed in terms of the integral length scale  $l_I$  through the turbulent Reynolds number  $R_T$ :

$$K = 0.157(u'/S_L)^2 R_T^{-1/2}$$
$$R_T = u' l_I / \nu$$

This leads to:

$$K = 0.157(\nu u'^3 / l_I)^{1/2} \cdot 1/S_L^2$$

Considering turbulent jets the prevailing turbulence intensity  $u'$  will be closely related to the velocity  $U$  in the opening. The turbulence length scale  $l_I$  will be closely related to the diameter  $D$  of the opening. Using this, the Karlovitz number used in the present study was chosen to be:

$$K = (\nu U^3 / D)^{1/2} \cdot 1/S_L^2$$

To arrive at a criterion for flame quenching in turbulent jets, i.e. at which Karlovitz number as defined will flames propagating through the opening be quenched, the results from experiments performed by Larsen (1998) were used.

These experiments were performed in a 2-chamber facility. Gas mixtures were ignited in a 1 litre primary chamber, which via a cylindrical hole was connected to a second open external chamber (Figure 13). The second chamber was transparent allowing for filming. Schlieren recordings were made of the flame propagation in the external chamber.

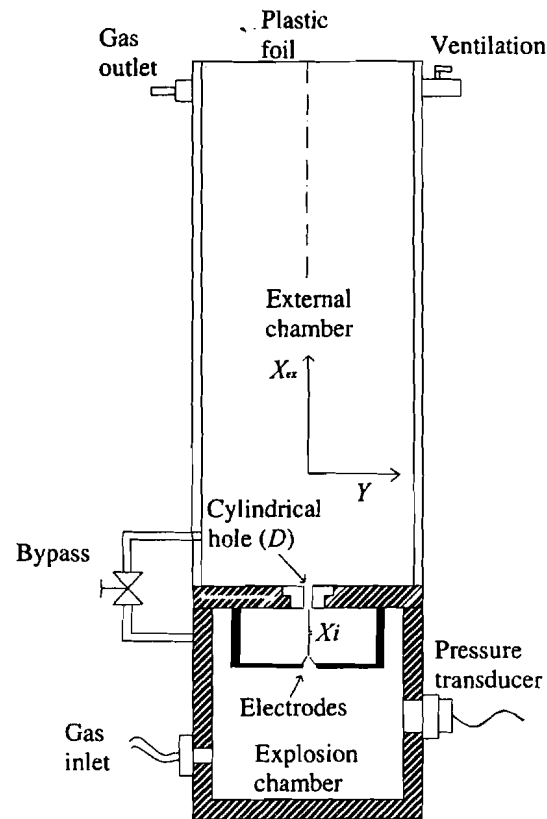


Figure 13 The University of Bergen explosion rig (1 litre).

The experiments involved variation of the ignition point, diameter of the cylindrical hole and variation of the concentration of the fuel-air mixture. All experiments were carried out with propane at atmospheric conditions.

For the purpose of the present study only results of a mixture of 4.2 % v/v propane/air were used. Typical results are plotted in Figure 14. The Figure shows the relationship between critical opening diameter and distance of the ignition source to the opening. The black dots represent points where in 10 shots ignition was always established in the external chamber whereas the open dots represent conditions where in none of the tests ignition of the mixture in the external chamber occurred. The initial decrease of critical diameter with increase of the distance between ignition source position and opening followed by an increase of critical diameter when the distance between ignition source position and hole is increased further clearly illustrates the existence of two different quenching processes. For short distances between ignition source and hole, heat losses to the cylindrical hole

determine the quenching process whereas for larger distance quenching in the turbulent jet dominates.

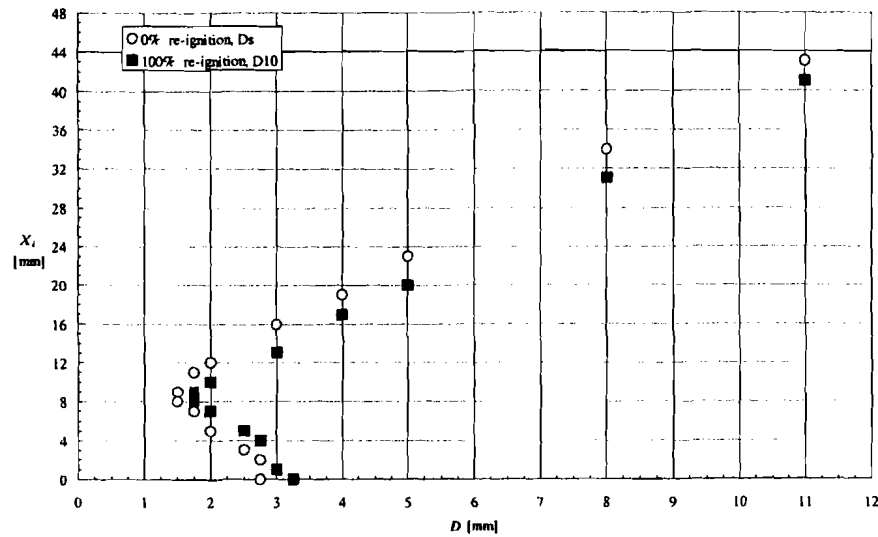


Figure 14 Critical opening diameter (D) as a function of the distance ( $X_i$ ) between ignition source position and opening between primary and second chamber. Primary chamber volume is 1 litre, a 4.2 % v/v propane-air mixture was used as a flammable mixture.

In order to be able to use the results reported by Larsen (1998) knowledge on the velocities in the opening at the moment of flame transmission should be known. Since such measurements were not carried out simulations were performed to generate these data. In the simulations a grid size was applied such that the hole size was represented by at least one cell.

From the calculated velocities and observed flame transmission phenomena a critical Karlovitz number was established as a function of the opening diameter. It was found that for opening diameters bigger than approximately 7 mm (there are no openings smaller than 7 mm in the full-scale CWT) the critical Karlovitz number is  $K=140-150$ .

As a next step the developed criterion was consolidated by comparing to the results of 1/4-scale experiments. To this end mainly Jet-A experiments were used (40 °C and 50 °C) considering 2-bay experiments carried out for this purpose and 6 bay all strong experiments (where quenching was observed as mentioned above: tests 44, 51



and 55, but also the results of tests 46, 48 and 53 were considered). In addition to that comparisons were made to some of the simulant fuel experiments.

The 2-bay experiments involved one partition with a single hole of varying dimensions (a 0.25 inch x 2 inch slot and circular openings with diameters of 1, 1.5 and 2 inch). The results of the simulations performed are summarised in Figure 15. The Figure shows that the criterion matches the results from the experiments for Jet-A 50 °C but the results from the Jet-A 40 °C experiments indicate that the criterion is not fully sound. According to the predictions a Karlovitz number of 203 would prevail for Jet-A at 40 °C in a 2-inch diameter hole at the moment of flame arrival indicating quenching. In the test, however, no quenching occurred.

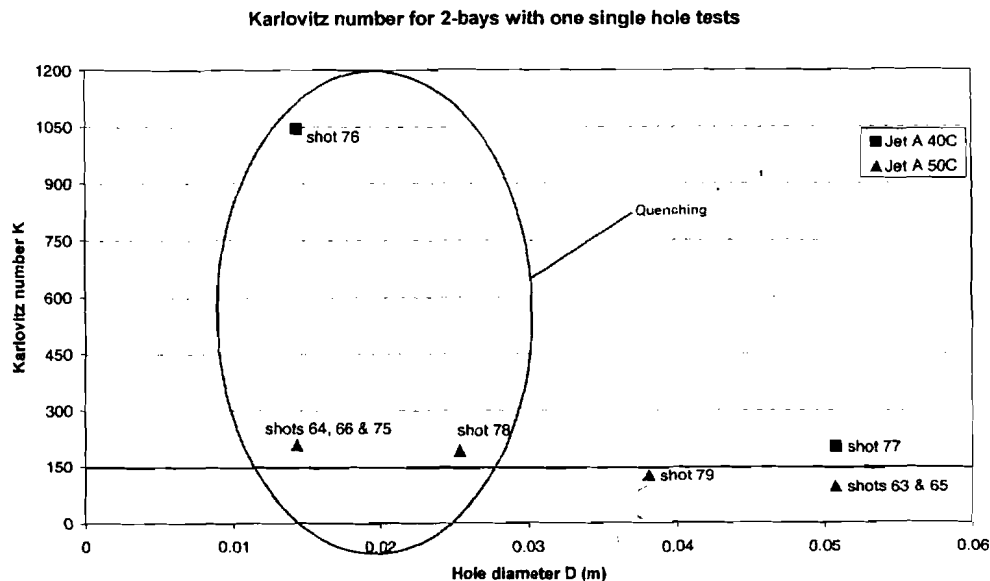


Figure 15 Comparison of  $K=150$  criterion with predictions for two-bay, single-hole experiments carried out with Jet-A at 40 °C and 50 °C. The encircled data points indicate in which tests quenching occurs in the experiments.

The criterion was also tested against 6-bay all strong tests carried out with Jet-A (40 °C) and Jet-A (50 °C). In these tests quenching was observed in several bays. The criterion can be checked by comparing the Karlovitz number at the moment of flame arrival at the first hole where the flame arrives with observations of quenching or not. The results of these simulations have been plotted in Figure 16. The Figure shows for several tests the occurrence of quenching or not and the respective

Karlovitz numbers predicted for each of the transmissions that potentially could have occurred. In test 44 (Jet-A 40°C) ignition was effected in bay 5 and combustion was only seen in bays 5 and 6. The Karlovitz number at the moment of flame arrival is  $K=248$ ,  $K=913$  and  $K=2738$  for the transmissions from bay 5 to 6, bay 5 to 3 and bay 6 to 4 respectively. Quenching was observed for the transmission into bays 3 and 4 but not for the transmission from bay 5 to 6. In test 51 (Jet-A 50 °C) the flame also only propagated through bays 5 and 6. For this test the Karlovitz number at the moment of flame arrival is  $K=141$ ,  $K=250$  and  $K=1144$  for the transmissions from bay 5 to 6, bay 5 to 3 and bay 6 to 4 respectively.

Test 53 exhibits a very strange behaviour. Upon ignition the pressure in the ignition bay starts rising up to approximately 0.6 bar. The combustion then seems to cease resulting in pressure decay. Suddenly, however, bay 1 is ignited whereas also combustion seems to take place in bays 3 and 4 (at least partially). Bays 5 and 6 do not show combustion. This strange behaviour is deviating from the combustion phenomenon described in the FLACS code and the results of this test can therefore not be used to consolidate the criterion.

Tests 46 and 48 (Jet-A, 40 °C) are tests where all bays are ignited. If we assume that the flame propagation from bay to bay would occur as predicted by the FLACS-code Karlovitz numbers of up to  $K=1924$  are seen, clearly far into the region where on the basis of the other Jet-A experiments (both 40 °C and 50 °C) reported above, quenching should have occurred. Comparing pressure-time histories in the ignition bay (bay 2) for the calculated Jet-A, 40°C and those measured, we see that the maximum pressure is considerably lower but, and more importantly, we also see a lower initial pressure rise in the experiments followed by a temporary plateau and even a slight pressure decrease before the pressure starts to increase strongly (Figure 17). It seems as if the explosion is occurring into two stages. First a mild explosion occurs running into especially bay 1. After a strong pressure in bay 1 occurs (finally up to 2.8 bar) the pressure in bay 2 starts to rise as well (up to approximately 1.5 bar) but not to the levels seen in any of the other bays. This secondary explosion in bay 2 is difficult to explain on the basis of "normal" explosion behaviour but potentially we see here a cool flame phenomenon which is not uncommon for hot surface ignition (D'Onofrio, 1980). The cool flame explanation is also supported by visual observations. The observed behaviour has also some similarities with the behaviour seen in test 53. Regarding the above-described behaviour also the results of these two tests were neglected.

In test 55 the transmission from bay 2 (ignition bay) to bay 1, from bay 2 to bay 3 and bay 3 to bay 4 can be described. Quenching occurs when propagating to bay 1 (K=256) and bay 3 (K=433). Transmission into bay 4 (K=121) is successful. Later the flame propagates into bay 5 and 6 as well but since the FLACS predictions used for estimation of Karlovitz numbers does not effectuate quenching when the criterion prescribes quenching pressure differentials across partitions may deviate from those seen experimentally.

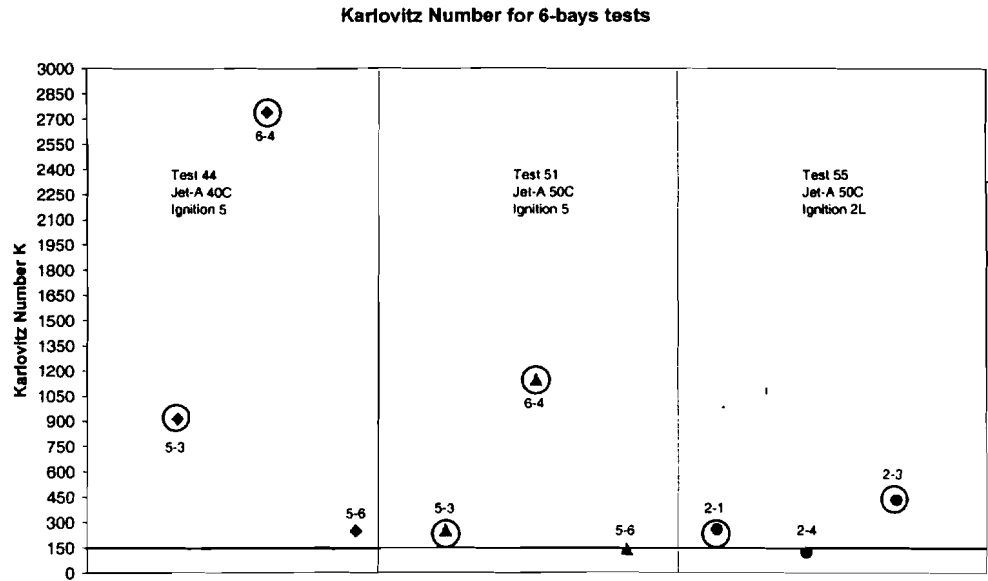


Figure 16 Comparison of K=150 criterion with predictions for six-bay, all strong experiments carried out with Jet-A at 40 °C and 50 °C. The encircled data points indicate in which tests quenching occurs in the experiments.

Fl Mar 24 11:26:28.2000 "Comparison FLAGB and experiments : show6 - pressure"

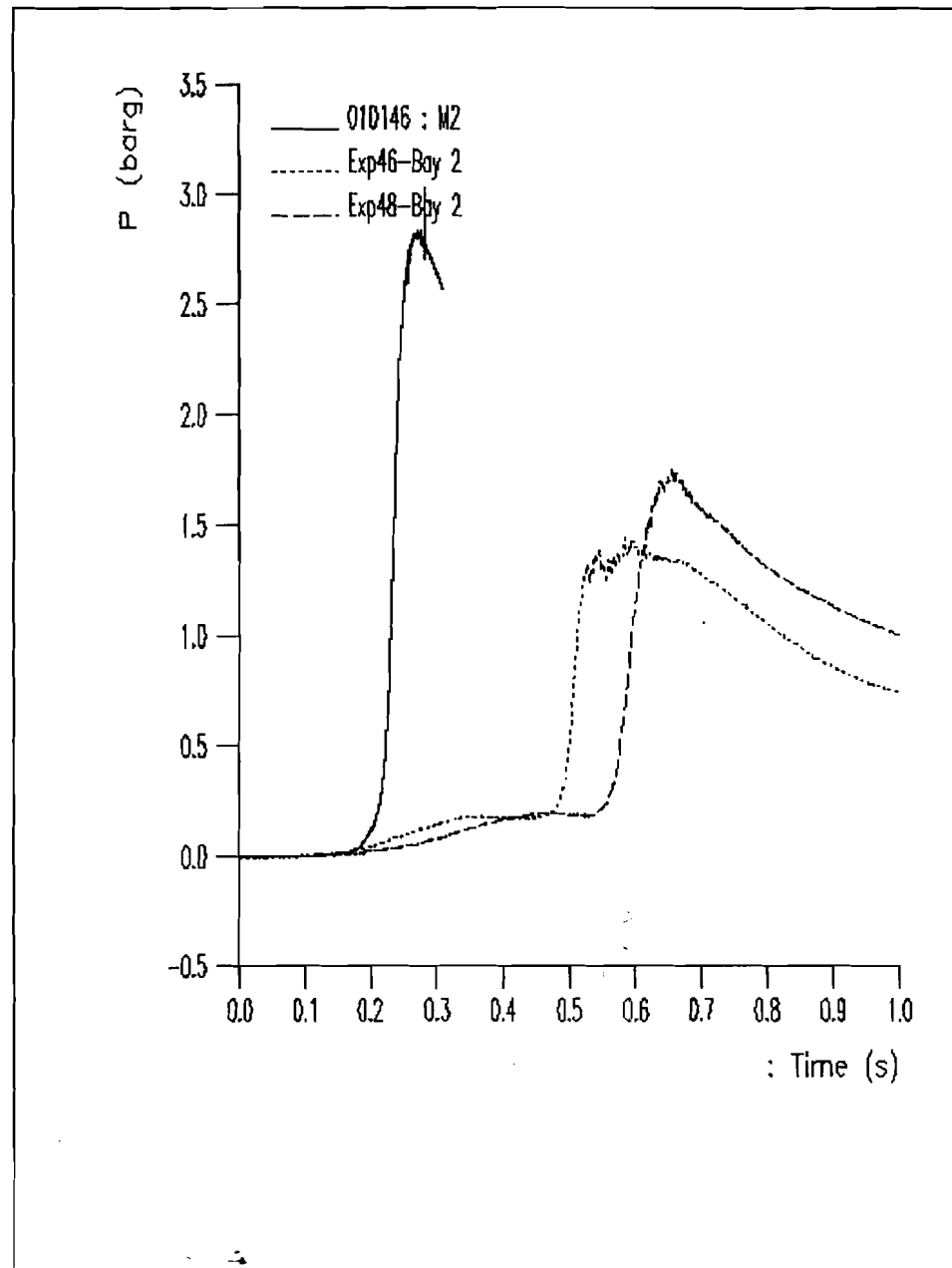


Figure 17 Predicted and measured (tests 46 and 48) pressure-time histories in bay 2 for a 6-bay, all strong experiment (Jet-A, 40 °C, ignition point 2L).

On the basis of these results the criterion derived from the experiments performed by Larsen (1998) was revised into a criterion representing a likelihood of transmission

as a function of Karlovitz number. The probability distribution is based on Jet-A experiments only and shown in Figure 18.

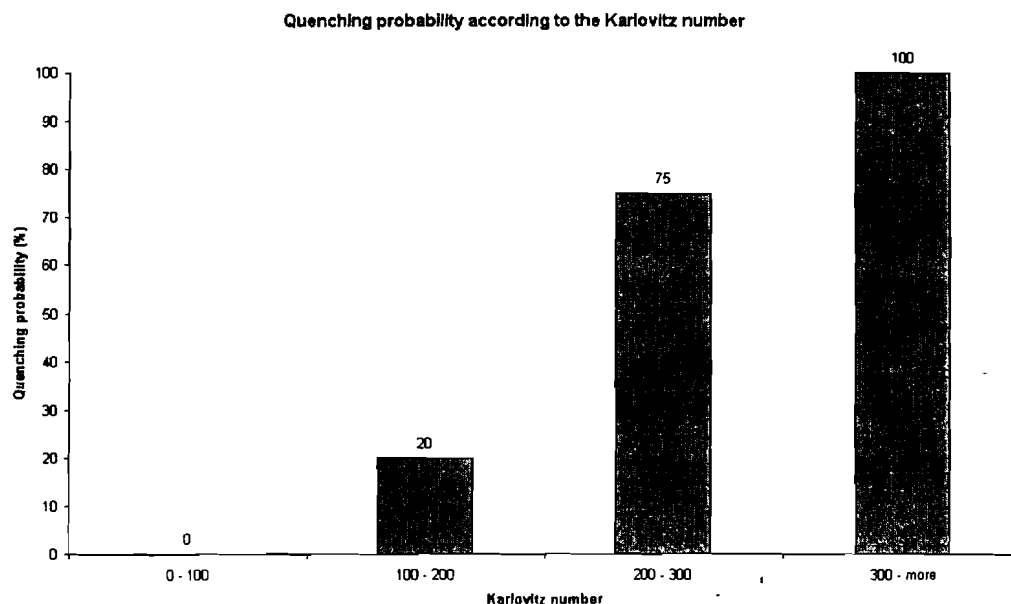


Figure 18 Probability of flame quenching in orifices as a function of Karlovitz number at the moment of flame arrival.

Although some differences are seen between the criterion obtained from the University of Bergen tests with propane and the Jet-A tests the relative difference can be described as small indicating that the criterion with confidence can be applied to hydrocarbon fuels with a reactivity comparable to that of ethane, propane and butane.

Simulations were also performed with simulant fuel (7 % hydrogen, 1.4 % propane) to investigate the criterion. Several initial conditions were studied and Karlovitz numbers were seen of up to  $K=1077$  implying that according to the criterion quenching should have occurred. In none of the simulant fuel tests, however, quenching was observed. The reason for this must be the fact that a fuel with a considerable content of hydrogen behaves very differently than a simple hydrocarbon fuel. The strain rates required to extinguish flames in hydrogen-air would be higher than for hydrocarbon-air mixtures, at the same burning velocity. A simple criterion just based on burning velocity therefore cannot accommodate for the differences between hydrocarbon fuels and fuels containing lots of hydrogen.

Inclusion of a Lewis number dependency accounting for the high molecular diffusivity of hydrogen may be a solution here (a criterion based on the product of the Karlovitz number and the Lewis number:  $K.L_e$ ). Perhaps such a criterion may also account for the differences seen between Jet-A at 40 °C and Jet-A at 50 °C (the quenching behaviour of Jet-A at 50 °C agreed very well with the original criterion obtained for stoichiometric propane whereas some deviations were seen for the Jet-A at 40 °C). The Lewis number would account for the slightly different thermal diffusivity of the two Jet-A mixtures. Also the Zeldovich number (nondimensional activation energy), plays an important role in quenching. Another explanation for the differences between Jet-A 50 °C and Jet-A 40 °C may be the slightly better representation of the combustion properties of Jet-A 50 °C compared to Jet-A 40 °C (see Figures 11 and 12).

## 6 SIMULATIONS PERFORMED

During the investigation the (modified) FLACS code was used for several purposes. The majority of the 1/4-scale tests in which simulant fuel was used were simulated in order to investigate and qualify the properties of the code regarding predicting the outcomes of explosions in both the 1/4-scale experimental set-up and the full-scale Center Wing Tank.

Secondly the ignition source location within the 1/4-scale experimental set-up was varied in order to confirm findings of Sandia National Laboratories. Sandia performed simulations with their tool varying the ignition location all over the 1/4 scale set-up to investigate both the sensitivity of the ignition source location and to find locations where the observed damage agrees with observed predicted loadings. The FLACS simulations concern a sub-set of the Sandia simulations.

The third set of simulations reported here concern predictions of loading on partitions in the full-scale Center Wing Tank starting from eight ignition source positions (7 fuel probes and the compensator) and two Jet-A fuel temperatures (40 °C and 50 °C).

### 6.1 Model validation: comparison to 1/4-scale experiments

The 1/4-scale experimental programme has been described briefly in section 3.3 (See Shepherd et al., 1998, Brown et al., 1999 and Shepherd et al, 2000 for details). Initially experiments were performed using a simulant fuel consisting of 1.4 % v/v propane and 7 % v/v hydrogen. The majority of these experiments that resulted in valid data and in which no liquid fuel were introduced were simulated using FLACS. Both tests in which all or some of the partitions were allowed to fail and in which all partitions were strong were considered. These simulations were used to validate the FLACS for this very application.

Figure 20 shows how the 1/4-scale rig was represented in FLACS and some moments of flame propagation of an explosion ignited in bay 3. Dimensions and other properties of openings, vents and partitions of the 1/4-scale rig were based on information made available by the California Institute of Technology (1997). The moments of flame propagation show how the flame after a relatively slow initial

phase shoots from bay to bay via the connecting holes causing turbulence and considerably faster explosions in these other bays.

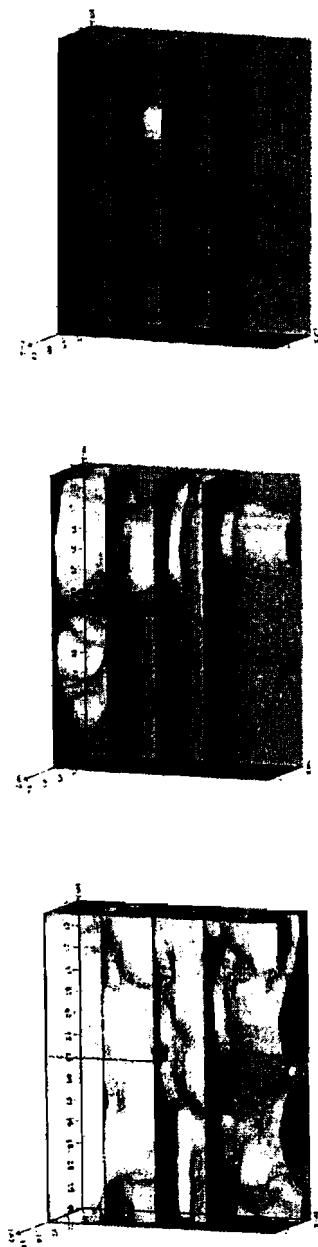


Figure 20 The 1/4-scale rig as represented in FLACS and some moments of flame propagation in this rig as predicted by FLACS.



For some bays (especially bays 3, 4, 5 and 6) flames can enter a bay from more than one direction due to the presence of several surrounding bays. This could for some scenarios lead to a very big sensitivity of change of ignition position.

In Figures 21-24 examples are given of simulated 1/4-scale experiments, all considering the simulant fuel. Each Figure shows the pressure development in bays of the CWT and the pressure differences across the partitions.

Figure 21 presents the results of simulations of test 10. In this test (from test series Alpha, see section 3.3) only one partition was present (MS). The partition was not allowed to fail. Ignition was effected in bay 5 ((co-ordinates: X=0.14 m, Y=1.016 m, Z= 0.228 m) see Section 3.3). The pressure-time histories in bay 1 and 2 (monitoring points M16 and M15) and the pressure-time histories in bays 3-6 (monitoring points M11-M14) are more or less similar as they were measured in the same bay in this very test configuration. We see that the pressure in the ignition bay (M11-M14) gradually increases whereas the pressure in the second bay increases much less fast. The pressure increase in the second bay is controlled by flow from the ignition bay into this bay through the hole in the partition connecting the two bays. Upon the moment of the flame entering the second bay the turbulence generated by the flow through the holes causes the combustion rate in the second bay to be much faster than in the ignition bay. As a result the pressure in the second bay rises sharply exceeding the pressure in the ignition bay already after 10 ms after the moment the flame entered the second bay. This causes the flow through the holes to reverse. Now a strong flow is established into the ignition bay causing turbulence here and thereby an acceleration of the explosion in the ignition bay. Comparing the pressure-time histories of simulation and experiment (Figure 21a) we see that the initial pressure rise in the ignition bay is stronger in the simulation which can be explained by a slightly more reactive mixture than in the experiment. This may also explain the differences during the further course of the explosion. In the second bay the pressure reaches approximately 4.9 bar in the simulation partly due to pre-compression effects (partly due to the higher heat of combustion). In the experiment the pressure reaches 3.9 bar. Also the pressure rise is considerably sharper in both the ignition bay and second bay. Figure 21b presents the pressure differences across the MS. Consequently the pressure difference across the MS is much higher in the simulation than in the experiment. In the experiment a forward directed pressure

Mon Jan 24 11:15:36 2000 "Comparison FLACS and experiments : shot10 - pressure"

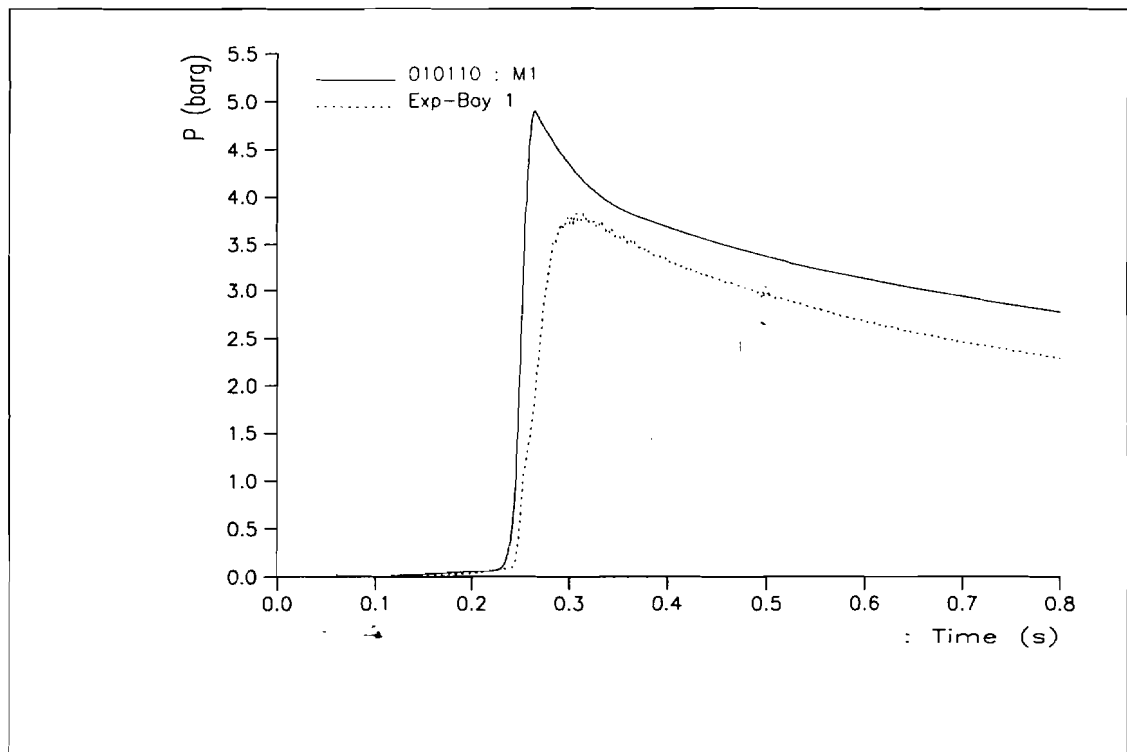
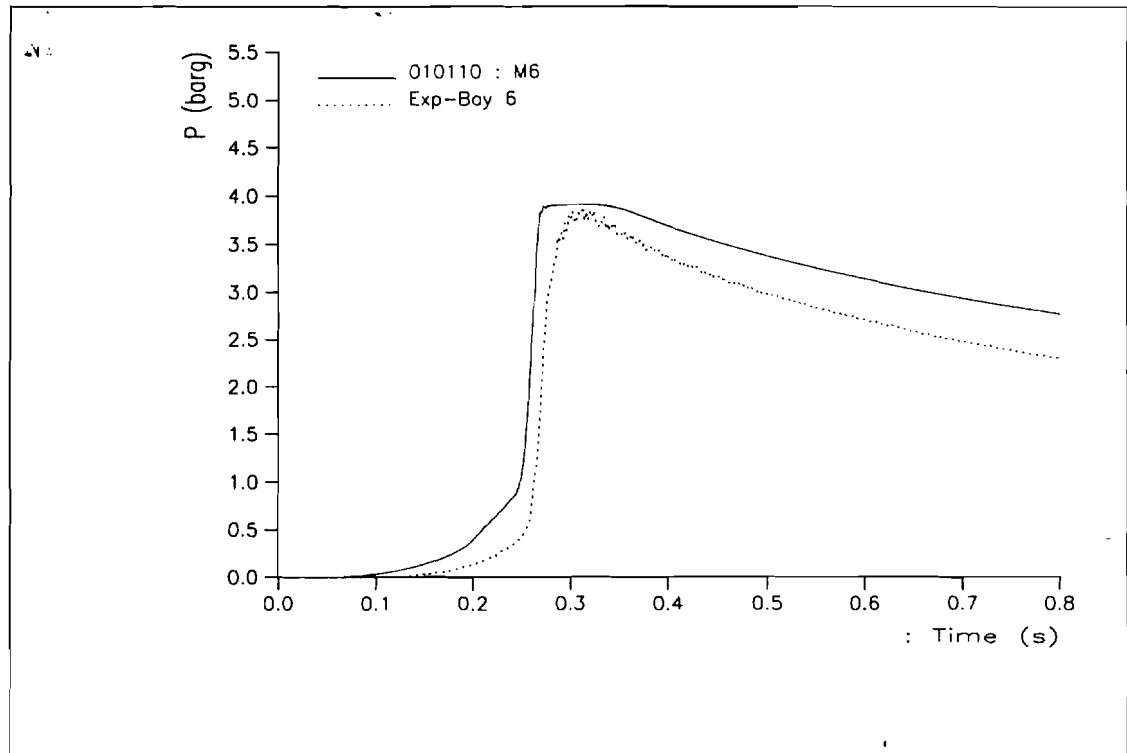


Figure 21a Comparison of predictions and experiment for absolute pressure in the two bays in test 10.

Mon Jan 24 11:19:31 2000 "Comparison FLACS and experiments : shot10 - panels pressure"

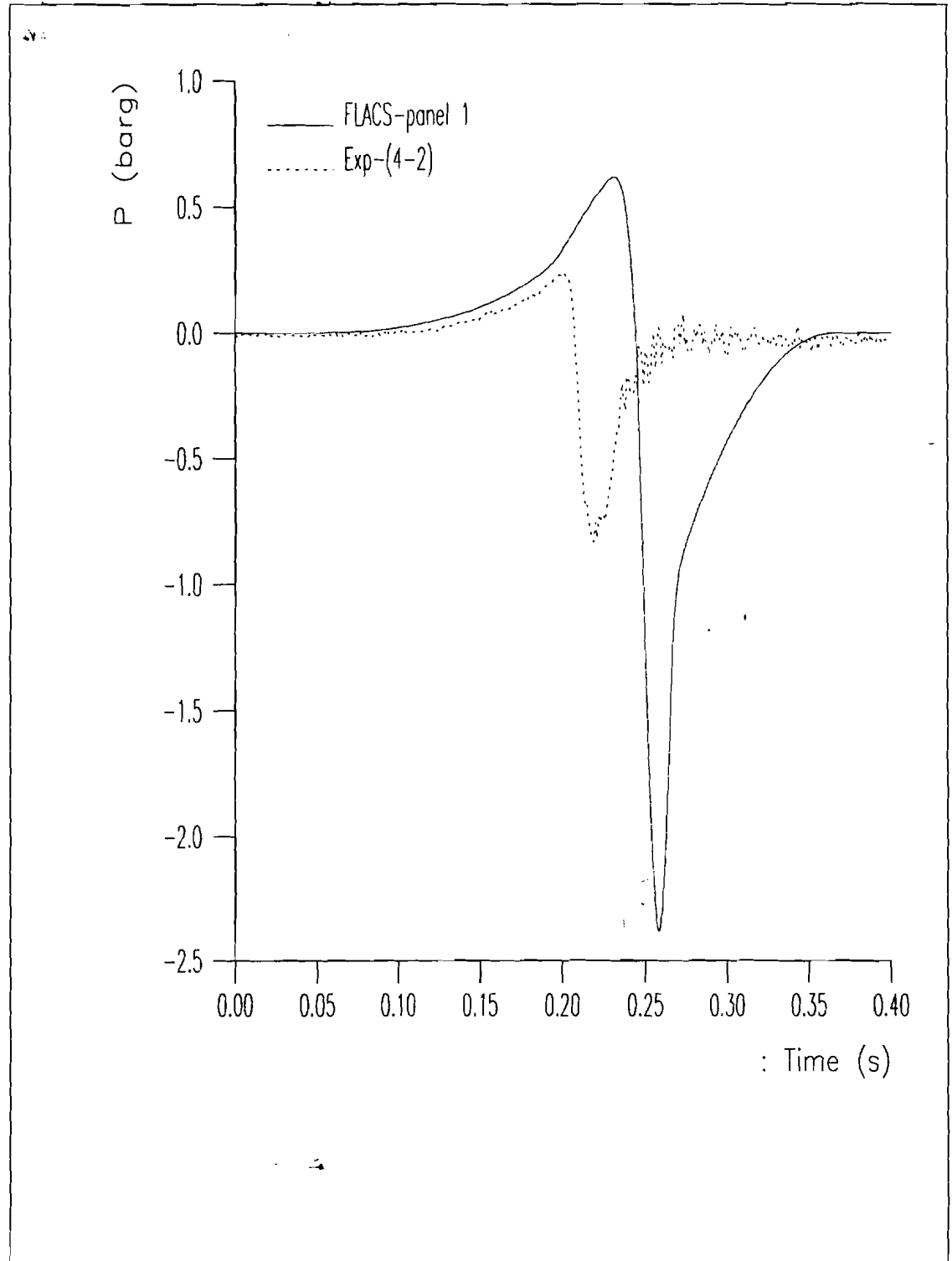


Figure 21b Comparison of predictions and experiment for pressure differences across the single partition (MS) in test 10.

difference of 0,241 bar and an aft directed pressure difference of 0,83 bar were seen. In the simulation these pressure differences were 0,62 bar and 2,38 bar respectively.

Figure 22 compares simulation and experimental results of test 5. Test 5 is a six-bay test (Beta-series) where all partitions were strong. Ignition was effected in bay 3 ((co-ordinates: X=0.394 m, Y=1.016 m, Z= 0.228 m) see Section 3.3). Figure 22a presents the absolute pressures in each bay showing that first of all the maximum pressure in each bay is considerably higher in the simulations than in the experiment (0.4 - 0.6 bar and 1.4 bar in bay 4). This may again be due to a higher heat of combustion of the mixture used in the simulation than in reality. No indications are seen of a higher initial combustion rate as seen in the simulation of test 10. It is unlikely that the difference in maximum pressure can be explained by a too low heat loss in the simulation.

Nevertheless we see that the shape of the pressure difference-time histories (Figure 22b) across all panels is very similar in simulation and experiment. Also the absolute values of the simulation are very close to the experimental values. It should be mentioned that the pressure measurement in bay 1 failed resulting in non-valid measurements of the pressure difference across SWB2.

Figure 23 compares simulation and experiment for a test (test no. 39) where ignition was effected at one of the potential ignition locations, i.e. one of the fuel probes ((ignition location 2L: co-ordinates X=0.535 m, Y=0.66 m, Z= 0.051 m) see Section 3.3). Also in this test all partitions were present and strong. Figure 23a shows the absolute pressures compared to those found in the experiments. Again as seen for test 5 the absolute pressures are overpredicted. The explanation is similar as for test 5. The simulation reproduces some features seen in the experiment, such as occurring at the moment of maximum pressure in bay 4.

Also many of the features seen in the pressure differences (Figure 23b) across the partitions obtained from the experiment are reproduced. Across SWB1 (between bays 3 and 5), however, an extra forward pointing peak is predicted.

Figure 24 shows an example of a test where failure of some of the partitions was assumed. In this test, test 17, the FS, SWB3 and a manufacturing panel in SWB2 were assumed weak (failure pressure 20 psi (1.378 bar)). Ignition was effected in bay 5 ((co-ordinates: X=0.14 m, Y=1.016 m, Z= 0.228 m) see Section 3.3). The absolute pressures are well reproduced (Figure 24a) although again a clear

Mon Jan 24 10:29:23 2000 "Comparison FLACS and experiments : shot05 - pressure"

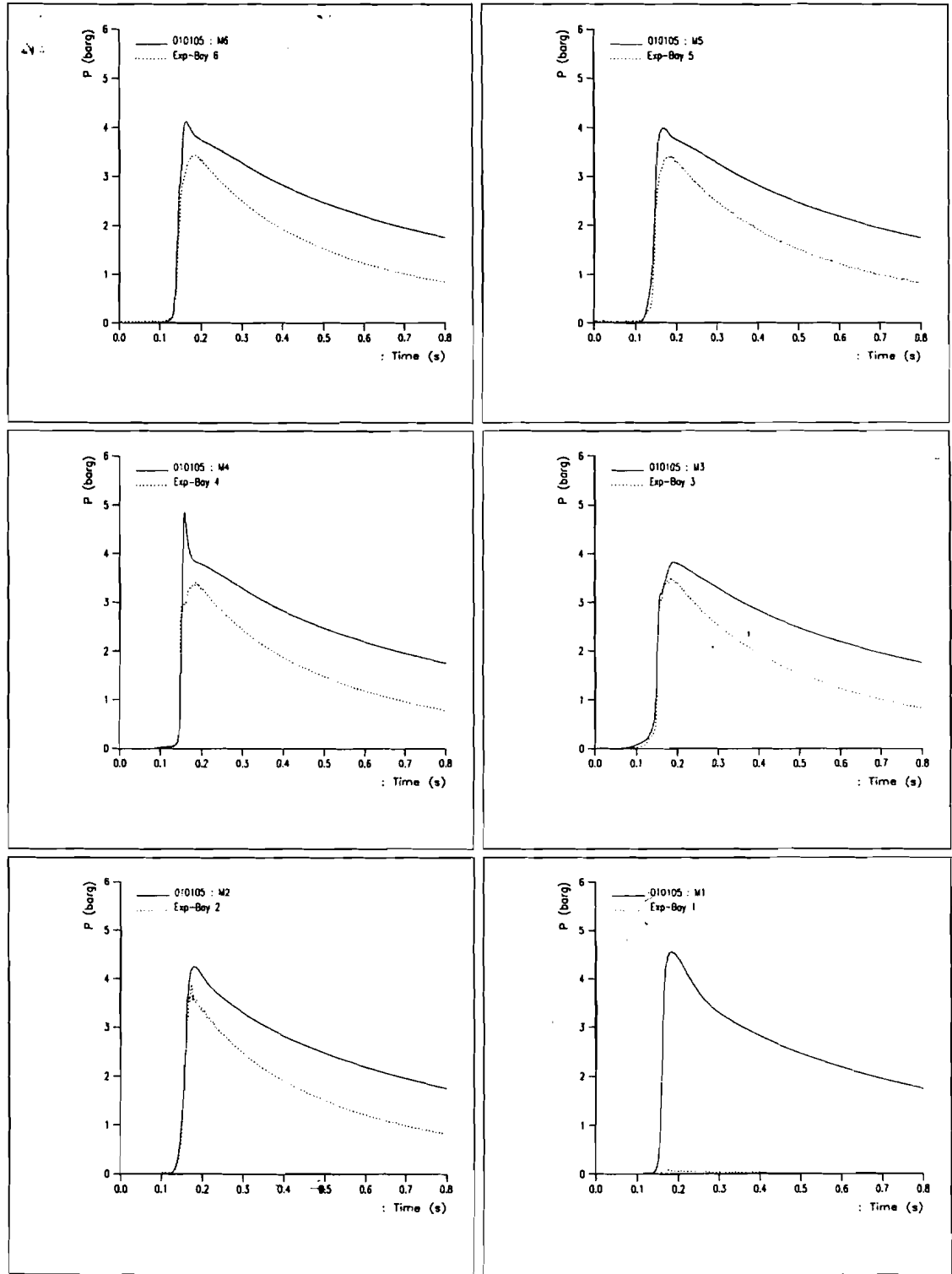


Figure 22a Comparison of predictions and experiment for absolute pressure in each bay in test 5.

Mon Jan 24 11:49:33 2000 "Comparison FLACS and experiments : shot05 - panels pressure"

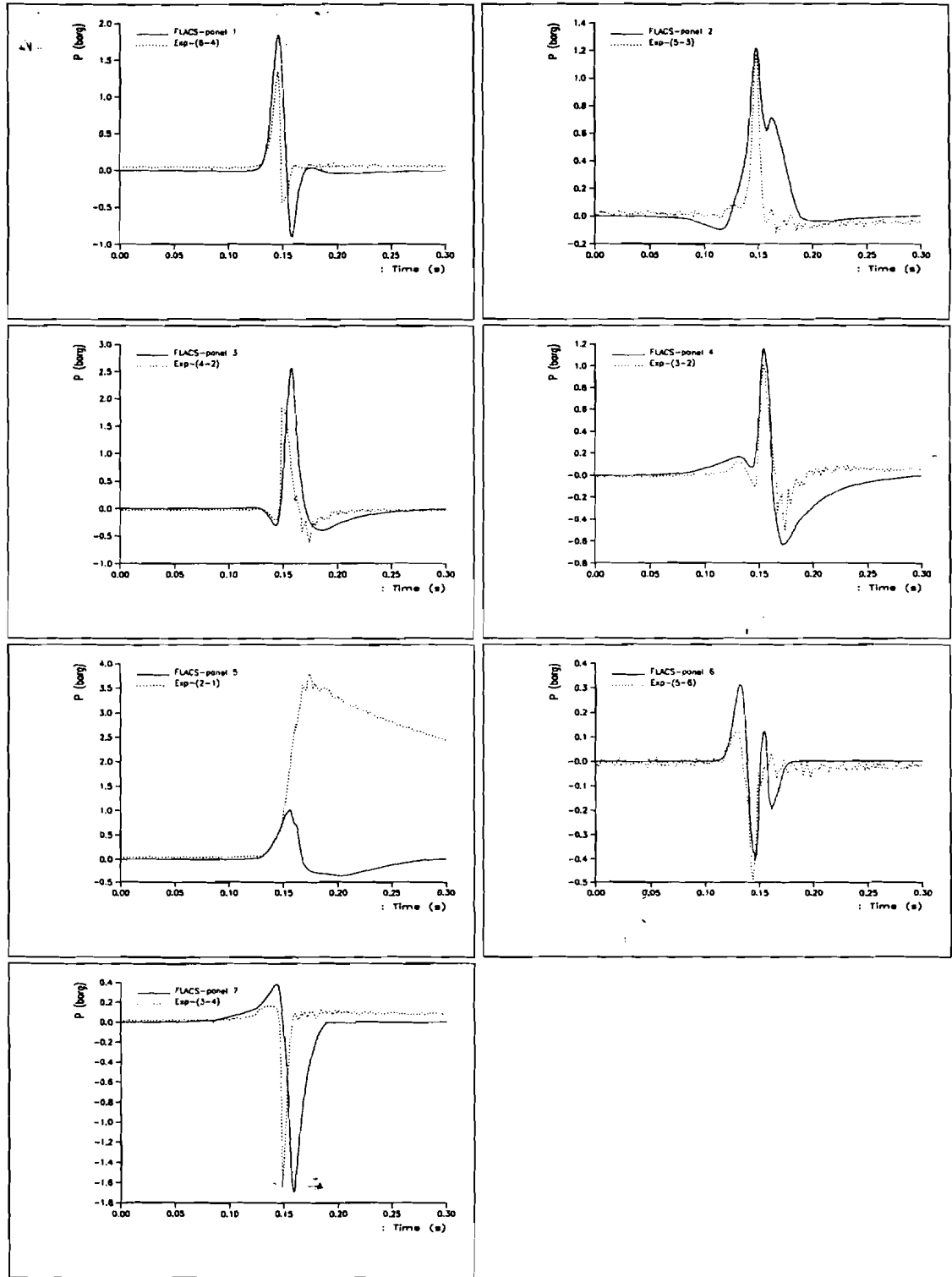


Figure 22b Comparison of predictions and experiment for pressure differences across each partition in test 5.

Mon Jan 24 10:34:45 2000 "Comparison FLACS and experiments : shot39 - pressure"

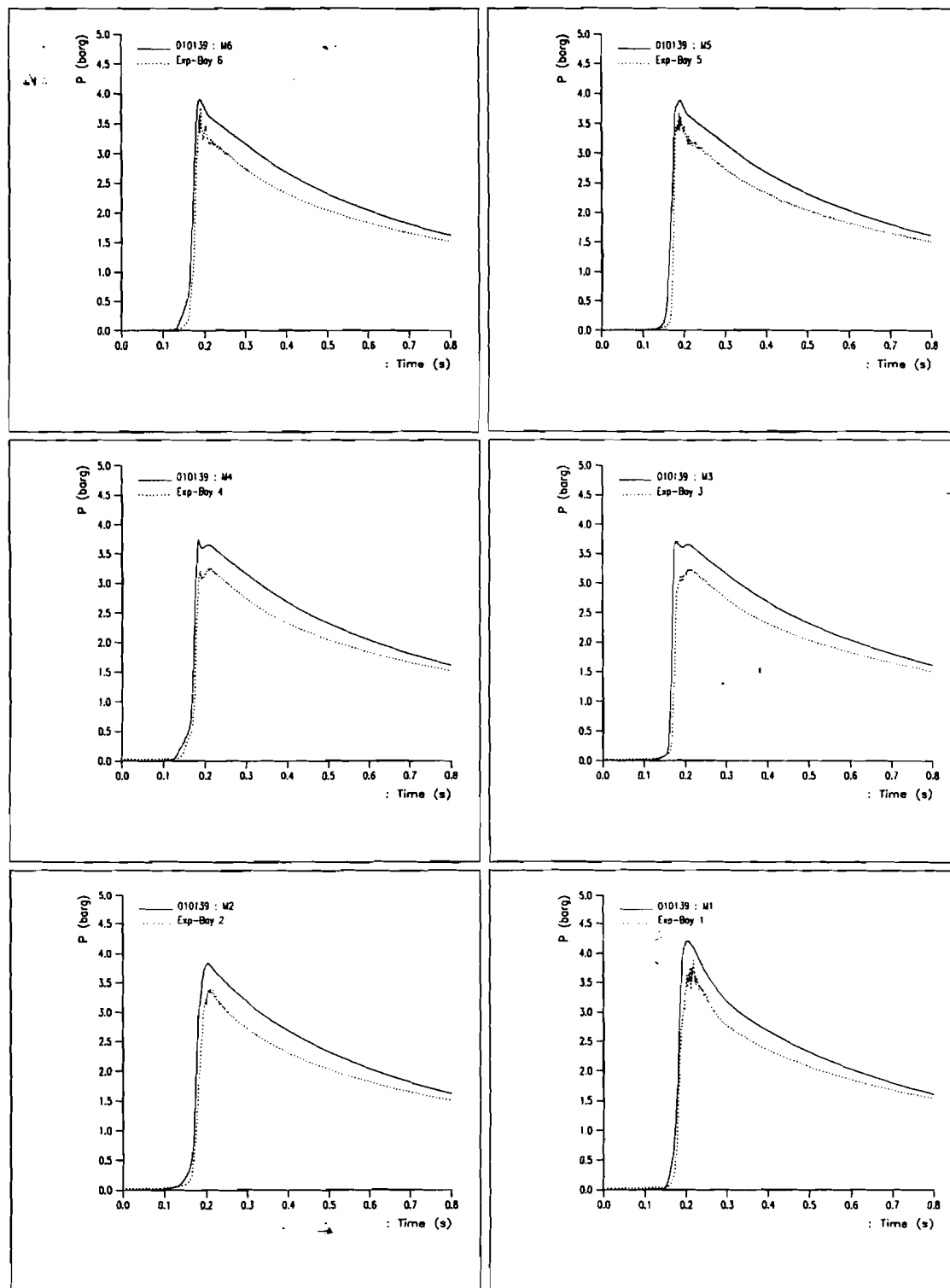


Figure 23a Comparison of predictions and experiment for absolute pressure in each bay in test 39.

Mon Jan 24 11:52:17 2000 "Comparison FLACS and experiments : shot39 - panels pressure"

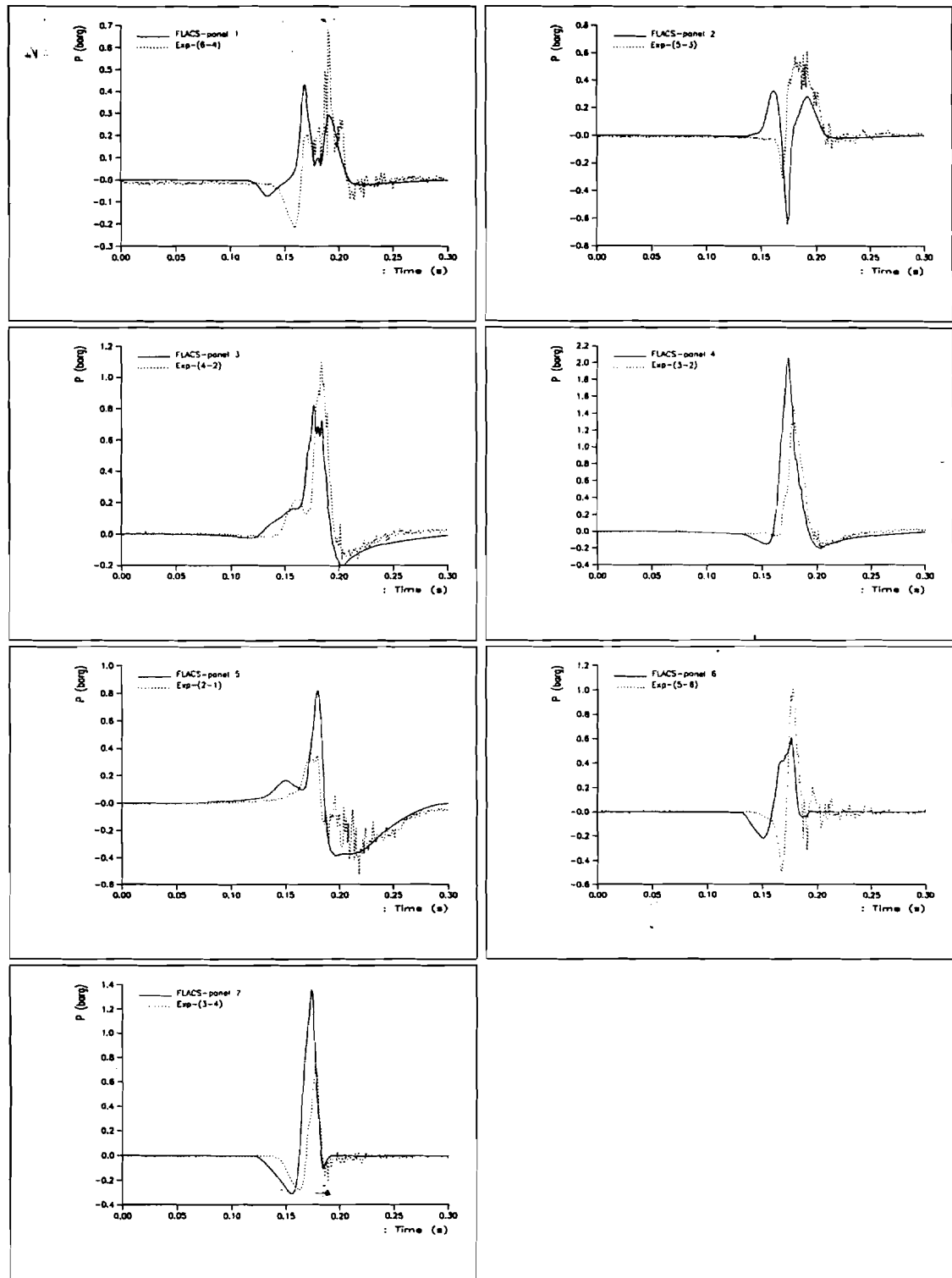


Figure 23b Comparison of predictions and experiment for pressure differences across each partition in test 39.



overprediction is noticed for the bays 3-6 partially due to a too high heat of combustion used in the simulations. The pressure decay is however, well described in these bays. The pressure decay is dominated by the flow through the openings between the bays. The heat loss is now less important for the pressure decay. The failure pressure of the panel in SWB2 seems to be too high in comparison to the assumed experimental conditions and therefore assumed in the simulations as well. The latter may have an impact on the entire course of the event after failure of this panel.

Considering the pressure differences (Figure 24b) across the various partitions we see that most peaks seen in the experiments are seen in the simulations as well. Some of these are slightly disguised as they almost coincide with other peaks as seen i.e. for the pressure differences across MS (bays 4-2 and 3-2).

Mon Jan 24 10:59:45 2000 "Comparison FLACS and experiments : shot17 - pressure"

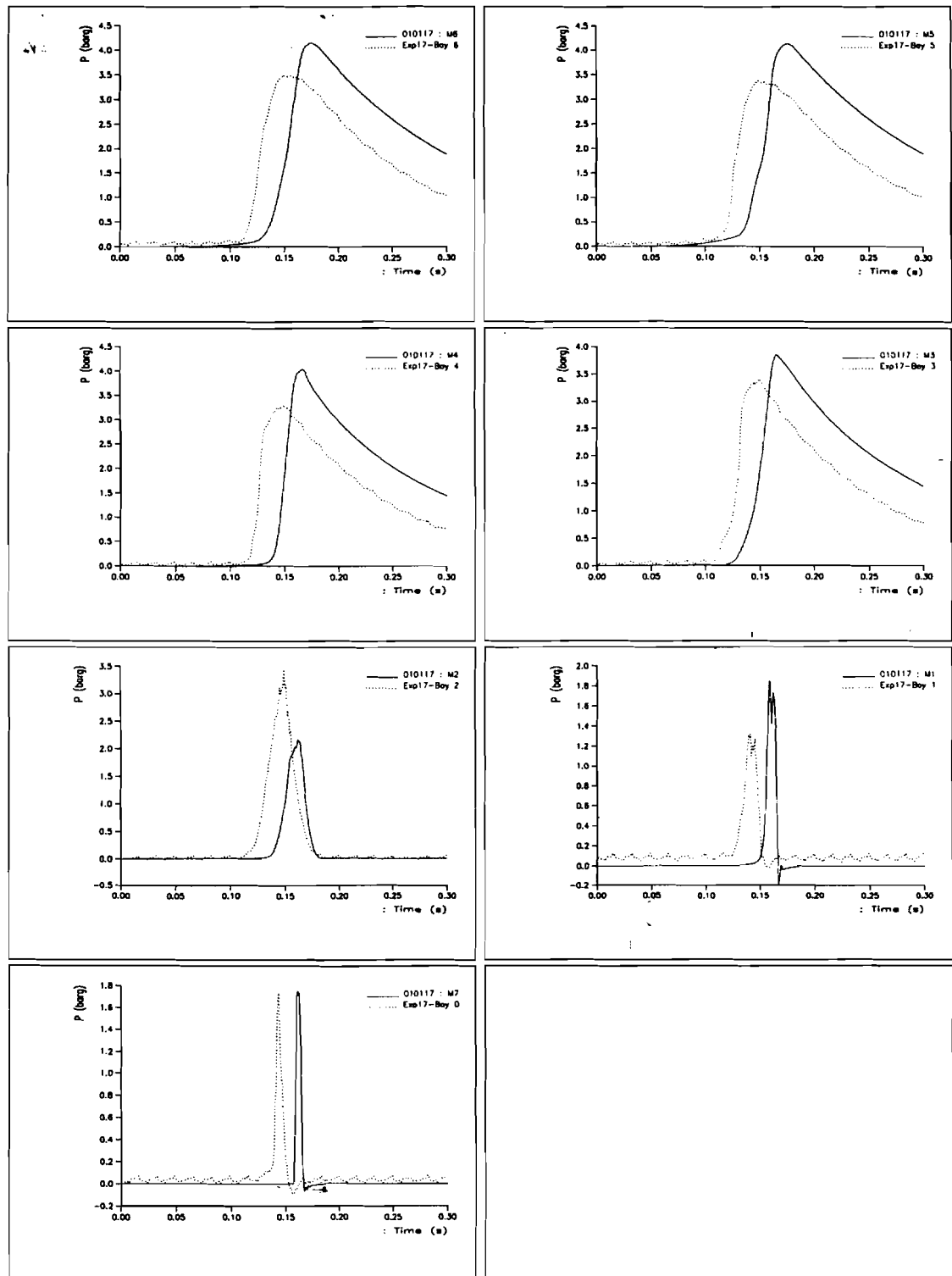


Figure 24a Comparison of predictions and experiment for absolute pressure in each bay in test 17.

Mon Jan 24 11:08:17 2000 "Comparison FLACS and experiments : shot17 - panels pressure"

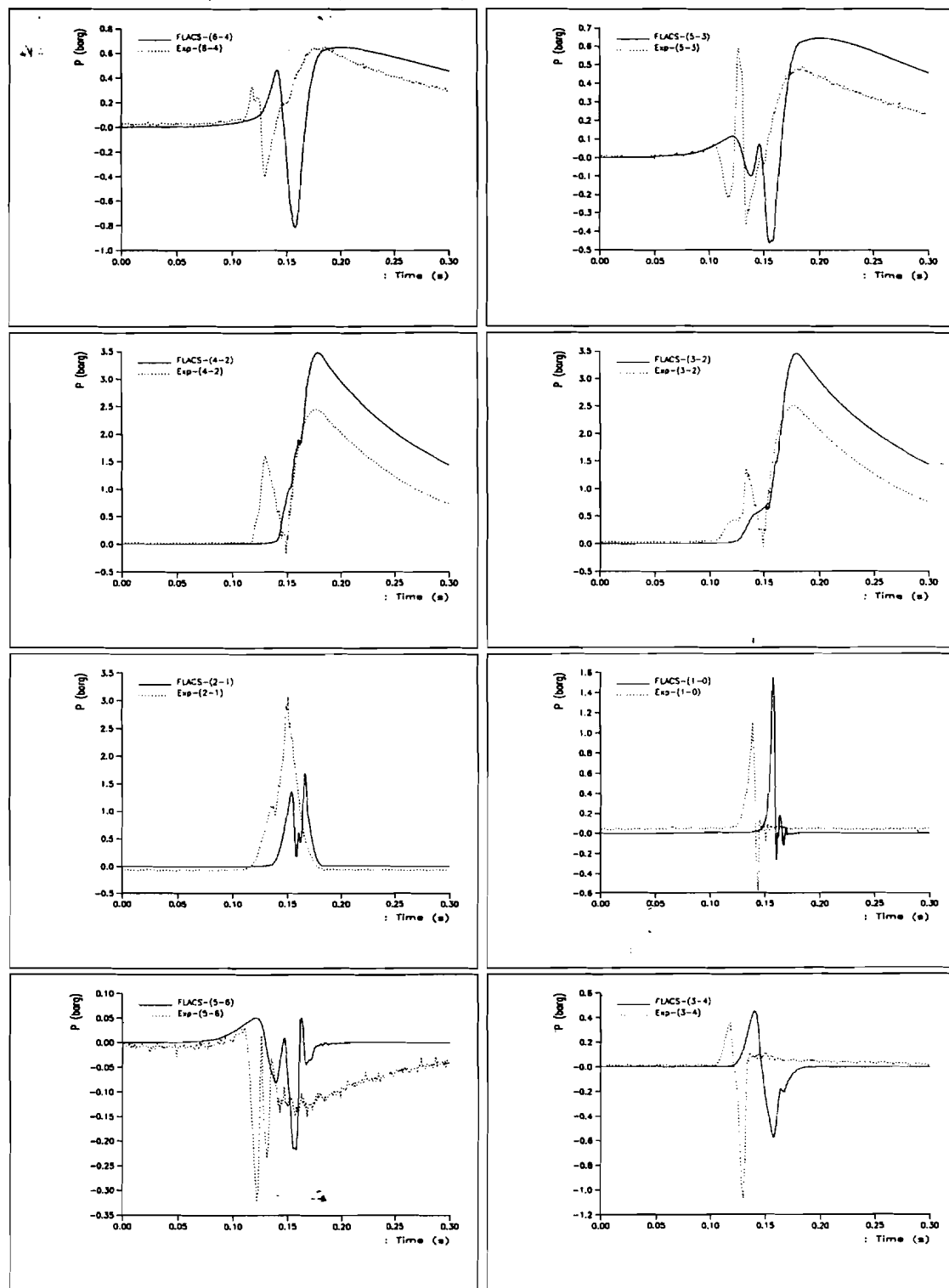


Figure 24b Comparison of predictions and experiment for pressure differences across each partition in test 17.

During the replica test-series (see section 3.3) several experiments were repeated in order to investigate the repeatability. A different way of judging the quality of the simulations/predictions instead of direct comparison to the measured pressure difference time-histories is comparing the maximum forward and aft directed pressure differences as calculated by FLACS to those of the experiments of the replica test series. Examples are shown in Figures 25 to 27.

Figure 25 shows a comparison of the FLACS predictions for tests 31a and 31b (All strong, ignition in bay 5, initial temperature 27.5 °C- 28.0 °C, initial pressure 82 kPa, vented). The Figure shows first of all that there is a reasonable agreement between FLACS predictions and test results regarding trends. The pressure differences seen in the tests are however higher, both forward and aft, than in the simulation. Another feature seen is the relatively big variations between the two experiments in spite of the initial conditions being similar. It should also be remarked that these tests had the liquid fuel manifold open which results in flow and in some cases flames propagating through the tubing causing jets or ignition.

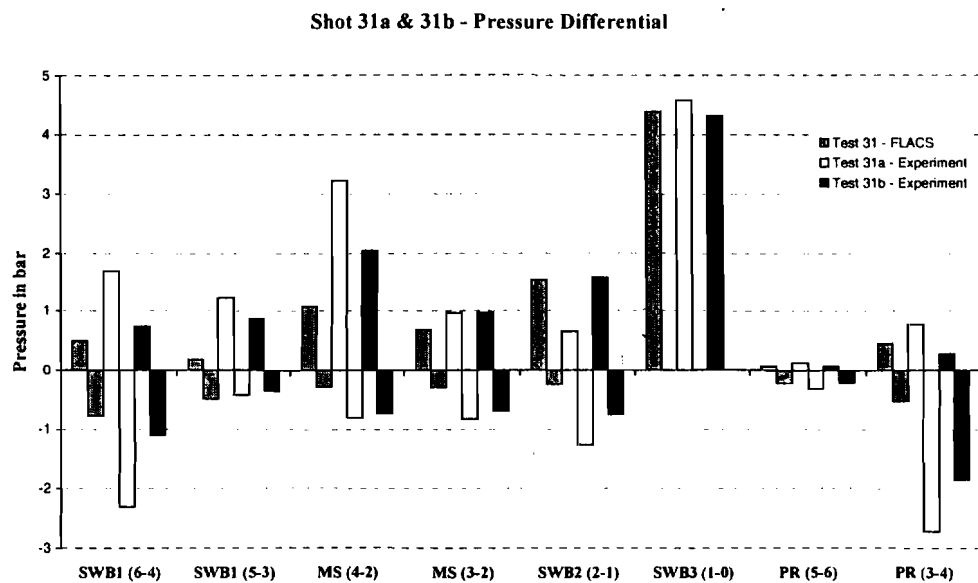


Figure 25 Comparison of predicted and measured pressure differences across the various partitions in the 1/4-scale CWT (forward (positive) and aft (negative) directed). Tests 31a and 31b: test conditions: all strong, ignition in bay 5, initial temperature 27.5 °C- 28.0 °C, initial pressure 82 kPa, vented.

Figure 26 presents similar results for tests 34 and 34a (All strong, ignition in bay 1, initial temperature 39.0-38.7 °C, initial pressure 82 kPa, vented). Again FLACS

seems to predict trends also seen in the experiments but the agreement between simulation and experiment varies from partition to partition. For some partitions the agreement is better with experiment 34 (SWB1, PR (bay3-bay4)) and sometimes the agreement is better with experiment 34a (MS (bay4-bay2), PR (bay5-bay6)). This highlights also the variations in the experiments.

Figure 27 shows a third example (Test 35, 35a and 35b; all strong, ignition in bay 2, initial temperature 40.0 °C - 40.1 °C, initial pressure 82 kPa, vented). This test was repeated twice and although the repeatability for some of the partitions is very good, for others quite some variations can be observed. FLACS seems to follow the trends again but predicts lower pressure differences than seen in the experiments. This may be related to the underprediction of the heat of combustion.

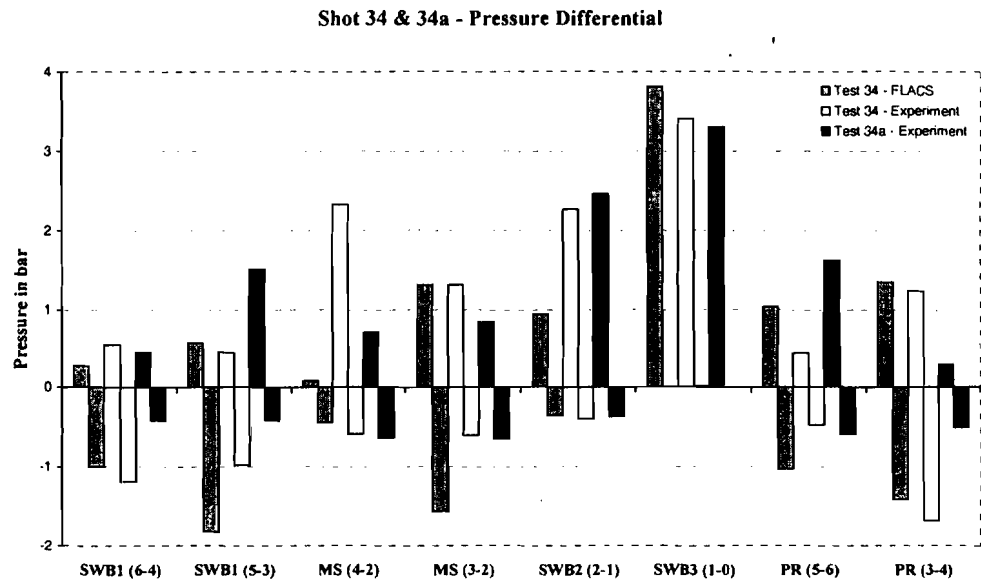


Figure 26 Comparison of predicted and measured pressure differences across the various partitions in the 1/4-scale CWT (forward (positive) and aft (negative) directed). Tests 34 and 34a; test conditions: all strong, ignition in bay 1, initial temperature 39.0-38.7 °C, initial pressure 82 kPa, vented.

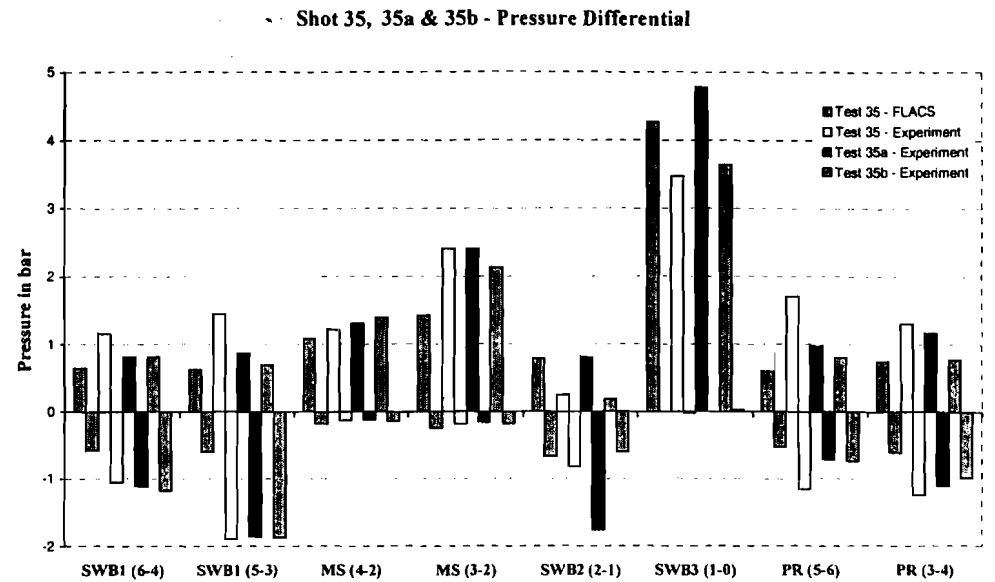


Figure 27 Comparison of predicted and measured pressure differences across the various partitions in the 1/4-scale CWT (forward (positive) and aft (negative) directed). Test 35, 35a and 35b; test conditions: all strong, ignition in bay 2, initial temperature 40.0 °C - 40.1 °C, initial pressure 82 kPa, vented.

All simulations performed for the 1/4-scale simulant fuel tests have been used to investigate the quality of the predictions. The quality of the predictions expressed in systematic average deviations and standard deviation can be used in the rule-based analysis of the accident as developed by Combustion Dynamics (Thibault, 1999).

Table 2 presents a summary of the deviations between FLACS predictions and experiments performed for all strong configurations (in total 22 tests, viz. tests 4, 5, 6, 7, 9, 10, 11, 12, 15, 16, 25, 31a, 31b, 32, 33, 34, 34a, 35, 35a, 35b, 36 and 39). Only pressure differences across the various partitions were considered in the exercise since these in general are the only loads that need to be taken into account. Moreover these pressures are a result of a very complex explosion process where small differences in time of arrival at openings in the partitions may give big variations (the pressure differences will tell the worst story regarding the quality of the code in comparison to the experiments and the repeatability of the experiments). It should be remarked that the results in a few of these tests have been affected by difficulties (in test 6 ignition of bay 1 occurred via the fuel manifold, in test 9 there was a liquid jet fuel residue, in test 35 the filament broke) affecting the presented statistics as well.

The Table presents for each partition and for each direction of the loading the average overall deviation of the predicted pressure difference compared to the average measured pressure difference  $\{[(\sum p_{i,sim}/n - \sum p_{i,exp}/n)] / \sum p_{i,exp}/n\} * 100$ . Further the average relative deviation  $\sum \{[(p_{i,sim} - p_{i,exp}) / p_{i,exp}] * 100\} / n$  and the standard deviation of this parameter are given.

The table shows that if the average overall deviation of the predictions in one force direction is small it is large in the other direction. A small average overall deviation may still lead to a relatively big relative deviation and superposed standard deviation.

To judge the relative deviation of the simulations compared to the experiments one should also take into account the standard deviation of the repeated experiments. Table 2 presents the standard deviation of repeated experiments compared to the average pressure difference measured in these experiments. A comparison to all repeated experiments (13 in total: test nos. 4, 31a, 31b, 32, 33, 34, 34a, 7, 6, 35, 35a, 35b and 36) and repeated experiments where the temperature was held constant (7 in total: test nos. 31a, 31b, 34, 34a, 35, 35a and 35b) is shown. The population of the experiments with constant initial temperature is relatively small (7). The table shows that the repeatability of the experiments where the initial temperature was held constant is slightly better than where the initial temperature varied.

Figure 28 shows how the simulations compare to the measured pressure differences across SWB2 (front direction). As the Figure shows big variations are seen per scenario in spite of the average deviation of only 2% (See Table 2).

Figure 29 and Figure 30 show how the repeatability of the experiments is, taking into account all experiments (Figure 29) and only experiments where the initial temperature was held constant (Figure 30).

Table 2 Statistics of all-strong simulant fuel simulations and experiments.

Partition	Force direction	FLACS simulations vs. experiments		Repeatability experiments (all)	Repeatability exp. (constant T)
		Average deviation (%)	Average relative deviation +/- standard dev. (%)	standard dev. (%)	standard dev. (%)
SWB2	front	-2	-64+/-126	45	54
	aft	35	20+/-39	36	37
port MS	front	5	-9+/-73	22	12
	aft	-59	-90+/-167	27	7
stbd MS	front	41	18+/-89	43	31
	aft	-6	-27+/-104	17	7
port SWB1	front	39	40+/-39	46	37
	aft	-1	-42+/-123	24	22
stbd SWB1	front	42	23+/-69	54	25
	aft	12	-30+/-101	46	32

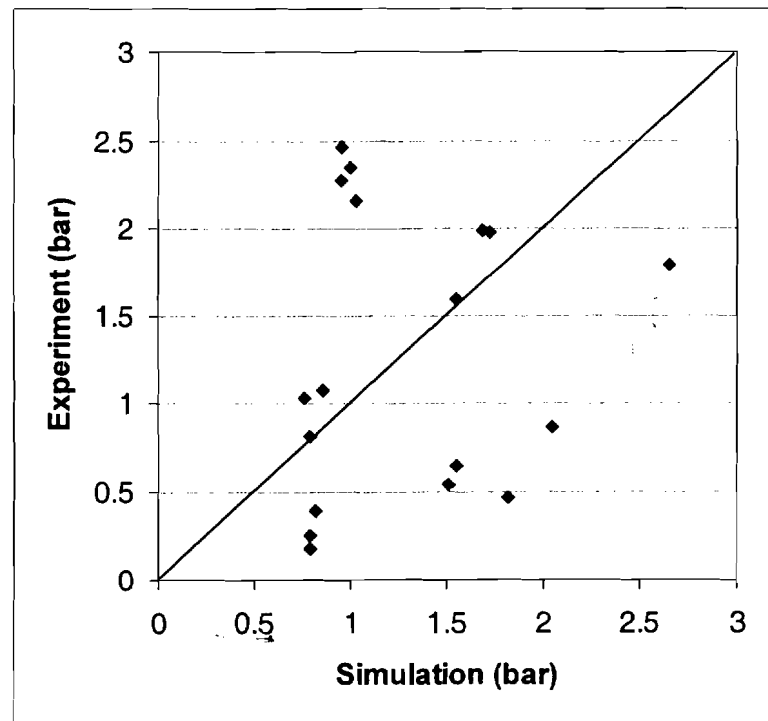


Figure 28 Comparison simulations and experiments for pressure differences acting on SWB2 in the forward direction.



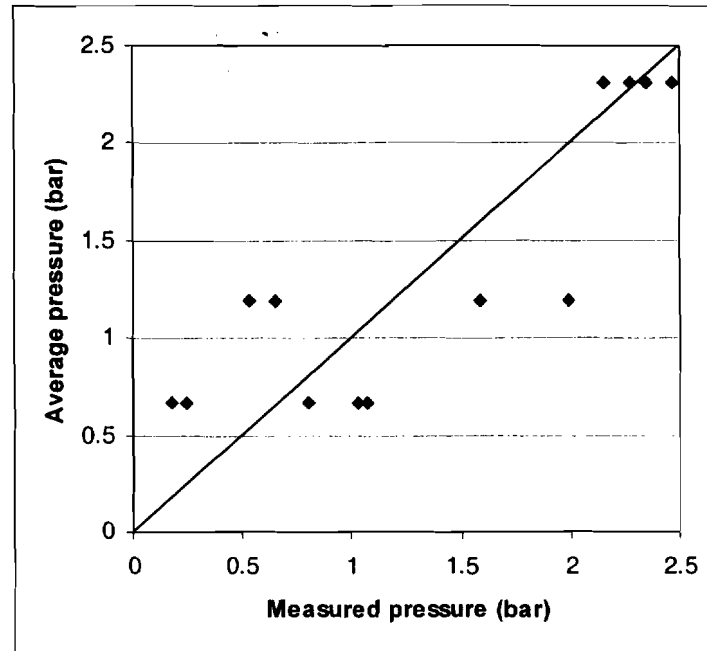


Figure 29 Distribution experimental pressure around average value for various investigated scenarios (all experiments).

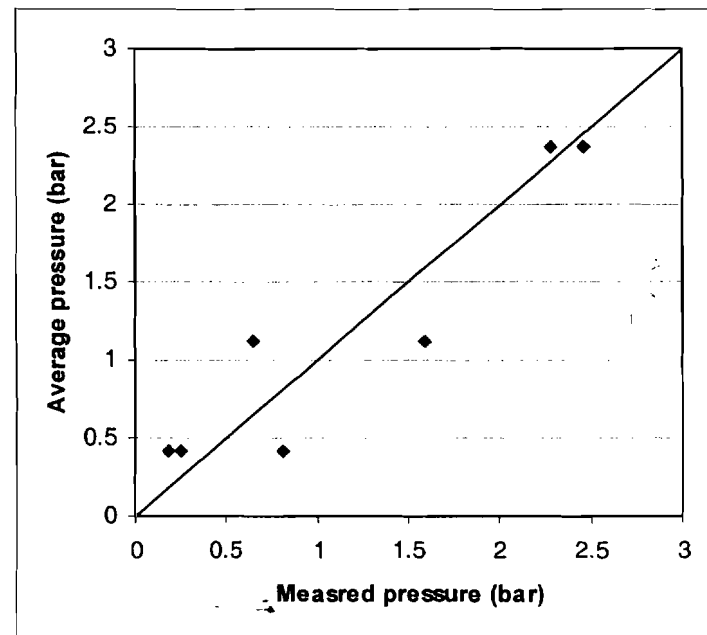


Figure 30 Distribution experimental pressure around average value for various investigated scenarios (experiments involving constant initial temperature).

## 6.2 Predictions: effect of ignition position: 1/4 scale

The most optimal way of determining the location of the ignition source would be to simulate the explosion loads for any position in the Center Wing Tank and to see for which ignition locations the damage seen after the accident corresponds to the loads. For the observed damage evaluation we refer to Thibault (2000). This procedure should ideally been carried out for several gas mixture compositions and perhaps even gas mixture distributions.

The Sandia explosion model (Baer and Gross, 1998) calculates considerably faster than the FLACS code implying that such sensitivity studies can be carried out faster with the Sandia code than with FLACS.

At Sandia a large number of simulations was performed to investigate the sensitivity of ignition source position in the 1/4-scale CWT facility. These simulations were carried out at three horizontal slices through the CWT (one high level, one mid-level and one low-level slice) with a high resolution (3 cm distance between ignition source positions).

An example of a result presentation of the Sandia simulations is shown in Figure 31. The Figure shows the effect of ignition source position on the pressure difference across SWB1 between bays 5 and 3. The force that is considered is acting in the forward direction. The Figure presents the value of the pressure difference across this partition at each ignition source position used. In this case only ignition sources in the mid-level slice through the CWT are shown.

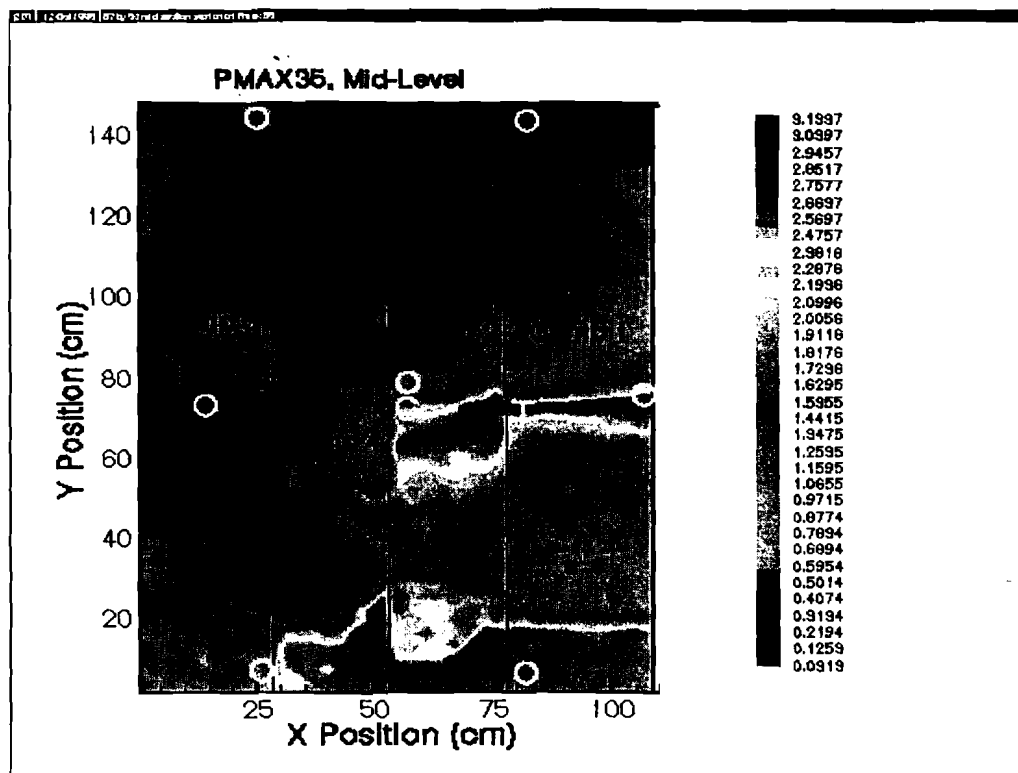


Figure 31 Results of ignition sensitivity study carried out by Sandia considering forward-directed force on SWB1 between bays 3 and 5. Ignition effected with 3 cm resolution at mid-level horizontal slice through CWT.

The Figure shows that the loads acting on this very partition can vary very strongly when the ignition is relocated slightly. Very high pressure differences seem to occur when ignition is effected close to the centre of axis of the starboard side of bay 1 and 2. A similar high pressure zone is observed towards the outskirts of the starboard side of bays 1 and 2.

Using FLACS, similar simulations were performed for a limited area inside the 1/4-scale CWT. A more coarse resolution was used in the FLACS simulations than in the Sandia simulations. The area that was considered (ignition source position) concerns the central area of bay 2 only (full length and central 37.5 % of width) at three horizontal slices, midway, near the bottom and near the roof of the CWT.

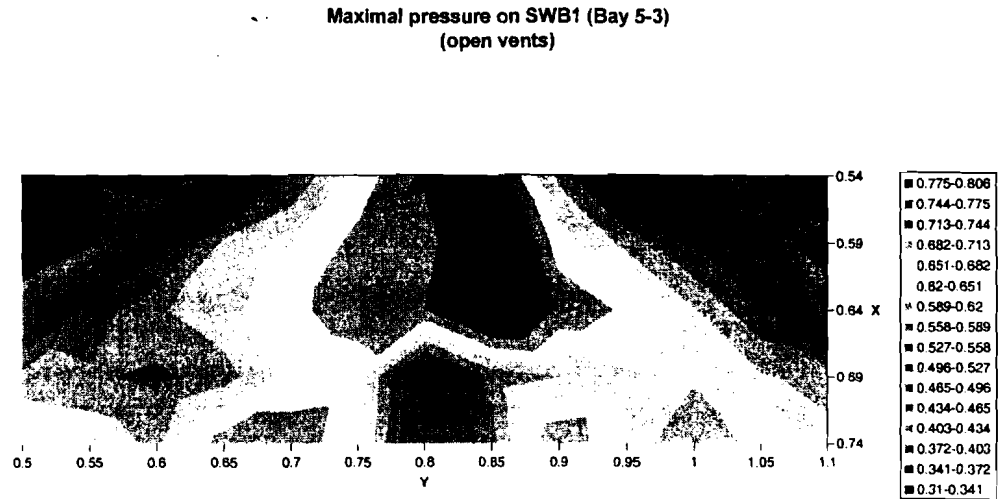


Figure 32 Results of ignition sensitivity study carried out with FLACS considering forward-directed force on SWB1 between bays 3 and 5. Ignition effected with 5 cm resolution at mid-level horizontal slice through CWT (i.e. central region of bay 2).

Figure 32 shows the results of ignition effected at mid-level in bay 2 on the force acting forward on the part of SWB1 separating bays 5 and 3. A comparison with the results presented in Figure 31 shows that the simulations performed with FLACS confirm the findings of the Sandia simulations qualitatively. On the other hand it should be observed that where FLACS predicts an increase of the forward directed force on SWB1 when moving from starboard to port close to in the central area of the bay the Sandia code predicts a decrease of the loading FLACS predicts an increase. The absolute values of the pressure difference are also considerably higher according to the Sandia code than they are according to the FLACS predictions.

Both the FLACS and Sandia predictions can be used to perform a rule based scenario analysis as put forward by Combustion Dynamics (Thibault, 1999) assuming that the 1/4-scale experiments using the simulant fuel are sufficiently representative of what happened on full-scale with Jet-A.

### 6.3 Predictions: effect of ignition source position: full-scale

An analysis to investigate the effect of the ignition source position was performed for the real Center Wing Tank geometry. The variation of the ignition source

position was limited to the seven fuel probe positions and the position of the compensator. The geometry schematically shown in Figure 33 is based on the details given in Shepherd et al. (1997a). The representation of the geometry takes into account the fact that the fuel tank is higher on the front end than it is near the RS (Figure 1). The width is not changing. To take the smaller volume of the bays near the RS into account the height of the bays has been varied accordingly across the length of the CWT. This is the only possibility to represent the inclination of the tank on a Cartesian grid. The ribs on some of the partitions of the Center Wing Tank (See Figure 34) and other details such as some baffles were not taken into account. These ribs and baffles could act as obstacles generating additional turbulence during an explosion event. The various openings in the partitions and the manufacturing door in SWB2 were represented. These were located and sized as in reality although minor differences with respect to position had to be introduced to account for the varying height of the various bays. To accommodate the annular holes around the vents running from bays 3 to 1 and 6 and 1, separate holes were introduced with the same cross section. These holes were positioned right next to the vents.

The manufacturing door in SWB2, the FS and SWB3 were allowed to fail. The properties of these panels were chosen as follows:

FS: failure pressure 0.48 bar<sup>3</sup>, weight 1168 kg, area 13.0 m<sup>2</sup>

SWB3: failure pressure 1.5 bar, weight 221 kg, area 13.0 m<sup>2</sup>

The failure pressure of the manufacturing panel in SWB2 was a variable and adjusted to give a desired moment of failure relative to the failure of SWB3. The panel has a weight of 2.8 kg and an area of 0.44 m<sup>2</sup>. Thibault (1999) present the results of a calculation assuming that the manufacturing door in SWB2 failed due to keel beam loading. This loading would be produced through a combination of pressurisation of the CWT, and the successive failure of SWB3, FS and the fuselage. His calculation shows that the panel must have failed during a period lasting 0-24 ms after the failure of FS.

---

<sup>3</sup> The failure of FS was based on either the impact time of SWB3 on FS which occurred according to calculations 16 ms after failure of SWB3 or the time when the pressure differential across FS exceeds 0.482 bar which is the failure pressure of FS when a neighbouring beam (SWB3) has already failed (which ever first occurred).

Thus a total of 32 full-scale CWT simulations were performed covering the following situations:

Initial temperature 50 °C, moment of failure of manufacturing panel 24 ms after failure of FS, eight ignition positions

Initial temperature 50 °C, moment of failure of manufacturing panel at moment of failure of FS, eight ignition positions

Initial temperature 40 °C, moment of failure of manufacturing panel 24 ms after failure of FS, eight ignition positions

Initial temperature 40 °C, moment of failure of manufacturing panel at moment of failure of FS, eight ignition positions

The 8 ignition source positions have been given in Figure 33 and in Table 3.

Table 3 Ignition source positions used during full-scale simulations

<b>ID</b>	<b>Item</b>	<b>Location</b>
<b>1</b>	<b>Fuel probe</b>	<b>Bay 1 port</b>
<b>2</b>	<b>Fuel probe</b>	<b>Bay 1 mid</b>
<b>3</b>	<b>Fuel probe</b>	<b>Bay 1 starboard</b>
<b>4</b>	<b>Fuel probe</b>	<b>Bay 2 mid, high</b>
<b>5</b>	<b>Compensator</b>	<b>Bay 2 mid, low</b>
<b>6</b>	<b>Fuel probe</b>	<b>Aft Bay 5 port</b>
<b>7</b>	<b>Fuel probe</b>	<b>Aft Bay 6 mid</b>
<b>8</b>	<b>Fuel probe</b>	<b>Aft Bay 6 starboard</b>

The results of the simulations considered especially the loading of each partition as a function of time and the possibility of flame quenching in the various orifices upon flame arrival. The simulations were, however, performed without quenching taking place, i.e. the flame propagated throughout the entire CWT also in situations where according the criterion of Figure 18 quenching should have occurred.

Typical results that were obtained for the pressure-time histories in each bay and the pressure differentials across partitions are shown in Figure 35 and 36. It should be emphasised once more that these simulations were performed with quenching not taking place implying that both the pressure-time histories in each bay and the pressure differences across each partition may differ from what is shown in Figures 35 and 36. A summary of the results is given in Figures 37 to 48 presenting the maximum positive (resulting in a force in forward direction) and negative pressure difference (resulting in a force in aft direction) across each partition for all 32 simulations. The Figures show that there is small relative variation between the loading on the partitions between bays 3 and 2, 4 and 2, 2 and 1 (SWB2) and 1 and 0 (SWB3) for each of the scenarios. For the latter two partitions this may be partially due to the failure of the manufacturing door and partition respectively. The loading on the partitions between bays 5 and 3 and 6 and 4 is much more varying but is relatively small as an absolute value (between 1.5 bar to 1 bar).

The simulations predict that the occurrence of quenching on full-scale is very common. As an example Table 4 presents an overview of Karlovitz numbers obtained in each hole at the moment of flame arrival for 8 simulations performed assuming the following initial conditions: Initial temperature 40 °C, moment of

failure of manufacturing panel at moment of failure of FS. Although the table is based on simulations assuming that flame propagation continues resulting in potentially smaller pressure differences across a hole and therefore lower flow velocities than would have been the case if the flame would not propagate into a neighbouring bay the Karlovitz numbers are still very high in general, indicating quenching.

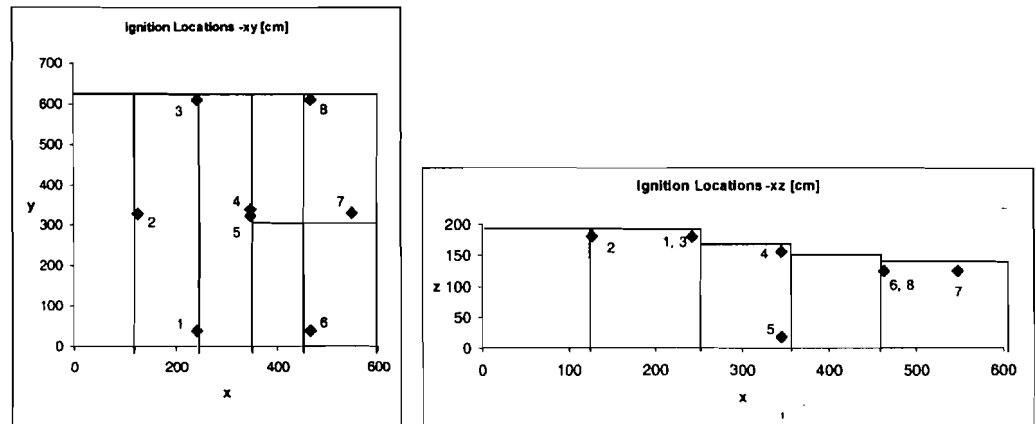


Figure 33 Representation of the Center Wing Tank in FLACS.



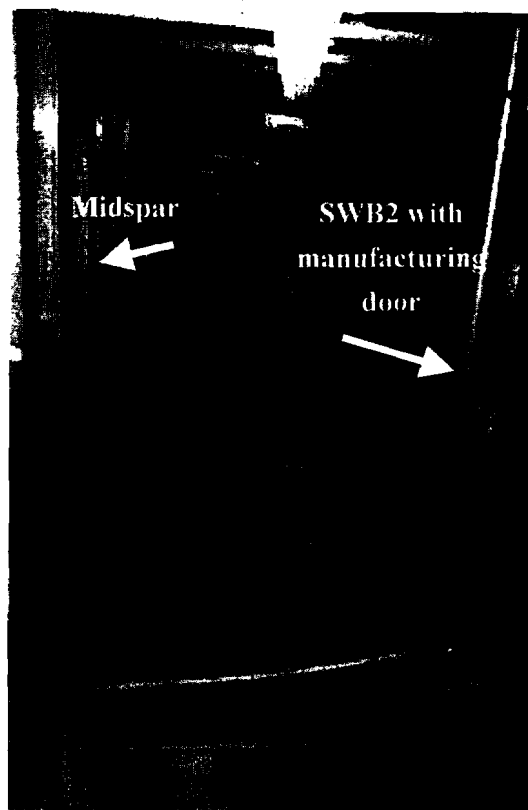


Figure 34 View inside Center Wing Tank of Boeing 747-100 (bay 2 in between MS and SWB2), showing the manufacturing panel in SWB2 and the ribs on the MS. Further the baffles on the floor should be noted.

It should be emphasised that the velocity through the holes was calculated on the basis of the pressure difference across the hole using standard orifice equations:

$$U = \frac{C_D}{\rho_u} \left\{ \frac{2\rho_u \gamma_u P}{\gamma_u - 1} \left( \frac{P_a}{P} \right)^{2/\gamma_u} \left[ 1 - \left( \frac{P_a}{P} \right)^{(\gamma_u - 1)/\gamma_u} \right] \right\}^{0.5}$$

where

- $\rho_u$  density ( $\text{kg/m}^3$ )
- $C_D$  discharge coefficient of the hole (=0.8)
- $\gamma_u$  specific heat ratio (=1.4)
- $P$  absolute pressure upstream (Pa)
- $P_a$  absolute pressure downstream (Pa)

This formula accounts for subsonic flow, i.e. when  $\frac{P_a}{P} \geq \left(\frac{2}{\gamma_u + 1}\right)^{\gamma_u/(\gamma_u - 1)}$

Otherwise, for a supersonic flow, the equation to apply is

$$U = C_D \left( \frac{\gamma_u P}{\rho_u} \left( \frac{\gamma_u + 1}{2} \right)^{(1 + \gamma_u)/(\gamma_u - 1)} \right)^{0.5}$$

The pressures upstream and downstream are measured at the moment of the flame arrival at the considered hole. In the FLACS calculations the flow velocity through the holes was based upon the average pressures in each of the two relevant bays.

The specific heat ratio  $\gamma_u$  is assumed as constant during the chemical reaction and equal at 1.4.

$\rho_u$  represents the density of the mixing just before the hole at the time of the flame arrival at the hole. The density can be defined as a function of the pressure based on the initial conditions:

$$\rho_u = \rho_o \left( \frac{P}{P_o} \right)^{1/\gamma}$$

where

- $\rho_o$  initial density of the mixing ( $\text{kg/m}^3$ )
- $P_o$  initial absolute pressure (bar)
- $P$  absolute pressure (upstream) at flame arrival (bar)
- $\gamma$  specific heat ration (=1.4)

The density used in these equations was calculated by FLACS directly from local prevailing conditions.

As mentioned above the FLACS simulations indicate that quenching would be a common event on full-scale as also was seen during the 1/4-scale experiments. Using the Karlovitz number - "probability of quenching" relationship as developed on the basis of 2-bay and 6-bay tests and shown in Figure 18, the full-scale simulations

were reviewed regarding the possibility and likelihood of transmission into neighbouring bays starting from the bay in which ignition was effected.

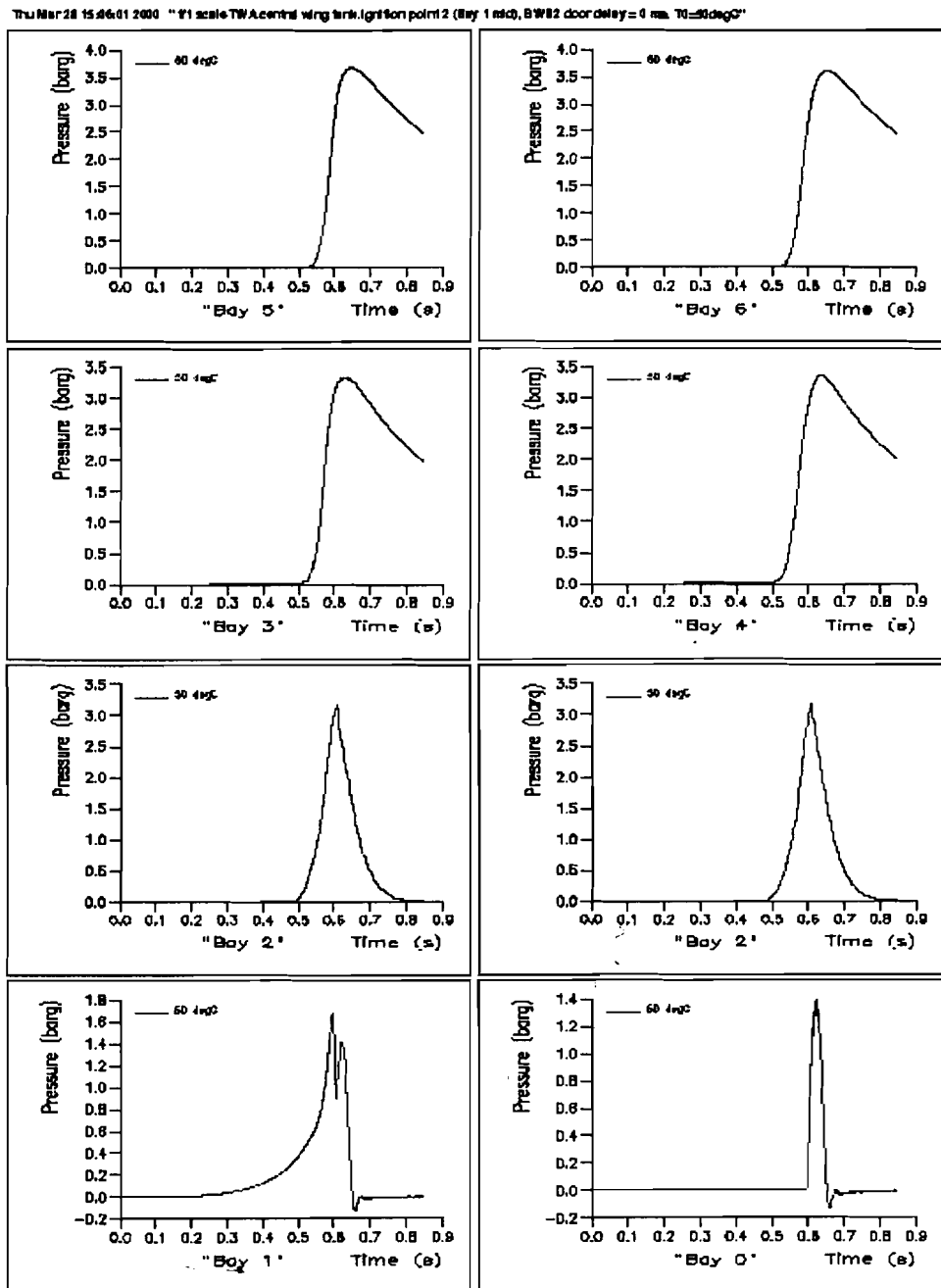


Figure 35 Prediction of pressure-time histories in each bay of the full-scale CWT assuming a fuel temperature of 50 °C and ignition at ignition point 2 (see Figure 33).

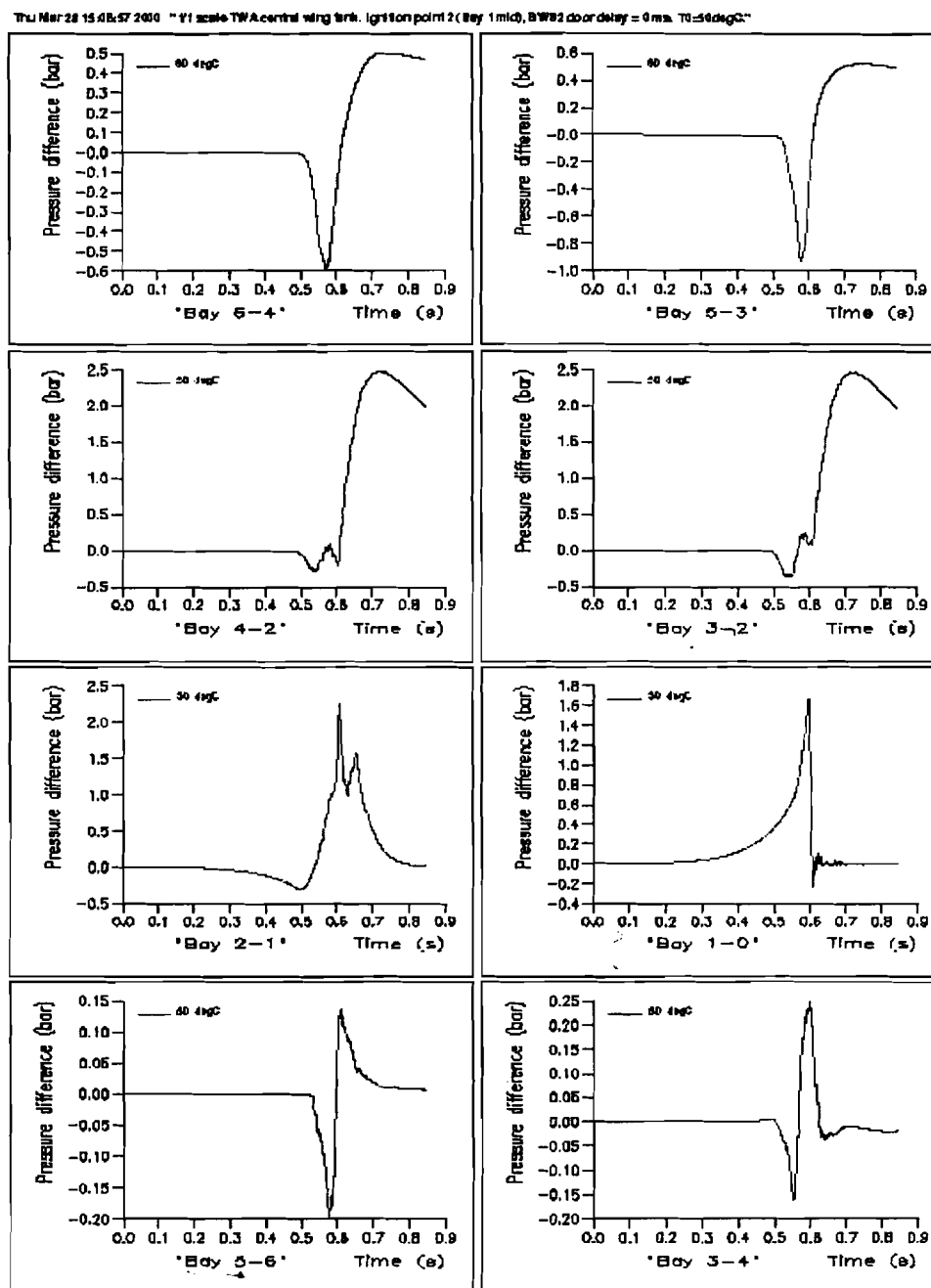


Figure 36 Prediction of pressure difference time histories across each partition of the full-scale CWT assuming a fuel temperature of 50 °C and ignition at ignition point 2 (see Figure 33).

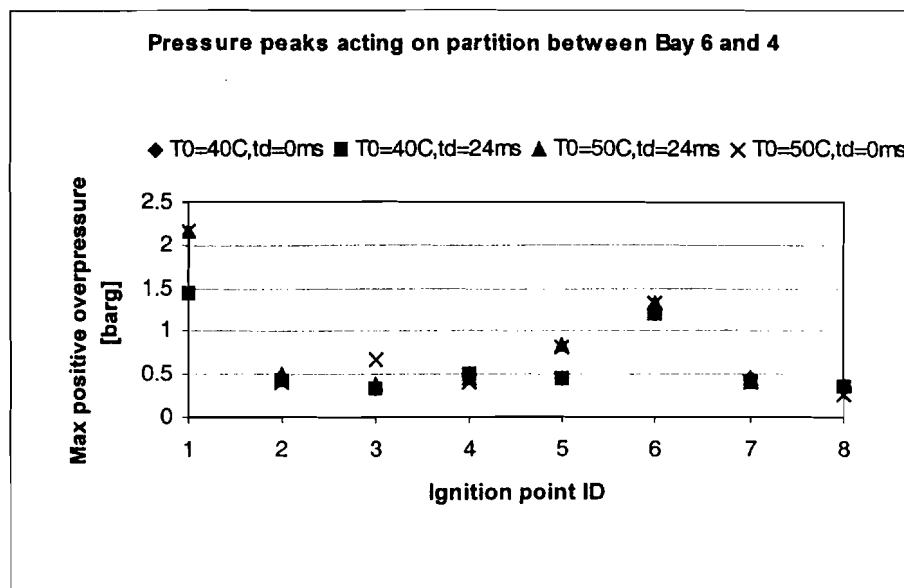


Figure 37 Maximum positive pressure load (resulting in forward directed load) acting on the partition between bays 6 and 4 for each of the 32 chosen explosion scenarios.

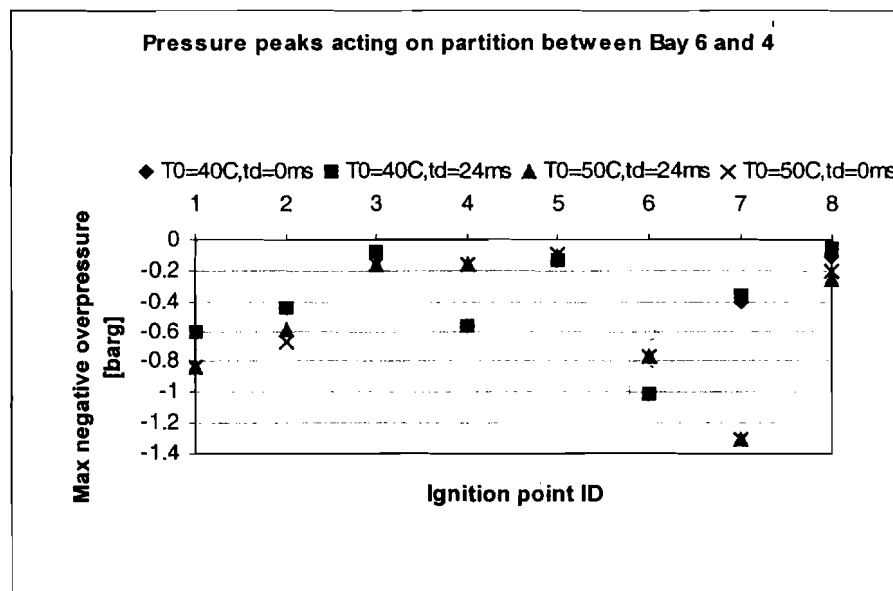


Figure 38 Maximum negative pressure load (resulting in aft directed load) acting on the partition between bays 6 and 4 for each of the 32 chosen explosion scenarios.

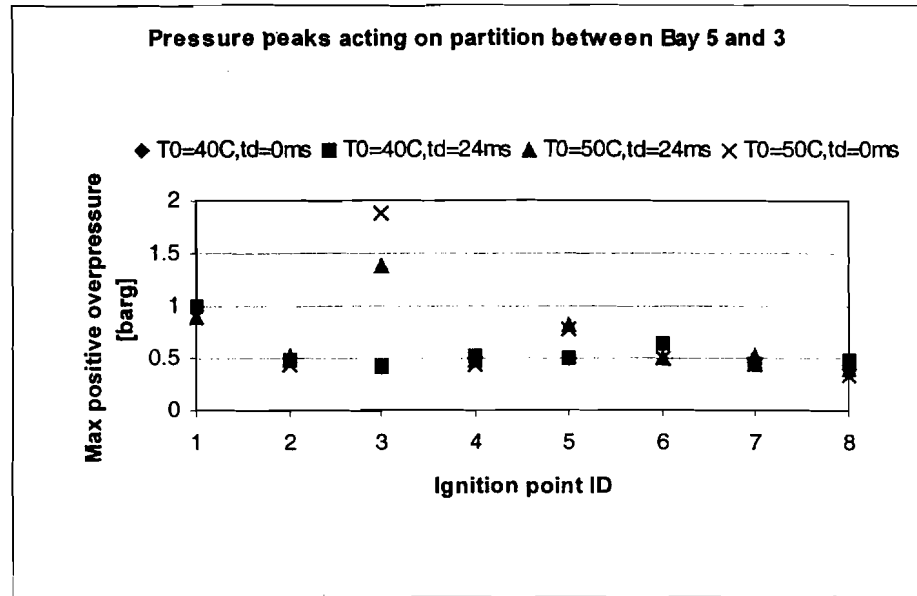


Figure 39 Maximum positive pressure load (resulting in forward directed load) acting on the partition between bays 5 and 3 for each of the 32 chosen explosion scenarios.

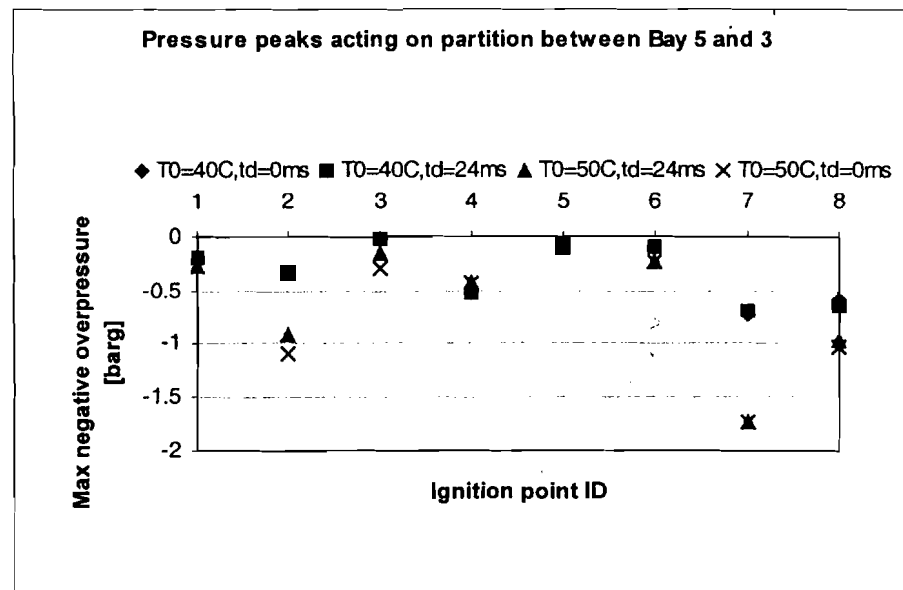


Figure 40 Maximum negative pressure load (resulting in aft directed load) acting on the partition between bays 5 and 3 for each of the 32 chosen explosion scenarios.

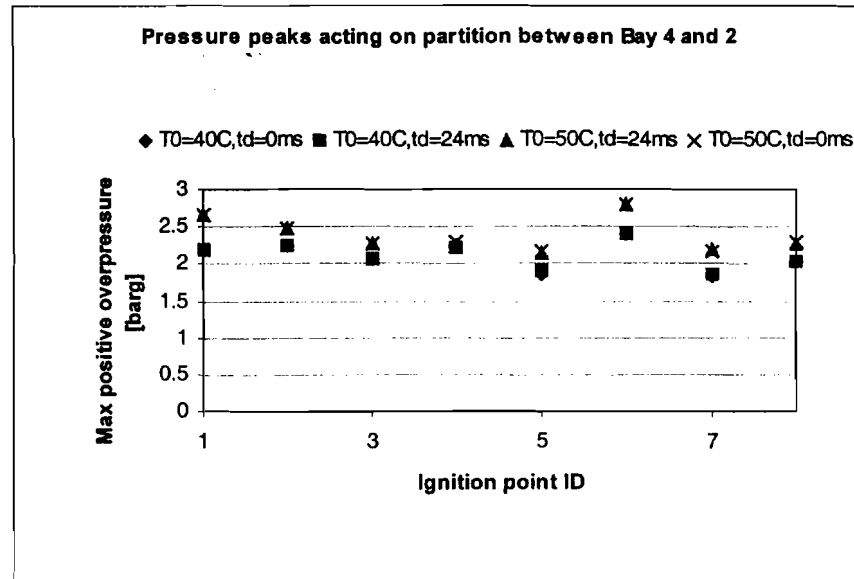


Figure 41 Maximum positive pressure load (resulting in forward directed load) acting on the partition between bays 4 and 2 for each of the 32 chosen explosion scenarios.

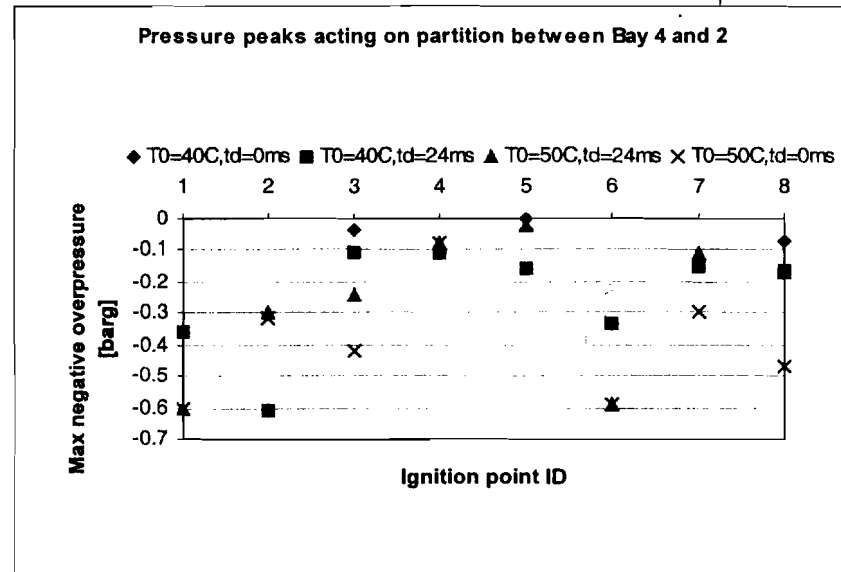


Figure 42 Maximum negative pressure load (resulting in aft directed load) acting on the partition between bays 4 and 2 for each of the 32 chosen explosion scenarios.



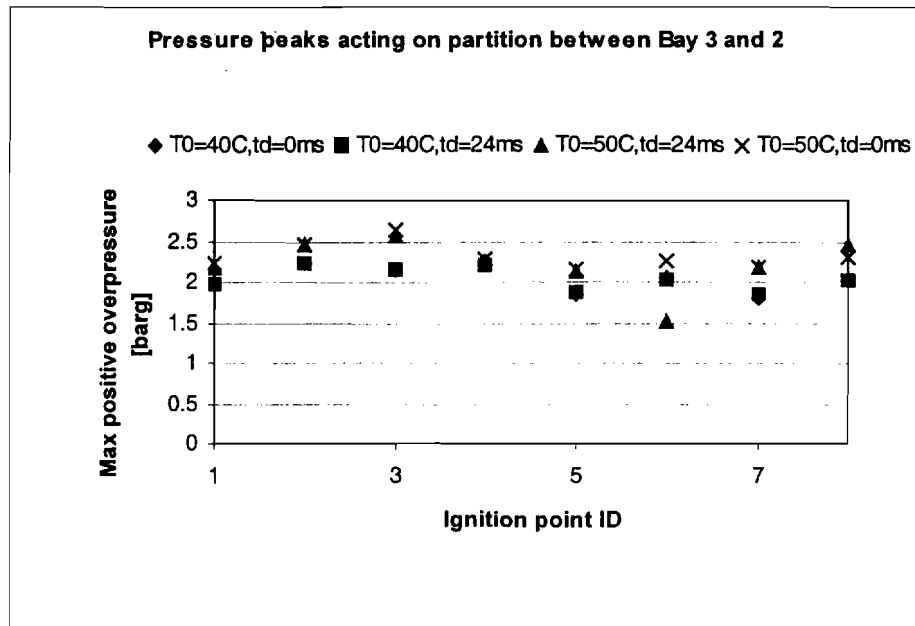


Figure 43 Maximum positive pressure load (resulting in forward directed load) acting on the partition between bays 3 and 2 for each of the 32 chosen explosion scenarios.

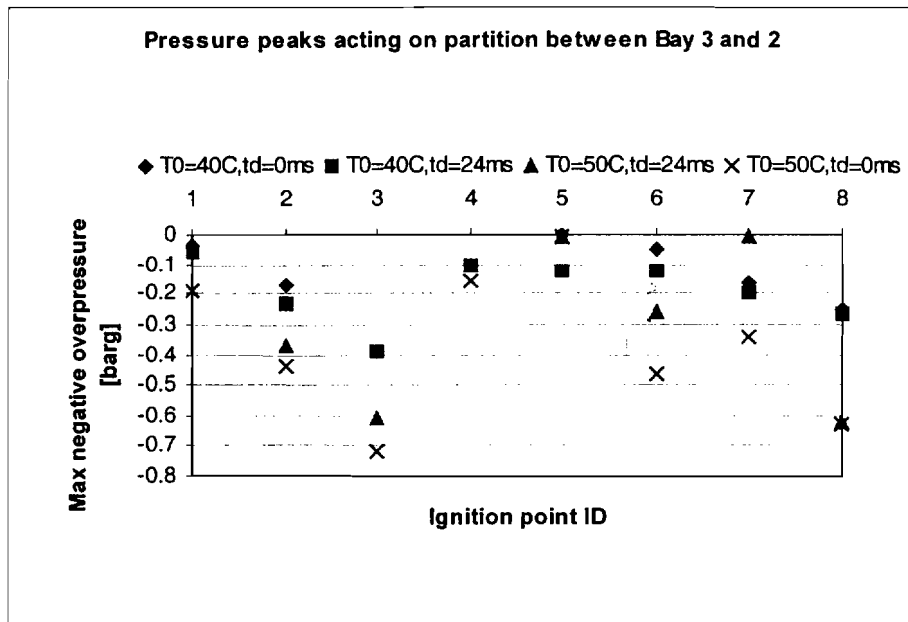


Figure 44 Maximum negative pressure load (resulting in aft directed load) acting on the partition between bays 3 and 2 for each of the 32 chosen explosion scenarios.

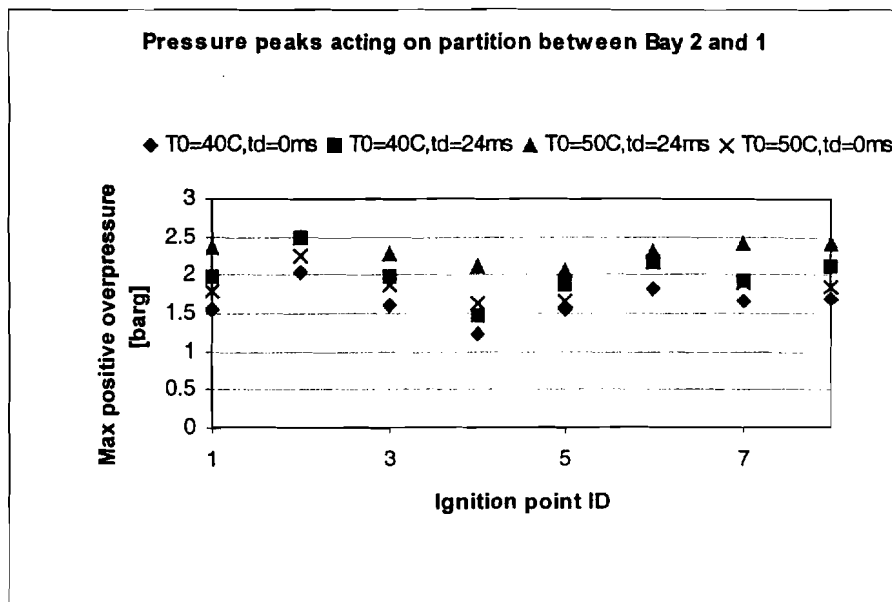


Figure 45 Maximum positive pressure load (resulting in forward directed load) acting on the partition between bays 2 and 1 for each of the 32 chosen explosion scenarios.

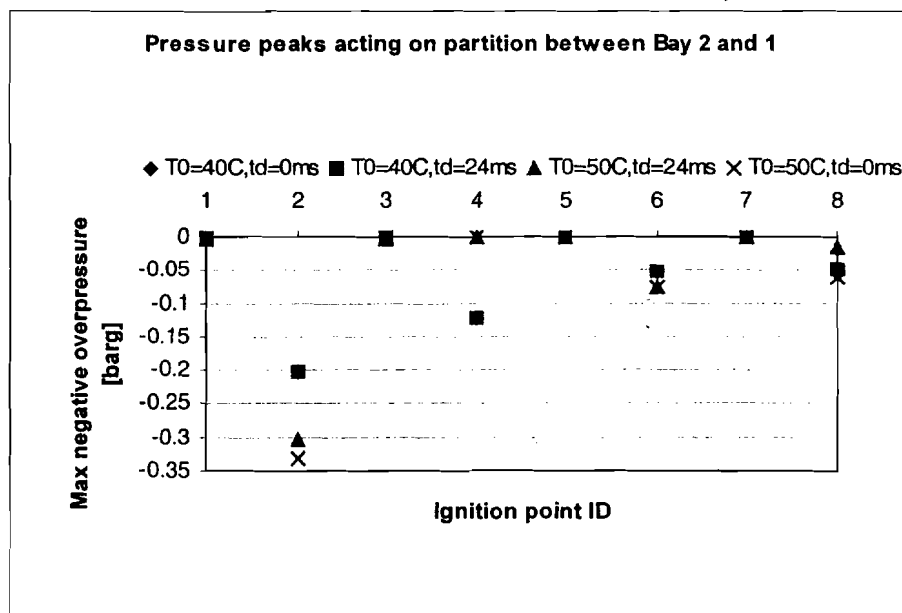


Figure 46 Maximum negative pressure load (resulting in aft directed load) acting on the partition between bays 2 and 1 for each of the 32 chosen explosion scenarios.

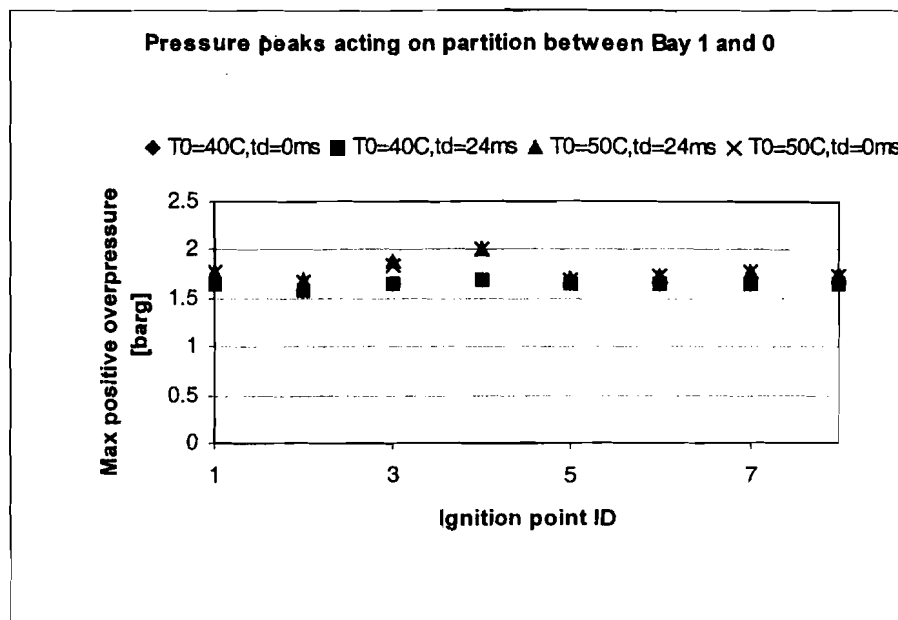


Figure 47 Maximum positive pressure load (resulting in forward directed load) acting on the partition between bays 1 and 0 for each of the 32 chosen explosion scenarios.

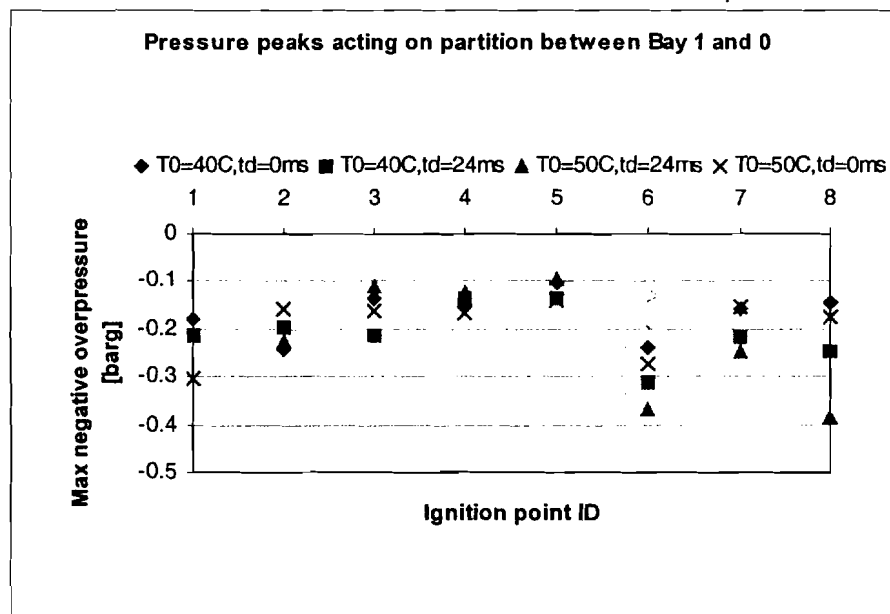


Figure 48 Maximum negative pressure load (resulting in aft directed load) acting on the partition between bays 1 and 0 for each of the 32 chosen explosion scenarios.

Table 4 Overview of Karlovitz number predicted in each hole present in the CWT for the following initial conditions: initial temperature 40 °C, moment of failure of manufacturing panel at moment of failure of FS, eight ignition positions (IP1-IP8).

	Partition	Passage	D hole (m)	IP1	IP2	IP3	IP4	IP5	IP6	IP7	IP8
9	Partial rib (SWB1/MS)*	lower shear ties	0.0747	282	933	-	-	52	-	561	983
10	Partial rib (SWB1/MS)*	lower shear ties	0.0747	-	1106	-	-	52	-	639	-
11	Partial rib (SWB1/MS)*	lower shear ties	0.0747	-	1103	709	-	33	-	656	-
12	Partial rib (SWB1/MS)*	upper shear ties	0.0629	-	1069	-	-	59	-	694	-
13	Partial rib (SWB1/MS)*	upper shear ties	0.0629	-	2512	-	-	-	-	693	-
14	Partial rib (SWB1/MS)*	upper shear ties	0.0629	-	2228	1187	468	-	1174	-	-
15	Partial rib (SWB1/MS)*	upper shear ties	0.0629	-	2238	1177	560	-	1176	-	-
16	Partial rib (SWB1/MS)*	upper shear ties	0.0629	672	2306	1163	601	210	1170	-	-
17	Partial rib (RS/SWB1)*	lower shear ties	0.0669	-	254	-	-	378	-	22	-
18	Partial rib (RS/SWB1)*	lower shear ties	0.0669	-	210	-	257	209	-	230	-
19	Partial rib (RS/SWB1)*	lower shear ties	0.0669	638	-	-	521	222	-	135	-
20	Partial rib (RS/SWB1)*	lower shear ties	0.0669	976	931	-	647	344	-	25	-
21	Partial rib (RS/SWB1)*	lower shear ties	0.0669	1082	1091	-	620	325	935	-	-
22	Partial rib (RS/SWB1)*	lower shear ties	0.0669	1096	1089	-	592	370	1057	165	-
23	Partial rib (RS/SWB1)*	lower shear ties	0.0669	1082	1087	-	576	205	1046	37	-
24	Partial rib (RS/SWB1)*	upper shear ties	0.0572	-	-	-	143	507	-	0	1110
25	Partial rib (RS/SWB1)*	upper shear ties	0.0572	-	-	-	176	514	-	-	1103
26	Partial rib (RS/SWB1)*	upper shear ties	0.0572	-	-	1223	-	506	-	4	1063
27	Partial rib (RS/SWB1)*	upper shear ties	0.0572	-	-	1257	-	505	604	0	1094
28	Partial rib (RS/SWB1)*	upper shear ties	0.0572	1189	1015	1244	-	546	1053	0	1113
29	Partial rib (RS/SWB1)*	upper shear ties	0.0572	1191	935	1256	-	514	946	5	893
30	Partial rib (RS/SWB1)*	upper shear ties	0.0572	-	1067	1252	232	476	998	0	-
31	Partial rib (RS/SWB1)*	upper shear ties	0.0572	1192	1169	1254	662	438	1120	0	-
32	Partial rib (RS/SWB1)*	upper shear ties	0.0572	1176	1176	1254	675	516	1124	-	-
69	Partial rib (RS/SWB1)*	Fuel flow hole	0.1270	782	773	811	444	53	781	3	463
70	Partial rib (RS/SWB1)*	Fuel cross feed line	0.0159	2149	2196	2172	1235	-	2159	0	-
71	Partial rib (RS/SWB1)*	Fuel jettison line	0.0191	1981	2035	-	1142	416	1989	0	-
72	Partial rib (RS/SWB1)*	APU fuel line	0.0064	3488	3541	3722	1841	1215	3359	0	-
33	SWB1	lower stringer hole port	0.0731	604	897	-	1025	-	-	-	1173
34	SWB1	lower stringer hole stbd	0.0731	-	-	-	1052	-	1202	-	195
35	SWB1	upper stringer hole port	0.0521	363	674	-	985	-	41	185	1375
36	SWB1	upper stringer hole stbd	0.0521	727	710	231	923	402	-	-	-
37	SWB1	Fuel vent circum ***	0.0095	789	2091	725	726	997	-	-	19
68	SWB1	Fuel Vent pipe ****	0.0889	-	811	-	-	-	4009	966	64
38	SWB1	Refuel Manifold port	0.0127	1560	1577	-	2499	687	1026	709	2866
39	SWB1	Refuel Manifold stbd	0.0127	-	1810	-	2506	-	7480	-	253
40	SWB1	Jettison	0.0064	-	2369	-	3147	-	12803	-	-
41	SWB1	Scavenge	0.0064	-	2563	-	-	1390	2438	1743	3283
42	SWB1	Flow hole port	0.0699	-	753	-	1023	449	482	338	1161
43	SWB1	Flow hole stbd	0.0699	-	734	-	1005	-	2633	-	207
44	MS	lower stringer hole port	0.0702	-	-	-	-	-	-	1130	1193
45	MS	lower stringer hole stbd	0.0702	-	-	-	-	-	5404	-	263
46	MS	upper stringer hole port	0.0521	332	-	-	-	-	218	1000	8693
47	MS	upper stringer hole stbd	0.0521	-	-	326	-	-	7183	475	249
48	MS	Fuel vent circum port ***	0.0095	758	243	-	1528	-	380	3173	3815
49	MS	Fuel vent circum stbd ***	0.0095	-	-	764	1372	-	3330	1768	278
64	MS	Fuel vent pipe port ****	0.0889	-	722	-	-	850	222	1801	5170
67	MS	Fuel vent pipe stbd ****	0.0889	-	806	-	-	-	4668	907	135
50	MS	Refuel Manifold port	0.0191	-	-	-	-	-	852	1864	-
51	MS	Refuel Manifold stbd	0.0191	-	-	-	-	-	1539	1692	0
52	MS	Scavenge	0.0064	-	-	3259	-	23	3061	522	-
53	MS	Flow Hole port	0.0643	-	-	-	-	-	159	1133	1243
64	MS	Flow Hole stbd	0.0643	-	-	-	-	-	1068	1044	-
56	SWB2	lower stringer hole stbd	0.0660	-	-	-	549	877	643	1315	-
56	SWB2	lower stringer hole port	0.0660	-	-	-	559	569	-	1129	591
57	SWB2	upper stringer hole port	0.0521	30	852	-	719	1090	355	1290	1295
58	SWB2	upper stringer hole stbd	0.0521	-	-	36	633	1124	1007	1497	-
59	SWB2	Fuel vent circum port ***	0.0095	62	2201	-	1780	2567	903	2771	1811
60	SWB2	Fuel vent circum stbd ***	0.0095	-	-	57	1505	2239	1528	2803	530
65	SWB2	Fuel vent pipe port ****	0.0889	-	715	-	-	-	-	-	5564
66	SWB2	Fuel vent pipe stbd ****	0.0889	-	800	290	-	-	5137	784	194

For each of the four main starting conditions (1. Jet-A 40 °C, failure of manufacturing panel 24 ms after failure of FS; 2. Jet-A 40 °C, failure of manufacturing panel at moment of failure of FS; 3. Jet-A 50 °C, failure of manufacturing panel 24 ms after failure of FS; 4. Jet-A 50 °C, failure of manufacturing panel at moment of failure of FS) the transmission to neighbouring bays was considered for the eight defined potential ignition positions. The results are

presented in Figures 49 to 52. For each condition (starting condition and ignition point) the CWT is shown. The bays which would be ignited (with 100 % certainty) according to the criterion are shown as solid green fields. Bays with a probability of ignition lower than 1 have been given different shading. These probabilities are derived directly from the "Karlovitz number classes" as given by the criterion of Figure 18. The bays that are "white" do not ignite. To illustrate why bays are considered not to be able to be ignited the lowest Karlovitz number at any hole in the relevant partition has been given at the moment that the flame reaches the first hole in that particular partition. If the Karlovitz number exceeds  $K=300$  ignition is not possible. Blue arrows indicate the direction of the main load in case of ignition of the bay. A question mark indicates that no conclusion can be made for that particular bay. The main reason for the latter is related to the fact that the simulations were performed without effecting quenching when it should have occurred.

# Jet A - 40 C

FS & SWB2 failed 0.016 s after SWB3

✘ Ignition location	K : Minimum Karlovitz number when quenching occurs
□ Ignition	← Load direction on panel
□ Ignition possible at 25 %	
? Indeterminate	

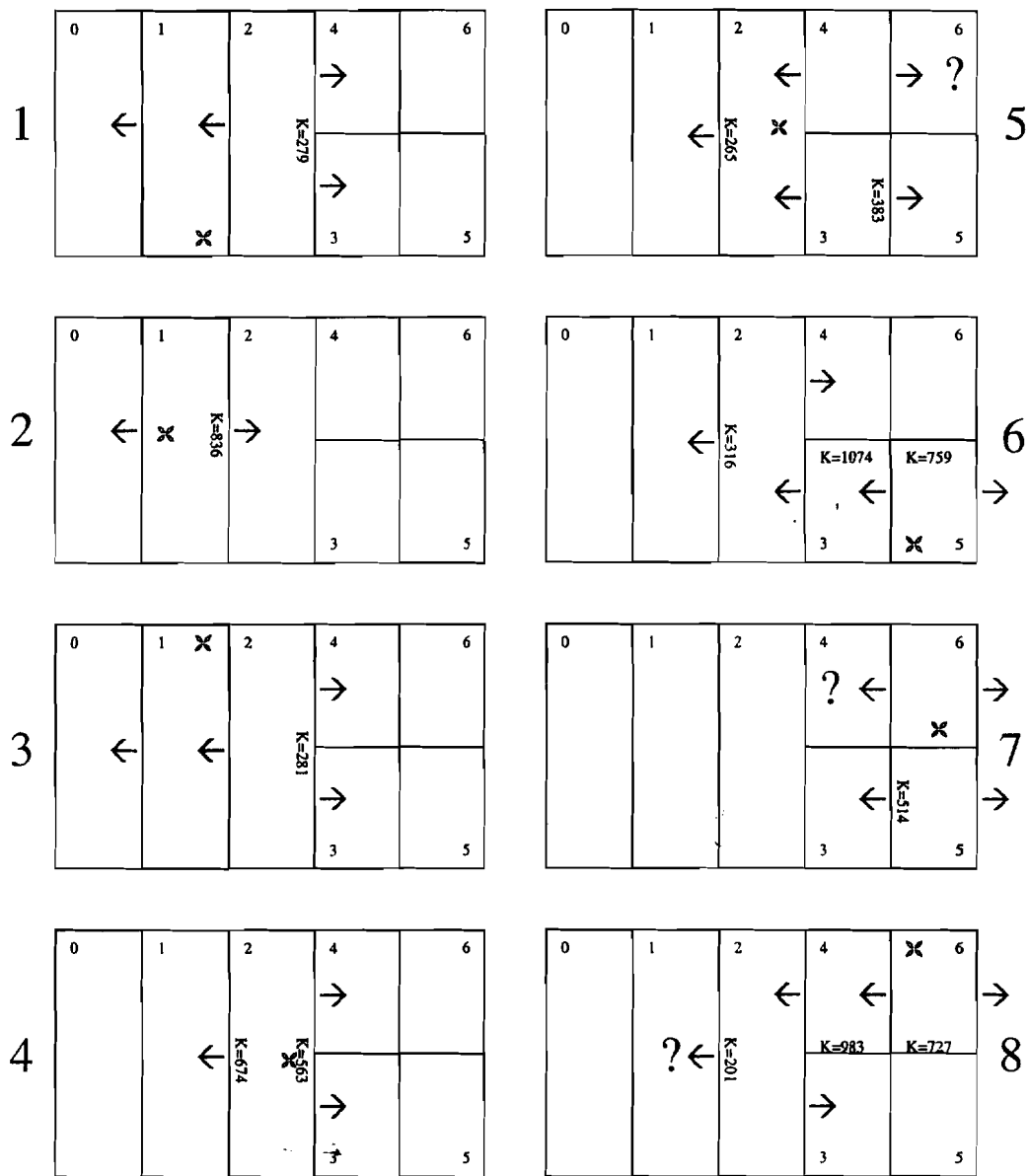


Figure 49 Bays in CWT where explosion will occur (indicated by solid green field) according to FLACS predictions supported by a quenching criterion for 8 different ignition positions (initial conditions: initial temperature 40 °C, moment of failure of manufacturing panel 0 ms after failure of FS).

# Jet A - 40 C

FS failed 0.016 s after SWB3  
 SWB2 failed 0.024 s after FS

✘ Ignition location	K : Minimum Karlovitz number when quenching occurs
□ Ignition	● Load direction on panel
□ Ignition possible at 25 %	
? Indeterminate	

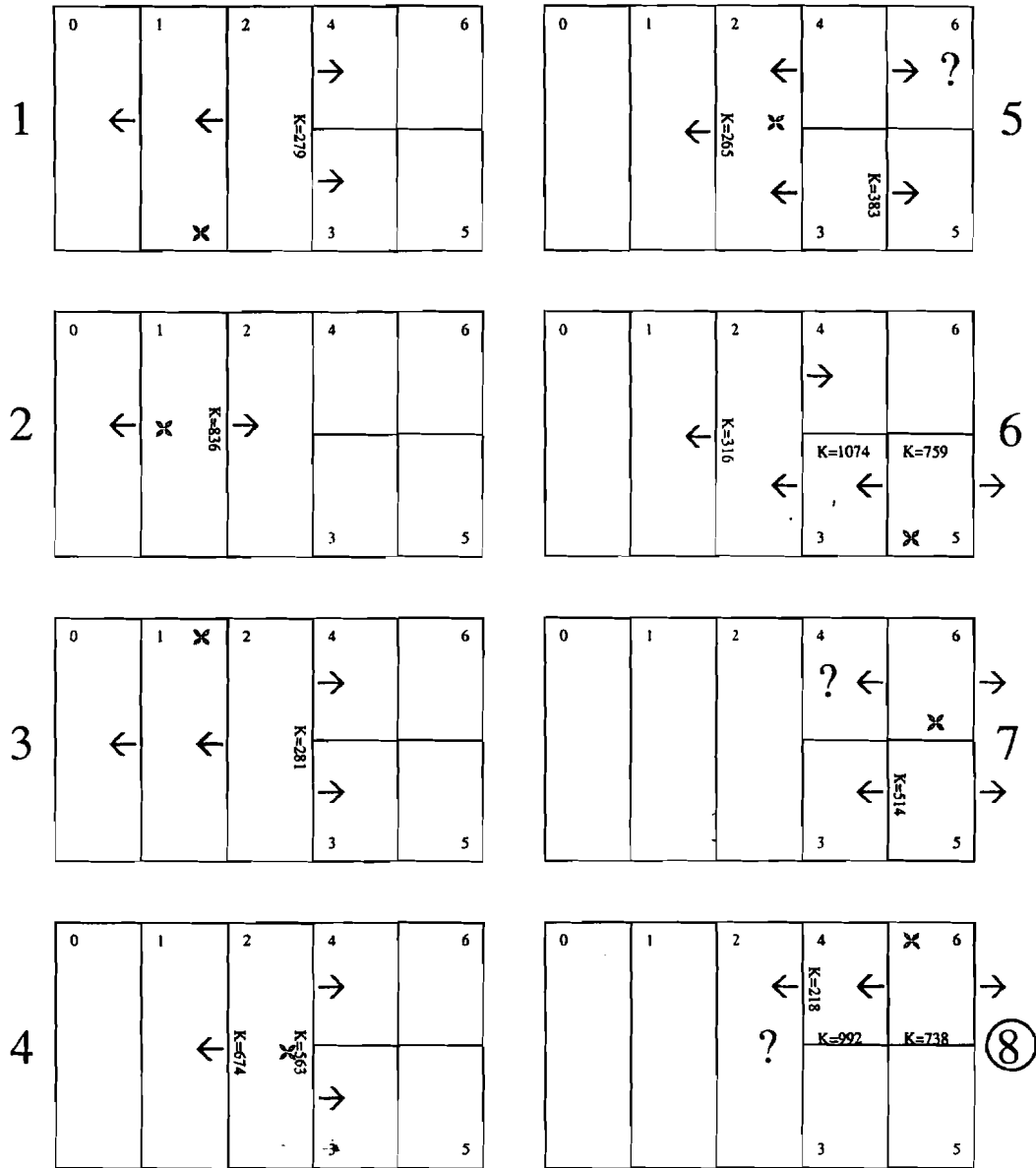


Figure 50 Bays in CWT where explosion will occur (indicated by solid green field) according to FLACS predictions supported by a quenching criterion for 8 different ignition positions (initial conditions: initial temperature 40 °C, moment of failure of manufacturing panel 24 ms after failure of FS).

# Jet A - 50 C

FS & SWB2 failed 0.016 s after SWB3

✖ Ignition location  
? Indeterminate

□ Ignition  
□ Ignition possible at 80 %  
□ Ignition possible at 64 %  
□ Ignition possible at 25 %

□ Ignition possible at 20 %  
K : Minimum Karlovitz number when quenching occurs  
← Load direction on panel

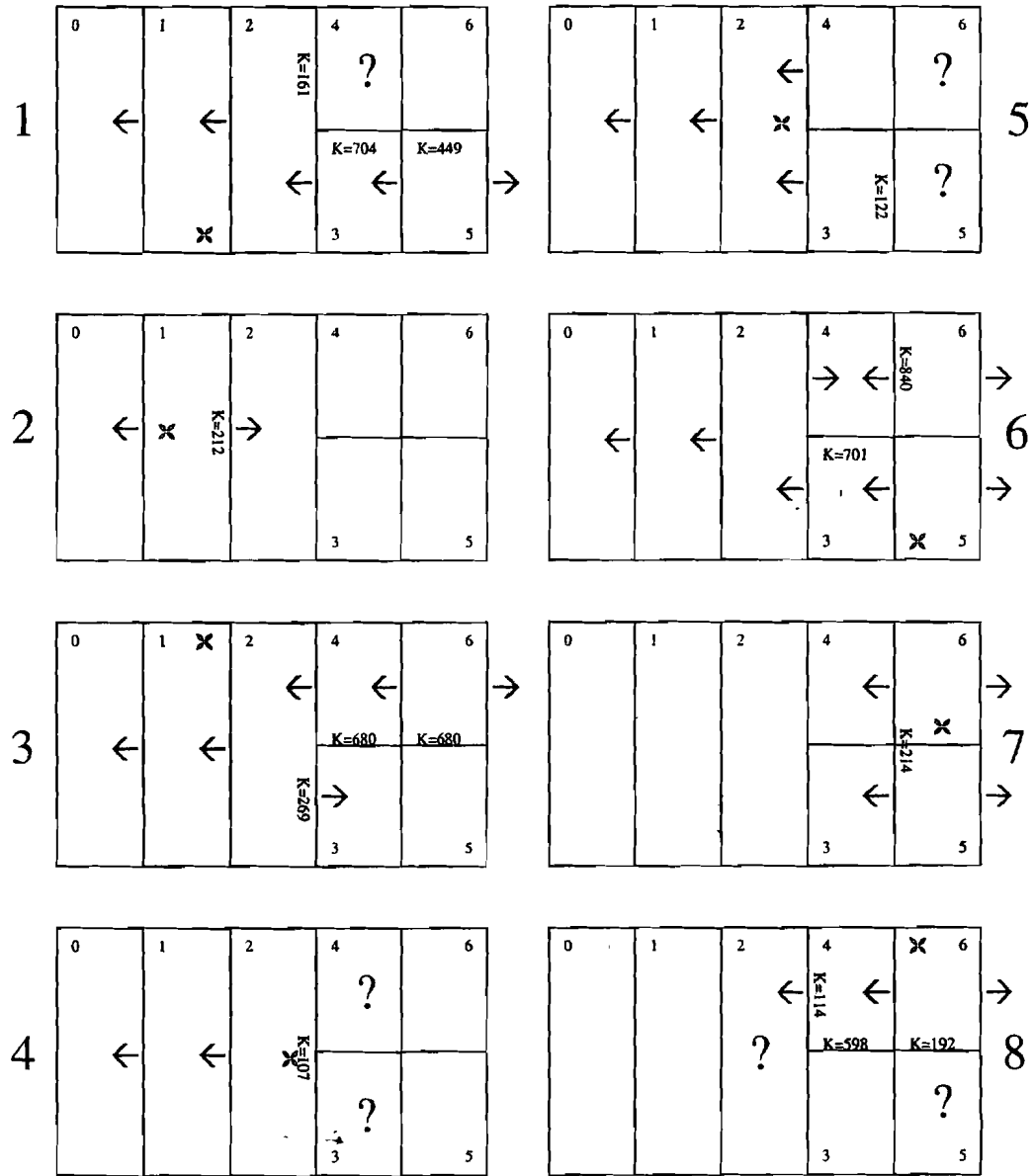


Figure 51 Bays in CWT where explosion will occur (indicated by solid green field) according to FLACS predictions supported by a quenching criterion for 8 different ignition positions (initial conditions: initial temperature 50 °C, moment of failure of manufacturing panel 0 ms after failure of FS).



# Jet A - 50 C

FS failed 0.016 s after SWB3  
 SWB2 failed 0.024 s after FS

<input type="checkbox"/> Ignition	<input type="checkbox"/> Ignition possible at 20 %
<input type="checkbox"/> Ignition possible at 80 %	K : Minimum Karlovitz number when quenching occurs
<input type="checkbox"/> Ignition possible at 64 %	
<input type="checkbox"/> Ignition possible at 25 %	<input type="checkbox"/> Load direction on panel
<input checked="" type="checkbox"/> Ignition location	
? Indeterminate	

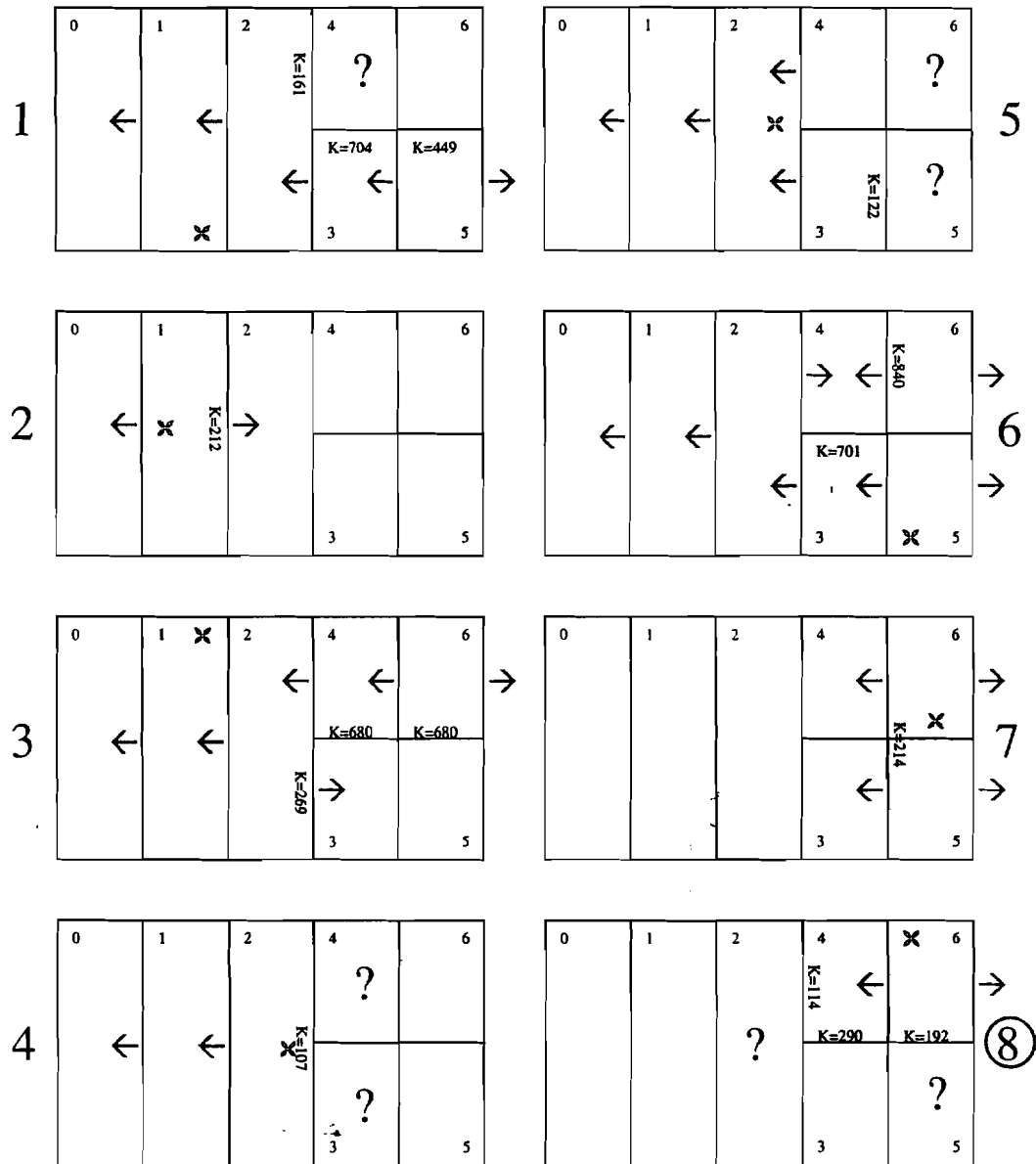


Figure 52 Bays in CWT where explosion will occur (indicated by solid green field) according to FLACS predictions supported by a quenching criterion for 8 different ignition positions (initial conditions: initial temperature 50 °C, moment of failure of manufacturing panel 24 ms after failure of FS).

The Figures clearly show that explosions of Jet-A at both 40 °C and 50 °C do not propagate into all bays according to the FLACS predictions and the criterion used (this is consistent with observations observed in the 1/4-scale experiments). Sometimes the explosion does not even propagate any further than the ignition bay such as ignition in bay 1 mid (ignition point 2, Jet-A 40 °C and 50 °C) and bay 2, mid, high (ignition point 4; Jet-A 40 °C). Very often the flame propagates into the neighbouring bays only, but does not propagate further. The subsequent rate of pressure rise in the secondary bay is so strong that flow velocities through holes into bays adjacent to the secondary bay are very high upon flame arrival, causing quenching.

Ignition in the front area of the CWT (bay 1) causes in general an explosion in bay 1 and 2 only. In case of Jet-A, 50 °C the explosion may propagate further down the tank with a certain probability. Similarly, ignition in the central area of the CWT (bay 2) causes the explosion to affect the central area of the CWT only although again for 50 °C the explosion may propagate further (probability < 1) both towards the aft and front. Finally, ignition in the aft of the CWT (bays 5 and 6) causes the flame to affect the bays in the aft of the tank (bays 3, 4, 5 and 6). Propagation to the middle and front sections of the CWT is seen for the case with ignition in bay 5 but also here with a probability < 1.

Considering the Karlovitz number expression used in the present study ( $K = (vU^3/D)^{1/2} \cdot 1/S_L^2$ ) one would expect quenching to be less likely on full-scale than on 1/4-scale. Keeping all other factors the same  $K \sim D^{1/2}$  indicating that K decreases with scale. To compensate for this increase of scale the flow velocity through the hole has to increase. Hydrodynamic and diffusive-thermal instabilities occurring on the flame surface cause on increase of the flame speed with distance. Tests performed at Christian Michelsen Research in a large unobstructed tent show that the burning velocity increases by a factor of 2.25 for stoichiometric methane-air mixtures and by a factor of 2.6 for stoichiometric ethane-air and propane-air mixtures within a distance of 2 m due to these instabilities. These instabilities have a bigger influence on the explosions in the full-scale rig where the flame can propagate over a 4 times larger distance than is possible in the 1/4-scale rig. The instabilities would cause stronger pressure rises in the full-scale tank causing higher velocities in the holes, partially compensating for the larger hole dimensions. A velocity increase by a factor of 1.6 would compensate for a factor of 4 in linear scale.

The effect of the hydrodynamic instabilities have been taken into account in FLACS by an empirical relationship which is a function of distance from the point of ignition (R):

$$S_{QL} = S_L (1 + aR)^{1/2} \quad (a = \text{a factor depending on the type of gas})$$

The explosions in secondary bays are dominated by turbulent combustion. A larger scale results in a faster combustion as well. In FLACS the turbulent combustion model that is used describes this. For both low and high intensity turbulence the turbulent burning velocity ( $S_T$ ) is directly related to the integral turbulent length scale ( $l$ ) according to

$$S_T \sim l^{0.196}$$

Hence the combustion in secondary bays would be faster in larger scale than in smaller, causing a higher rate of pressure rise in large scale than in small scale for a fixed fraction of the compartment combusted. This would increase the velocity in the holes between adjacent bays, increasing the Karlovitz numbers and the likelihood of quenching. This argument suggests that the quenching could be more important in full scale than in the 1/4-scale experiments. However, lacking experimental confirmation, the role of scale in quenching cannot be decisively determined.

The results of the Figures 49 to 52 together with the numerical data of Figures 37 to 48 allow for applying the rule-based analysis as developed by Thibault (1999).

## 7. DISCUSSION

In this chapter the level of confidence into the CFD-predictions as presented above is discussed.

The simulations of the simulant fuel 1/4-scale experiments highlight deviations between simulations and experiments. The average deviation of the pressure differences across the partitions seen in all-strong simulant fuel experiments is in one case more than 50 %. The simulations also show a systematic deviation of the pressure difference, which is present in only one direction: if the deviation of the pressure difference between simulation and experiment for many scenarios and for a certain partition is big in one direction it appears to be small in the other direction. This behaviour may perhaps be explained by the fact that no attempts were made to correct for the slight difference seen between the reactivity of the fuel as represented in FLACS and the real reactivity of the simulant fuel (See Figure 10). No work was done to support this statement.

The average relative deviation between simulations and experiments is in the same order of magnitude as the standard deviation of repeated experiments whereas the standard deviation of the simulations is about twice the standard deviation of repeated experiments indicating that the simulations are clearly deviating.

A good comparison between pressure differences seen in 1/4-scale Jet-A experiments and simulations could not be performed due to quenching in several of the experiments whereas the majority of the explosion simulations were performed assuming no quenching. Other experiments in which quenching did not occur could not be used due to anomalous combustion behaviour.

Since quenching appears to play a dominating role on full-scale the quality of the developed quenching criterion is very important. The criterion was developed on the basis of experiments performed with propane on small-scale and is effectively based on three parameters (combined in a single number the so-called Karlovitz number): burning velocity, orifice dimensions and flow velocity through the orifice. The parameters are lump parameters and do not address local effects happening in the jet downstream of the hole. Data not measured in the experiments were estimated on the basis of simulations of the same experiments.

It appeared possible to define a single Karlovitz number above which quenching always occurred. It should be emphasised that the Karlovitz number addresses quenching by turbulent flow only. The flame quenching by thermal effects (occurring when ignition is effected very close to a hole) is not described.

The Jet-A experiments performed to verify the quenching criterion confirmed the validity for Jet-A 50 °C whereas for Jet-A, 40 °C small deviations made it necessary to improve the criterion slightly. The improved criterion can, however, be considered as validated to some degree for both fuel (Jet-A) and scale (in the 1/4-scale rig the 2-bay experiments involved holes with dimensions similar to those in the real CWT. The propane experiments performed by the University of Bergen and used to develop the quenching criterion were performed with openings where the largest of these had dimensions similar to the smallest holes of the CWT). Much more work is needed, however, to have a fully validated quenching criterion for Jet A.

In the real-scale CWT simulations holes were in general represented as subgrid orifices. This implies that at positions where an orifice was present the cell face was made porous, thus representing the relative size of the opening. The criterion was, however, developed representing orifices ongrid. Therefore a study was performed to investigate the effect of grid size on the effective Karlovitz number. The study showed that subgrid representation of orifices is satisfactory and that the grid size dependency is limited. Table 5 shows results of the effect of grid size on the Karlovitz number and other parameters in 11 holes in SWB2 upon ignition in bay 1 (ignition point 2) at full-scale with Jet-A 40 °C.

Table 5 Effect of grid size on various parameters measured in holes in SWB2 (ignition point position 2 in bay 1; fuel: Jet-A, 40 °C).

Hole ID	Orifice description	Diam. (cm)	Size grid cell (cm)								
			12			8			6		
			t (s)	v (m/s)	K	t (s)	v (m/s)	K	t (s)	v (m/s)	K
55	Lower stringer hole stbd	6.6	1.127	150	836	1.167	159	911	1.116	151	846
56	Lower stringer hole port	6.6	1.127	150	836	1.167	159	911	1.116	151	846
57	Upper stringer hole stbd	5.21	1.127	150	941	1.167	159	1026	1.116	151	952
58	Upper stringer hole port	5.21	1.127	150	941	1.167	159	1026	1.116	151	952
59	Fuel vent circum port	0.95	1.127	150	2201	1.167	159	2399	1.116	151	2227
60	Fuel vent circum stbd	0.95	1.127	150	2201	1.167	159	2399	1.116	151	2227
65	Fuel vent pipe port	8.89	1.127	150	720	1.167	159	785	1.116	151	729
66	Fuel vent pipe stbd	8.89	1.127	150	720	1.167	159	785	1.116	151	729
61	Refuel Manifold port	1.27	1.127	150	1906	1.167	159	2077	1.116	151	1929
62	Refuel manifold stbd	1.27	1.127	150	1906	1.167	159	2077	1.116	151	1929
63	Flow hole	3.81	1.127	150	1100	1.167	159	1199	1.116	151	1113

t = moment of arrival of flame at first hole

v = flow velocity

K = Karlovitz number

The limited grid size dependency and the fact that the study shows that choice of a criterion based on lump parameters allows for predicting quenching conditions well gives some confidence in the full-scale predictions. Full-scale tests would, however, be needed to warrant full confidence.

The effect of hydrodynamic flame instabilities for Jet-A is described by the same empirical factor as found for stoichiometric propane and ethane. Whether this factor also can be used for the two Jet-A mixtures is an uncertainty but the simulations of the single bay Jet-A tests show that the rate of pressure rise for these two mixtures are well reproduced (Figures 11 and 12) indicating that there are no big deviations to be expected.

Other combustion related scaling parameters have been proven to be understood through the many validation exercises against a large data set of explosion experiments varying from laboratory scale facilities to full-scale offshore platform test facilities.

Therefore it is concluded that the full-scale predictions performed by FLACS can be used with some confidence.

The similarities seen in full-scale predictions for Jet-A 40 °C and Jet-A 50 °C also indicate that the effect of non-homogeneities in the gas distribution and knowledge about the exact temperature are limited in the investigated range of temperatures and associated gas concentrations.

The fact that the explosion propagates into a few bays only makes the necessity of being able to accurately predict the course of flame propagation and resulting pressure development in many coupled compartments less stringent.

In some of the experiments anomalous combustion behaviour was seen. The occurrence of cool flames could possibly explain this behaviour. Cool flames could start a first stage of combustion in each bay. Propagation of cool flames in the CWT would probably be dominated by thermal/molecular phenomena whereas turbulent combustion does not play a role. Combustion rates of cool flames in Jet-A are unknown. Pressure increases due to the first stages of combustion could possibly start off a second more violent stage of combustion as seen in some bays in experiments where the anomalous combustion phenomena were observed. It should be emphasised that no attempt was made to support the suggestion of cool flames explaining the anomalous combustion phenomena.

Initiation of cool flames is especially seen at hot surfaces. Since hot filaments are used as an ignition source in the present 1/4-scale experiments, the occurrence of cool flames cannot be excluded there.

## 8. CONCLUSIONS

Using FLACS, a 3-D CFD based tool for predicting the consequences of gas explosions in complex geometries simulations were performed to support the investigation into the cause of the explosion in the Center Wing Tank of TWA-800.

The essential part of the work that was carried out consisted of three main phases:

- Improvement of the prediction tool for this special application
- Validation of the tool against 1/4-scale explosion experiments
- Prediction of the course of Jet-A explosions in the Center Wing Tank

The first two phases were necessary to be able to, to verify the possibility of, and to quantify the confidence in predictions of the course of explosions in the full-scale TWA-800 Center Wing Tank. Laboratory-scale and 1/4-scale explosion experiments performed by California Institute of Technology and ARA were used for the first two phases. The full-scale predictions were done for 8 potential ignition source locations and were used as input for the rule-based model developed by Combustion Dynamics to compare predicted loads with observed damage.

The improvement of the code consisted of the following phases:

- Representation of the simulant fuel used in the 1/4-scale explosion experiments and Jet-A mixtures at initial temperatures of 40 °C and 50 °C
- Representation of flame propagation through holes
- Heat transfer to the environment
- Development of a quenching criterion

The representation of the simulant fuel (a mixture of hydrogen and propane) was performed on the basis of existing subroutines in the FLACS-code itself. Comparison to explosion vessel tests and single bay 1/4-scale explosion tests show that the real mixture was slightly more reactive than represented in the FLACS-code. To represent the two Jet-A mixtures butane-air mixtures with equivalence ratios of ER=0.79 (laminar burning velocity of 43 cm/s) for the Jet-A mixture at 50 °C and ER=0.62 (burning velocity of 21.6 cm/s) for the Jet-A mixture at 40 °C, were used.

Flame propagation through holes was represented as porosities for holes smaller than the side of the grid. Comparison to specially designed experiments showed reasonable agreement.



Models for convective heat losses and heat loss due to radiation were included. The models represented the heat loss seen in experiments quite well.

A quenching criterion describing quenching of flames by turbulence generated in shear layers at holes in the CWT-partitions was developed on the basis of experiments performed at the University of Bergen with propane. The criterion based on a defined Karlovitz number uses lump parameters as input neglecting local effects. The criterion was successfully applied to 1/4-scale Jet-A experiments. Small changes to the criterion made it possible to apply it with confidence for full-scale predictions.

Application of the quenching criterion to tests performed with the simulant fuel showed that quenching should have been observed in these experiments as well. The presence of hydrogen in the simulant fuel is probably the main cause that the quenching criterion cannot be applied for the simulant fuel.

Deviations seen in FLACS pressure load predictions on partitions in simulant fuel 1/4-scale experiments may be explained by the slightly deviating reactivity of the simulant fuel used in FLACS. No attempt was made to improve this deviation.

Predictions of full-scale CWT explosions using eight ignition source locations for Jet-A at 40 °C and 50 °C showed that the flame very often quenched at the orifices in the partitions. As a result combustion was not predicted in all bays. This was seen for both Jet-A mixtures. The potential damage due to explosions at both temperatures is very similar although there is a higher probability at 50 °C that more bays are affected. The effect of delay of the failing of the manufacturing panel (up to 24 ms after failure of the FS) is very small on this very behaviour although the propagation of a possible flame through the resulting opening was not taken into account considering flame quenching.

## 9. REFERENCES

- Abdel-Gayed, R.G., Bradley, D. and Lawes, M. (1987) *Turbulent burning velocities: a general correlation in terms of straining rates*, Proc.Roy. Soc. London A414, p.389-413
- Artnzen, B.J. (1998), *Modelling of Turbulence and Combustion for Simulation of Gas Explosions in Complex Geometries*, PhD Thesis Norwegian University of Science and Technology, MTF-report 1998:173 (D)
- Baer, M.R. and Gross, R.J. (1998), *A Combustion Model for the TWA 800 Center-Wing Fuel Tank Explosion*, Sandia National Laboratories Report no. SAND98-2043
- Bradley, D., Lau, A.K.C. and Lawes, M. (1992), *Flame stretch as a determinant of turbulent burning velocity*, Phil. Trans. R. Soc. London A (1992) 338, pp. 359-387
- Brown, L. L., Lynch, R.T. and Samaras, T.M. (1999) *TWA FLIGHT 800 1/4-Scale Fuel Tank Explosions Phase II. Fall 1998 & Spring 1999 Test Series Final Report*. ARA Report, Projects 4810 and 5057. July 22, 1999.
- California Institute of Technology (1997), *Venting and Passageways in the Caltech 1/4-Scale Model of 747-100 CWT*, Note 27 September 1997
- Gibbs, G.J. and Calcote, H.F.G. (1959), *Effect of Molecular Structure on Burning Velocity*, J. Chem. Eng. Data, vol.4, no.3
- Goodwin, D.G., TCC (ThermoChemical Calculator) Sandia,  
<http://adam.caltech.edu/tcc/>
- Hjertager, B.H. (1982), *Simulation of Transient Combustible Turbulent Reactive Flows*, Comb. Sci. Techn. Vol. 27, no. 5-6, pp. 159-170
- Kee, R.J., Rupley, F.M. and Miller, J.A. (1987), *The Chemkin thermodynamic data Base*, Sandia National Laboratories Report no. SAND87-8215

Kobayashi, H., Tamura, T., Maruta, K., Niioka, T. and Williamsn F.A. (1996), *Burning Velocity of Turbulent Premixed Flames in a High Pressure Environment*, 26<sup>th</sup> Symposium on Combustion, The Combustion Institute, pp. 389-396

Larsen, Ø. (1998), *A Study of Critical Dimensions of Holes for Transmission of Gas Explosions and Development and Testing of a Schlieren System for Studying Jets of Hot Combustion Products*, MSc Thesis, University of Bergen

Lee, J. J. and Shepherd, J. E. (1999) *Spark Energy Measurements in Jet A. Part II* GALCIT Report FM 99-7, Dec 3, 1999.

Lind, C.D. and Whitson, J.C. (1977), *Explosion Hazards Associated with Spills of Large Quantities of Hazardous Materials, Phase 2*, Report no. CG-D-85-77, US Department of Transportation, Coast Guard Final Report ADS 047585

Markstein, G.H. (1964), *Non-Steady Flame Propagation*, Pergamon Press, New York

Metghalchi, M. and Keck, J.C. (1980), *Laminar Burning Velocity of Propane-Air Mixtures at High Temperature and Pressure*, Combust. Flame, vol. 38, pp. 143-154

Nuyt, C. D., Shepherd, J.E., and Lee, J.J. (2000), *Flash point and Chemical Composition of Aviation Kerosene (Jet A)*. Explosion Dynamics Laboratory Report FM99-4, California Institute of Technology

D'Onofrio, E.J. (1980), *Cool-Flame and Auto-Ignition in Glycols*, Loss Prevention, pp. 89-95, 1980

Ratzel, A.C. and Shepherd, J.E. (1985), *Heat transfer resulting from premixed combustion*, in Heat Transfer in fire and Combustion systems (Edited by C.K. Law, Y. Jaluria, W:W: Yuen and K. Miyasaka), Publication HTD-45 of ASME, New York, NY, pp. 191-201

Renoult, J. (1999), *Comparison of FLACS and TCC*, Christian Michelsen Report no. CMR-99-F30045

Shepherd, J.E., Krok, J.C., Lee, J.J. and Birky, M.M. (1997a), *Jet A Explosions - Field Test Plan 1/4-Scale Experiments*, Explosion Dynamics Laboratory Report FM97-17, California Institute of Technology, Dec 6, 1997

Shepherd, J.E., Krok, J.C. and Lee, J.J. (1997b), *Jet A Explosion Experiments: Laboratory Testing*, Explosion Dynamics Laboratory Report FM97-5, California Institute of Technology

Shepherd, J. E., Krok, J. C., Lee, J. J., Brown, L. L., Lynch, R. T., Samaras, T. M., and Birky, M. M. (1998, July). *Results of 1/4-scale experiments, vapor simulant and liquid Jet A tests*. Explosion Dynamics Laboratory Report FM98-6, California Institute of Technology.

Shepherd, J. E., Krok, J. C. and Lee, J. J. (1999) *Spark Energy Measurements in Jet A*. GALCIT Report FM 97-9, May 3, 1999

Shepherd, J. E., Krok, J. C., Lee, J. J., Kaneshige, M. J., Brown, L. L., Lynch, R. T., Samaras, T. M., Kolly, J., and Birky, M. M. (2000). *Results of 1/4-Scale Testing: Simulant repeatability tests, Jet A vapor, and quenching*. Explosion Dynamics Laboratory Report FM00-2, California Institute of Technology.

Thibault, P. (1999), *Proposed CMR CFD Calculations. Effect of Initial Temperature, Ignition Location and SWB2 Door Release Delay*, Revision 2 of Working Paper of TWA-800 investigation, December 16, 1999

P. A. Thibault (2000) *A Rule-Based Analysis Method for the Evaluation of Explosion Scenarios*, Combustion Dynamics Ltd Report CDL-1010. July 2000 .

Van Wingerden, K., Storvik, I., Artzen, B., Teigland, R., Bakke, J.R., Sand, I.Ø. and Sørheim, H.R. (1993), *FLACS-93, a New Explosion Simulator*, Proceedings of the 2<sup>nd</sup> Int. Conf. On Offshore Structural Design against Extreme Loads, pp. 5.2.1-5.2.14, London, 1993

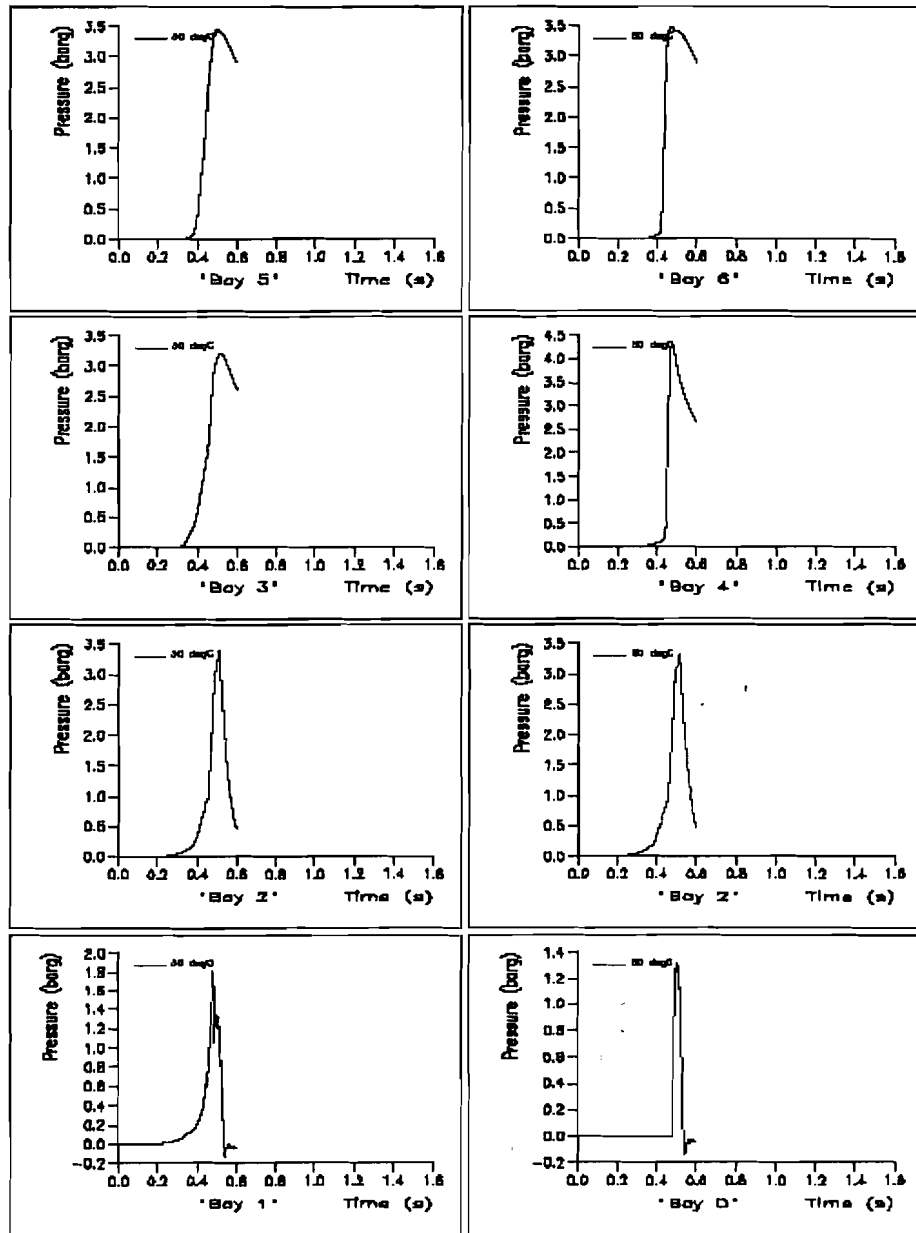
Van Wingerden, K., Hansen, O.R. and Storvik, I. (1995), *On the Validation of a Numerical Tool used for Explosion and dispersion Predictions in the Offshore Industry*, Fifth Int. Symp. on Loss Prevention in the oil and Gas Industry (Thompson, ed.), BHR Group Publication 15, pp. 201-219

## **ANNEX**

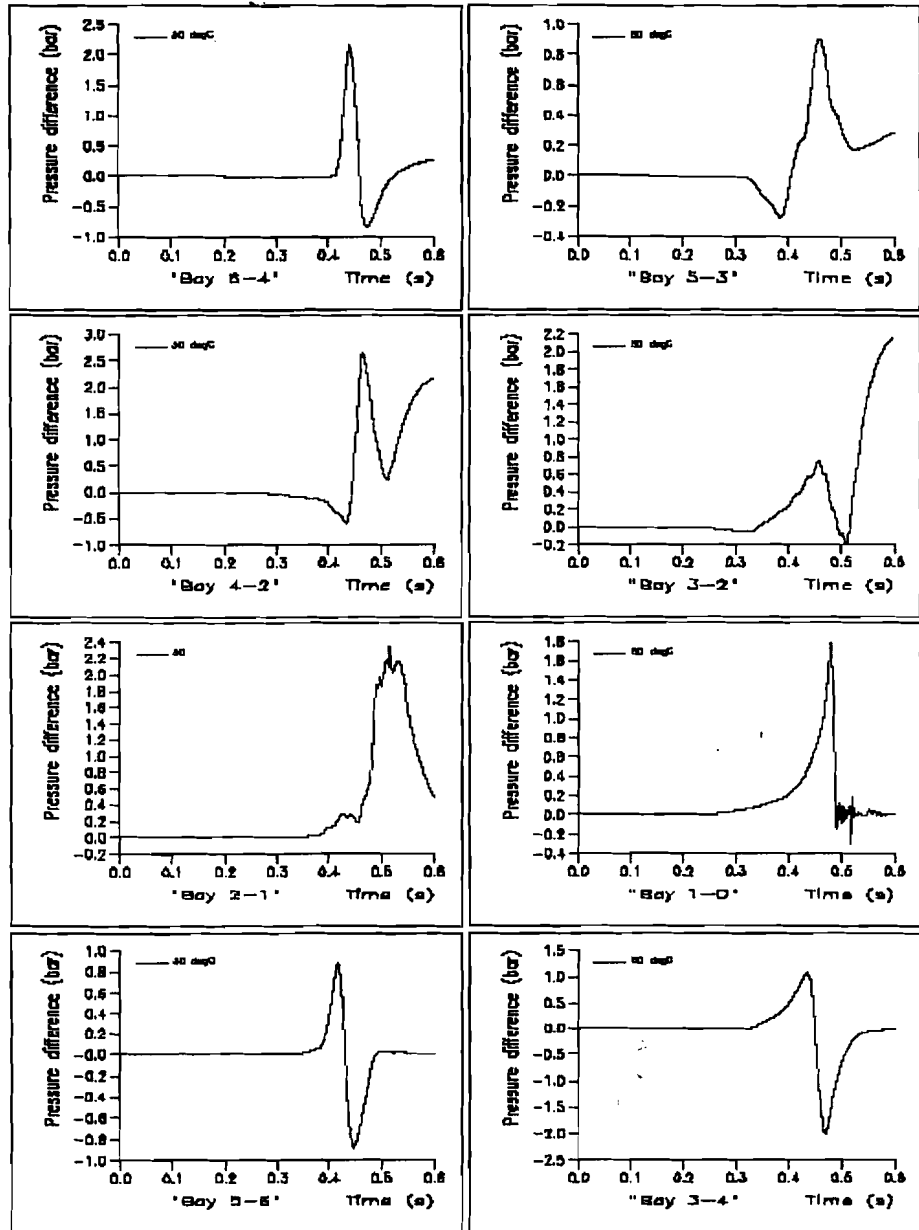
### **Predictions of pressure time histories of 32 full-scale explosions**

**Series 1: Initial temperature 50 °C, moment of failure of  
manufacturing panel 24 ms after failure of FS, eight ignition positions**

Tue Mar 23 15:07:55 2009 "M1 scale TWA central wing tank ignition point 1 (Bay 1 port), SWB2 door delay = 24 ms, TD=66degC"

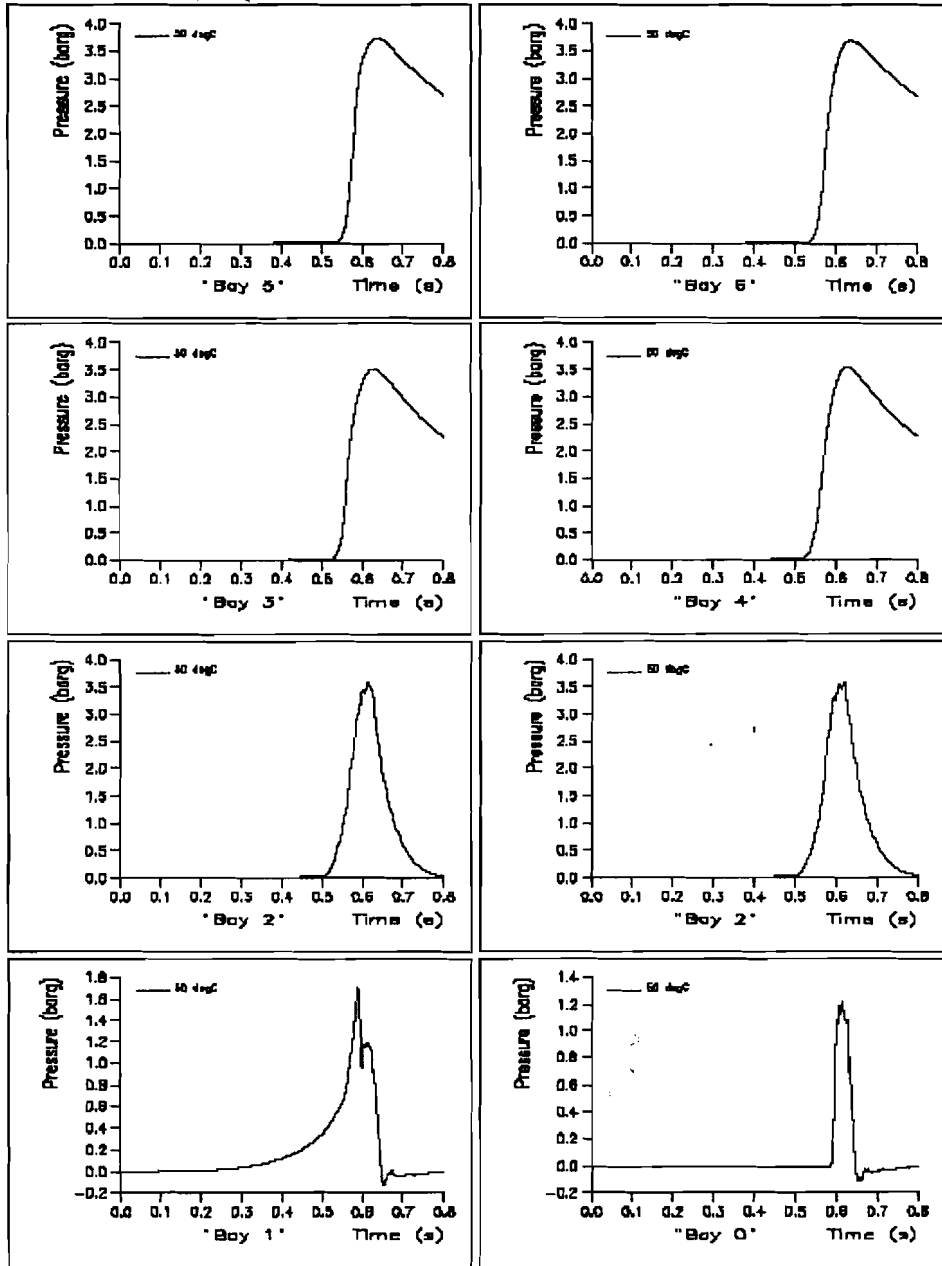


Thu Mar 23 15:10:00 2000 \*1/1 scale TWA central wing tank. Ignition point 1 (Bay 1 port), BWB2 door delay = 24 ms, T0=50degC\*

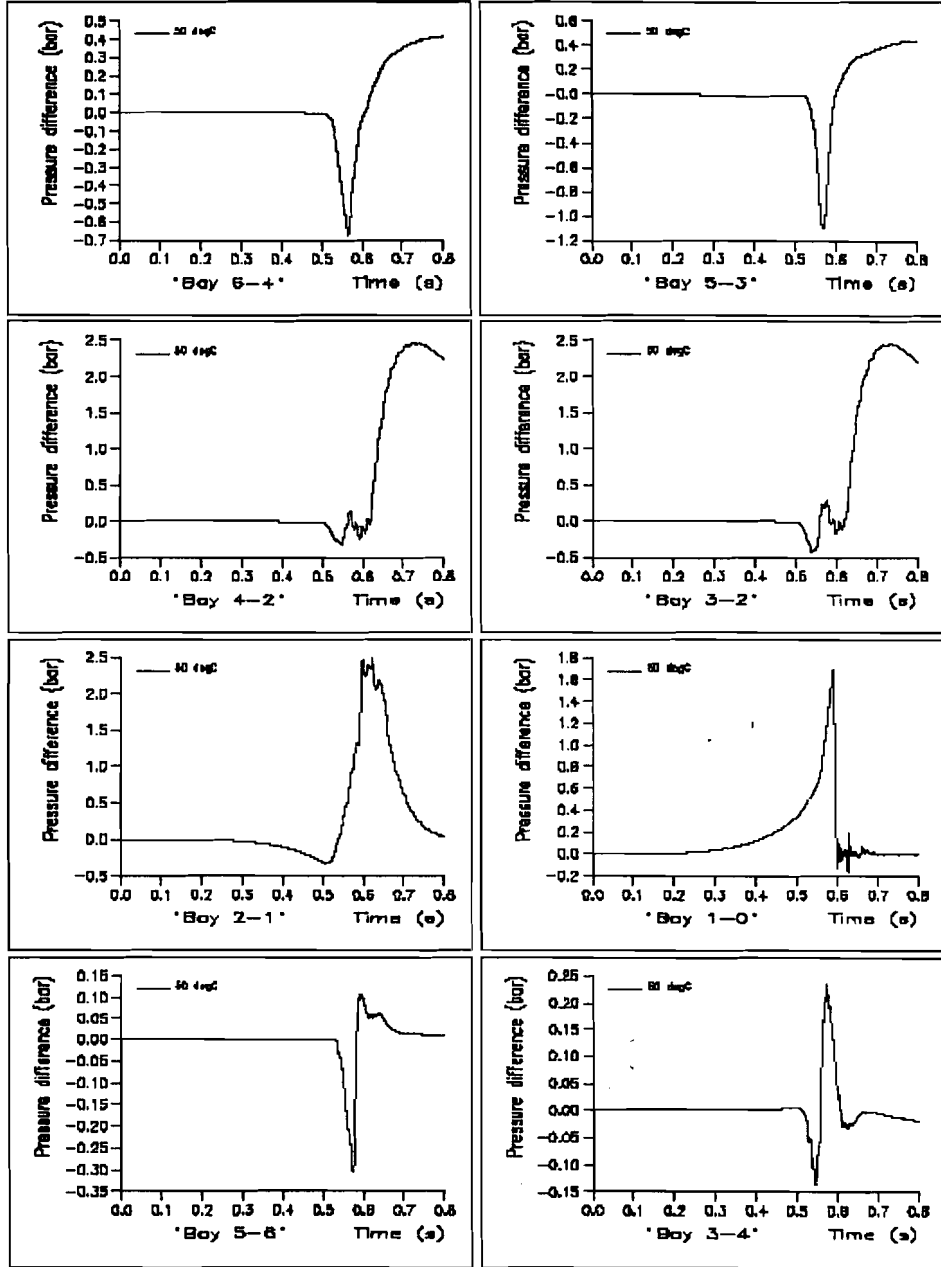




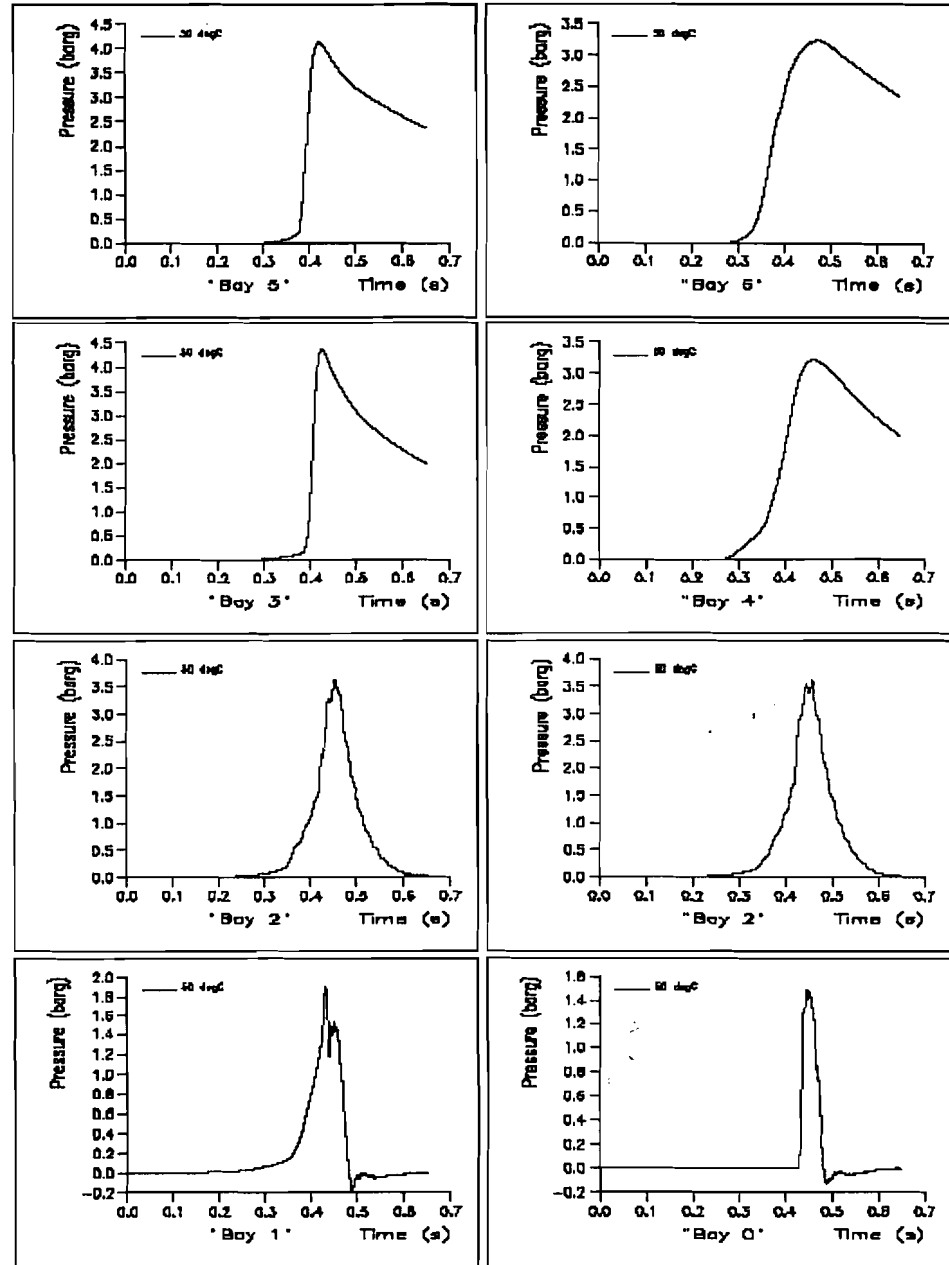
The Mar 23 15:58:52 2000 "U1 scale TWA center wing tank.ignition point 2 (Bay 1 mid), 3WB2 door delay = 24 ms, T0=50degC"



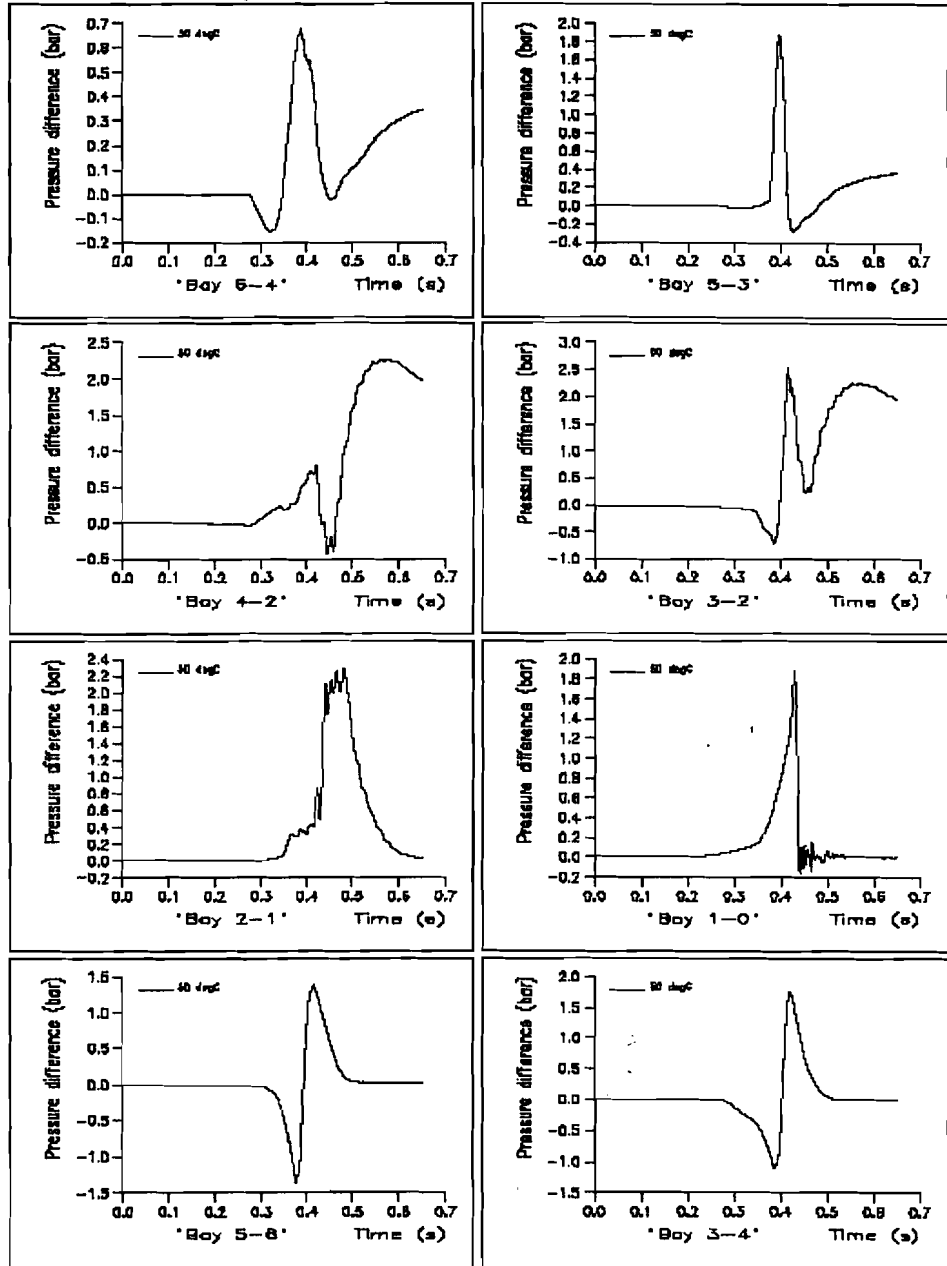
The Mar 23 15:18:57 2009 \*1/1 scale TWA central wing tank, Ignition point 2 (Bay 1 mid), SWB2 door delay = 34 ms, T0=50degC.\*



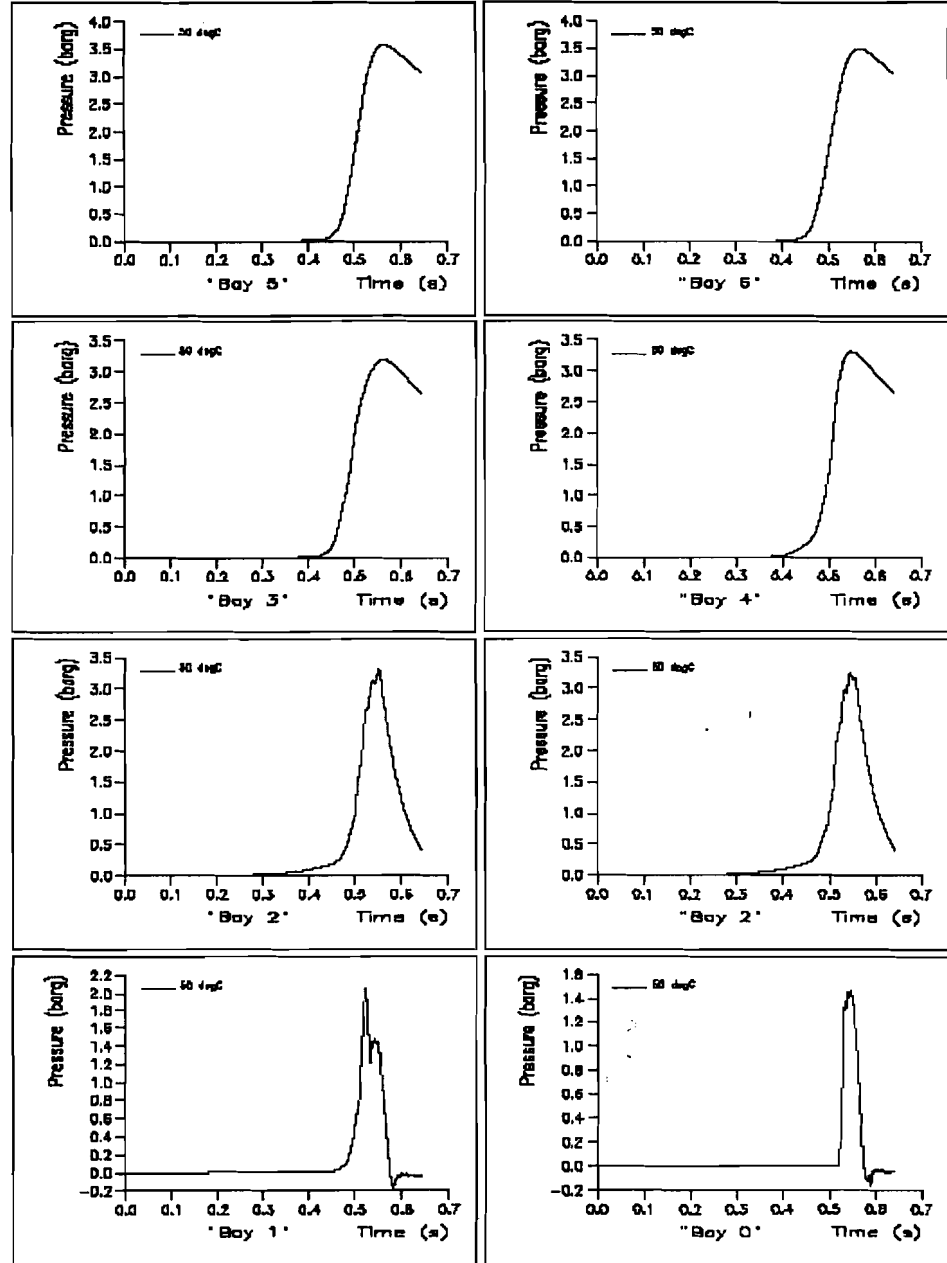
The Mar 23 15:08:10 2000 "U1 scale TWA central wing tank ignition point 3 (Bay 1 starboard, 0WB2 door delay = 24 ms, T0=50degC"



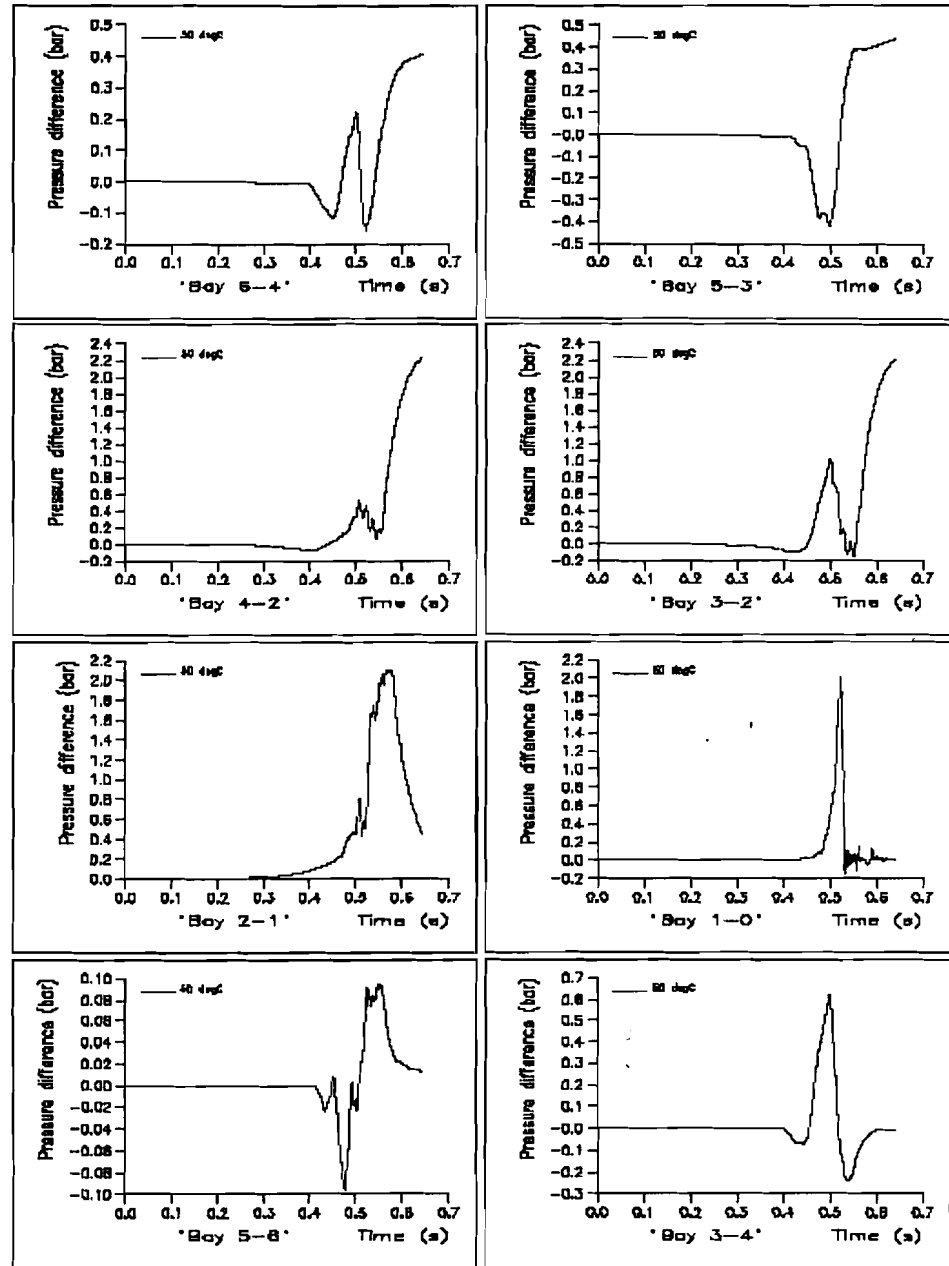
The Mar 23 15:10:16 2008 "U1 scale TWA central wing tank. Ignition point 3 (Bay 1 Midboard), BWB2 door delay = 24 ms, T=550degC."



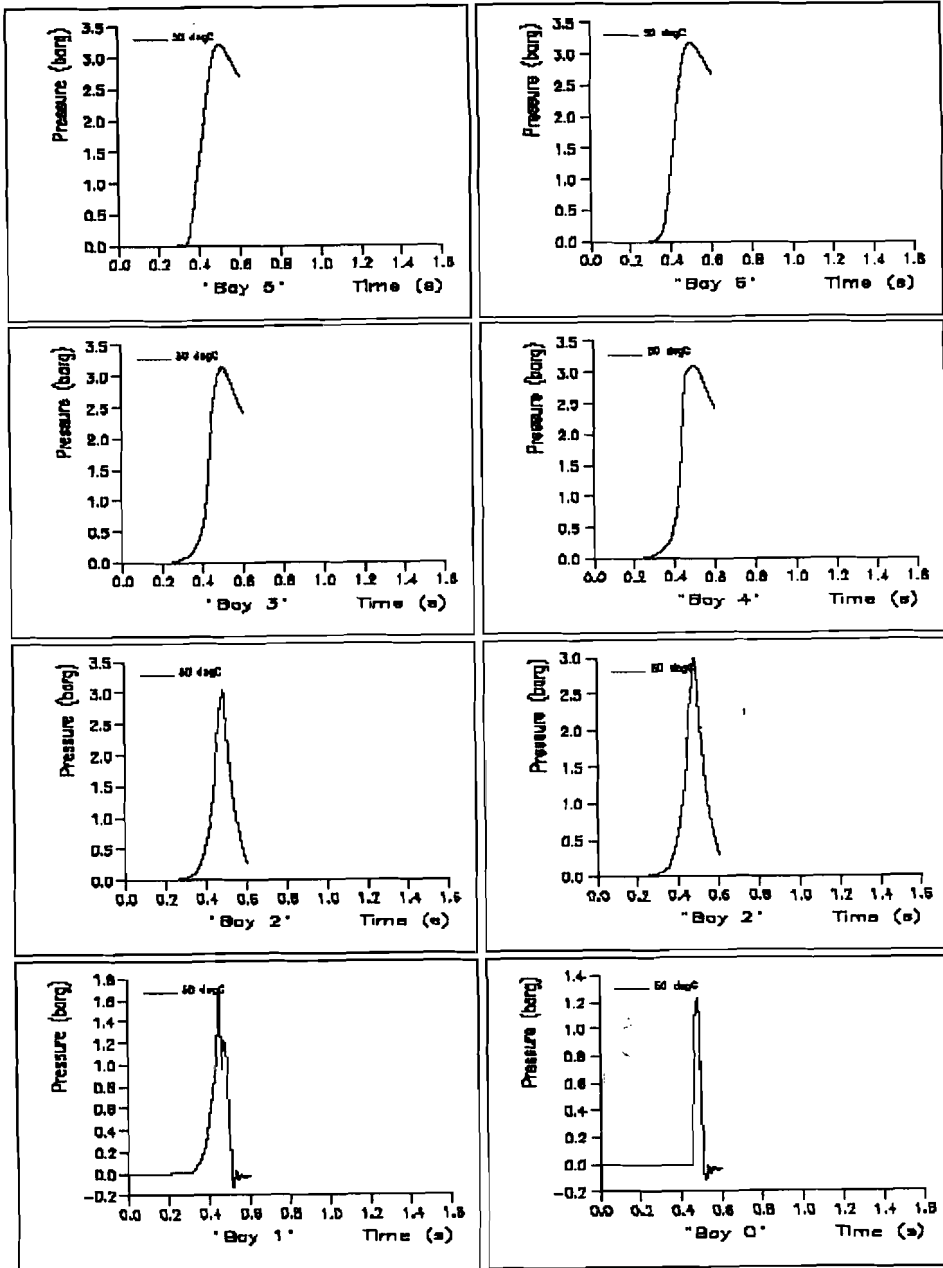
The Mar 23 15:08:17 2008 \*U1 scale TWA central wing tank, ignition point 4 (Bay 2 mid), SWB2 door delay = 24 ms, T0=50degC



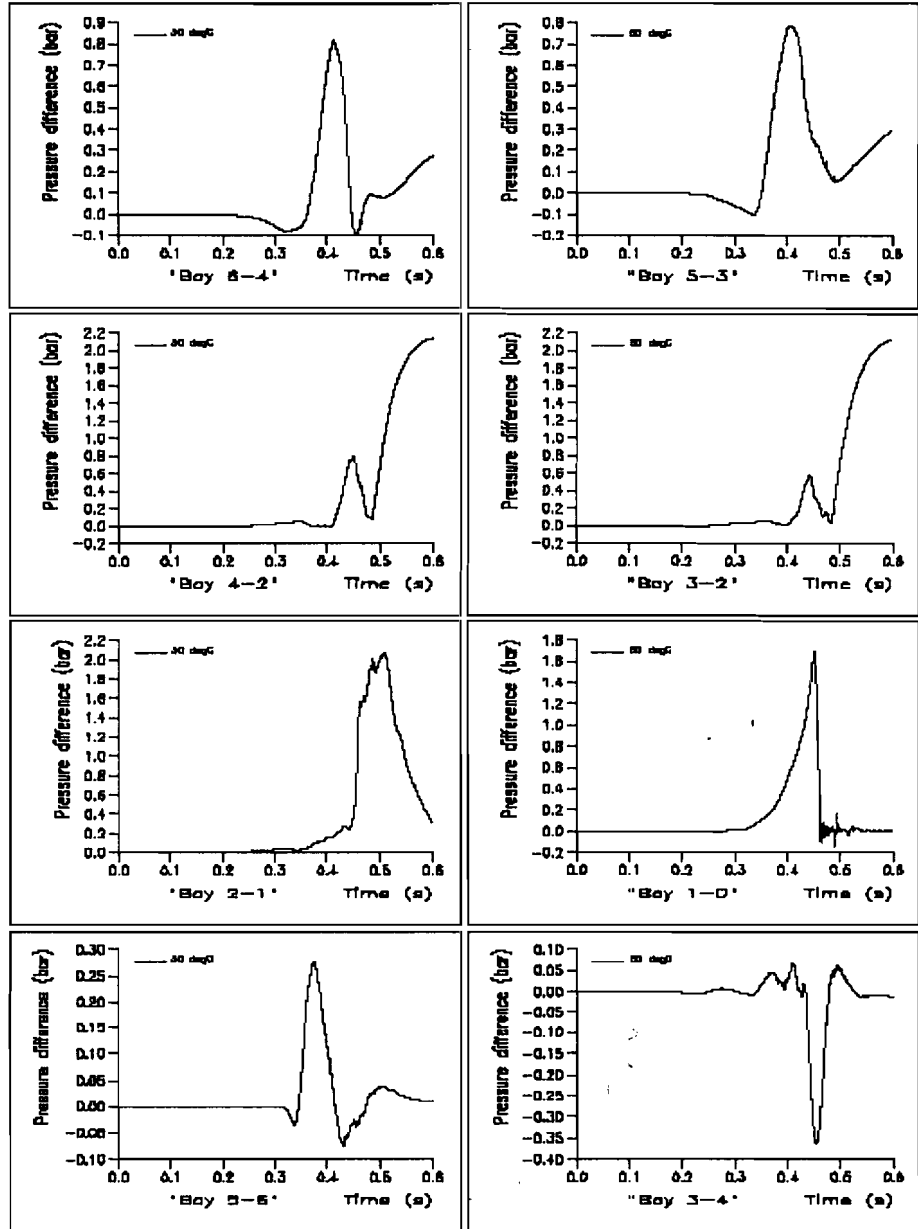
Thu Mar 23 15:10:23 2000 \*U1 scale TWA control wing tank, Ignition point 4 (Bay 2 mid), SYB2 door delay = 24 ms, T0=50degC.\*



The Mar 23 15:48:23 2000 \*1/1 scale TWA central wing tank ignition point 5 (Bay 2 mid), SWB2 door delay = 24 ms, TD=56degC

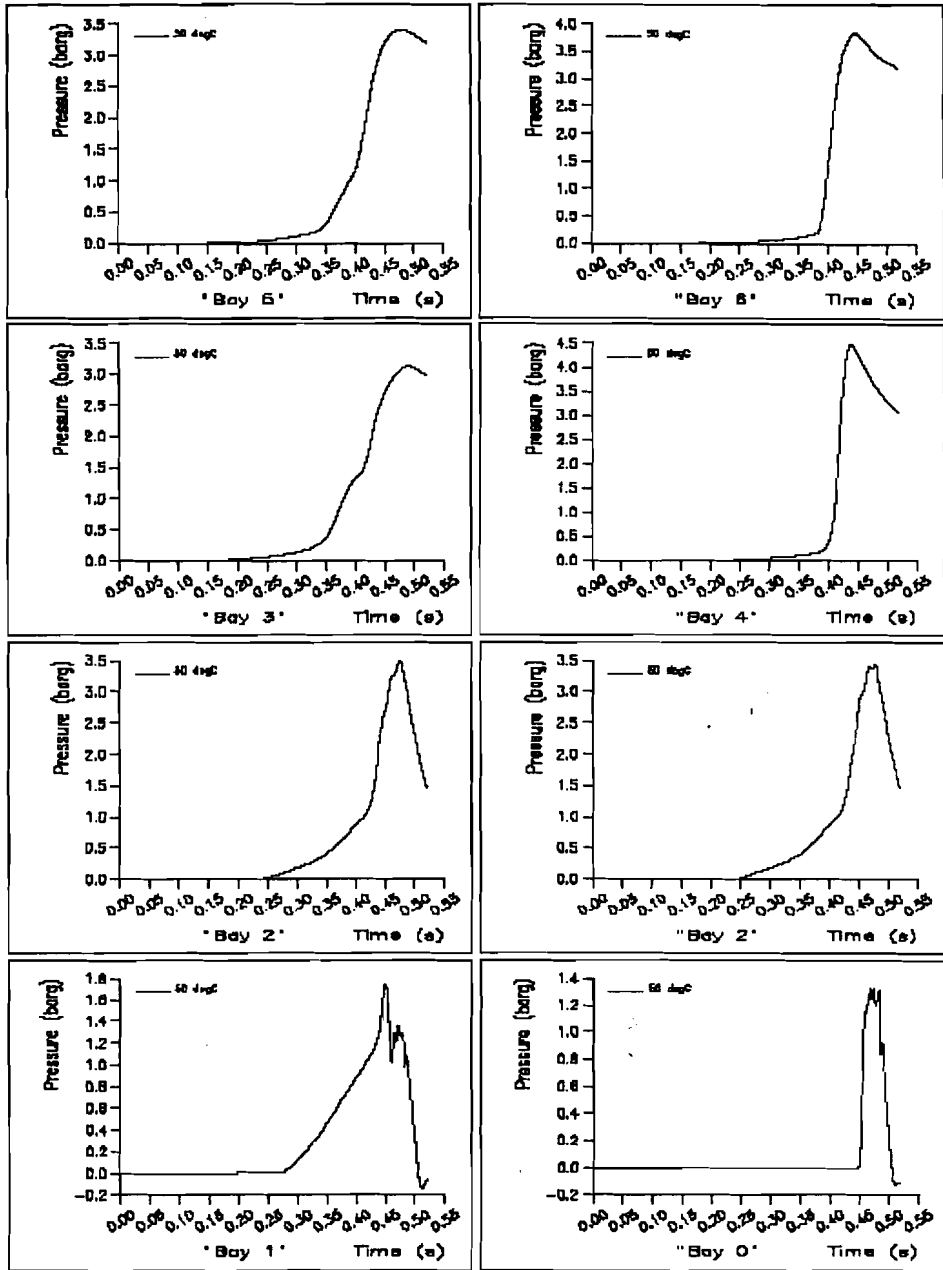


Thu Mar 23 15:10:29 2000 \*1/1 scale TWA central wing tank. Ignition point 1 (Bay 2 mid), SWB2 door delay = 24 ms, T0=50degC\*

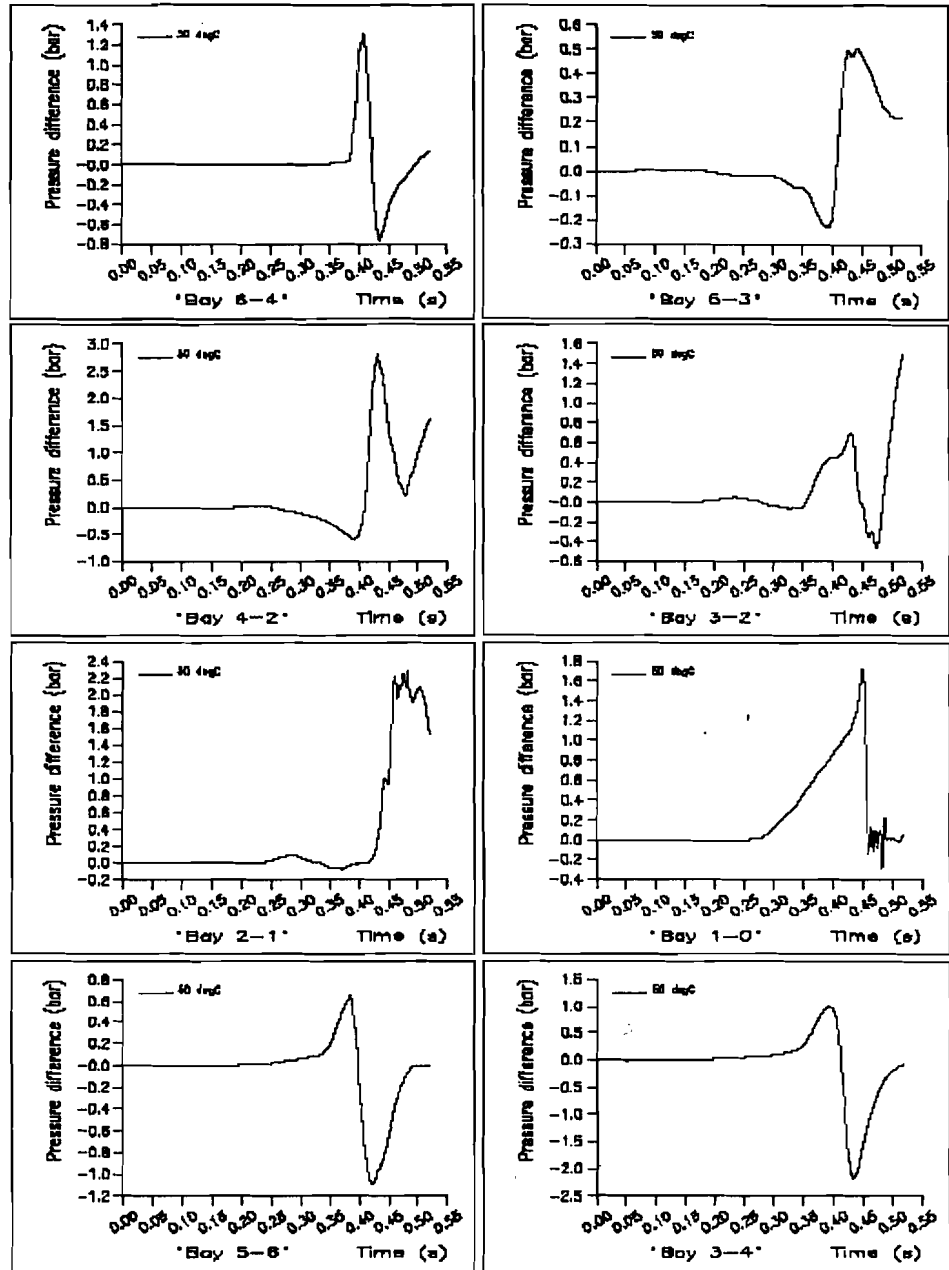




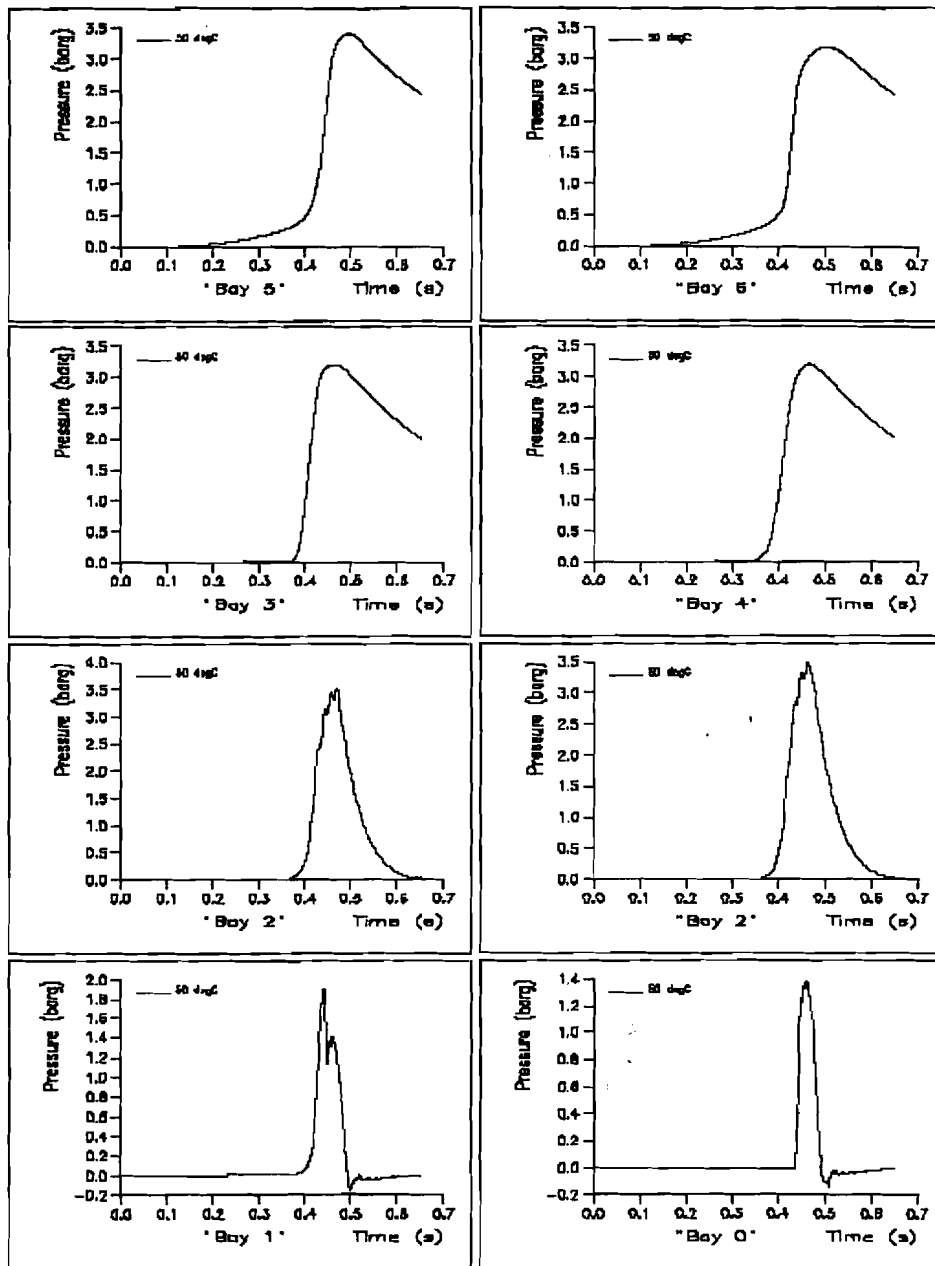
The Mar 23 15:08:29 2009 "1/1 scale TWA center wing tank ignition point 8 (AR Bay 5 port), BWB2 door delay = 24 ms, TD=50degC"



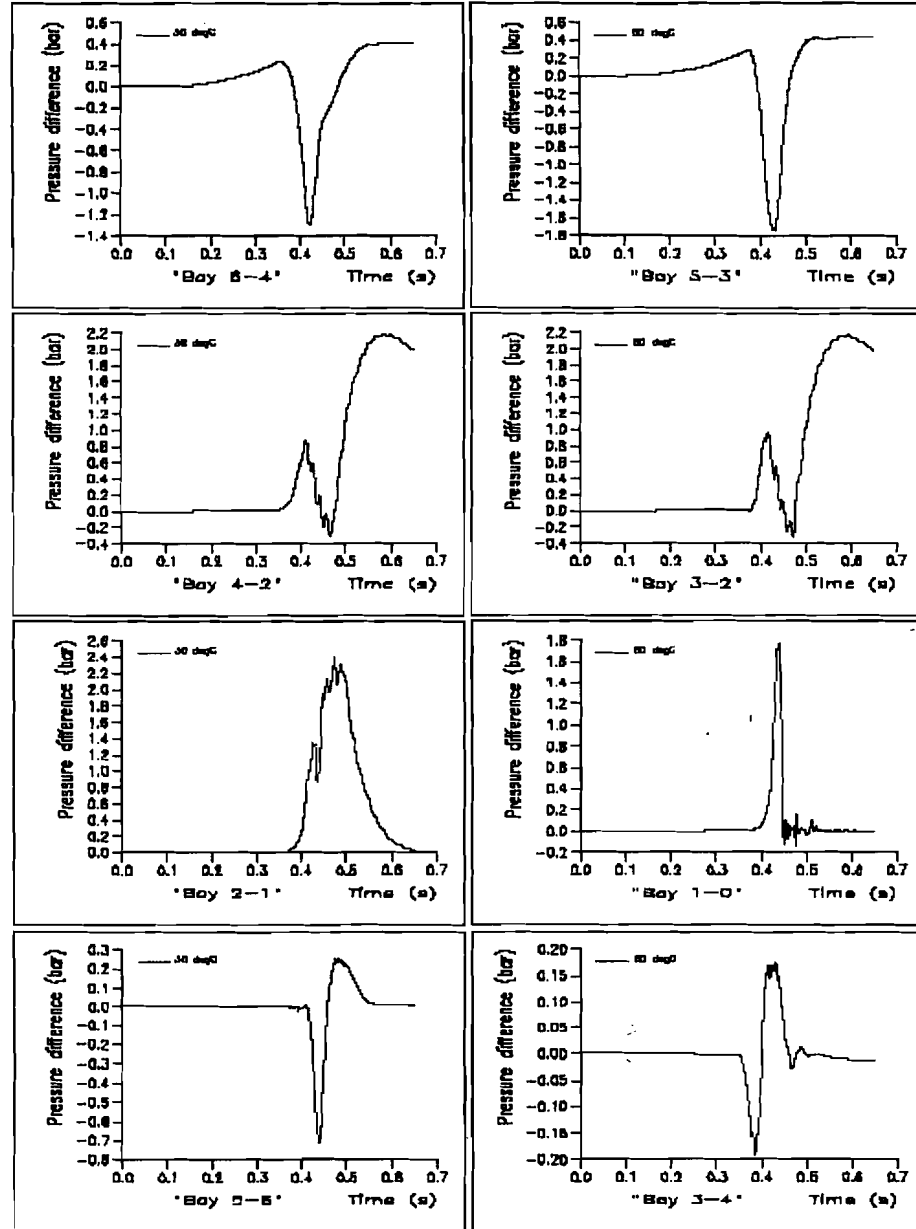
The Mar 23 15:18:35 2008 \*U1 scale TWA central wing tank. Ignition point 6 (AR Bay 5 port), SWB2 door delay = 24 ms, TB=500degC.\*



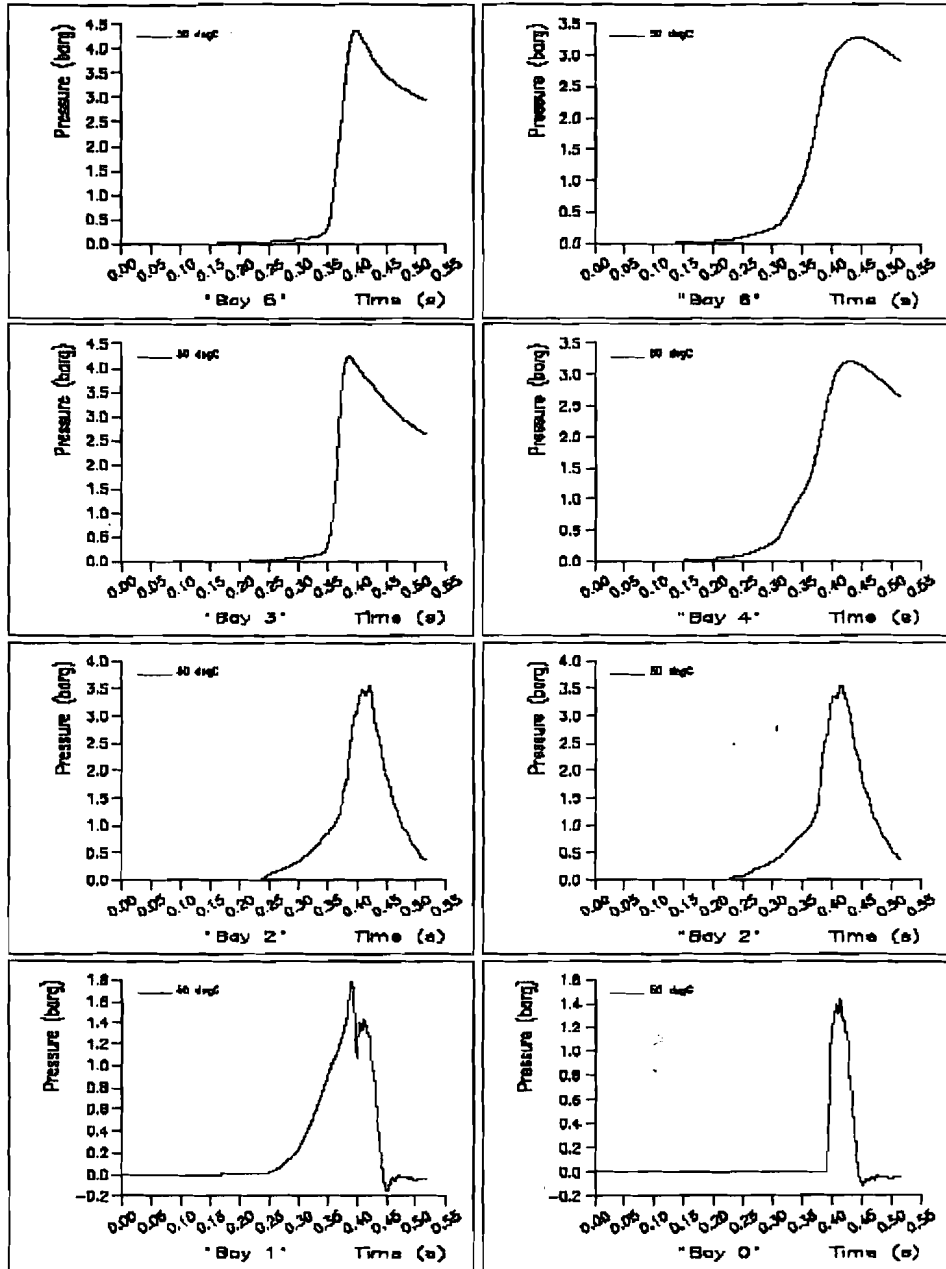
The Mar 25 15:58:35 2008 \*1/1 scale TWA central wing test. Ignition point 7 (All Bay 6 midl, BWB2 door delay = 24 ms, T0=50degC)



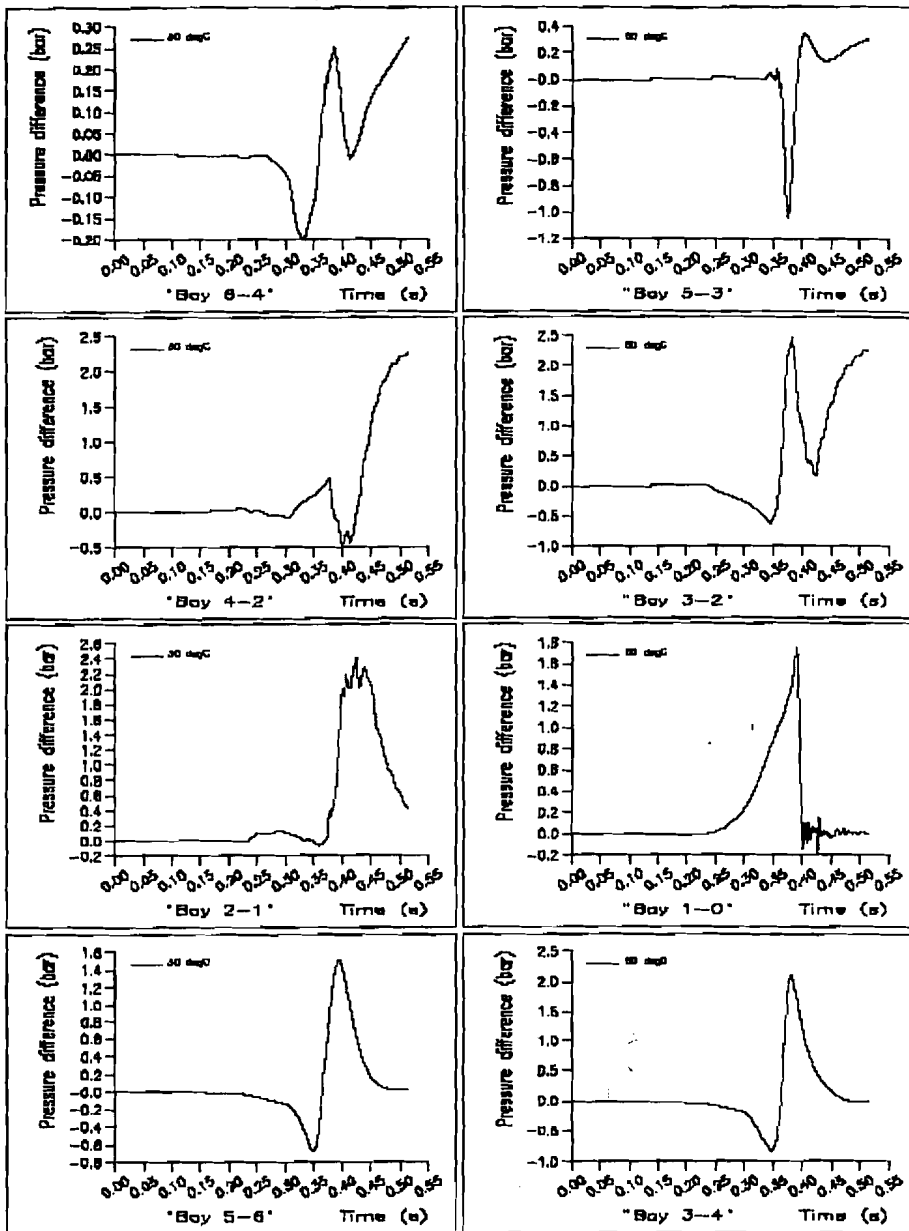
Thu Mar 23 15:10:41 2000 \*V1 scale TWA center wing tank. Ignition point 7 (AR Bay 8 mid), BWB2 door delay = 24 ms. TDe50degC.



The Mar 23 15:08:42 2008 \*U1 scale TWA central wing tank, Ignition point B (All Bay 6 starboard), SWB2 door delay = 24 ms, T=59degC\*

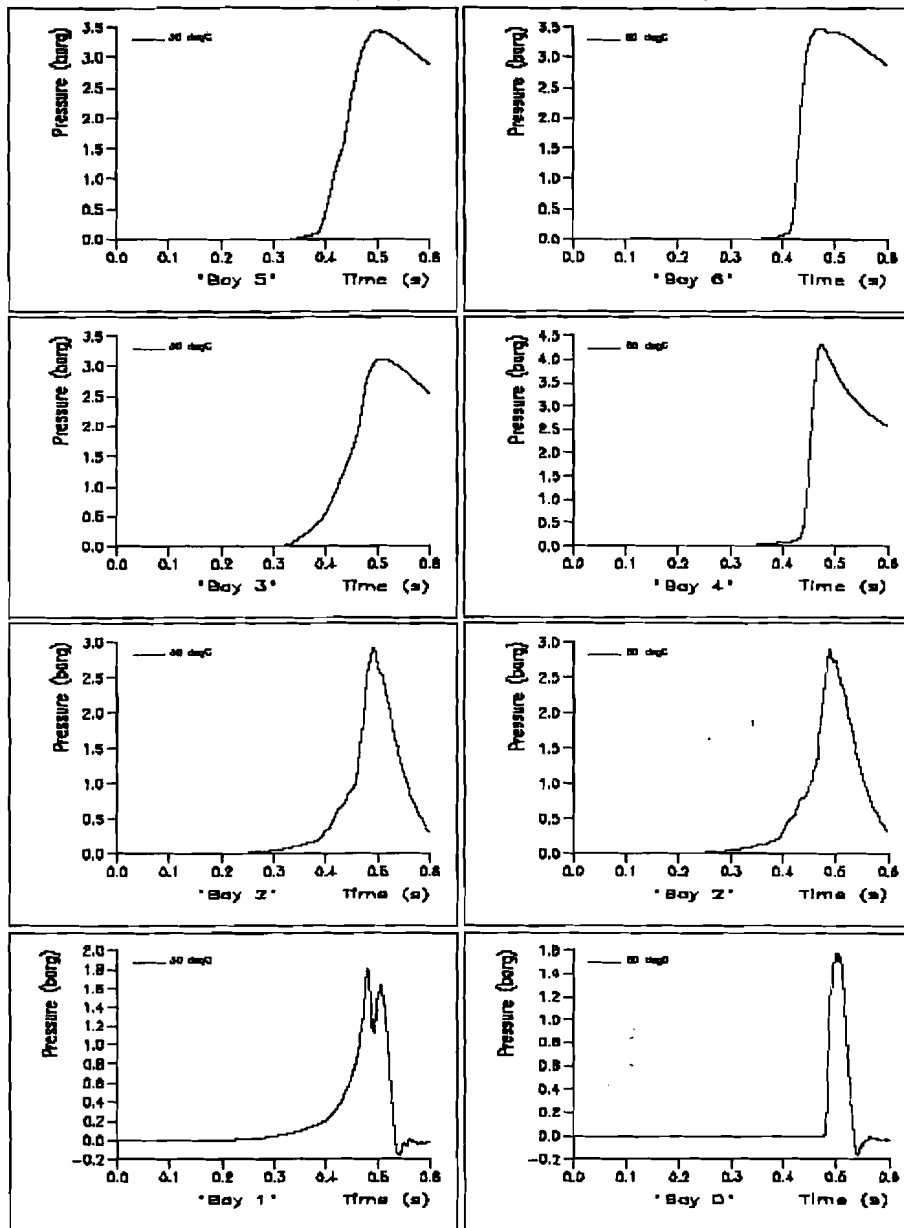


Thu Mar 23 15:10:44 2000 \*V1 south TWA central wing tank, Ignition point 8 (Aft Bay 6 starboard), OWS2 door delay = 24 ms, TD=60degC\*



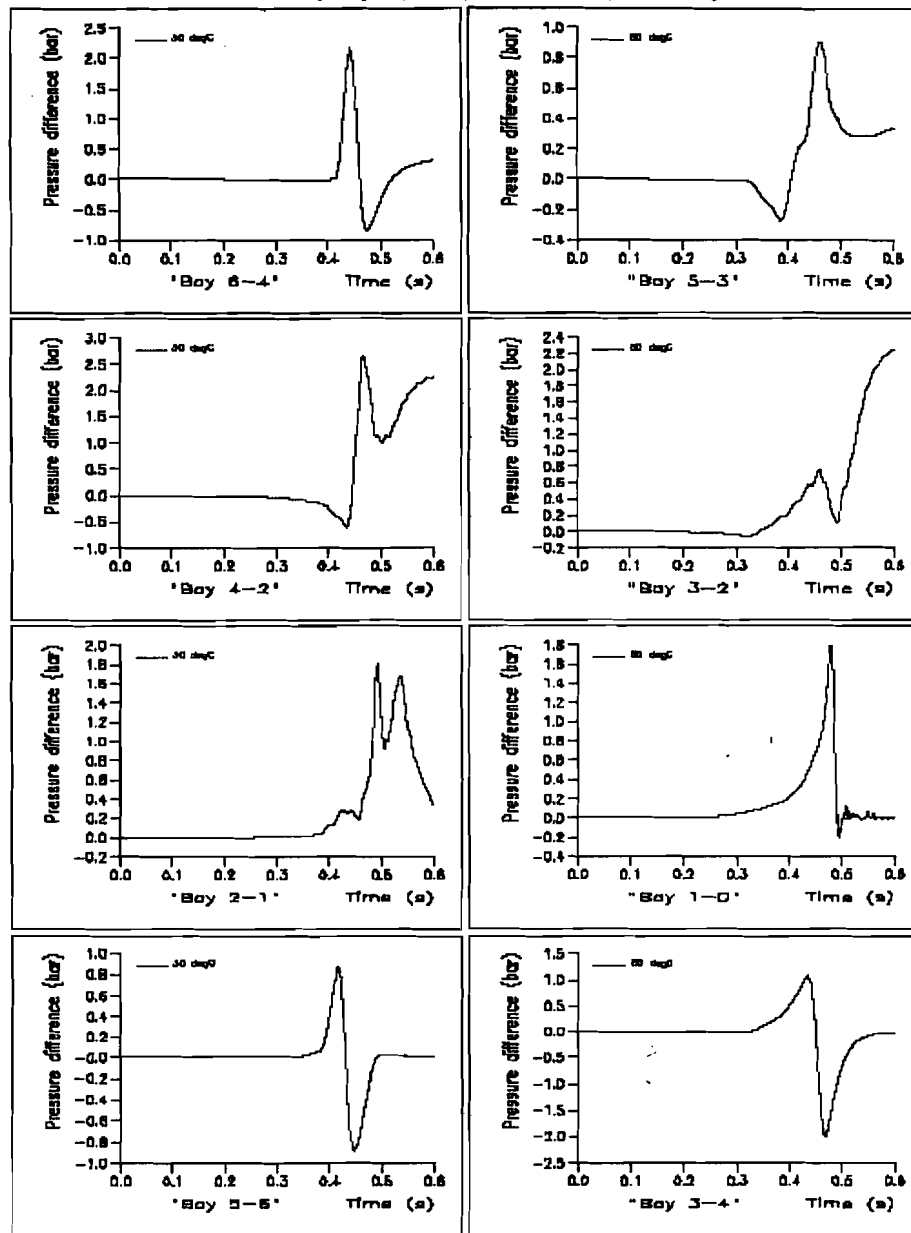
**Series 2: Initial temperature 50 °C, moment of failure of manufacturing panel at moment of failure of FS, eight ignition positions**

Thu Mar 23 15:06:29 2000 \*1/1 scale TWA central wing tank ignition point 1 (Bay 1 port), BWB2 door delay = 0 ms, T0=50degC

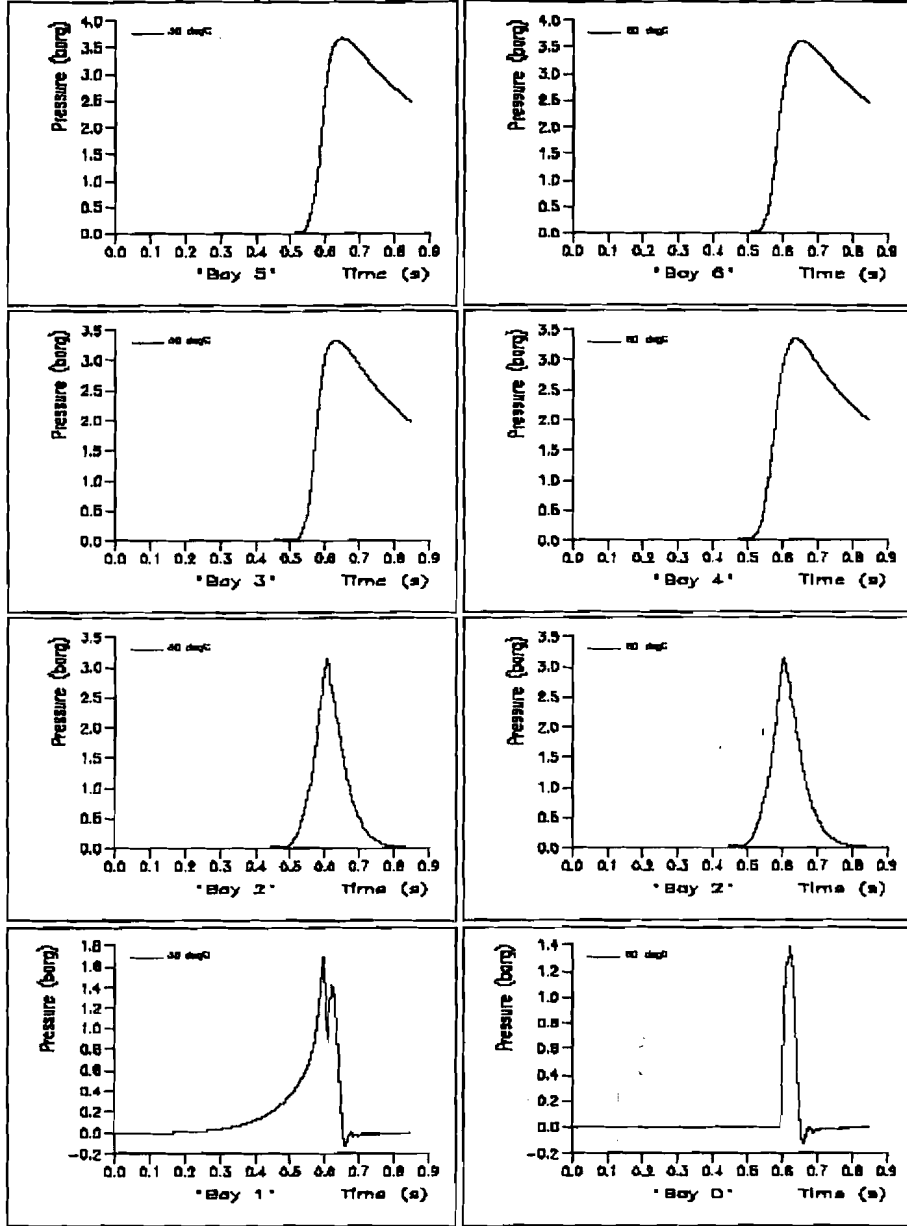




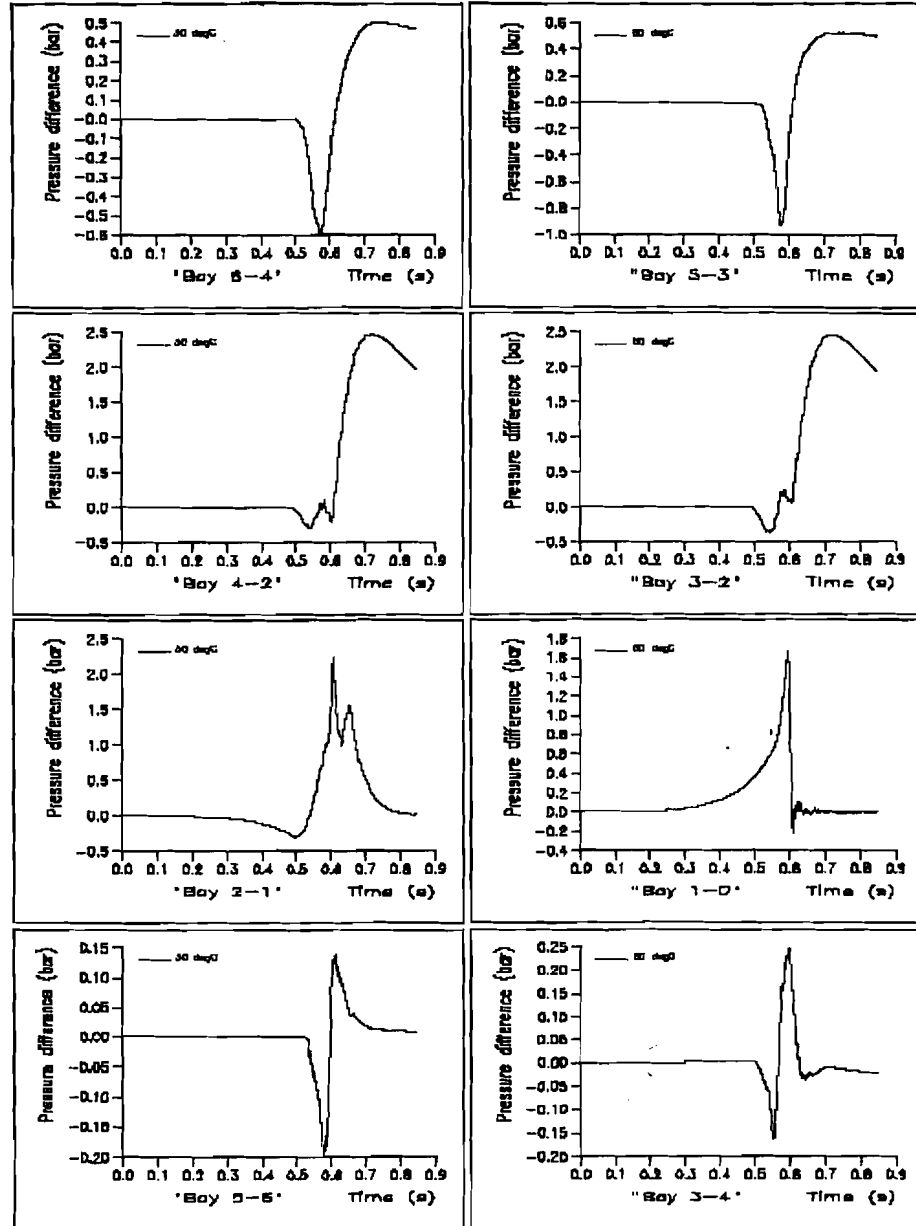
Thu Mar 23 15:08:49 2000 \*1/1 scale TWA central wing tank, Ignition point 1 Bay 1 pod1, SWB2 base delay = 0 ms, TD=50degC\*



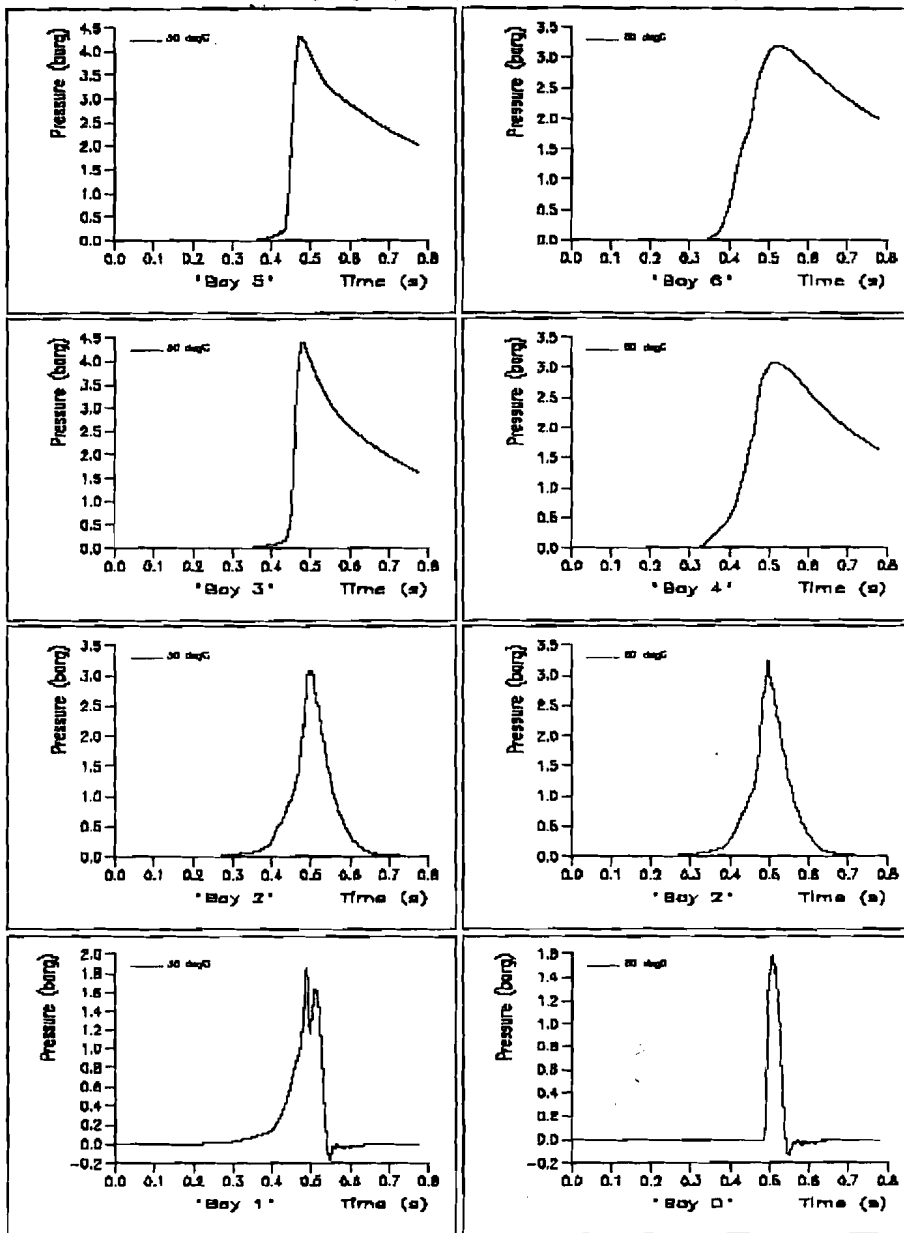
Thu Mar 23 15:06:51 2000 \*1/1 scale TWA center wing tank ignition point 2 (Bay 1 mid), SWB2 door delay = 0 sec, TD=50degC\*



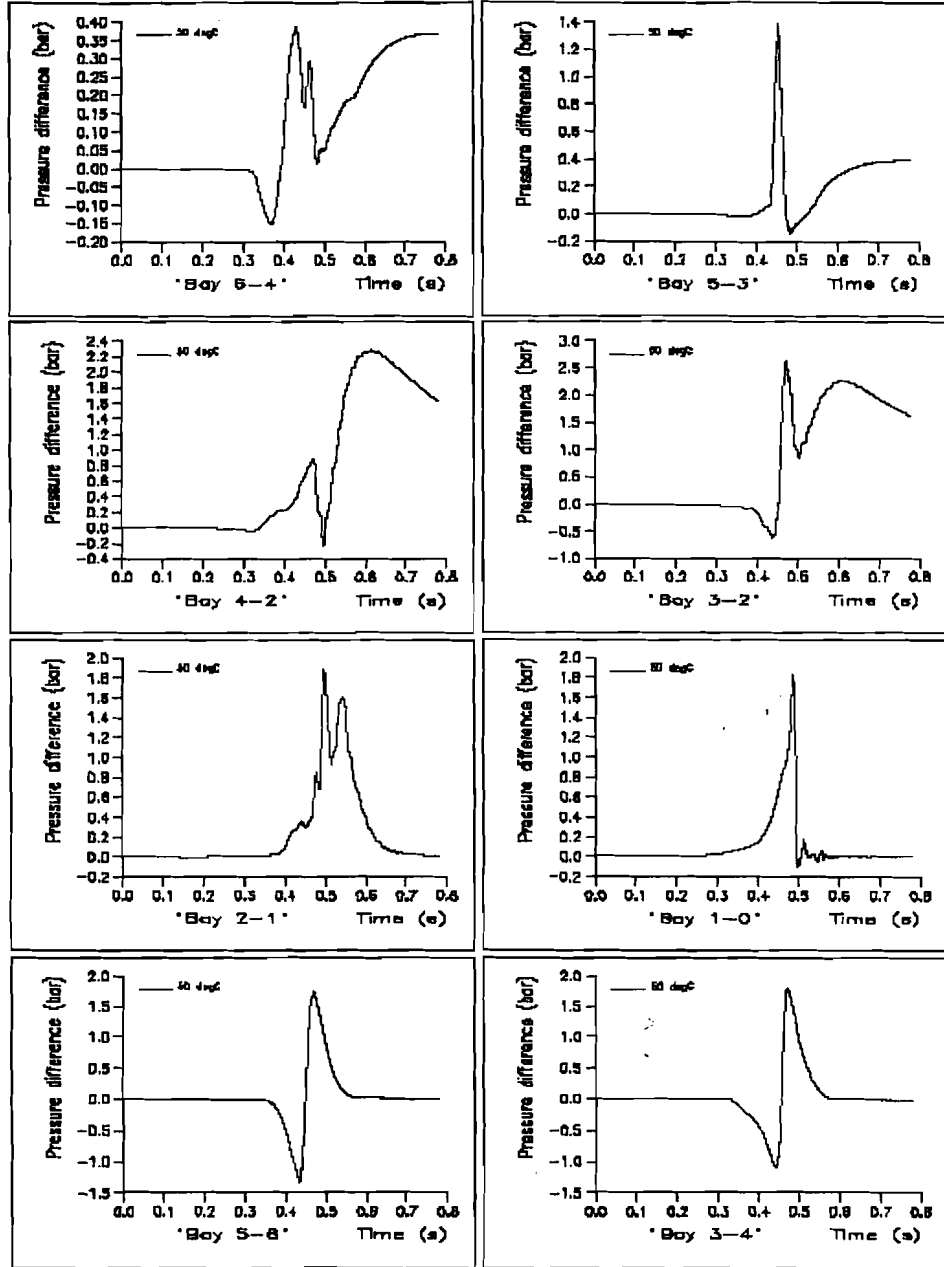
Thu Mar 23 15:00:57 2000 \*1/1 scale TWA control wing tank. Ignition point 2 (Bay 1 mid), RWB2 door delay = 0 ms. TD=50degC\*



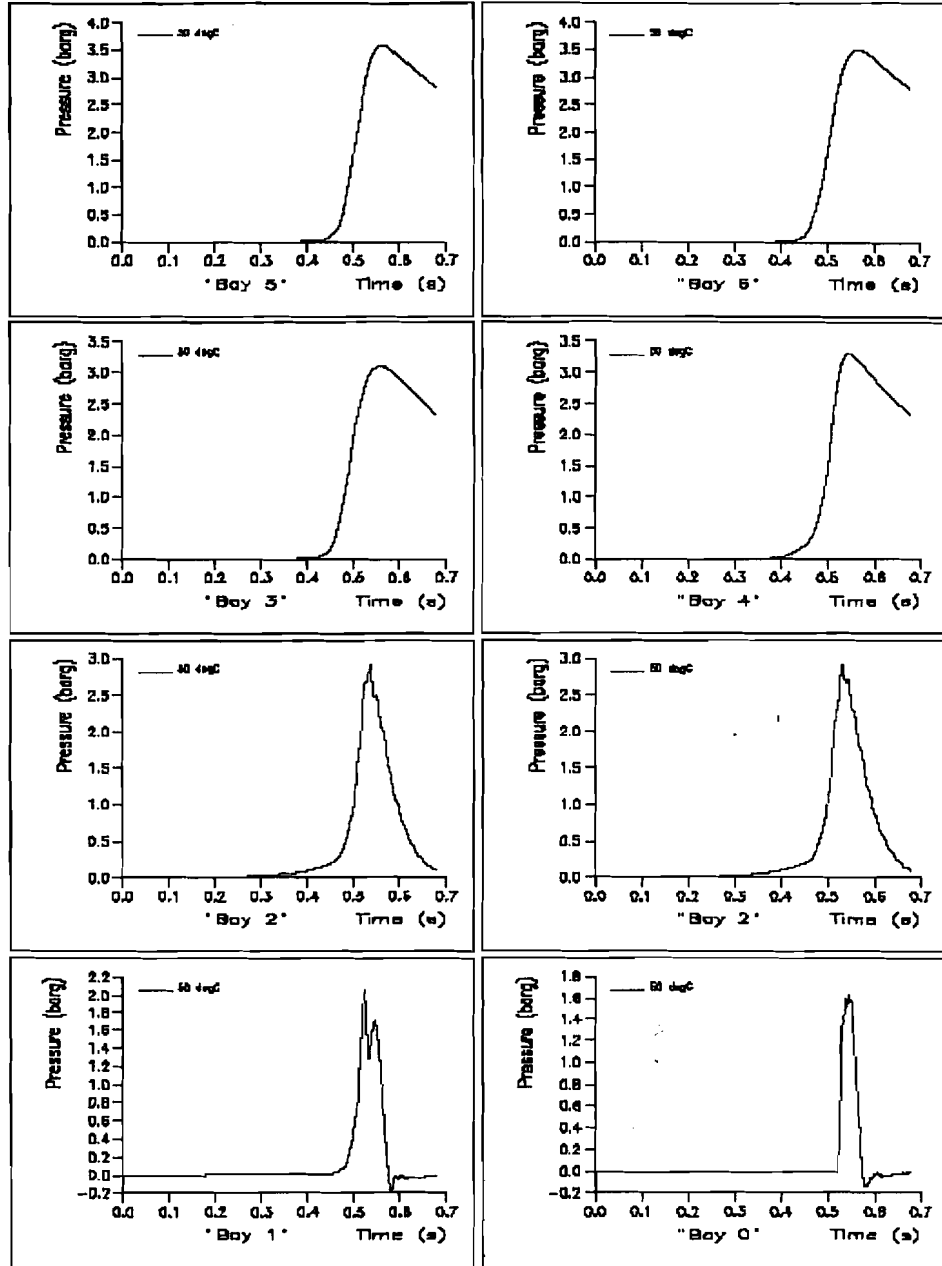
Thu Mar 23 15:06:23 2000 \*1/1 scale TWA center wing tank, ignition point 3, Bay 1 starboard, BWB2 door delay = 0 sec, T0=50degC\*



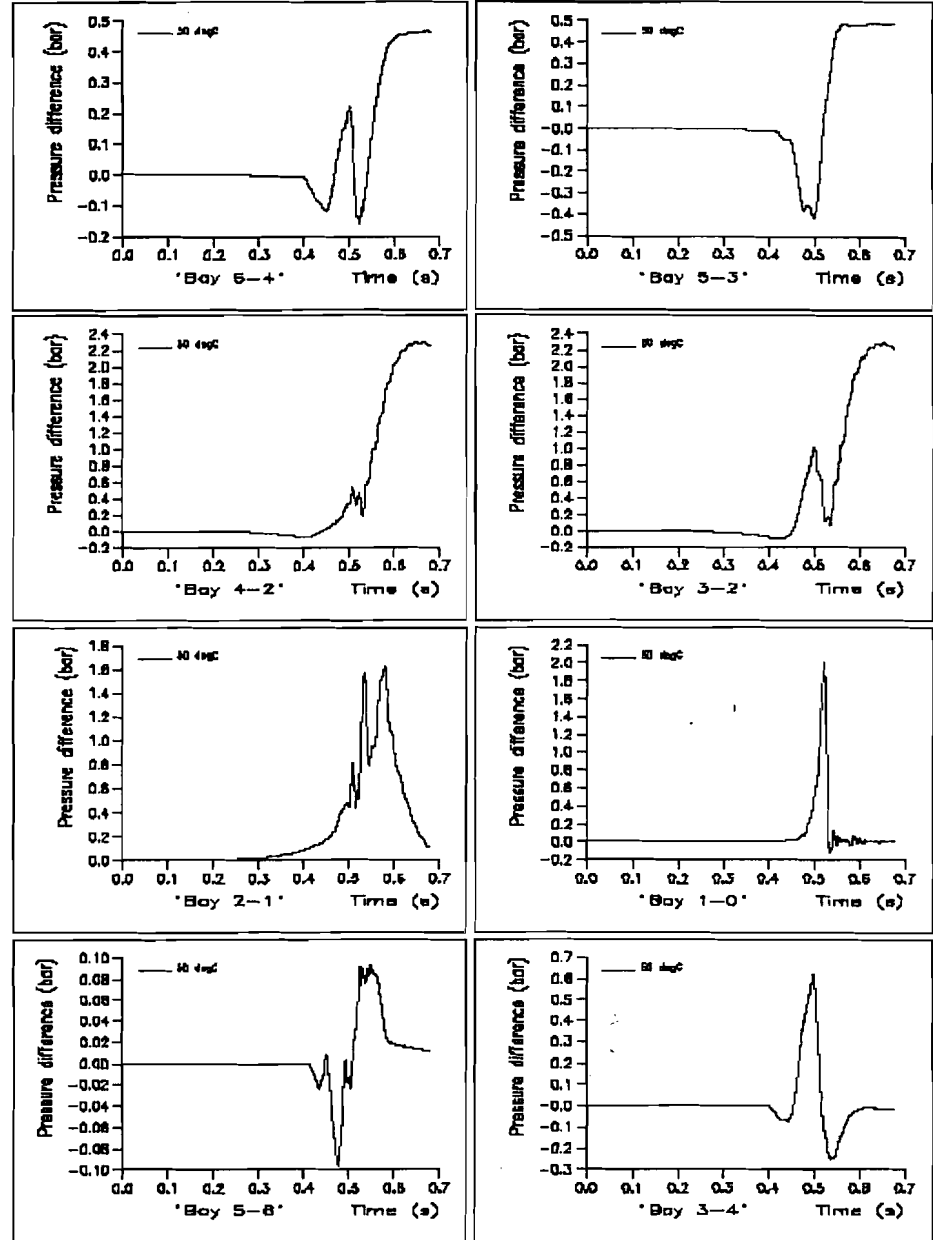
The Mar 23 15:09:47 2008 \*01 scale TWA central wing tank. Ignition point 3 (Bay 1 starboard), SWB2 door delay = 6 ms. T0=50degC.



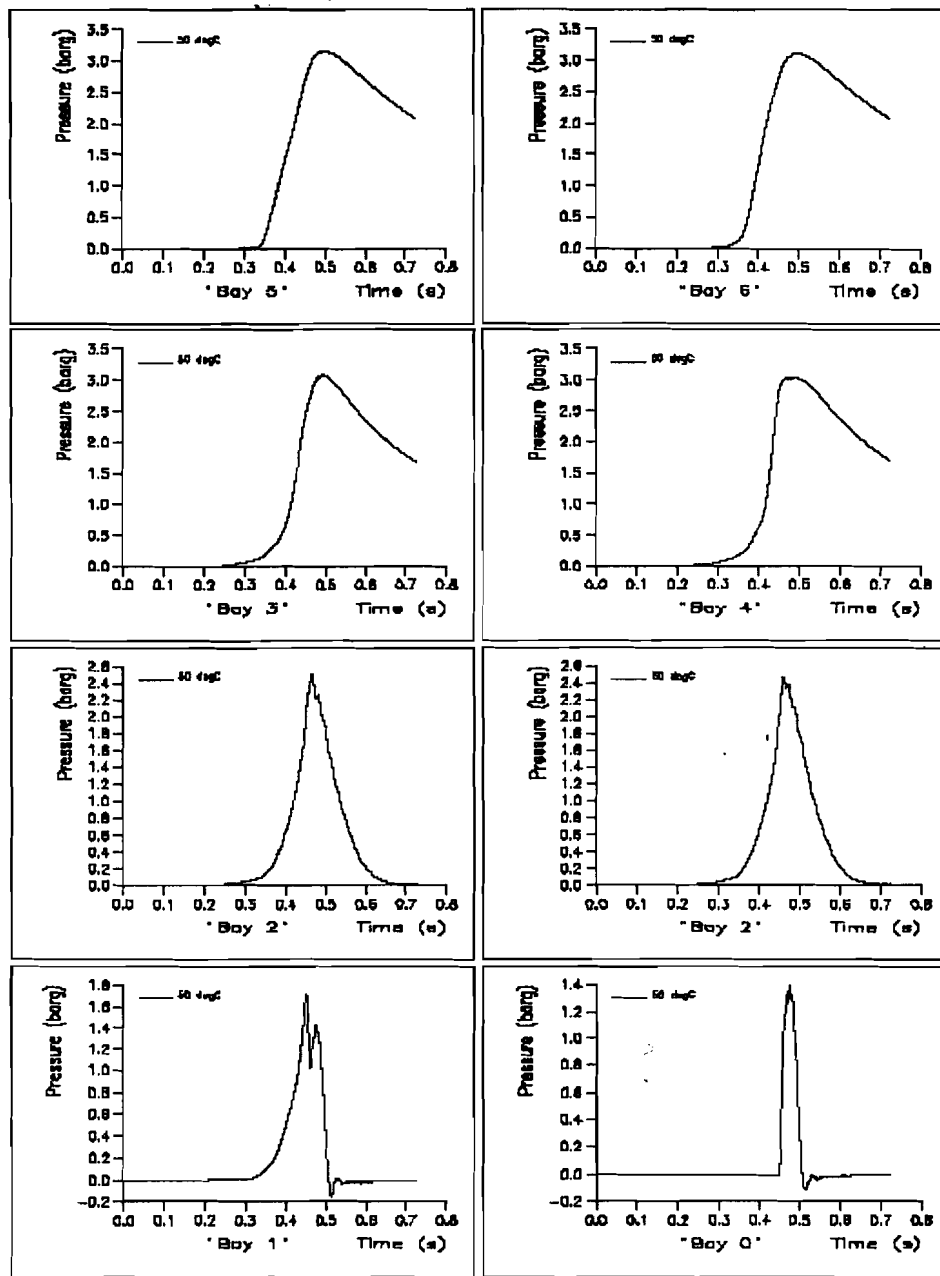
The Mar 23 15:46:41 2009 \*11 scale TWA central wing tank ignition point 4 (Bay 2 mid), SWB2 door delay = 8 ms, T0=50degC



The Mar 23 15:09:15 2009 "1/1 scale TWA central wing tank, ignition point 4 (Bay 2 mid), STWB2 door delay = 0 ms, T0=50degC."

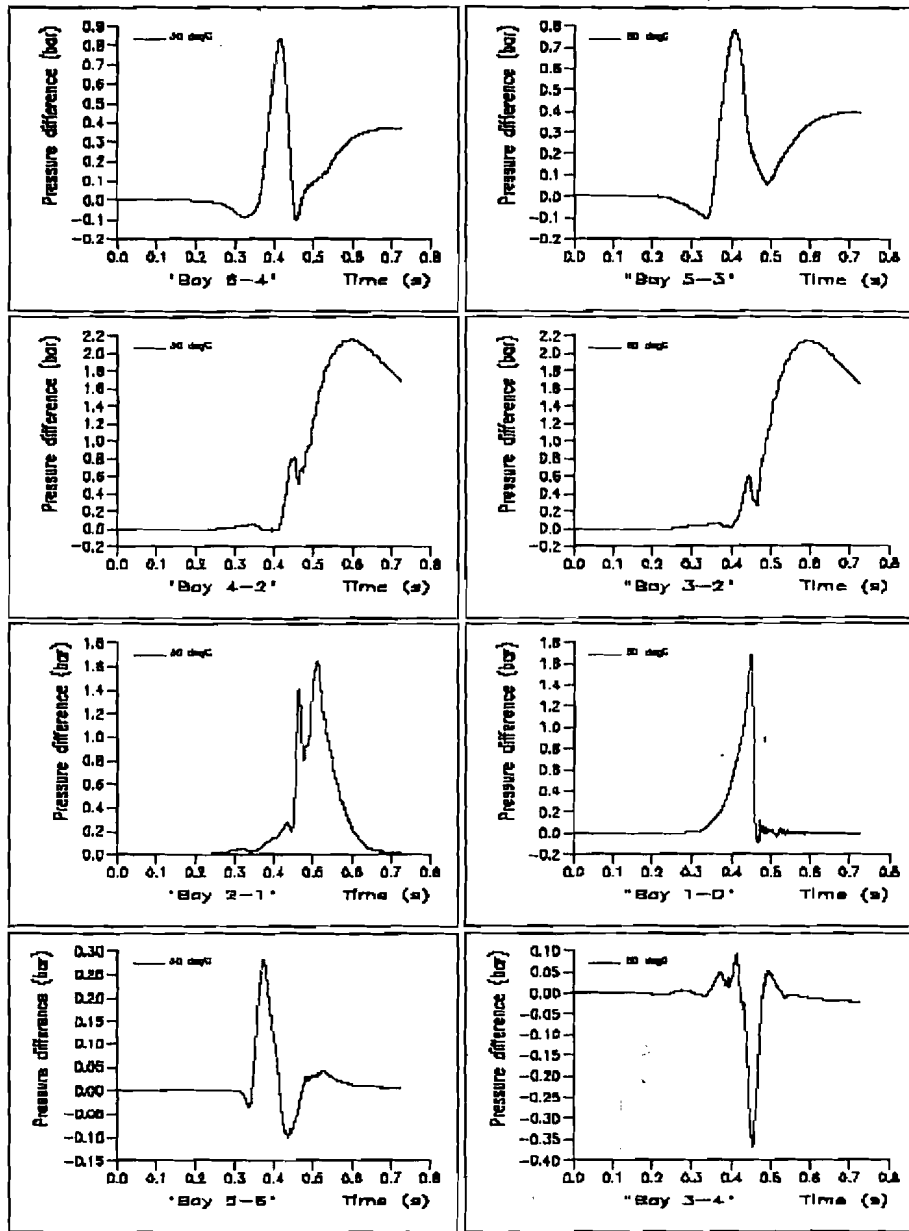


The Mar 23 15:44:57 2000 "1/1 scale TWA center wing tank ignition point 5 (Bay 2 mid), SWB2 door delay = 0 ms, T0=50degC"

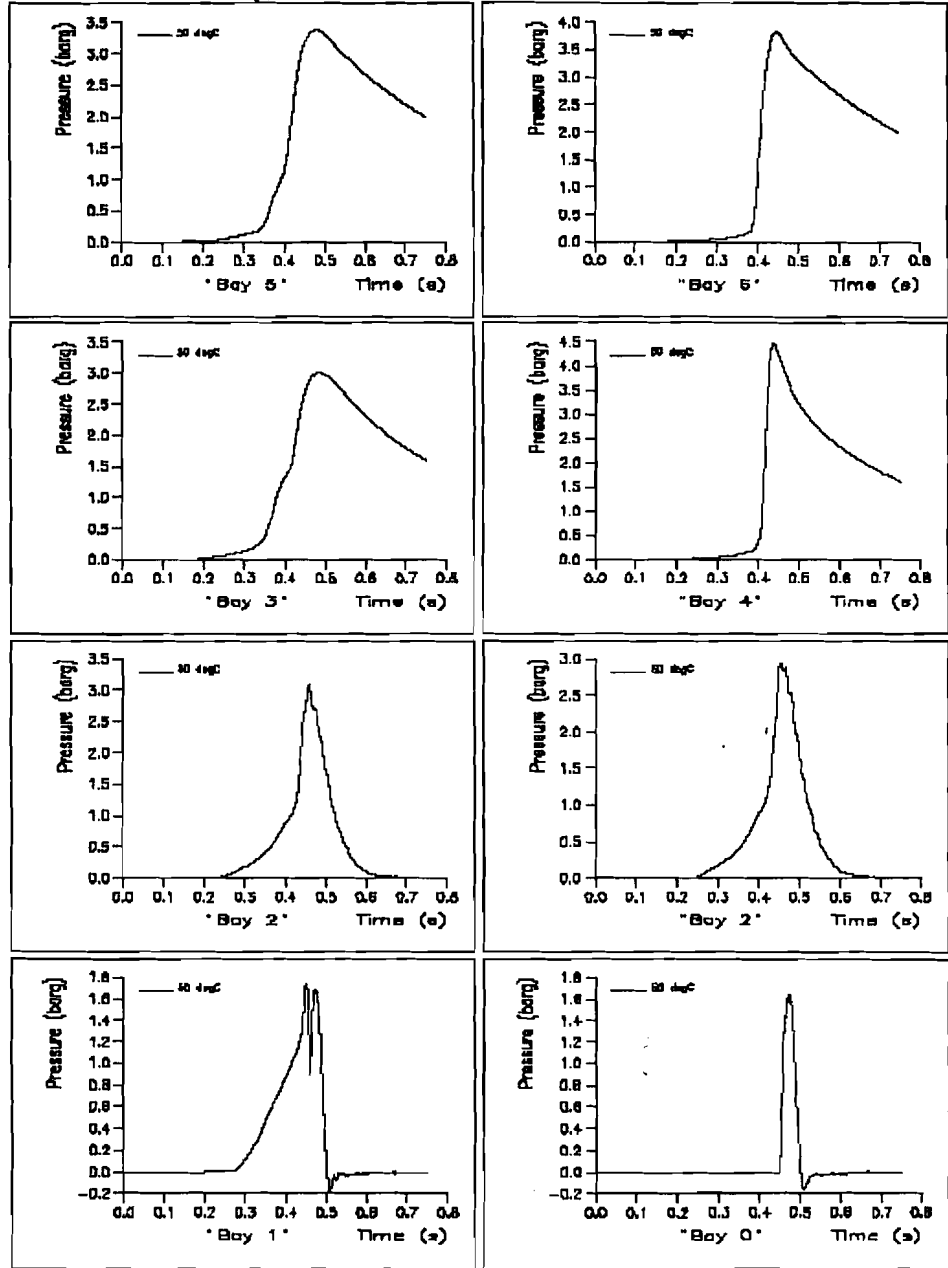




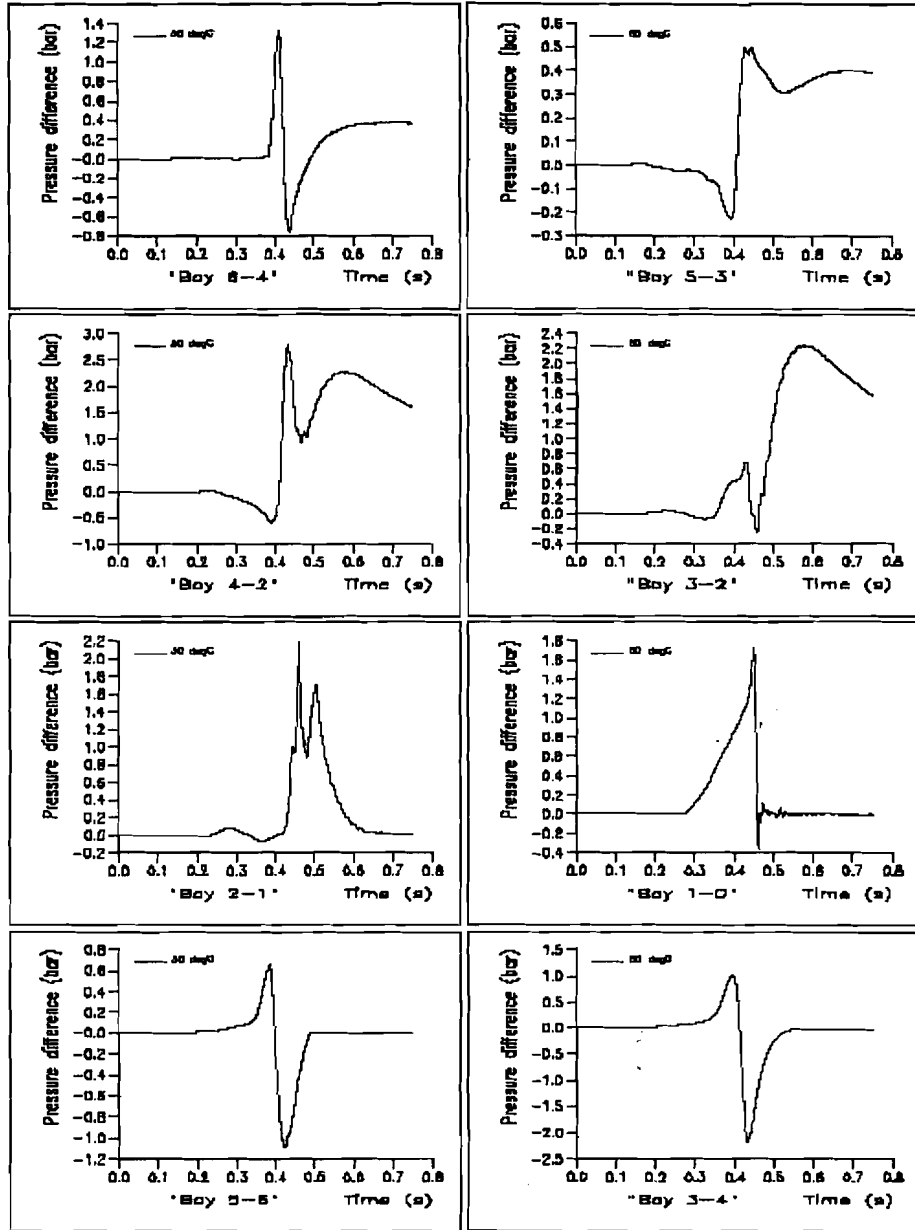
The Mar 23 15:50:24 2000 \*1/1 scale TWA center wing tank ignition point 4 (Bay 2 mid), 9W82 door delay = 0 ms, TD=60degC\*



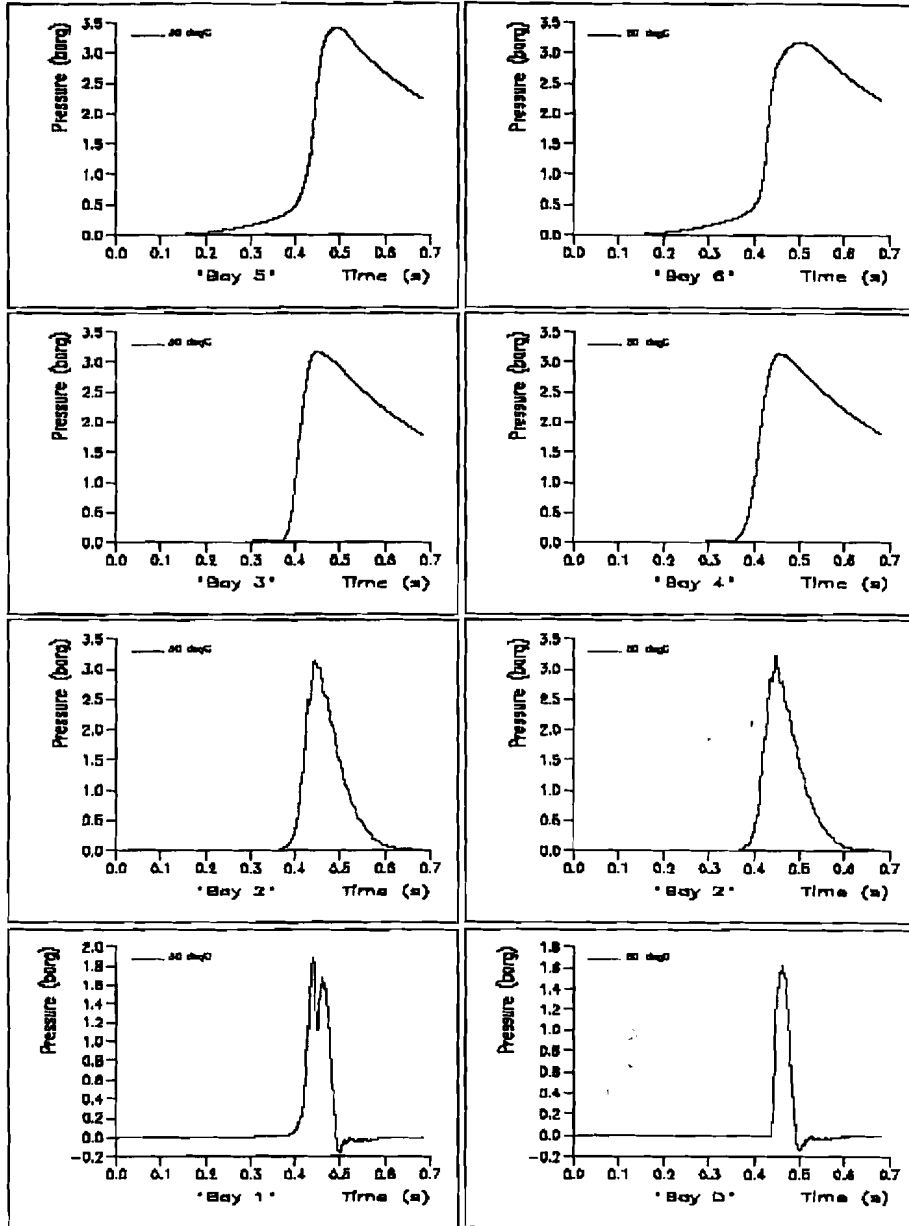
The Mar 23 15:07:21 2000 \*U1 scale TWA central wing tank, ignition point 6 (All Bay 5 port, BWB2 door delay = 0 ms, T=590degC)



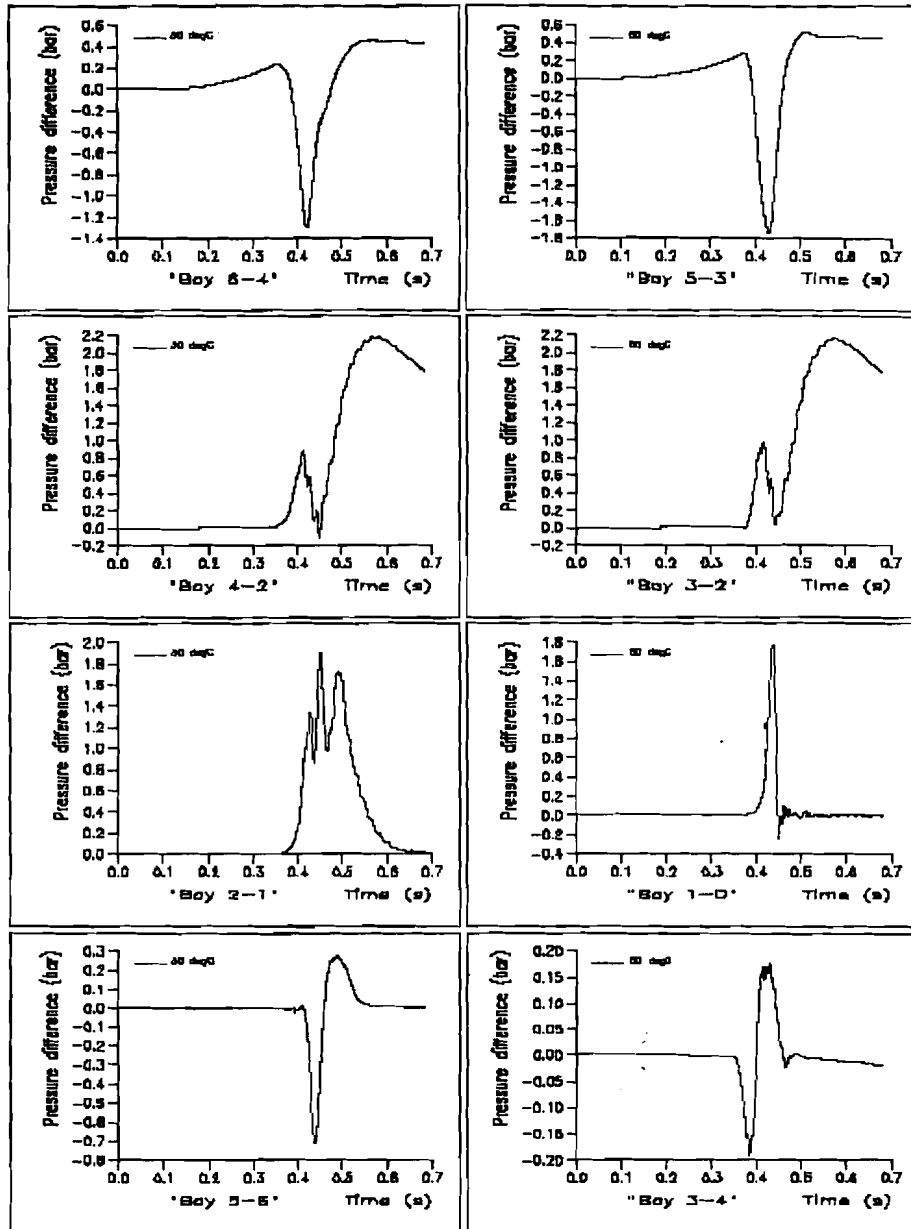
Thu Mar 23 15:00:33 2000 \*M1 scale TWA\_center wing tank, Ignition point 4 (AR Bay 5 port), SWB2 door delay = 0 ms, TD=50degC\*



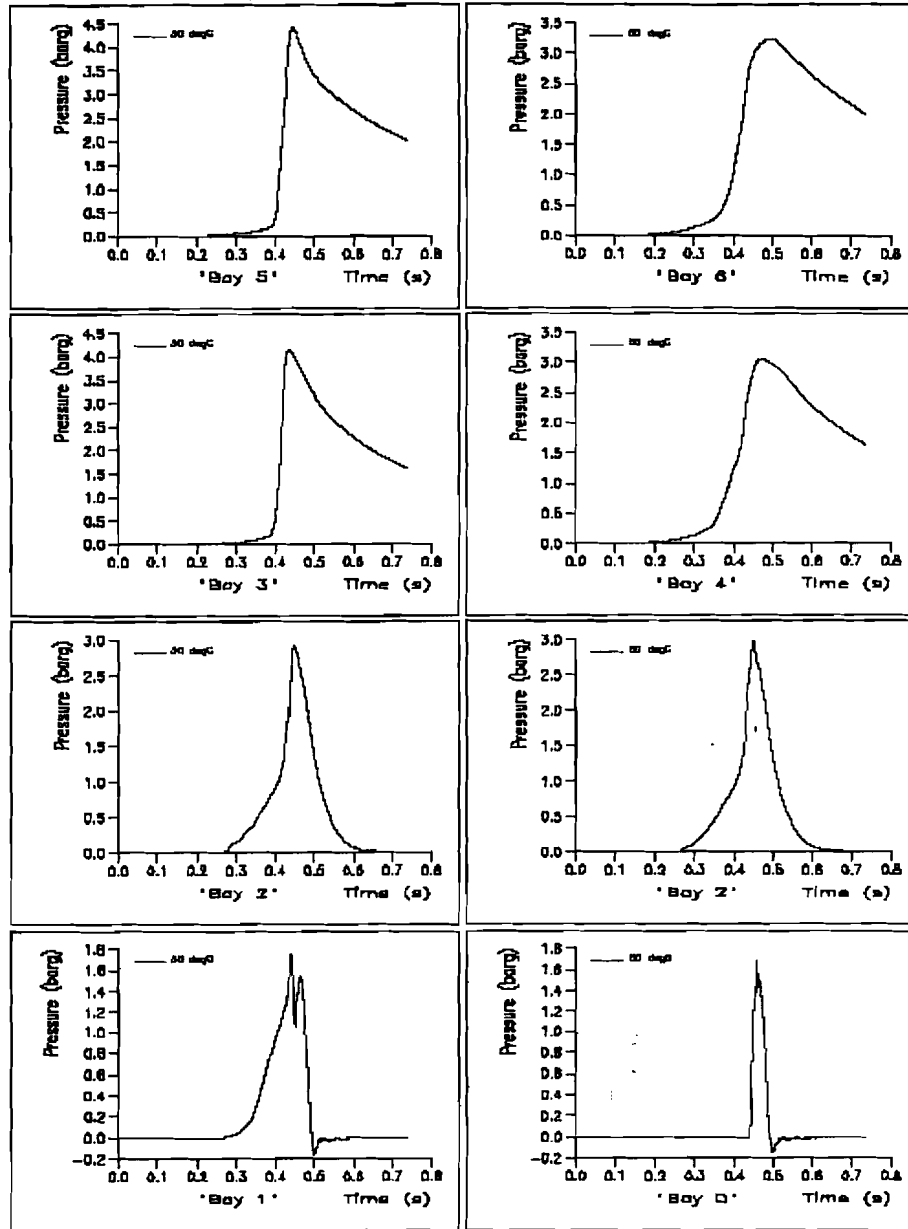
Thu Mar 29 15:47:33 2000 \*1/1 scale TW4 center wing tank ignition point 7 (Air Bay 6 mid), SWB2 door delay = 0 ms, TD=60degC



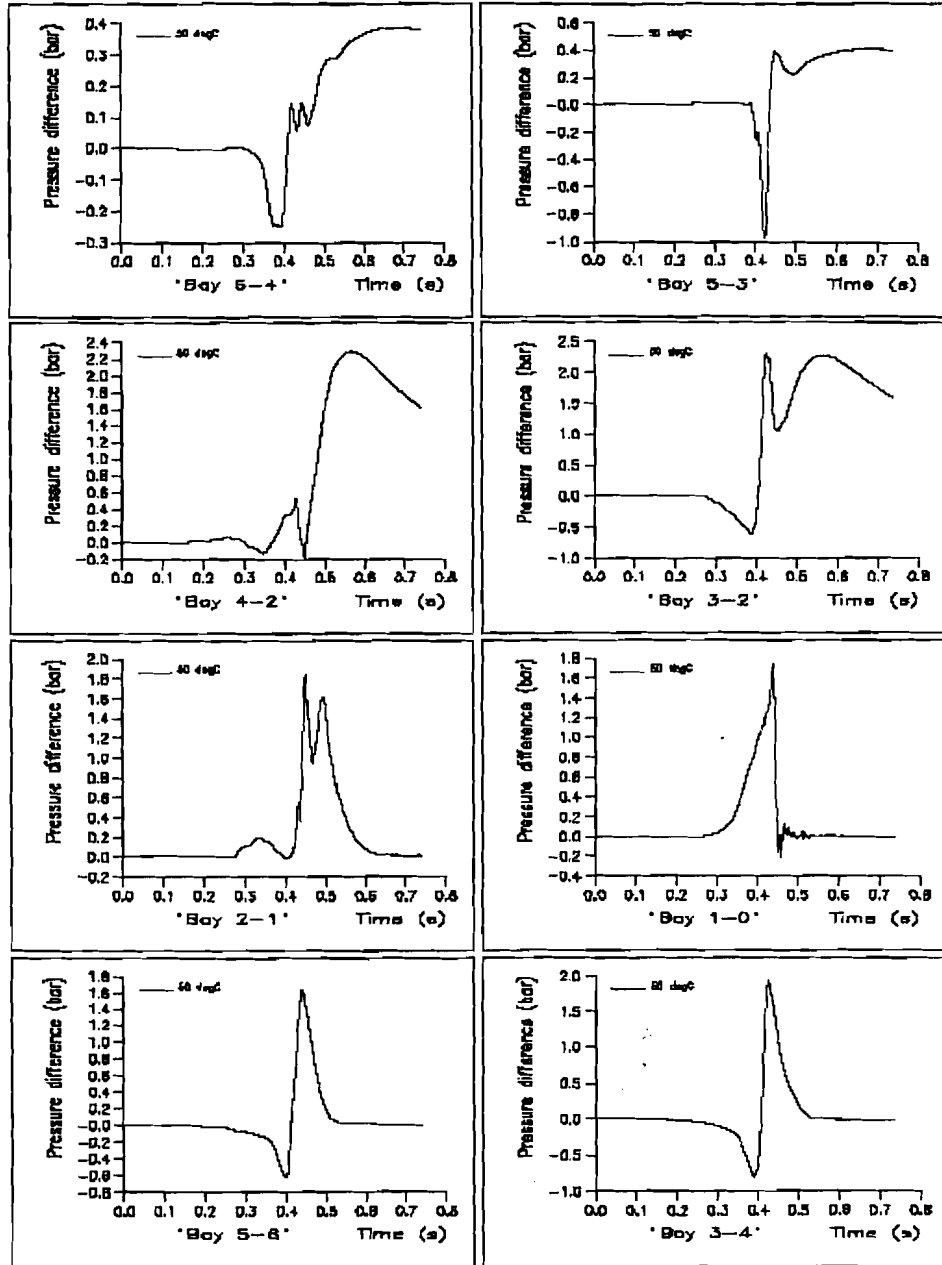
Thu Mar 23 15:46:43 2000 \*1/1 scale TWA central wing tank, Ignition point ? (AR Bay 6 mid), SWB2 door delay = 0 ms, T0=50degC\*



Thu Mar 22 15:07:47 2000 \*M1 scale TWA center wing tank, ignition point 8 (AR Bay 8 starboard), SWB2 door delay = 0 ms, TD=99degC



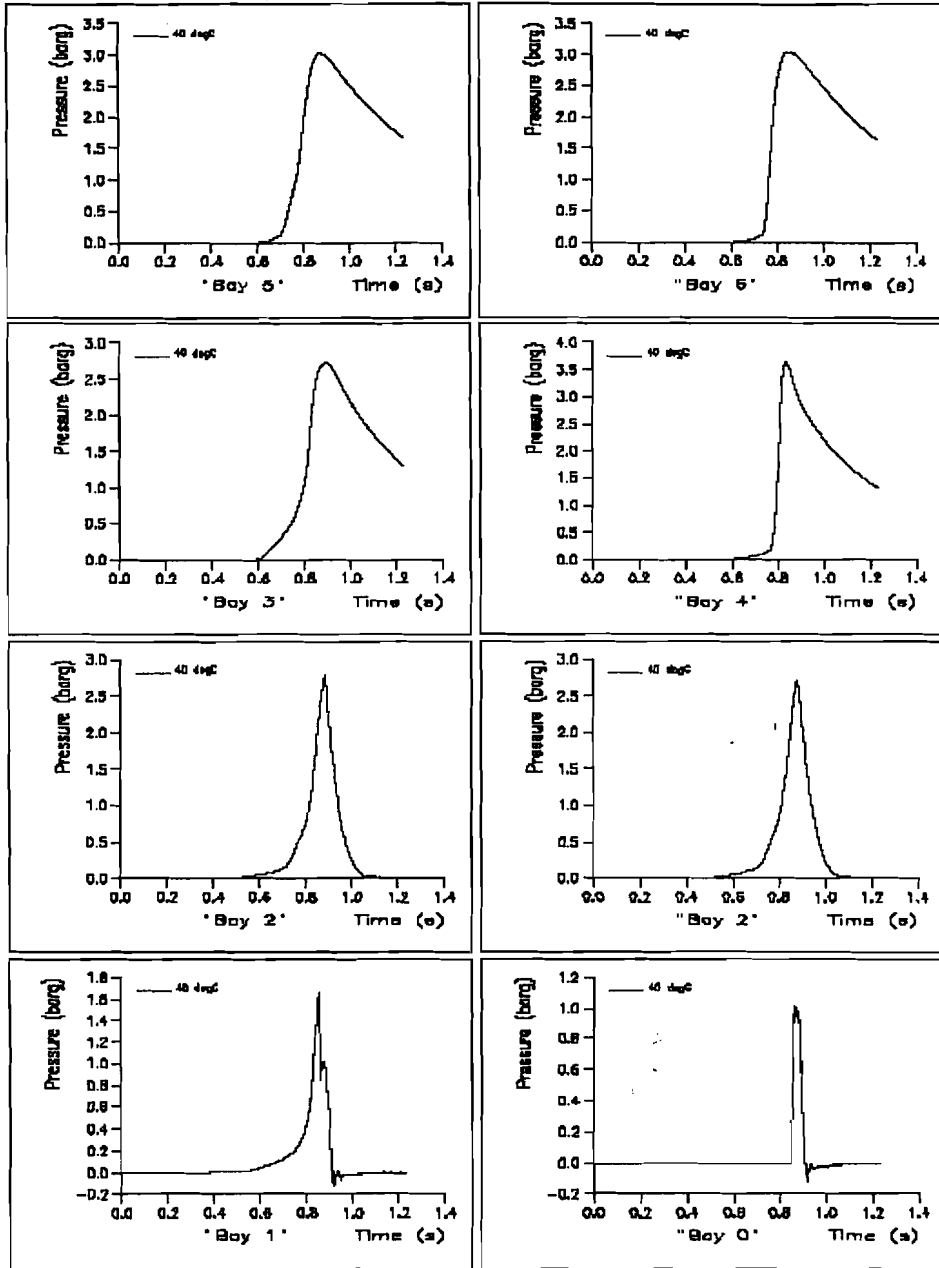
The Mar 23 15:09:52 2000 "1/1 scale TWA center wing tank, Ignition point 8 (AR Bay 8 starboard), SWB2 door delay = 0 ms, T0=50degC."



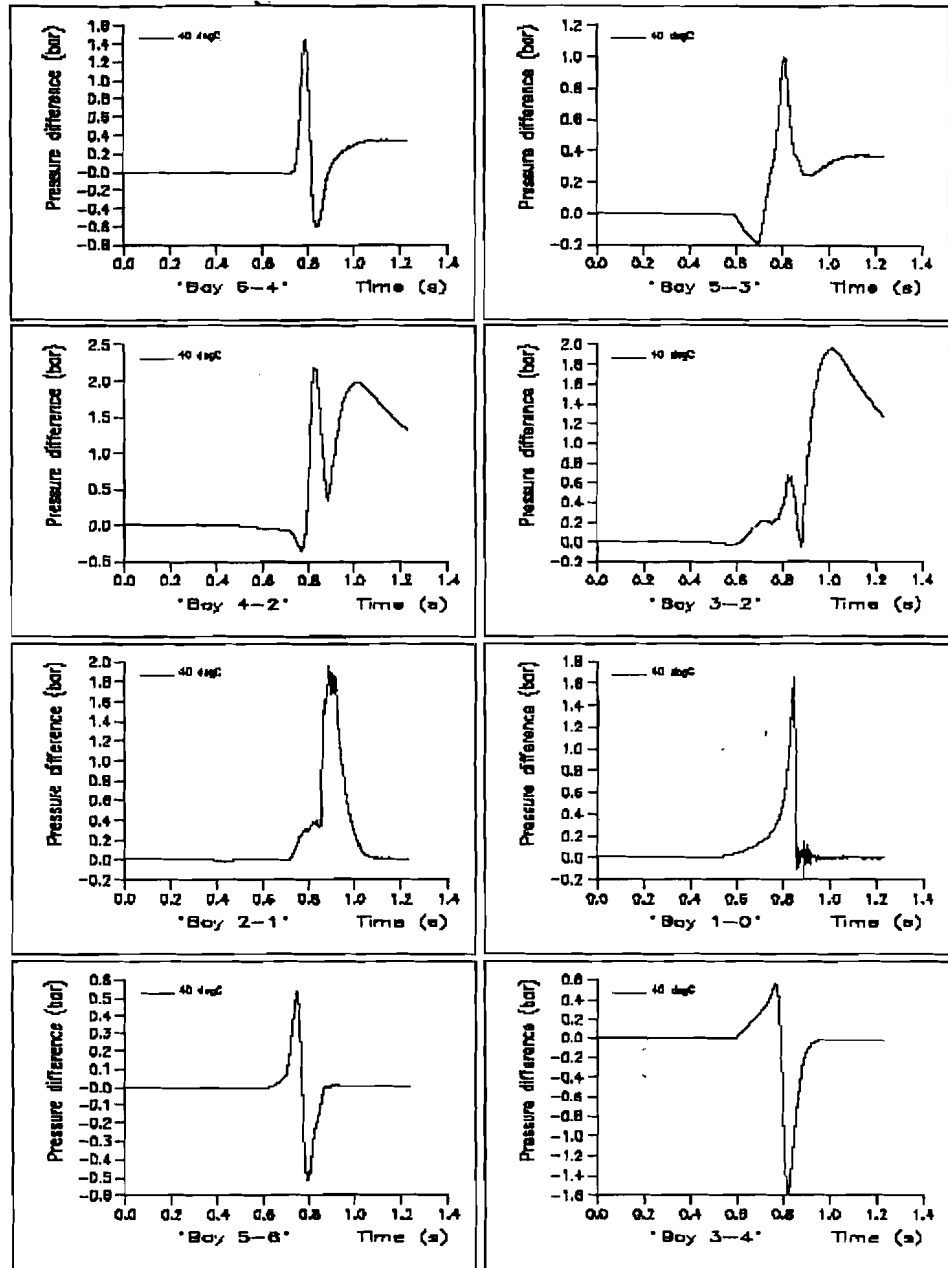
**Series 3: Initial temperature 40 °C, moment of failure of  
manufacturing panel 24 ms after failure of FS, eight ignition positions**



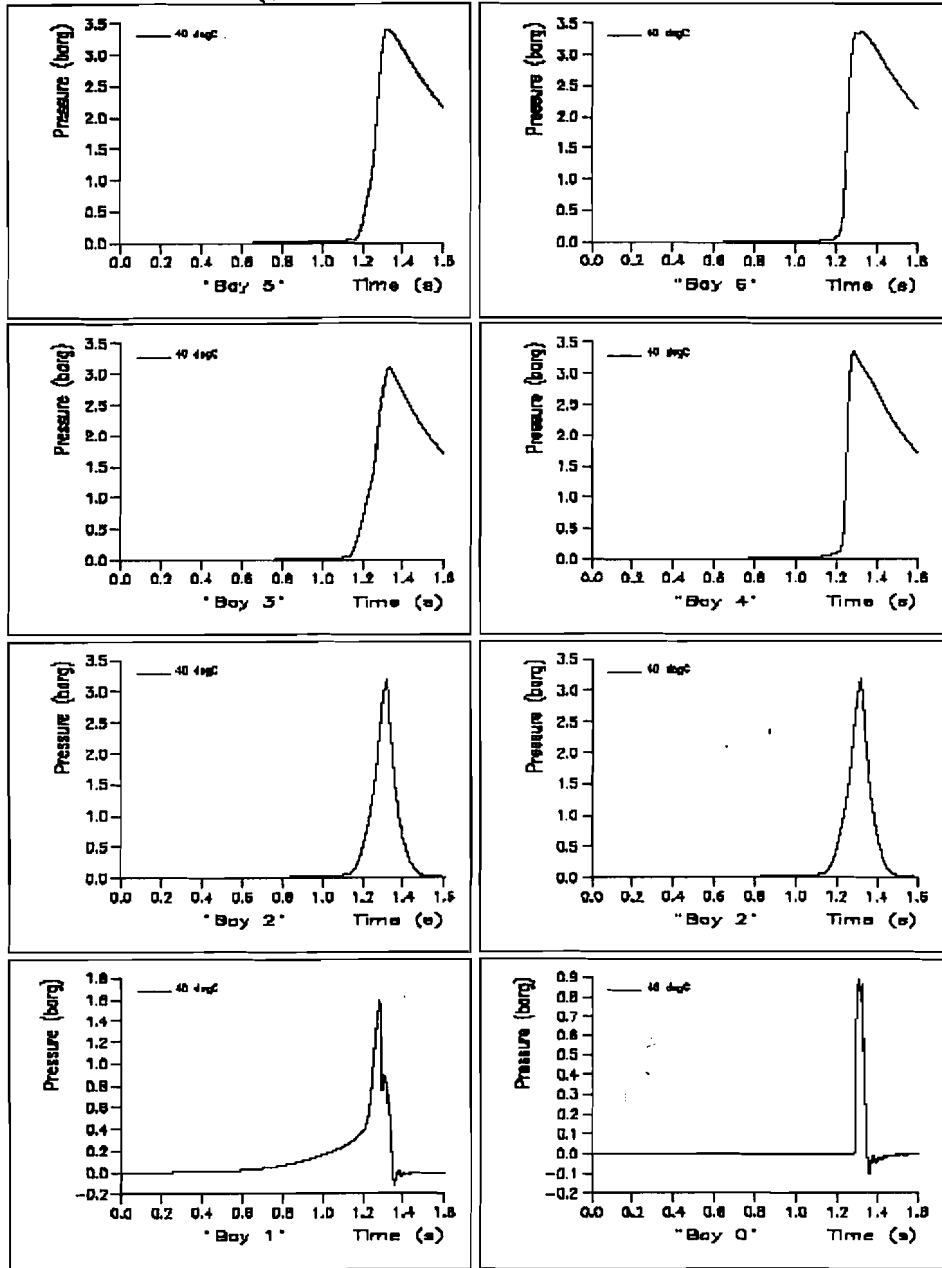
Mon Jan 24 08:51:28 2000 '1/7 scale TWA central wing tank ignition point 1 (Bay 1 port), SWB2 door delay = 24 ms, T0=40degC'



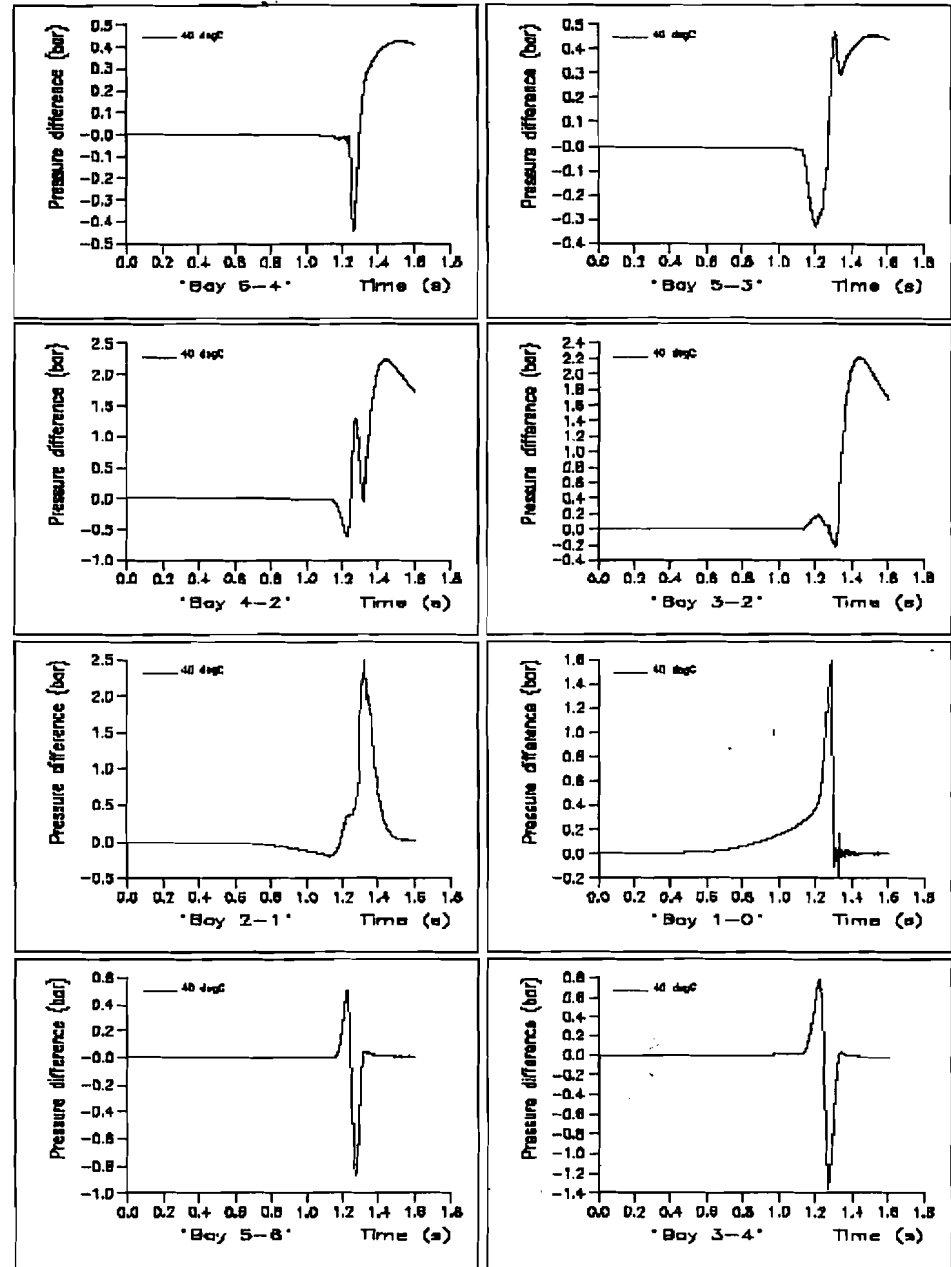
Mon Jan 24 09:45:52 2000 1/1 scale TWA central wing tank, Ignition point 1 (Bay 1 port), SWB2 door delay = 24 ms, T0=10degC



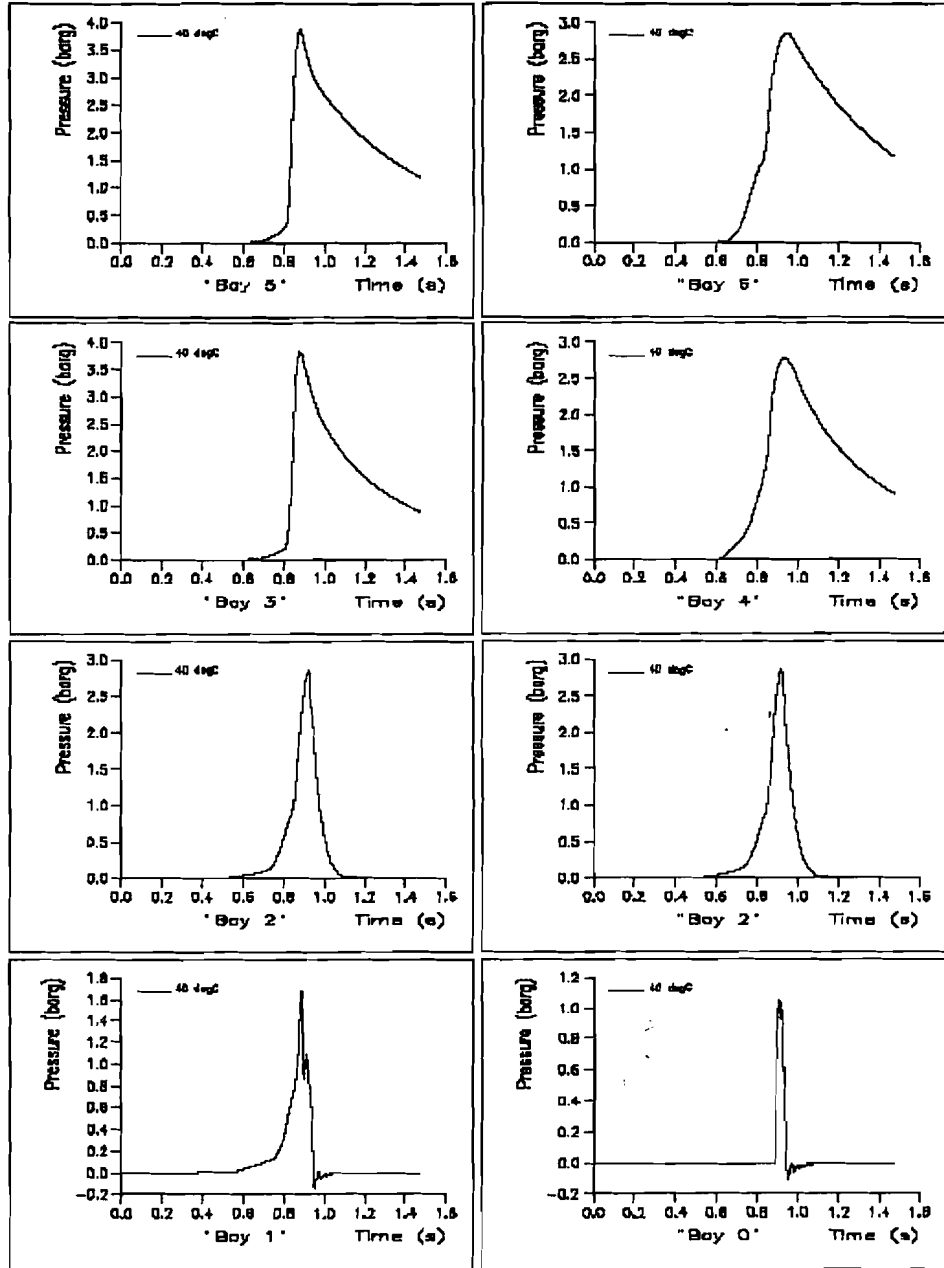
Mon Jan 24 08:51:42 2000 1/1 scale TWA central wing tank Ignition point 2 (Bay 1 mid), SWB2 door delay = 24 ms, T0=40degC



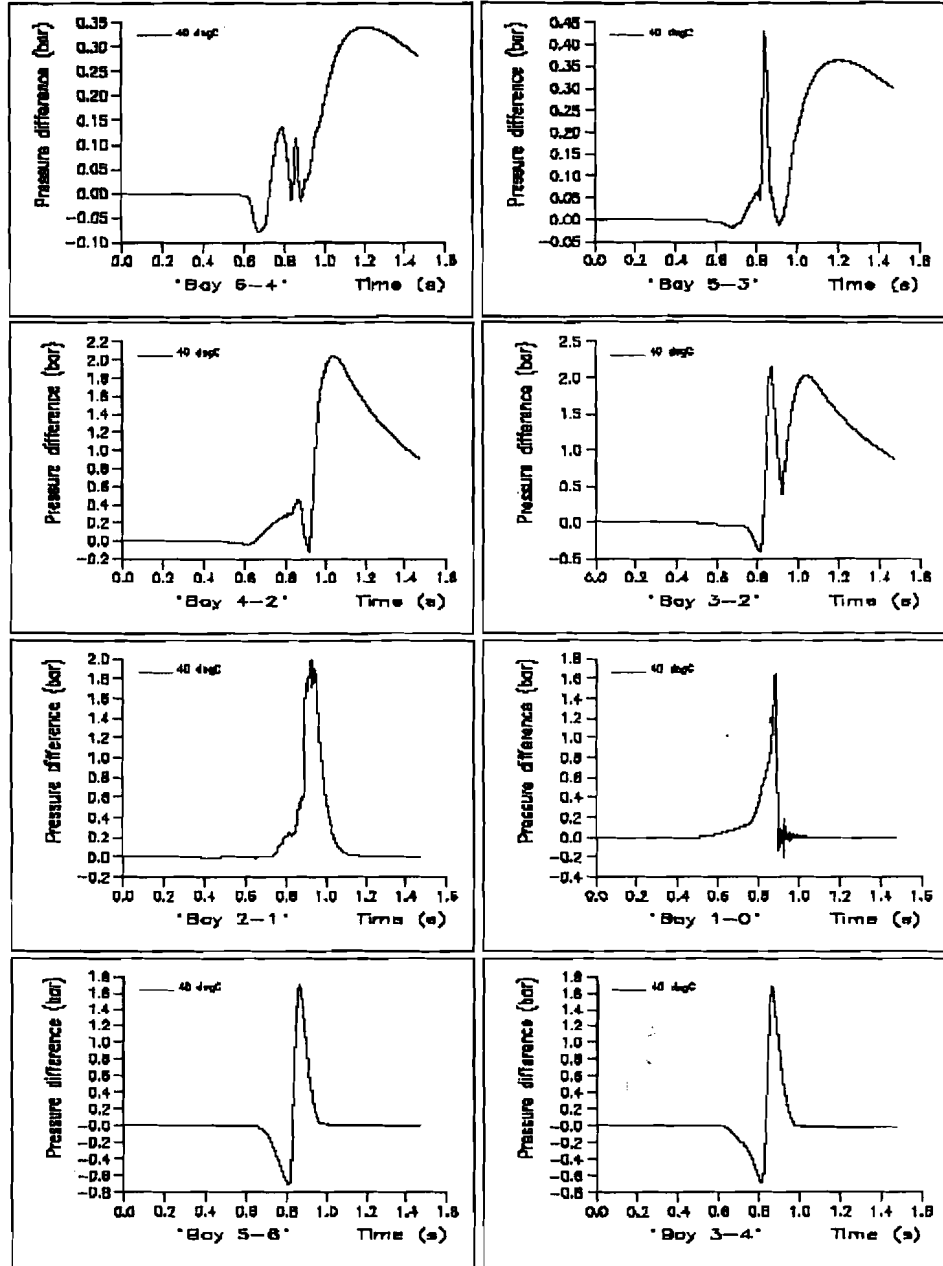
Mon Jan 24 08:48:11 2000 \*T1 scale TWA central wing tank, ignition point 2 (Bay 3 mid), SWB2 door delay = 24 ms, T0=40degC\*



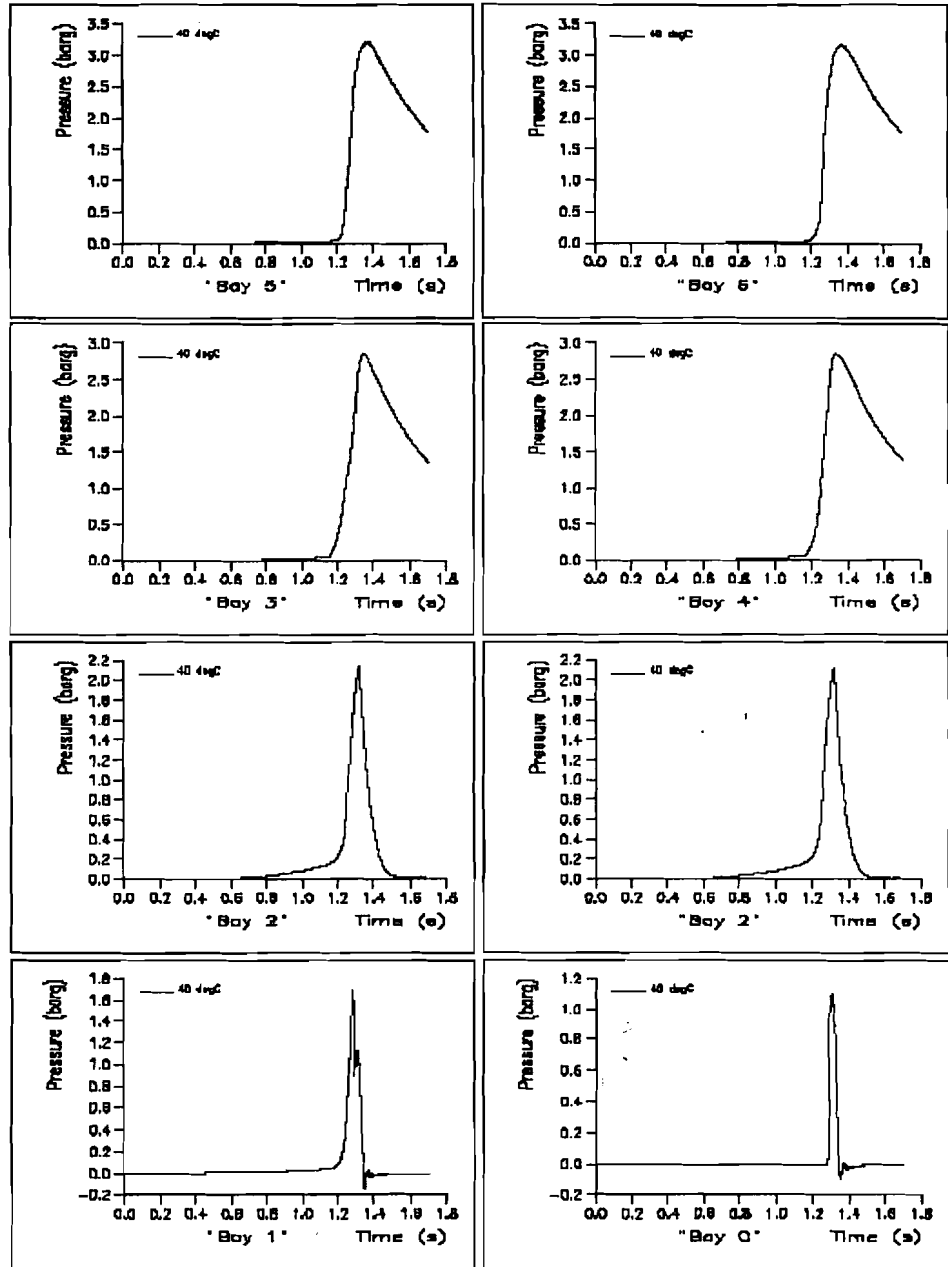
Mon Jan 24 08:51:56 2000 \*1/1 scale TWA center wing tank ignition point 3 (Bay 1 starboard), 50/B2 door delay = 24 ms, 10>40degC\*



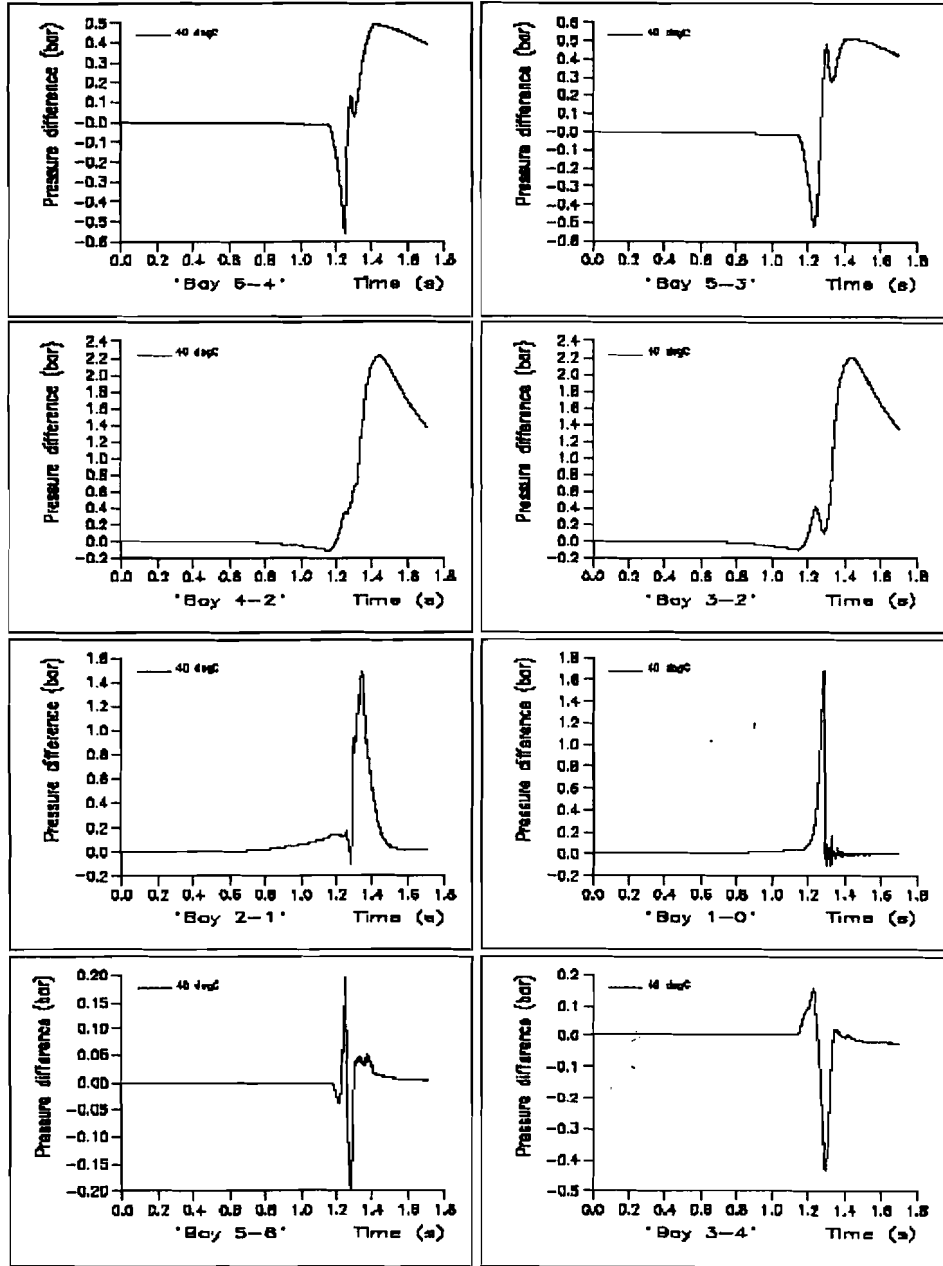
Mon Jan 24 08:48:32 2000 \*1/1 scale TWA\_center wing tank. Ignition point 3 (Bay 1 starboard), SWB2 door delay = 24 ms, T0=40degC.\*



Mon Jan 24 08:52:12 2000 '1/1' scale TWA central wing tank, Ignition point 4 (Bay 2 mid), SWB2 door delay = 34 ms, T0=40degC

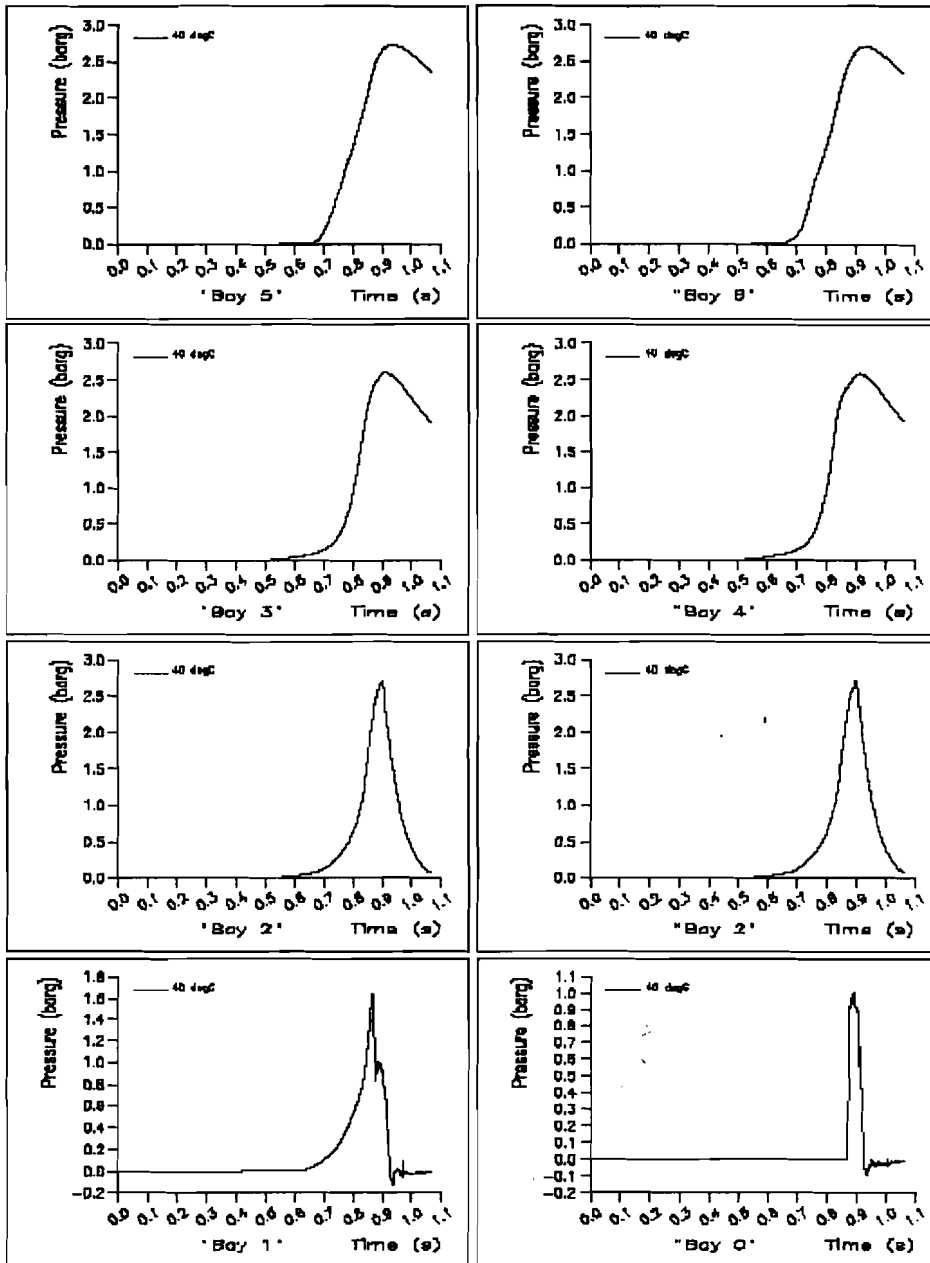


Mon Jan 24 09:05:21 2000 \*1/1 scale TWA central wing tank. Ignition point 4 (Bay 3 mid), SWB2 door delay = 24 ms. T0=0degC\*

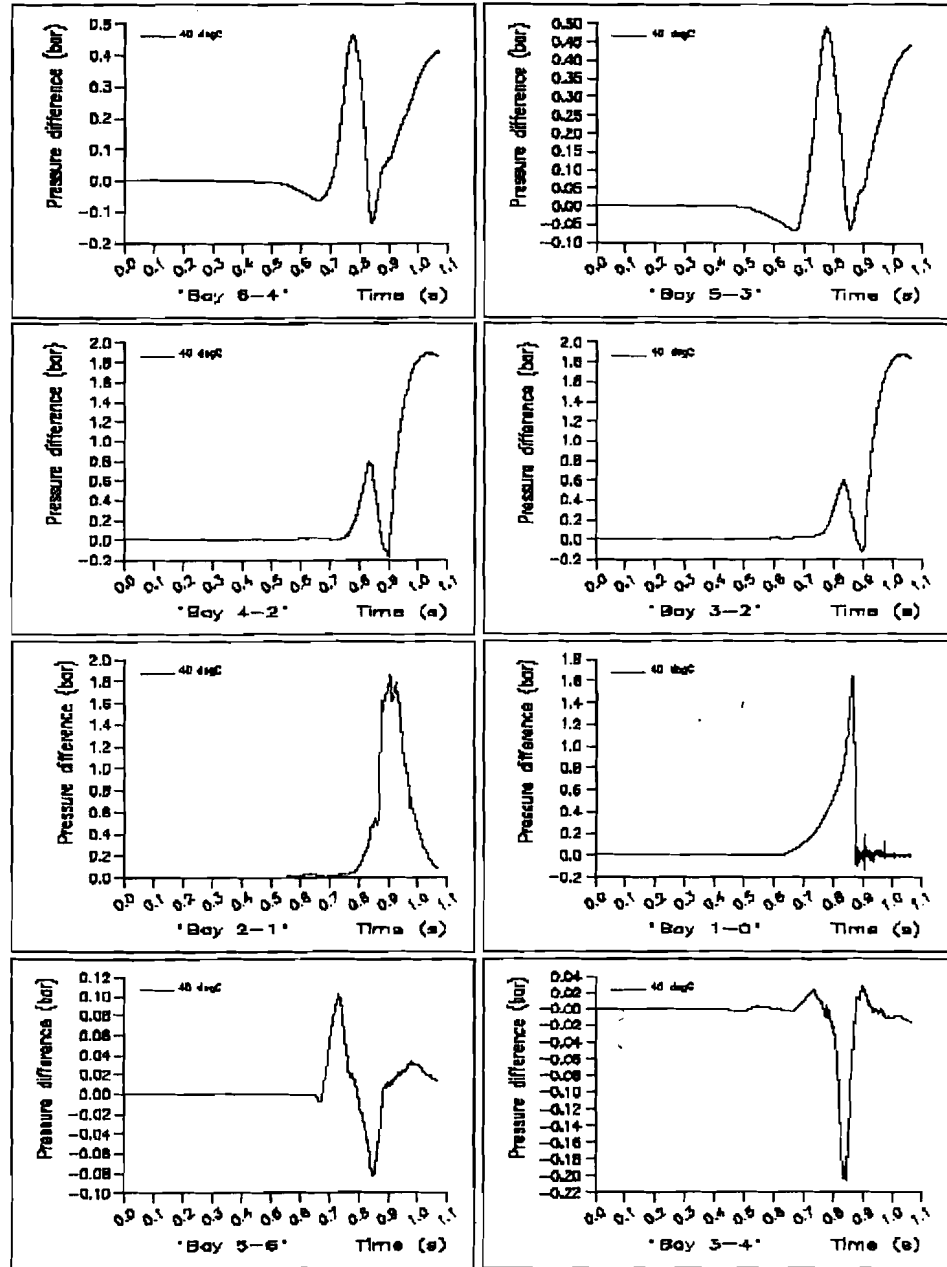




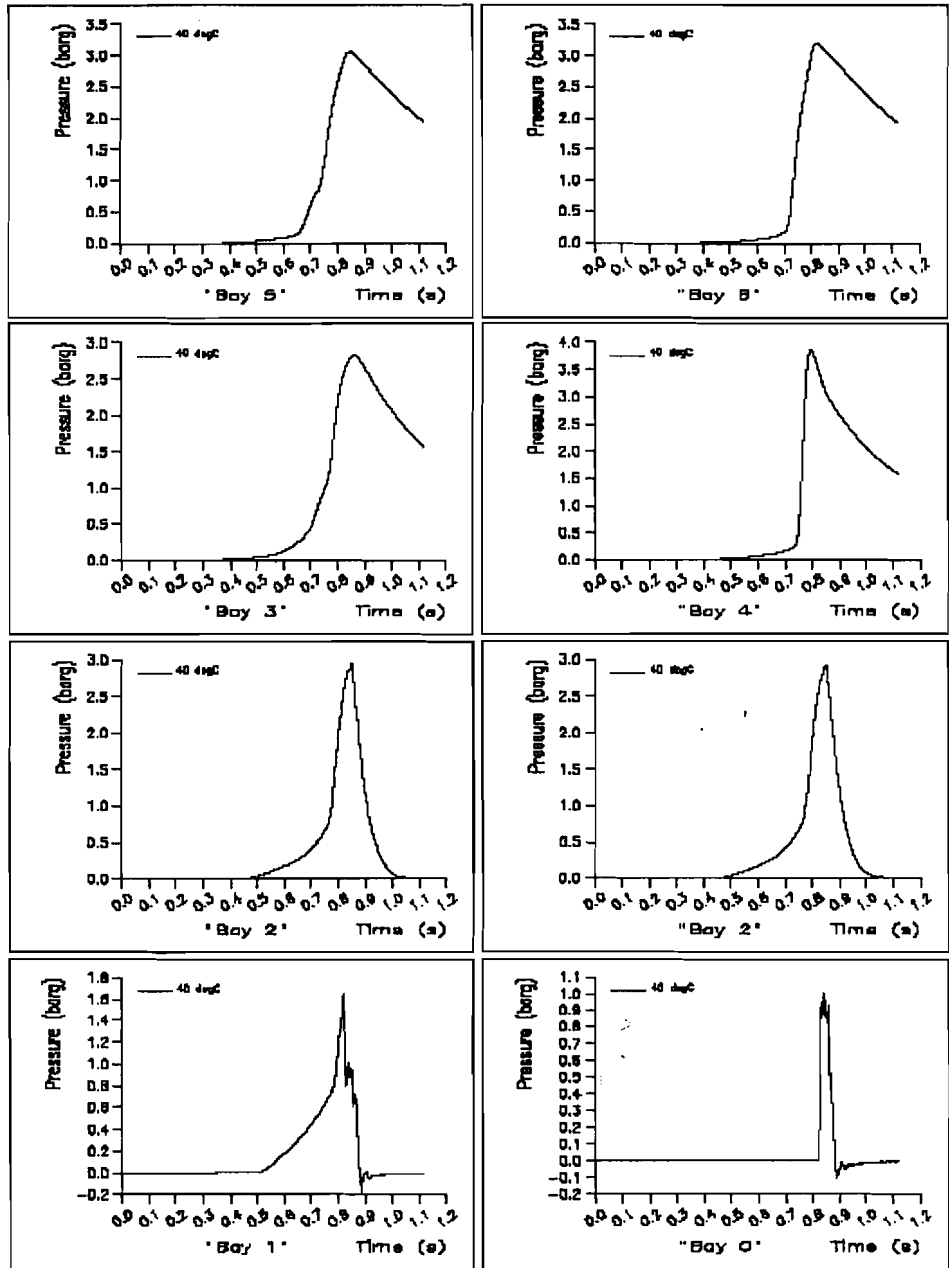
Mon Jan 24 08:52:23 2000 \*1/1 scale TWA central wing tank Ignition point 5 (Bay 2 mid), SWB2 door delay = 24 ms, T0=40degC



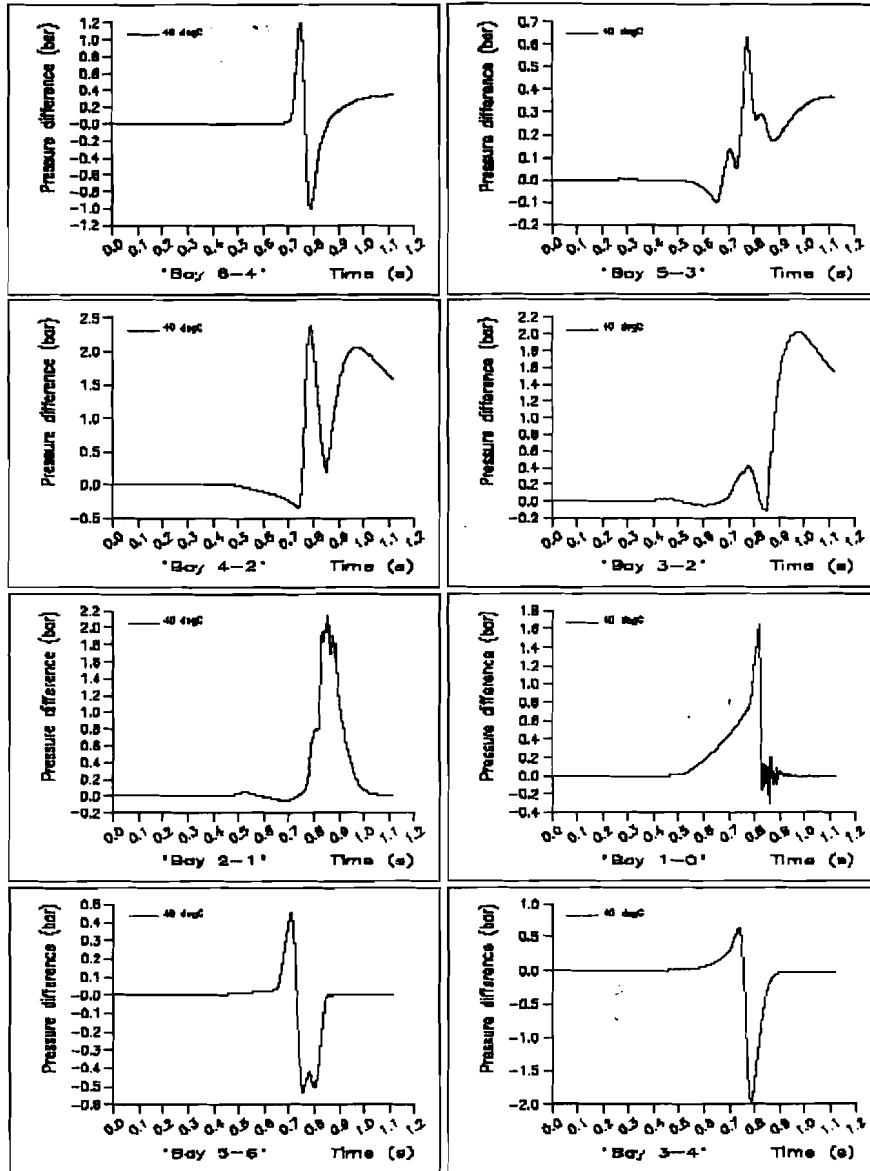
Mon Jun 24 08:47:14 2008 \*U1 scale TWA central wing tank, ignition point 5 (Bay 2 mid), SWB2 door delay x 24 sec, T0=46degC\*



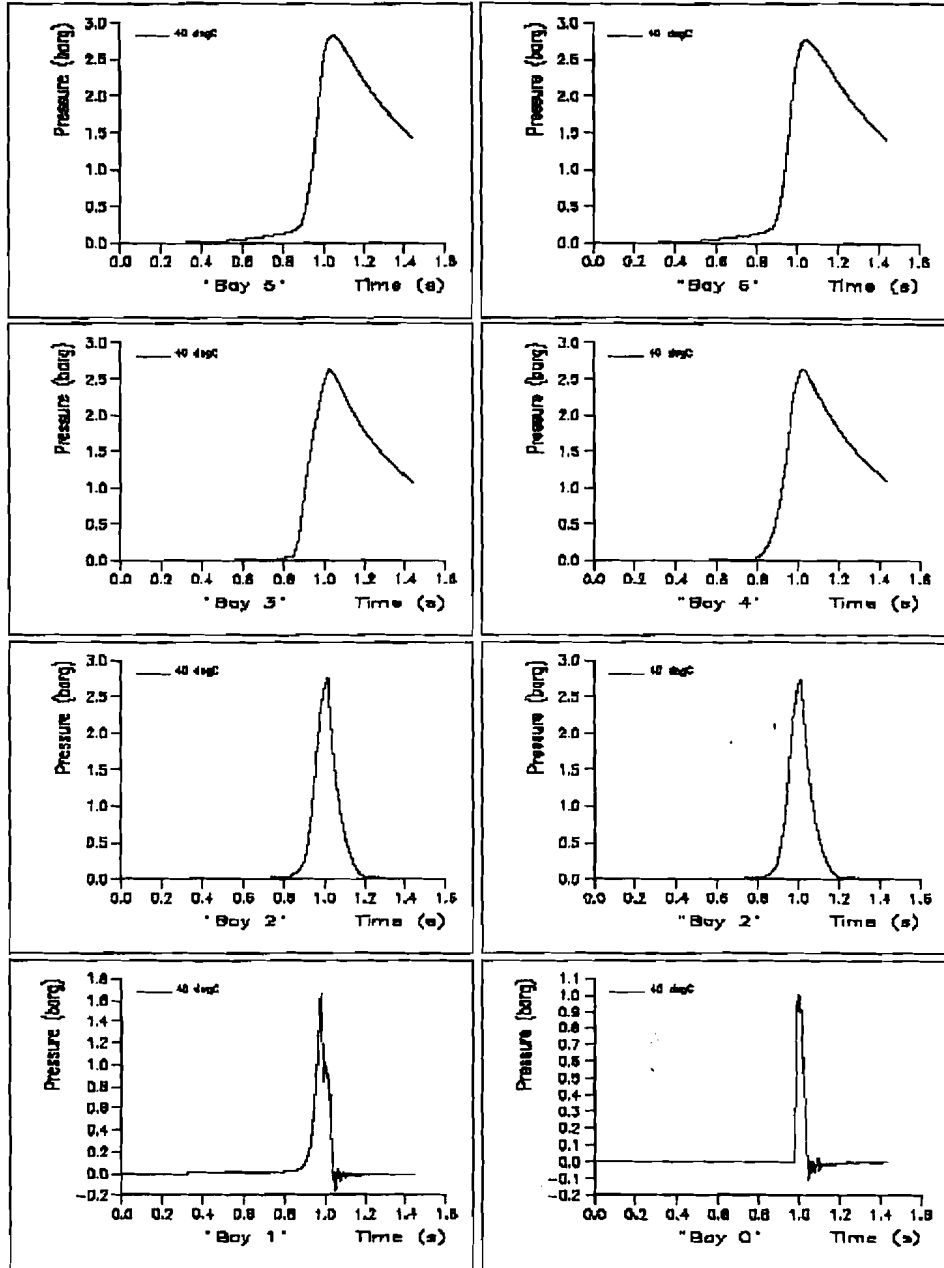
Mon Jan 24 08:52:33 2006 1/1 scale TWA center wing tank ignition point B (AB Bay 5 port), SW02 door delay = 24 ms, T0=40degC



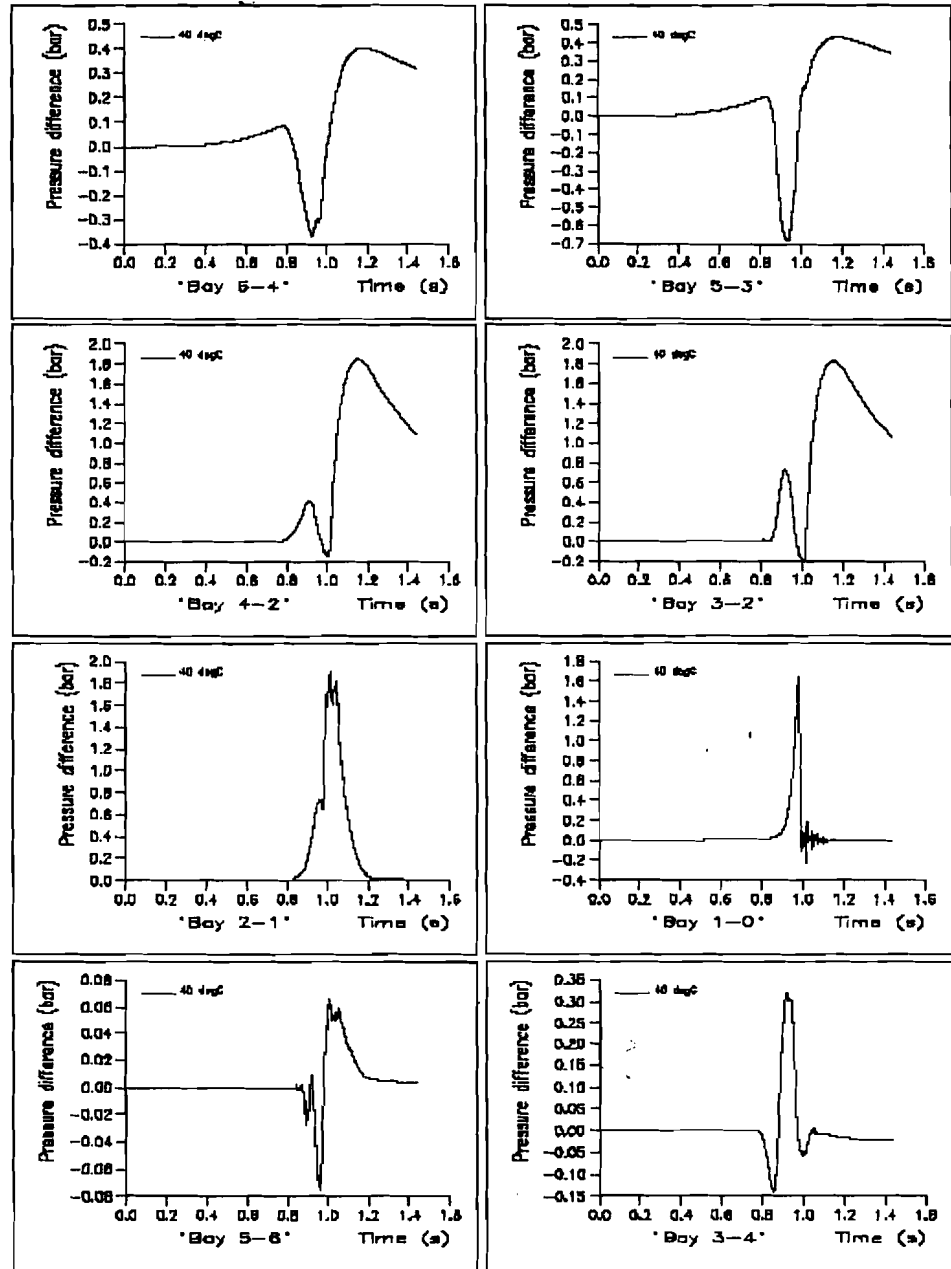
Mon Jan 24 08:05:40 2000 \*1/1 scale TWA center wing tank, ignition point 6 (Alt Bay 5 port), SWB2 door delay = 34 ms, TSo=40degC\*



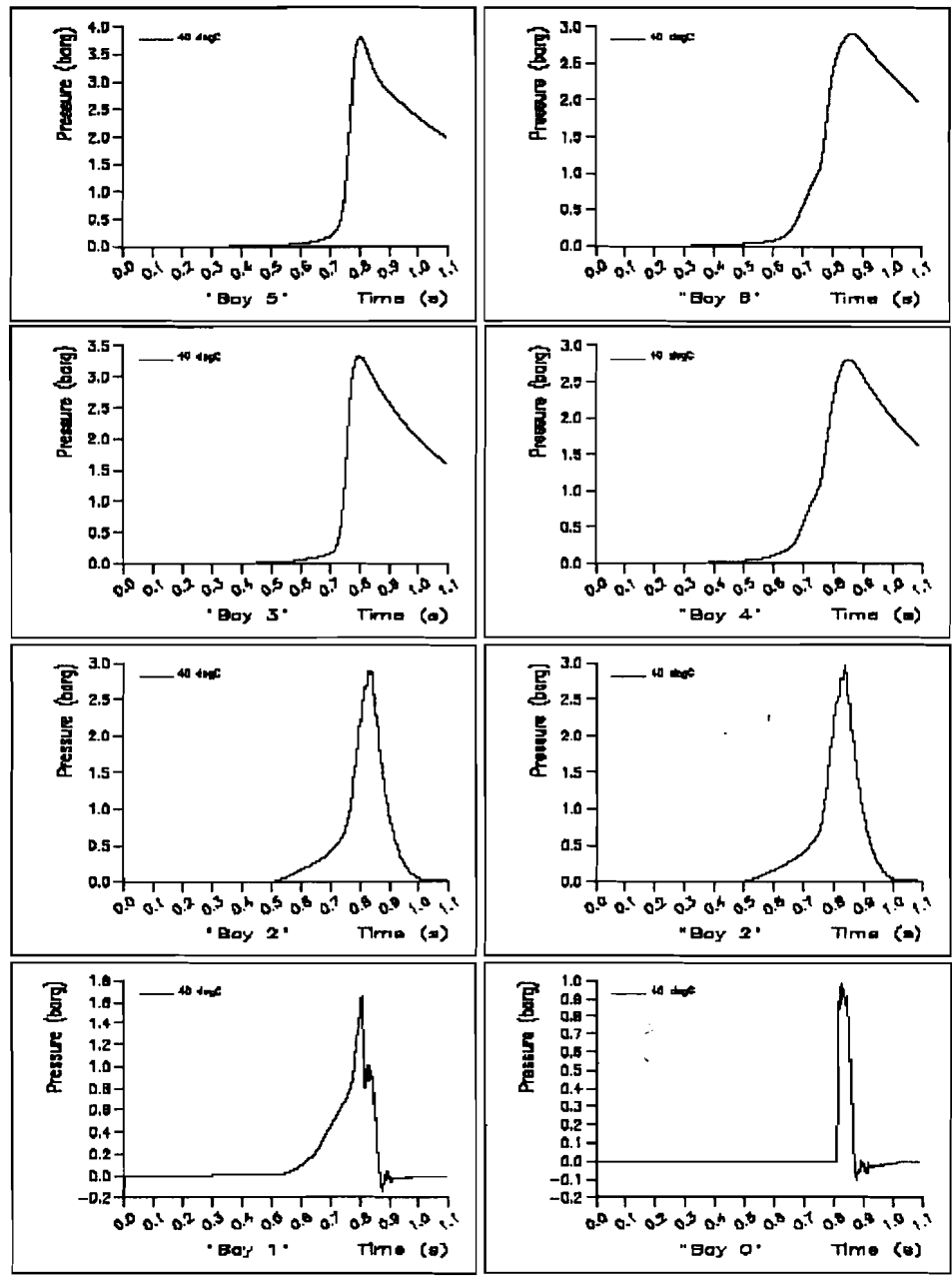
Mon Jan 24 08:52:47 2000 \*1/1 scale TWA center wing tank ignition point 7 (AR Bay 6 mid, SWB2 door delay = 24 ms. T0=40degC



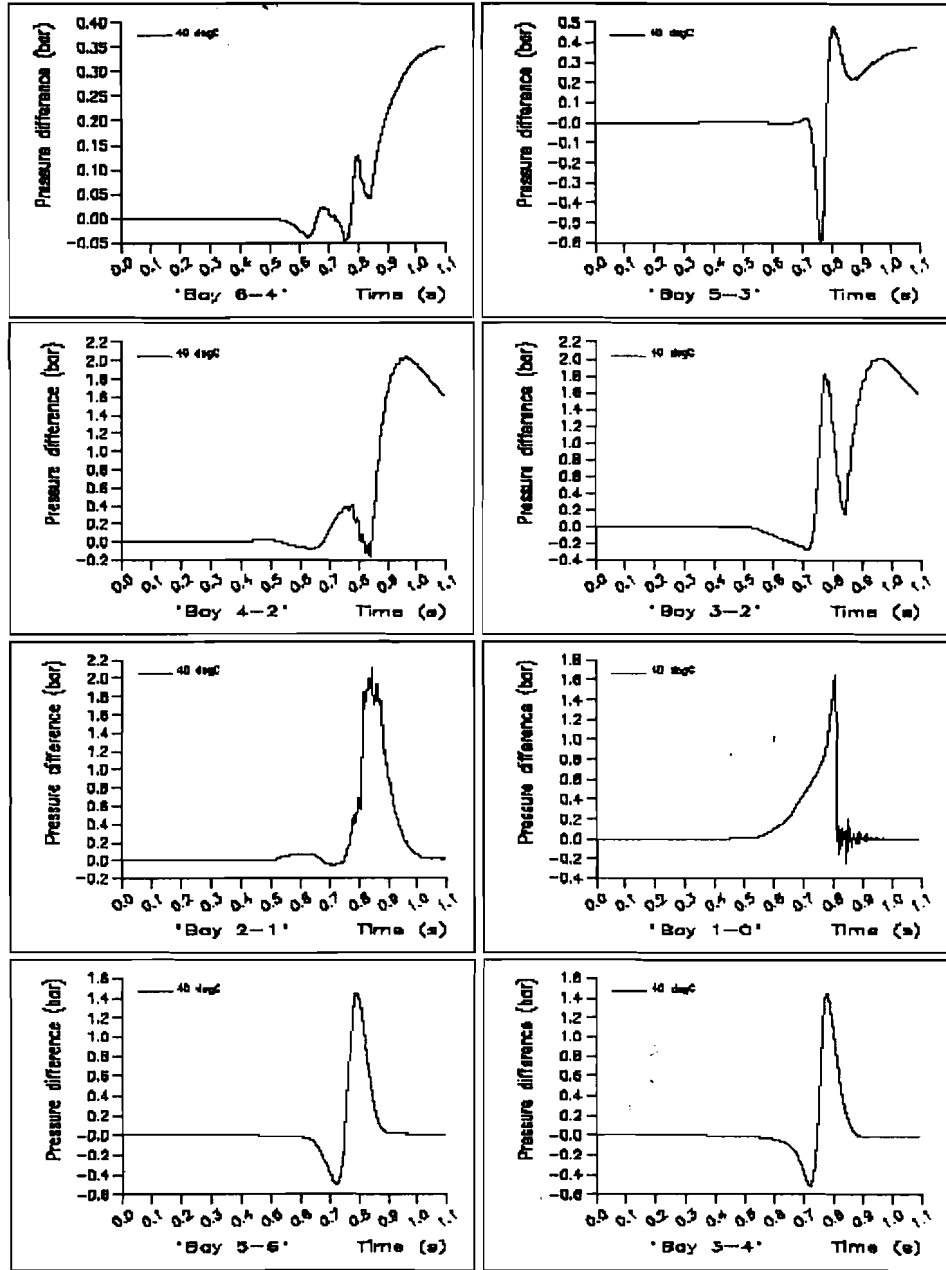
Mon Jan 24 09:05:59 2000 1/11 scale TWA center wing tank, ignition point 7 (AR Bay 6 mid), SWB2 door delay = 24 ms, T0=40degC.



Mon Jan 24 08:53:00 2000 \*1/1 scale TWA center wing tank Agribon point B (Aft Bay 6 starboard), SWB2 door delay = 24 ms, T0=40degC\*



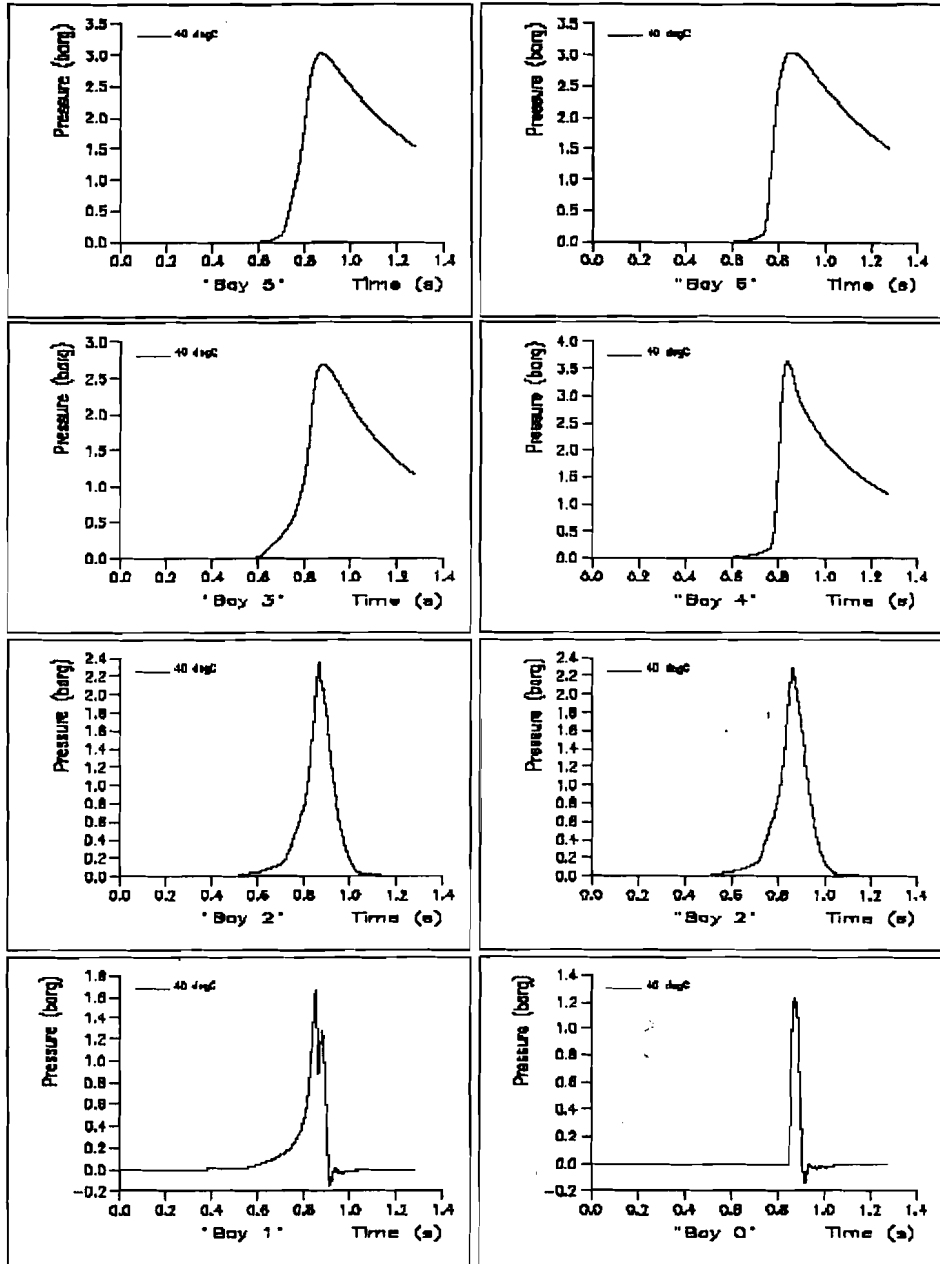
Mon Jan 24 08:46:07 2000 1/1 scale TWA central wing tank, Ignition point B (AR Bay 8 starboard), SWB2 door delay = 24 ms, T0=600degC.



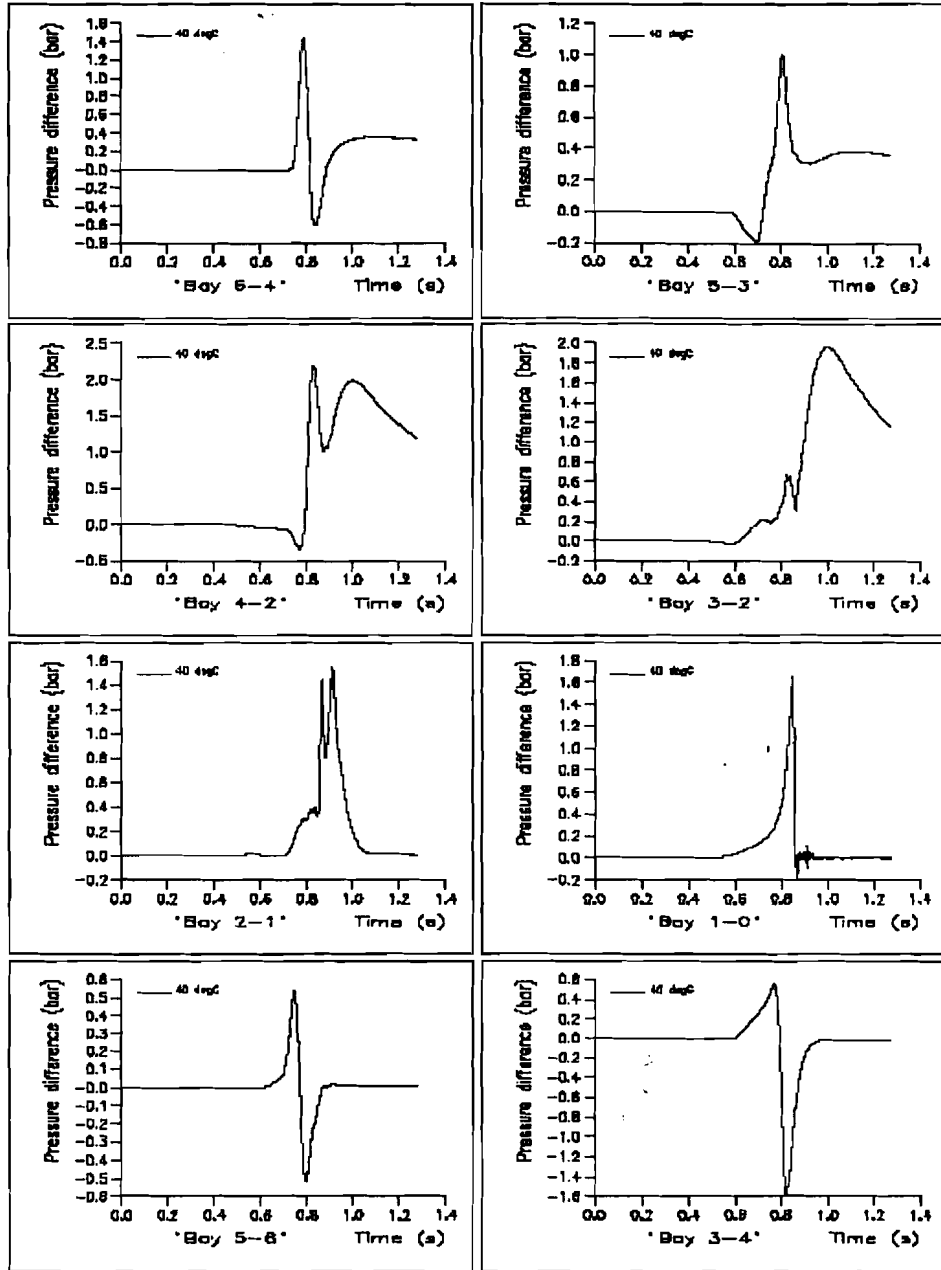


**Series 4: Initial temperature 40 °C, moment of failure of  
manufacturing panel at moment of failure of FS, eight ignition  
positions**

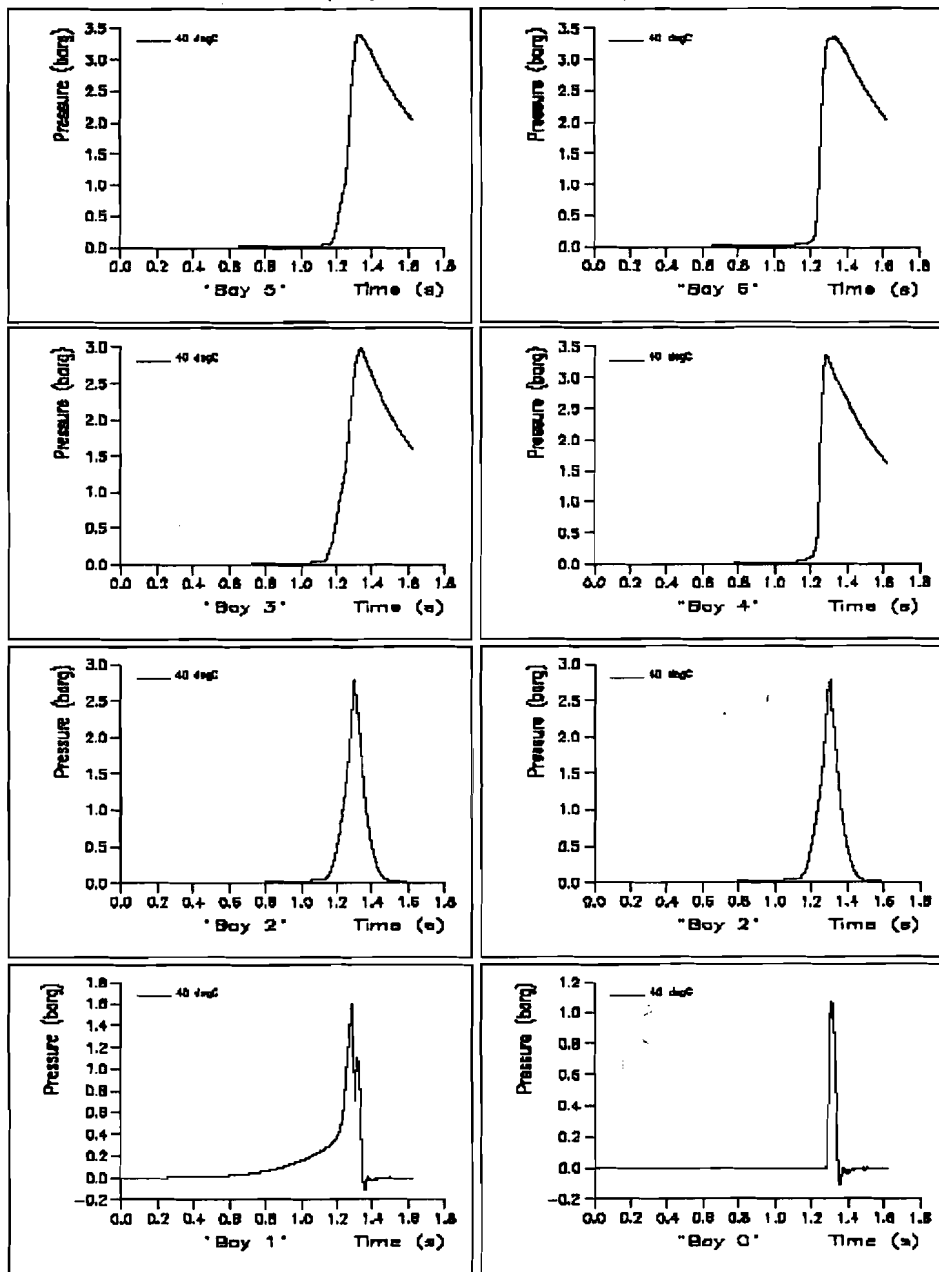
Mon Jan 24 15:03:16 2000 \*1/1 scale TWA Center wing tank Ignition point 1 (Bay 1 port), 3WB2 door delay = 0 ms, T0=40degC\*

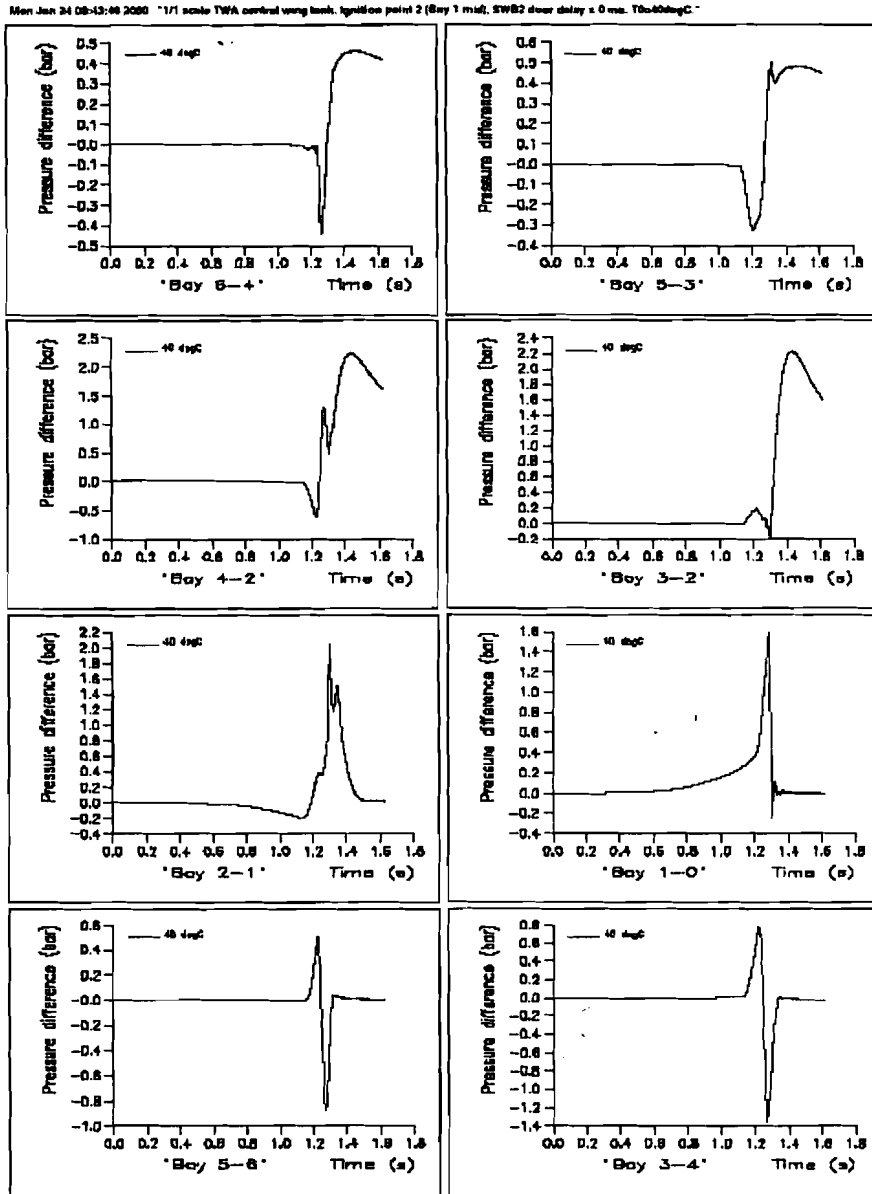


Mon Jan 24 08:43:24 2000 \*1/1 scale TWA center wing tank, ignition point 1 (Bay 1 port), SWB2 door delay = 0 ms, T0=80degC\*

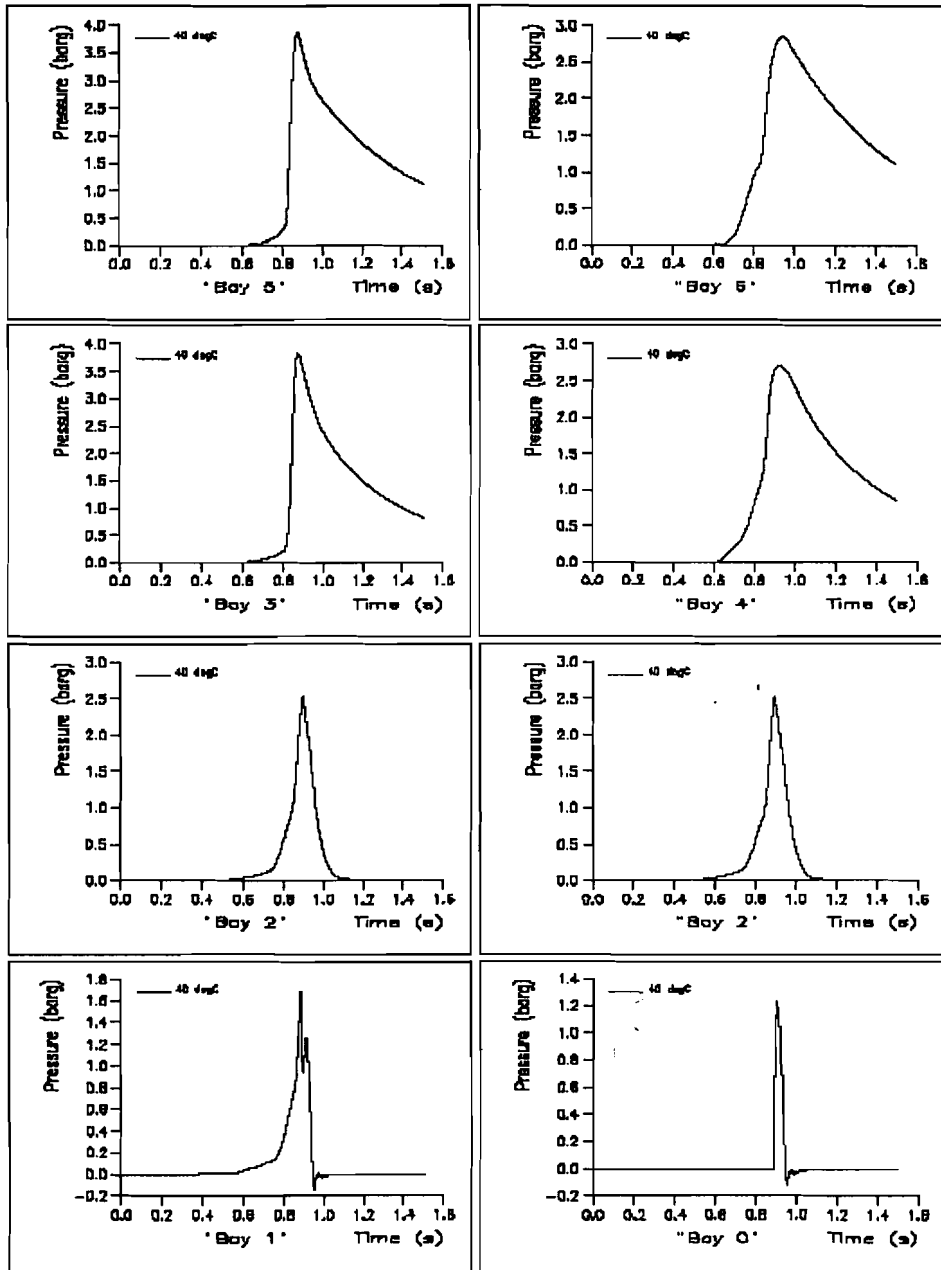


Mon Jan 24 08:48:39 2000 "1/1 scale TWA center wing tank ignition point 2 (Bay 1 mid), SWB2 door delay = 0 ms, 70x60degC"

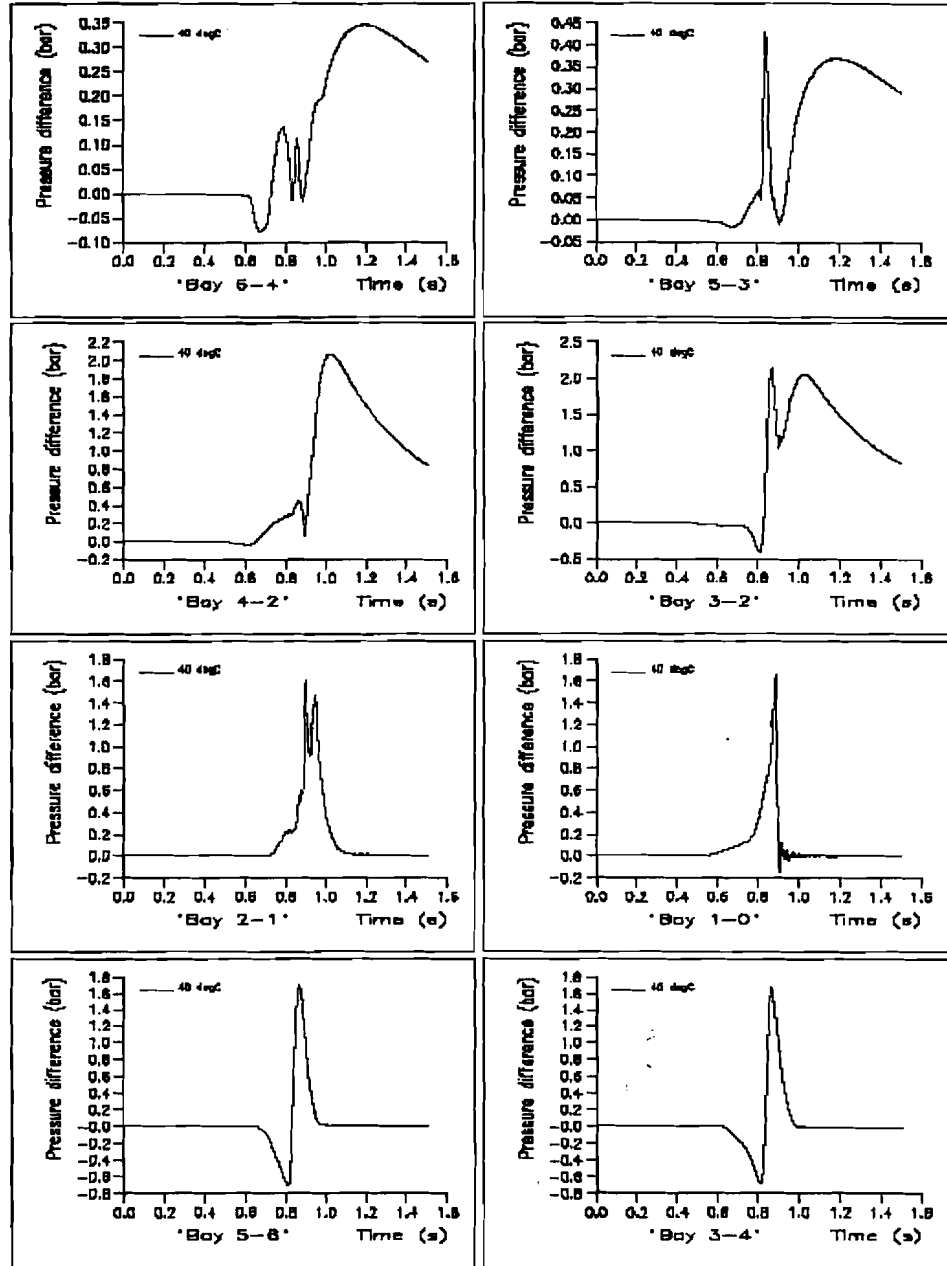




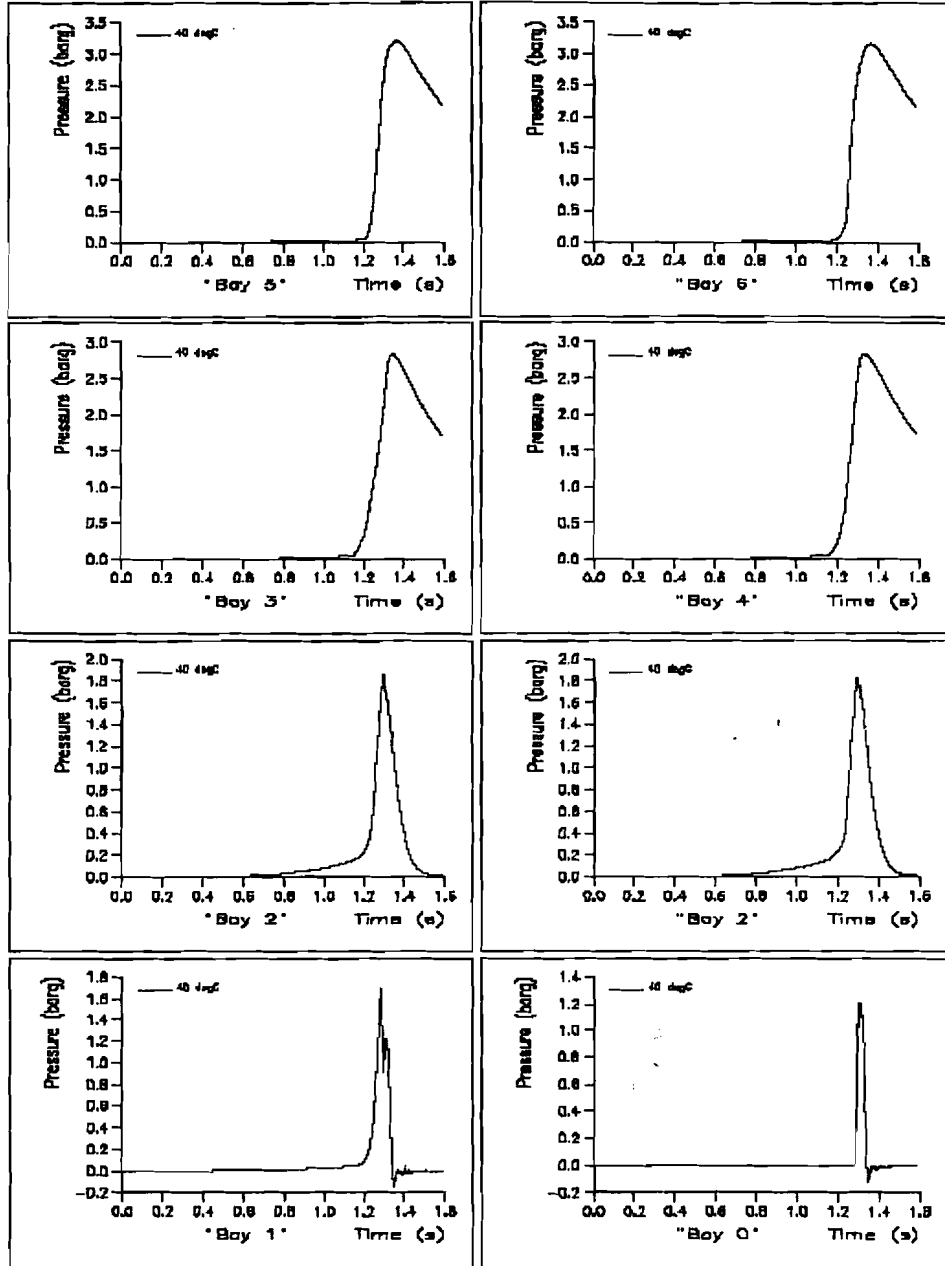
Mon Jan 24 08:48:56 2000 "1/1 scale TWA central wing tank ignition point 3 (Bay 1 starboard), SWB2 door delay x 0 ms, T0=40degC"



Mon Jan 24 08:44:08 2000 \*1/1 scale TWA, central wing tank, ignition point 2 (Bay 1 starboard), SWBD door delay = 0 ms, T0=104degC.\*

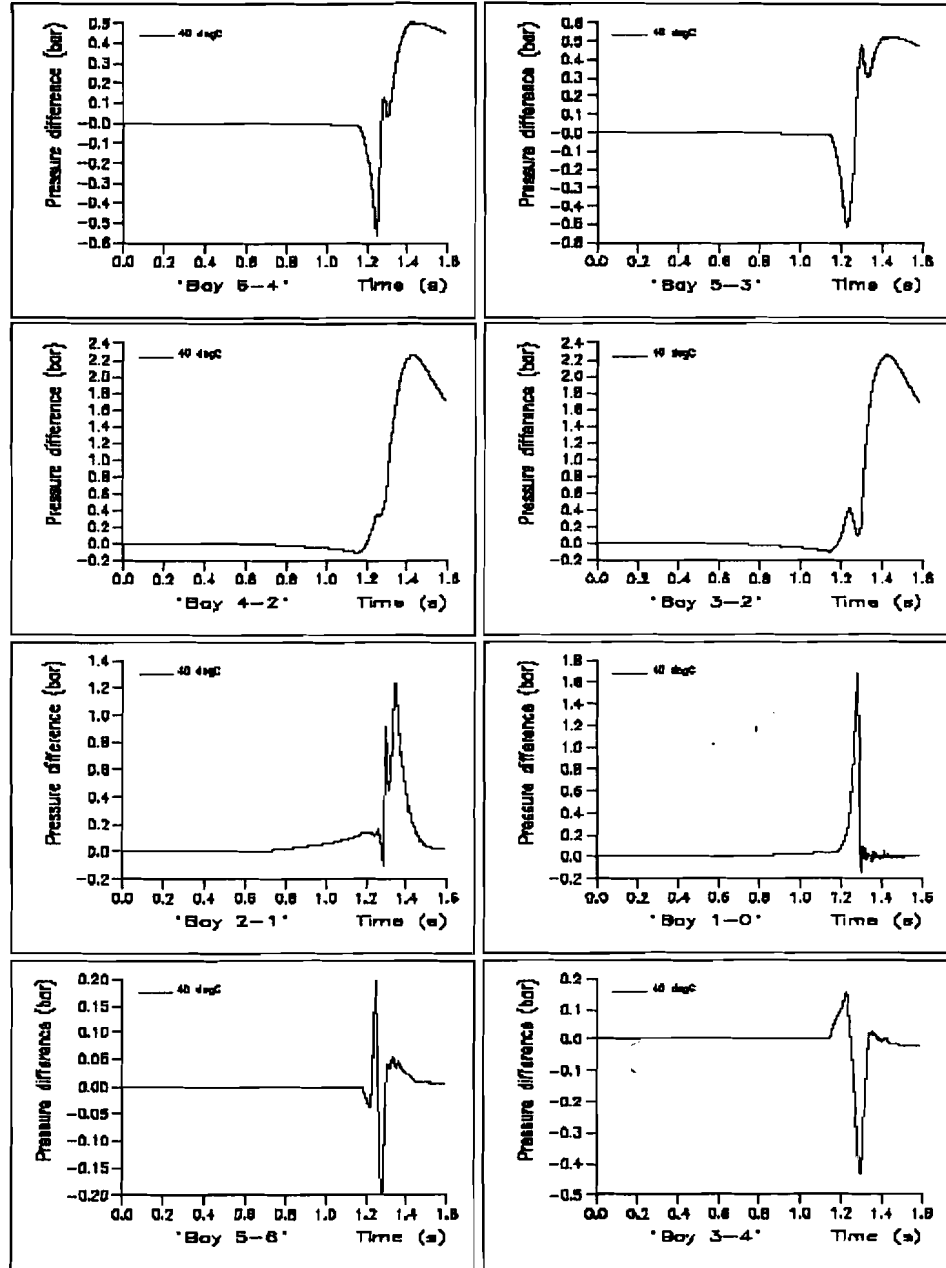


Mon Jan 24 08:10:11 2000 \*1/1 scale TWA center wing tank, ignition point 4 (Bay 2 mid), SWB2 door delay = 0 sec, T0=40degC\*

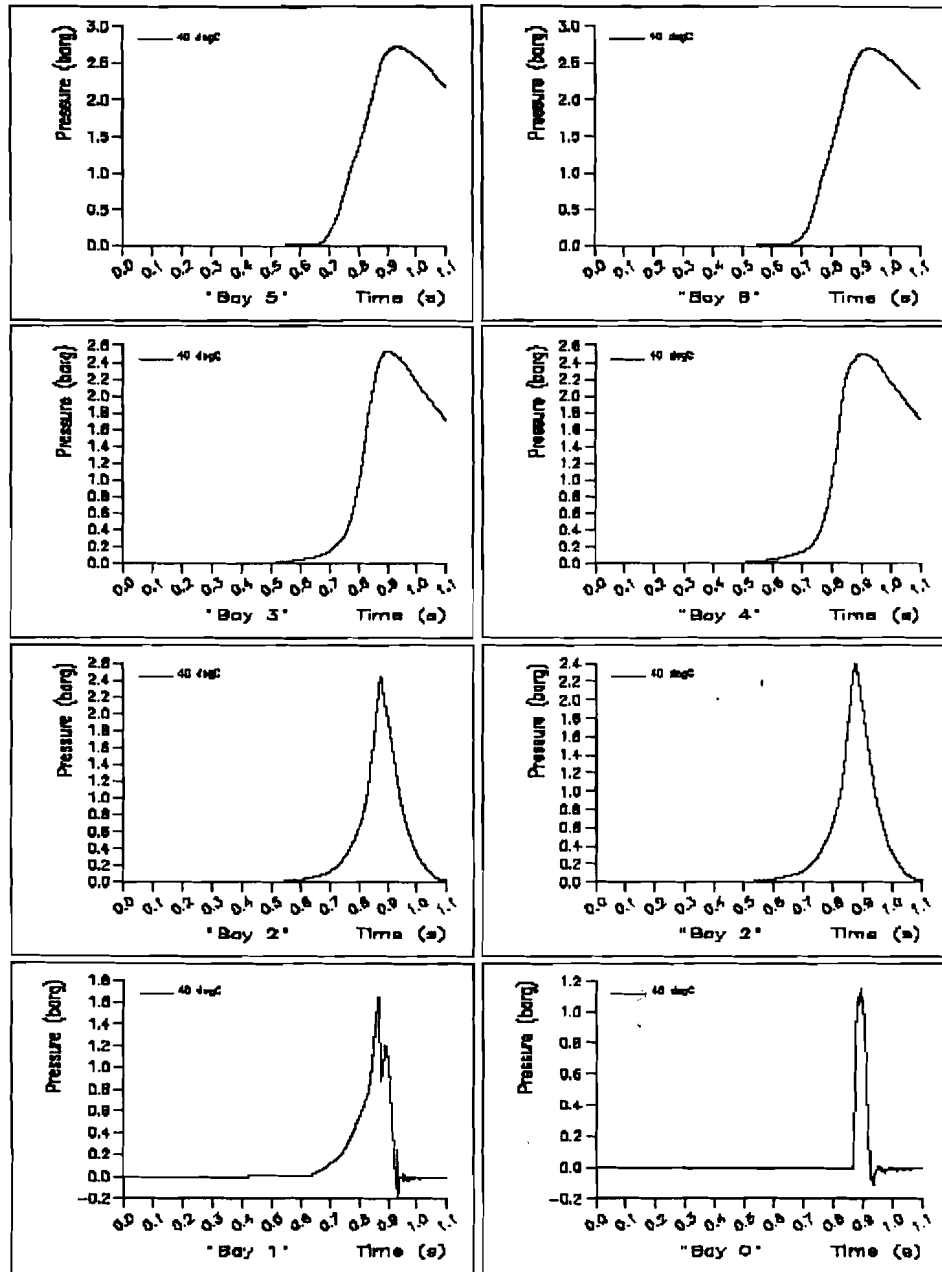


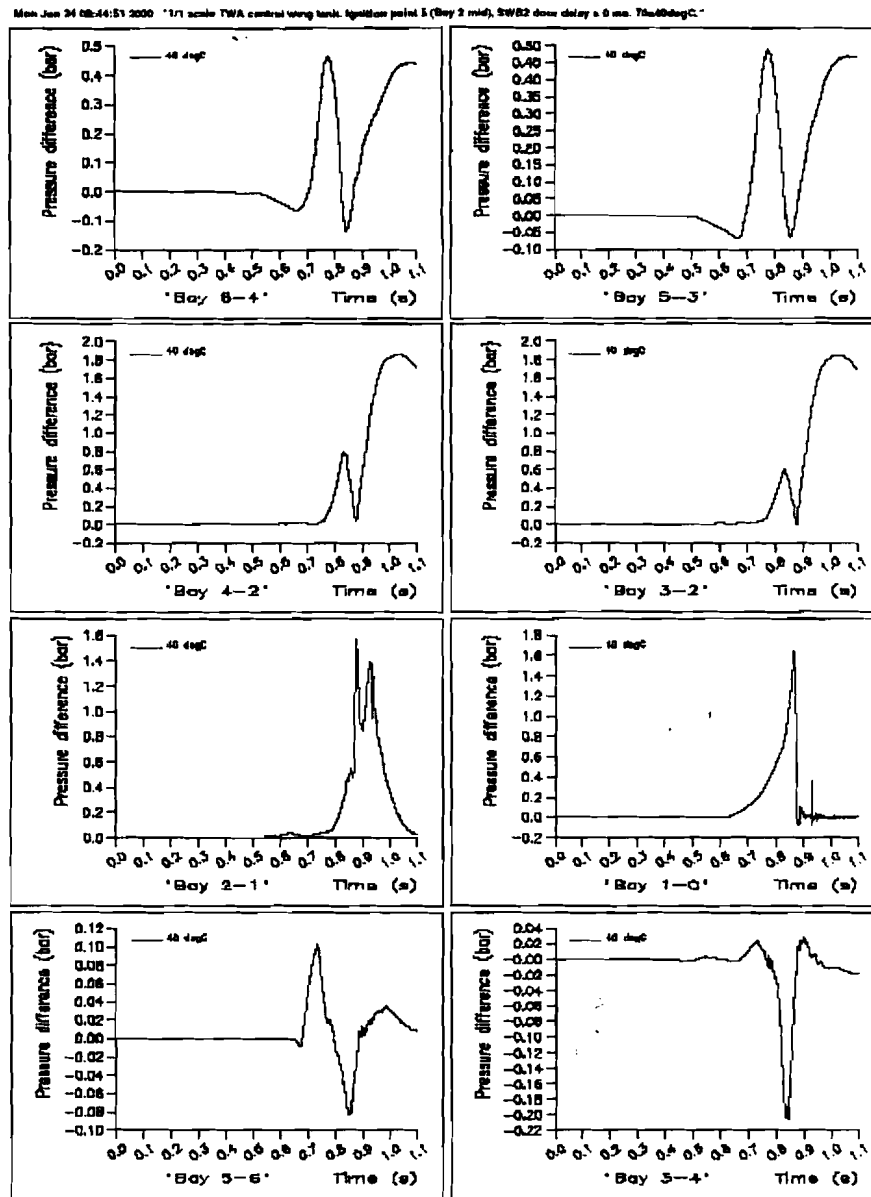


Mon Jan 24 08:44:25 2000 \*1/1 scale TWA central wing tank, Ignition point 4 (Bay 2 mid), SWB2 door delay = 0 ms, T3=0.00kgC\*

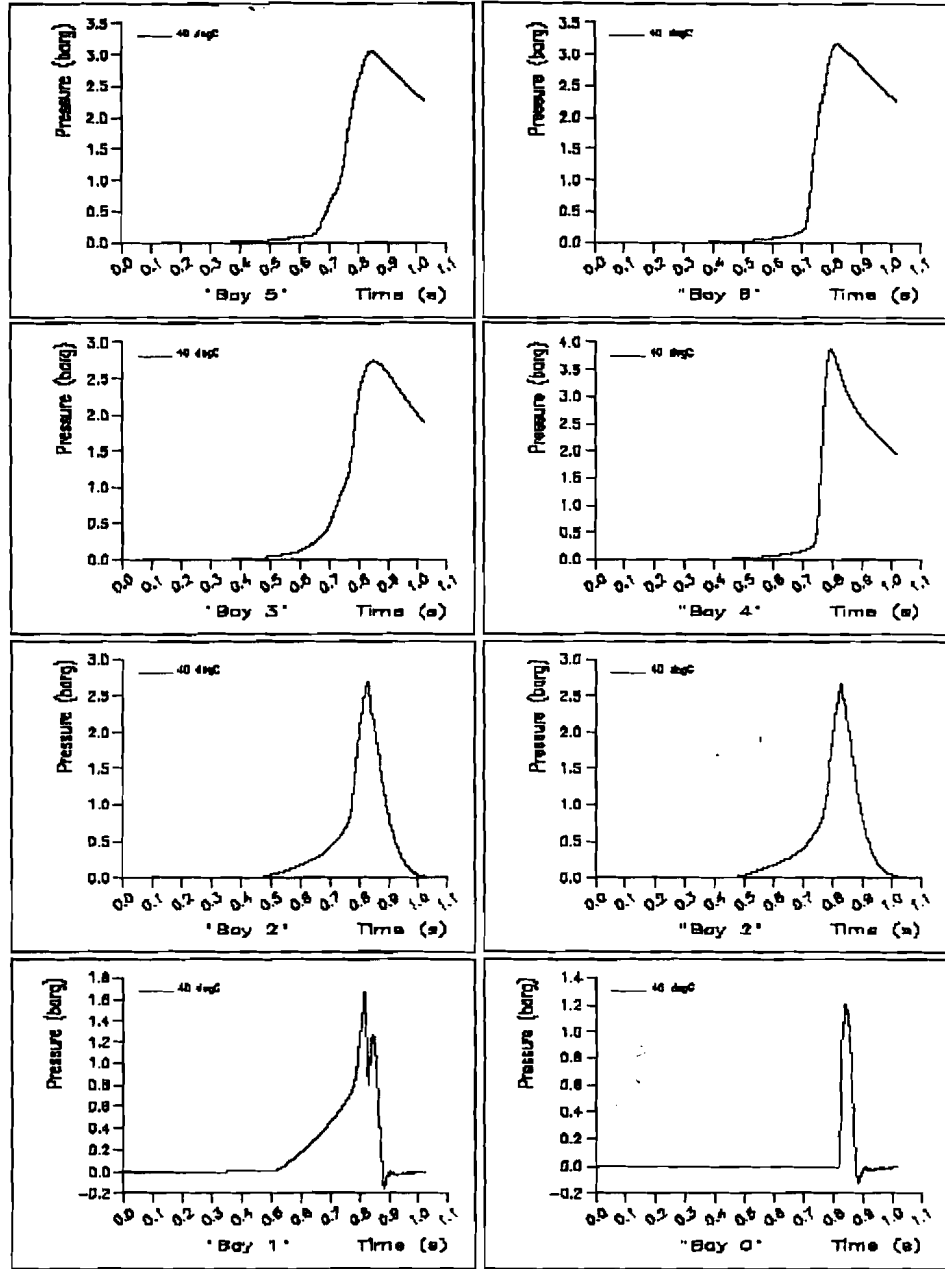


Mon Jun 24 08:49:23 2008 \*1/1 scale TWA central wing tank, ignition point 5 (Bay 2 mid), SWB2 door delay = 0 ms, T0:40degC

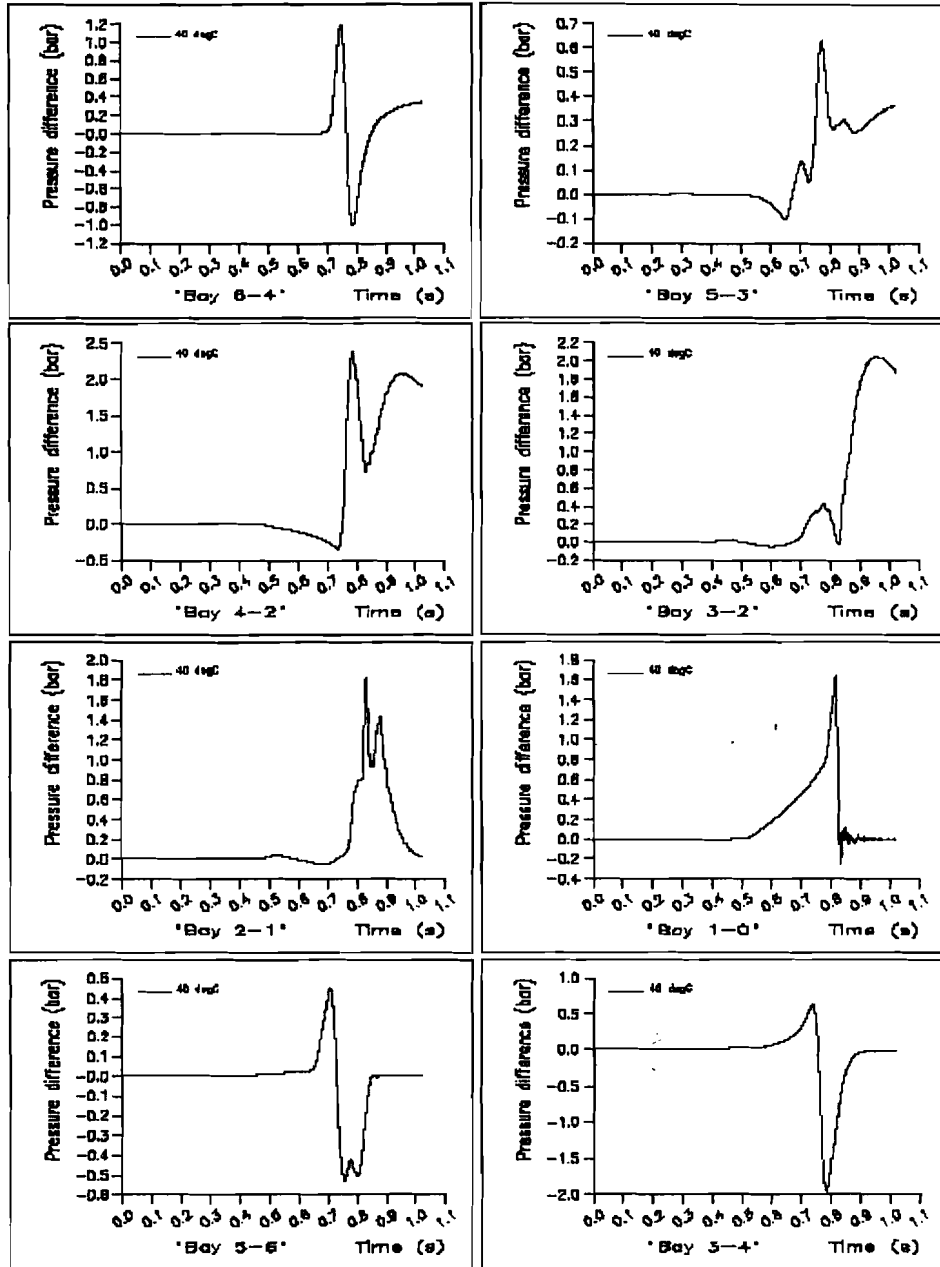




Mon Jan 24 15:05:04 2000 \*1/1 scale TWA central wing tank, ignition point 6 (Alt Bay 5 port), SWB2 door delay = 0 ms, T0=40degC

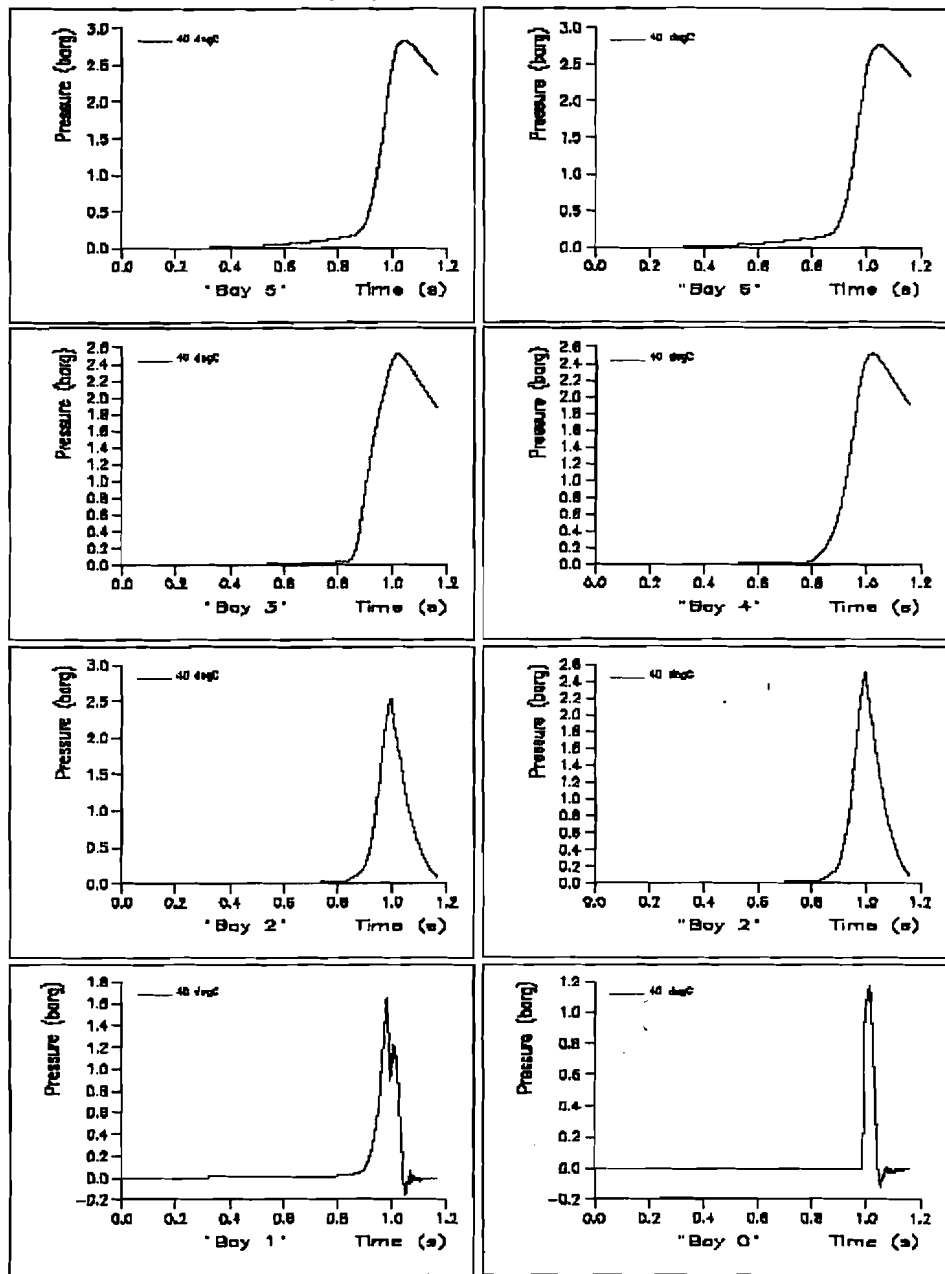


Mon Jan 24 08:45:05 2000 1/1 scale TWA center wing tank, ignition point 6 (AR Bay 5 port), SWB2 door delay = 0 ms, T0=40degC

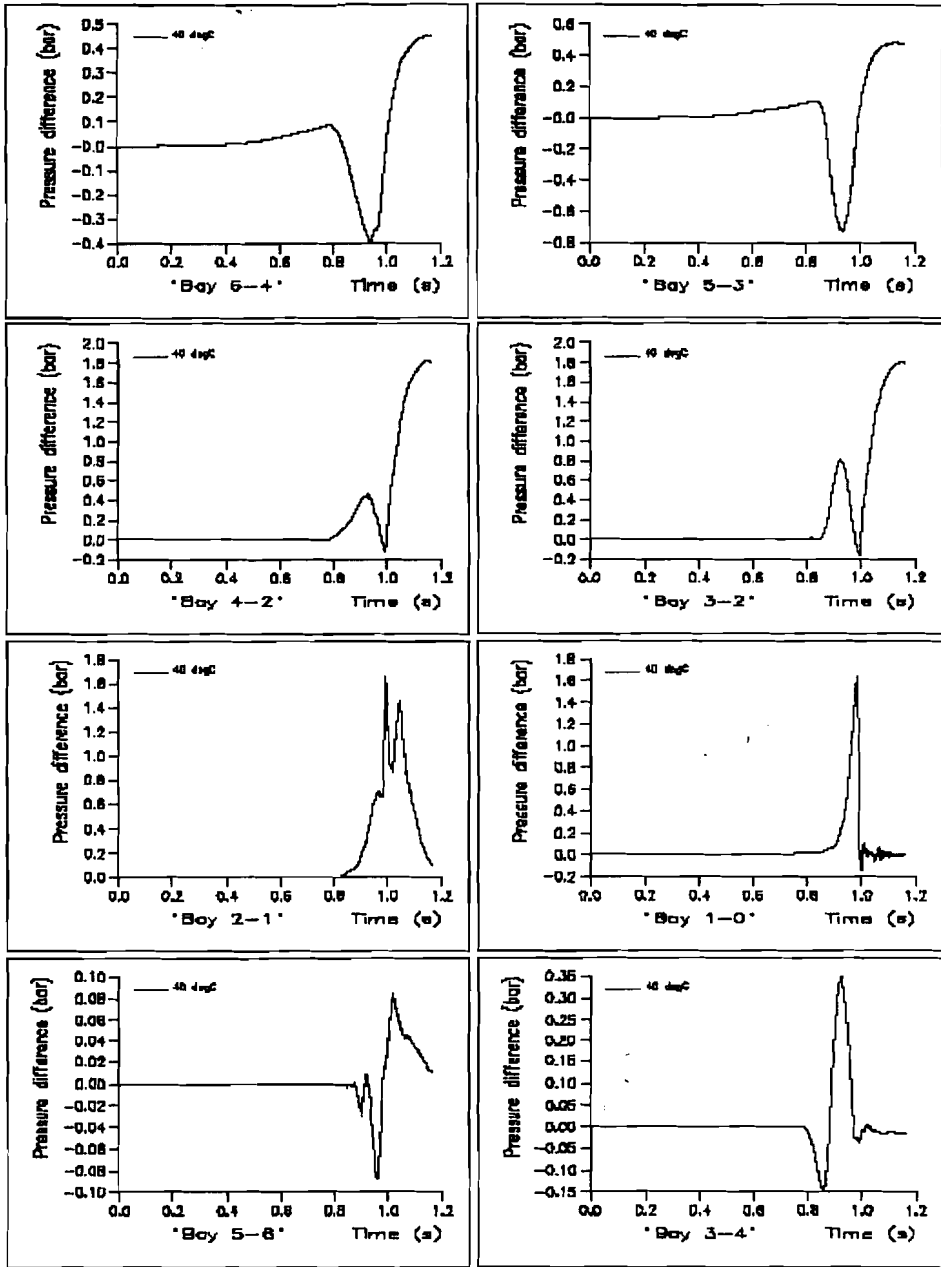


43

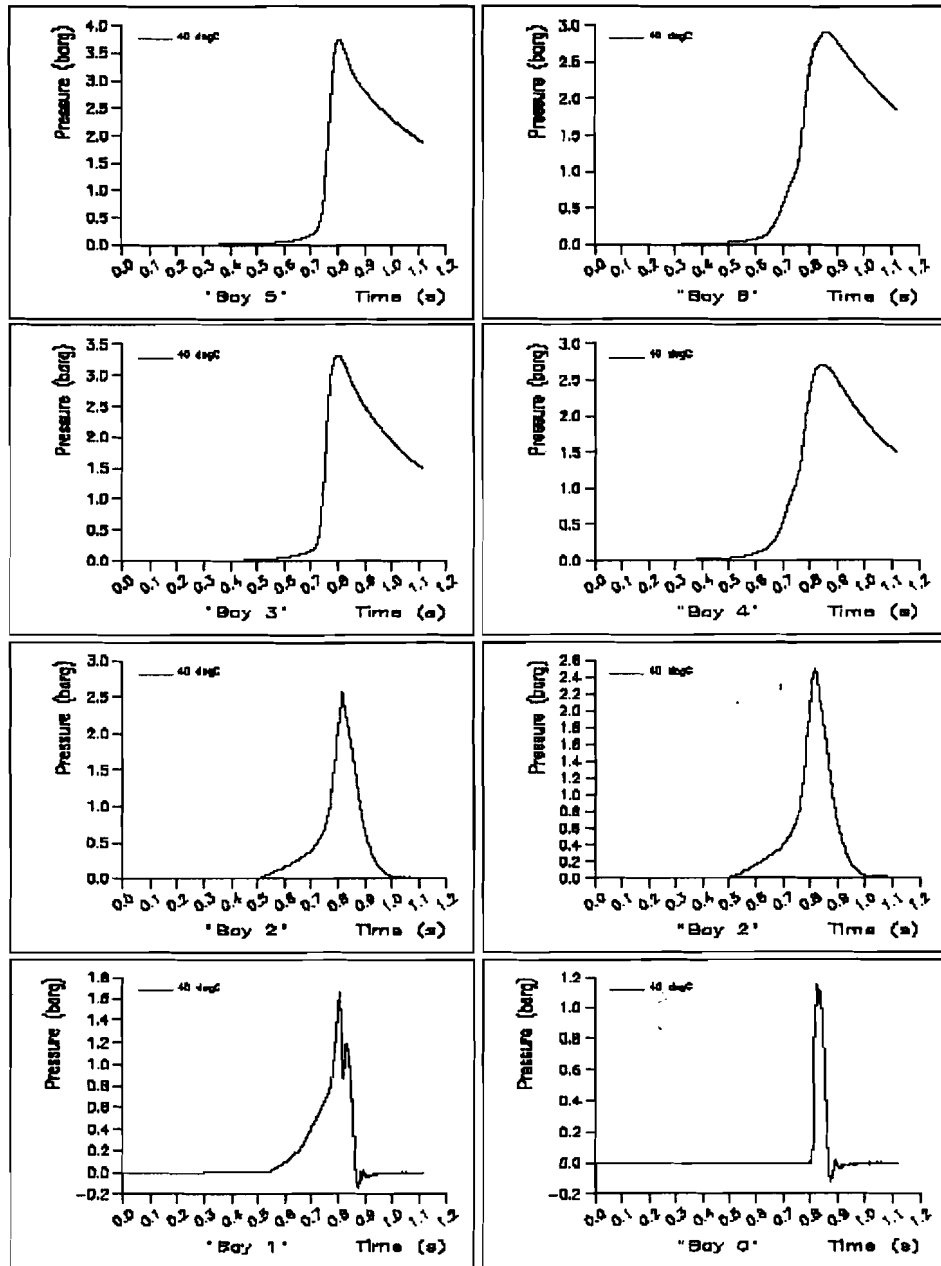
Mon Jan 24 09:51:06 2000 \*1/1 scale TWA central wing tank ignition point 7 (AR Bay 6 mid), SWB2 door delay = 0 ms, 10x00degC\*



Mon Jun 24 08:45:19 2008 \*1/1 scale TWA central wing tank, ignition point 7 (AR Bay 6 red), SWB2 door delay = 0 ms, T0=0.000000



Mon Jan 24 08:51:17 2000 \*1/1 scale TWA central wing tank ignition point B (Air Bay 5 starboard), SWB2 door delay = 0 ms, T0=40degC





Mon Jan 24 08:45:34 2000 \*1/1 scale TWA center wing tank: Ignition point B (AR Bay 6 starboard), SWB2 door delay = 0 ms, TD=40degC\*

